

# AGARD

ADVISORY GROUP FOR AEROSPACE RESEARCH & DEVELOPMENT  
7 RUE ANCELLE, 92200 NEUILLY-SUR-SEINE, FRANCE

DISTRIBUTION STATEMENT A

Approved for public release  
Distribution Unlimited

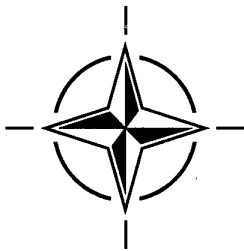
AGARD REPORT 815

## Loads and Requirements for Military Aircraft

(les Charges et les spécifications des avions militaires)

*Papers presented at the 83rd Meeting of the AGARD Structures and Materials Panel, held in Florence, Italy, 4-5 September 1996.*

19970506 074



NORTH ATLANTIC TREATY ORGANIZATION

# AGARD

ADVISORY GROUP FOR AEROSPACE RESEARCH & DEVELOPMENT

7 RUE ANCELLE, 92200 NEUILLY-SUR-SEINE, FRANCE

---

**AGARD REPORT 815**

## **Loads and Requirements for Military Aircraft**

(les Charges et les spécifications des avions militaires)

Papers presented at the 83rd Meeting of the AGARD Structures and Materials Panel,  
held in Florence, Italy, 4-5 September 1996.



North Atlantic Treaty Organization  
*Organisation du Traité de l'Atlantique Nord*

DTIC QUALITY INSPECTED 3

---

# The Mission of AGARD

According to its Charter, the mission of AGARD is to bring together the leading personalities of the NATO nations in the fields of science and technology relating to aerospace for the following purposes:

- Recommending effective ways for the member nations to use their research and development capabilities for the common benefit of the NATO community;
- Providing scientific and technical advice and assistance to the Military Committee in the field of aerospace research and development (with particular regard to its military application);
- Continuously stimulating advances in the aerospace sciences relevant to strengthening the common defence posture;
- Improving the co-operation among member nations in aerospace research and development;
- Exchange of scientific and technical information;
- Providing assistance to member nations for the purpose of increasing their scientific and technical potential;
- Rendering scientific and technical assistance, as requested, to other NATO bodies and to member nations in connection with research and development problems in the aerospace field.

The highest authority within AGARD is the National Delegates Board consisting of officially appointed senior representatives from each member nation. The mission of AGARD is carried out through the Panels which are composed of experts appointed by the National Delegates, the Consultant and Exchange Programme and the Aerospace Applications Studies Programme. The results of AGARD work are reported to the member nations and the NATO Authorities through the AGARD series of publications of which this is one.

Participation in AGARD activities is by invitation only and is normally limited to citizens of the NATO nations.

The content of this publication has been reproduced  
directly from material supplied by AGARD or the authors.

Published February 1997

Copyright © AGARD 1997  
All Rights Reserved

ISBN 92-836-0037-1



*Printed by Canada Communication Group  
45 Sacré-Cœur Blvd., Hull (Québec), Canada K1A 0S7*

# **Loads and Requirements for Military Aircraft**

**(AGARD R-815)**

## **Executive Summary**

Since the beginning of aircraft design and certification, loads and loads-related requirements have continued to evolve, while the initial conservative assumptions related to safety factors have remained essentially the same over the years.

The technology and analysis tools have also evolved substantially in several areas: for example the increased use of computational/experimental methods in the areas of maneuvering loads; the characterization of buffet; the increased use of stochastic methods for gust loads; and the improved knowledge of fatigue life impact on design.

On the other hand, the quest for lighter and higher performance aircraft led to the development of new technologies such as Electronic Flight Control Systems (EFCS) and thrust vectoring systems. With the increased use of these technologies and the improved quantification of factors influencing loads, the initial concept of safety factors and also some of the bases of military standards for military aircraft needed to be re-visited.

It was observed in the Workshop that there was not much advantage in trying to reduce the safety factors for a new aircraft but that it might be effective to do so for an aircraft modification after a change of role, for instance. Reserves were also expressed as to the danger of optimizing a design for an initial use. It was considered advisable to remain conservative in order to accommodate changes in role during the life of an aircraft, especially a fighter aircraft.

The effects of failures of EFCS on loads envelopes were also presented, showing that in certain cases an aircraft designed according to a functional EFCS could exceed the design load envelope when a failure of EFCS occurred, thus arguing for a certain conservatism in design.

It was concluded, that some level of conservatism was still required but that new criteria and methods should be investigated in order to propose standards for future aircraft design.

# Les charges et les spécifications des avions militaires

## (AGARD R-815)

### Synthèse

Depuis le début de l'ère du design et de la certification des aéronefs, les charges et leurs exigences n'ont cessé d'évoluer, tandis que les hypothèses conservatrices liées aux facteurs de sécurité sont demeurées les mêmes au fil des ans.

La technologie et les outils d'analyse ont aussi évolué grandement: usage de plus en plus prononcé des méthodes numériques et expérimentales dans le champ de détermination des charges de manœuvre, caractérisation des phénomènes dynamiques tels la rafale ("buffet"), l'utilisation de plus en plus poussée des méthodes probabilistes pour le calcul de charges dues aux turbulences et enfin, la connaissance accrue de la vie en fatigue anticipée sur les critères de design.

La recherche d'aéronefs de plus en plus performants et légers, de même que la progression rapide de l'ordinateur ont amené l'introduction de systèmes de commandes de vol électroniques et de poussée vectorisée.

Durant, l'atelier du sous-comité 73, plusieurs articles ont traité du concept de facteur de charge. Il fut noté que d'essayer de réduire le facteur de sécurité lors du design initial ne menait pas nécessairement à un gain significatif. Par contre, il en va autrement lorsqu'il s'agit de modifier un aéronef suite à un changement de rôle. Des réserves furent aussi émises quant au danger d'optimiser à l'extrême le design d'un aéronef pour l'usage initial, planifié durant la phase de design. Des exemples ont montré qu'un certain conservatisme est de rigueur à cet égard.

La caractérisation des différents phénomènes dynamiques pouvant influencer le design d'un aéronef muni d'un système de commande actif furent abordés. Les effets de la défaillance des systèmes de commandes actifs sur les charges d'aéronefs conçus en tenant compte de tels systèmes ont été présentés. On a observé notamment qu'un aéronef peut se retrouver à l'extérieur de son enveloppe de charges lors de la défaillance d'un système actif utilisé pour la réduction des charges structurales, suggérant un certain conservatisme lors du design.

Une table ronde a clos l'atelier, et la conclusion générale est à l'effet qu'un niveau de conservatisme était de rigueur lorsqu'il s'agit de modifier des facteurs de sécurité de charges d'aéronefs et que l'on devrait se pencher sur le besoin de redéfinir certains critères pour les prochains aéronefs.

# Contents

	Page
Executive Summary	iii
Synthèse	iv
Preface	vii
Structures and Materials Panels	viii
	Reference
<b>SESSION I</b>	
<b>Evolution de la Philosophie des Charges de Dimensionnement des Avions Militaires</b> <i>Evolution of Philosophy of Design Loads for Military Aircraft</i> by C. Petiau	1
<b>Probabilistic Approaches – Composite Design</b> by C.C. Chamis	2
<b>Determination and Verification of Operational Maneuver Parameters and Time Histories</b> by J. Molkenthin	3
<b>Flight Loads Derived from Operational Maneuvers</b> by H. Struck and C. Perron	4
<b>Paper 5 withdrawn</b>	
<b>A Comparison of Pressure Measurements between a Full-Scale and a 1/6-Scale F/A-18 Twin Tail during Buffet</b> by R.W. Moses and E. Pendleton	6
<b>SESSION II</b>	
<b>Paper 7 withdrawn</b>	
<b>The Impact of Dynamic Loads on the Design of Military Aircraft</b> by W. Luber, J. Becker and O. Sensburg	8
<b>Dynamic Loading Considerations in Design of Modern Combat Aircraft</b> by R. Chapman	9
<b>Les Charges au Sol lors des Phases de Roulage: Les Spécifications Civiles et Militaires</b> by G. Squeglia and O. Regis	10
<b>Paper 11 withdrawn</b>	

### SESSION III

<b>Evolution of F-16 Loads and Requirements</b>	<b>12</b>
by D.H. Gibson	
<b>Paper 13 withdrawn</b>	
<b>Impact of Electronic Flight Control System (EFCS) Failure Cases on Structural Design Loads</b>	<b>14</b>
by H.-M. Besch, H.-G. Giessler and J. Schuller	
<b>Influence of Thrust Vectoring System (TVS) on Structural Design Loads</b>	<b>15</b>
by K. Füllhas and M. Neubauer	
<b>Eurofighter 2000 Structural Design Criteria and Design Loading Assumptions</b>	<b>16</b>
by G.J. Watson	
<b>Paper 17 withdrawn</b>	

# Preface

The introduction of Electronic Flight Control Systems (EFCS) in aircraft has brought the need to re-visit some of the existing concepts such as limit loads and safety factors. The former are directly affected by the EFCS while the second are affected by a better knowledge of accurate load prediction method, structural analyses, material and production variability, and operations during service.

The objectives of the Workshop were the following:

- review the state-of-the-art for the limit load concept;
- review the state-of-the-art for fatigue and damage tolerance limits and the factors applied (scatter factors);
- investigate the different factors contributing to loads for actively controlled aircraft;
- investigate effects of EFCS failures on loads envelope;
- explore possible adverse effects of initial usage based design optimization;
- explore other avenues than “maneuver based” design;
- determine the possibilities of introducing stochastic methods in the aircraft design process.

The Workshop was organized in Florence Italy in September 1996. It brought together major aircraft manufacturers to share experiences and provided insights to help meet the objectives defined above.

It led to the creation of a working group on “Design Loads for Future Aircraft”.

Claude Perron  
Chairman,  
Sub-Committee on  
Loads and Requirements for Military Aircraft



# Structures and Materials Panel

**Chairman:** Prof. O. Sensburg  
Chief Engineer  
Daimler Benz Aerospace  
Militaerflugzeuge LM2  
Postfach 80 11 60  
81663 Munich  
Germany

**Deputy Chairman:** Prof. S. Paipetis  
Prof. of Applied Mechanics  
School of Engineering  
Dept. of Mechanical Engineering  
University of Patras  
26110 Patras  
Greece

## SUB-COMMITTEE MEMBERS

**Chairman:** Mr. C. Perron  
Bombardier Inc.  
Canadair, Military Aircraft Div.  
10,000 Cargo A-4 Street  
Montreal International Airport  
Mirabel, Quebec I7N 1H3  
Canada

<b>Members:</b>	E. Campo	IT	N. Livings	UK
	D. Chaumette	FR	D. Paul	US
	J. Coyle	US	O. Sensburg	GE
	P. Heuler	GE	D. Simpson	CA
	A. Humble	UK	J. Vantomme	BE
	J.P. Immarigeon	CA	G. Zennaro	IT
	R. Labourdette	FR		

## PANEL EXECUTIVE

Dr. J.M. CARBALLAL, SP

**Mail from Europe:**  
AGARD-OTAN  
92200 Neuilly-sur-Seine  
France

**Mail from US and Canada:**  
AGARD-NATO/SMP  
PSC 116  
APO AE 09777

Tel: 33 (0) 1 55 61 22 90 & 92  
Telefax: 33 (0) 1 55 61 22 99 & 98  
Telex: 610175F

**EVOLUTION DE LA PHILOSOPHIE DES CHARGES DE DIMENSIONNEMENT  
DES AVIONS MILITAIRES**  
**EVOLUTION OF PHILOSOPHY OF DESIGN LOADS  
FOR MILITARY AIRCRAFT**

C. PETIAU

Dassault Aviation, Direction Générale Technique  
78 Quai Marcel Dassault, Cedex 30  
92552 Saint-Cloud Cedex, France

**RESUME**

Après un rappel des principes de définition des charges de dimensionnement avec les anciens règlements, nous en montrons les difficultés pour le cas des avions de combat munis de Système de Commande de Vol Electrique (S.C.V.E.).

Nous avons dû évoluer vers un **processus intégré** couplant la définition des charges de dimensionnement et le réglage du S.C.V.E., et visant à garantir en final le maintient de l'avion dans un **domaine limite de résistance**.

Cette évolution a renforcé le principe de définition des charges limites comme **charges maximales attendues en service**, sans cependant devoir les rattacher à des manoeuvres types normalisées par un règlement.

Nous présentons les grandes lignes du processus actuel, qui fait intervenir :

- la définition d'**indicateurs de sévérité des charges** et la construction des opérateurs de calcul correspondants,
- le calcul systématique de ces indicateurs dans les simulations de mécanique du vol (simulateurs d'étude temps réel compris),
- les techniques d'optimisation mathématique, permettant de manier les taux d'échange entre performances de manoeuvre et dimensionnement structural.

Pour le cas général, nous écartons plutôt l'idée que ces évolutions puissent justifier une modification du coefficient de sécurité charges extrêmes/charges limites.

**ABSTRACT**

After a brief recall of the principles of design load definition resulting from classical regulations, we show the difficulties of their application for combat aircraft equipped with Electrical Flight Control System (E.F.C.S.).

This has led to an **integrated process**, where definition of design loads and setting of E.F.C.S. has been coupled, aiming finally to guarantee keeping the aircraft within a **limit strength domain**.

This evolution reinforces the definition principle of limit loads as **maximum loads to be expected in service**, yet, without need for links with regulation standard manoeuvres.

We present the main aspects of this process, which includes :

- the definition of **load severity indicators**, and the elaboration of corresponding calculation operators,
- systematic calculations of these indicators during flight mechanics simulations (including real time development flight simulators),
- use of mathematical optimization techniques, allowing to handle exchange rate between manoeuvre performances and structural sizing.

For general cases it is not proven that these evolutions could justify a modification of ultimate loads/limit loads safety factors.

## 1. CONTEXTE

Les charges « limites » des avions de combat sont classiquement définies comme les valeurs de charge « maximales » autorisées en service (AIR-20004-E), ou résultant de l'usage autorisé de l'avion \* (US-MIL-A-87221). Cette définition globale est complétée par la donnée de « conditions de charge » :

- manoeuvres types définies par des arguments simples (accélérations, braquages maximum des gouvernes, efforts maximum des servocommandes),
- rafale et turbulence atmosphérique,
- pressurisation,
- charges au sol,
- etc...

Pour certaines conditions de charge (rafale, charges au sol,...) les règlements proposent des procédures de calcul forfaitaires ; dans quelques cas, en particulier pour le calcul de « turbulence continue », les niveaux de charges limites sont définis à partir de la donnée de leur nombre d'occurrence.

L'intérêt apparent de ce système est :

- une définition relativement claire et explicite des cas de charge de dimensionnement pour le concepteur
- une relation qui semble aisée entre les charges de dimensionnement et les performances de manoeuvre

En pratique il reste bon nombre de difficultés liées à l'exhaustivité insuffisante des conditions de charges envisagées dans les règlements.

Ainsi, lors de manoeuvres contrées sur un avion à commandes classiques, un pilote peut solliciter la structure plus sévèrement que les charges limites, en restant en deçà des facteurs de charges et des braquages de gouvernes des conditions limites réglementaires.

\* noter la nuance avec le règlement civil (FAR/JAR 25) qui définit les charges limites comme les charges maximales attendues en service.

L'arrivée depuis 1975 des avions à commandes de vol électriques (Mirage 2000, Rafale) a amplifié ces difficultés, dans la mesure où les situations réelles de charges dimensionnantes ne correspondent pas aux configurations de manoeuvre envisagées par les règlements :

- les manoeuvres de facteur de charge stabilisées sont précédées et suivies de transitoires rajoutant localement des efforts,
- les manoeuvres contrées des règlements peuvent ne plus être réalisables, l'action du S.C.V.E. (Système de Commande de Vol Electrique) interdisant certaines situations
- de façon générale le S.C.V.E. est conçu pour dégager le pilote du soucis de surveillance des limites structurales (pilotage « care free »), tout en tirant le meilleur parti opérationnel des qualités de vol de l'avion ; il en résulte pratiquement que les limites structurales peuvent être atteintes quotidiennement avec des manoeuvres dynamiques complexes.

Cette situation pour les avions munis de S.C.V.E., nous a conduit, à faire évoluer sensiblement le processus d'établissement des charges de dimensionnement, en prenant mieux en compte l'esprit du règlement où les charges limites sont les charges maximales\*\* rencontrables en service, tout en pouvant s'affranchir de liens réglementaires entre les conditions de charges limites et des manoeuvres types standardisées.

\*\* voir en annexe, l'explicitation du terme « charges maximales ».

## 2. Processus d'établissement des charges de dimensionnement des avions de combat munis d'un S.C.V.E.

### 2.1 Principales idées directrices

- Le processus de définition des charges de dimensionnement est intégré au processus de conception du S.C.V.E. et à celui du dimensionnement de la cellule.
- On construit un premier jeu de charges à partir de configurations de manoeuvres relativement forfaitaires, reflétant les qualités de vol exigées de l'avion. L'expérience du constructeur détermine le choix de ces premiers cas de charge de dimensionnement
- Il en résulte un premier dimensionnement, qui définit lui-même un « domaine de résistance limite » de la cellule,
- Dans tous les cas de manoeuvre, le S.C.V.E. maintient l'avion dans le domaine de résistance limite \*,
- Si la règle précédente pénalise les performances opérationnelles de l'avion, le dimensionnement est revu pour élargir ponctuellement le domaine de résistance limite,
- Pour les charges dépendantes pour tout ou partie de l'environnement naturel ou de paramètres variables (rafales, turbulences, charges des atterrisseurs,...) on doit gérer un compromis entre les modèles forfaitaires des règlements, et les simulations numériques plus sophistiquées permettant l'analyse des occurrences de charge en fonction des occurrences de leurs causes.
- Le principe d'un coefficient de sécurité forfaitaire entre charges limites et charges extrêmes n'est pas remis en cause (voir § 3)

\* sauf cas très exceptionnels voulus par le pilote.

### 2.2 Organisation pratique

A partir des idées directrices énoncées et des capacités actuelles des moyens de calcul et d'essais, on aboutit au processus itératif d'établissement des charges suivant:

- **Phase de conception de l'avion** (avant projet et début de projet)
  - **Construction de modèles d'analyses**
    - ▲ modèle structural Elément Finis de l'avion complet, statique et dynamique, réduit dans une « base de charge » (voir références 1 et 2),
    - ▲ base des charges aérodynamiques obtenue par calcul numérique (C.F.D.) et recalage expérimental,
    - ▲ modèles non linéaire des composants mécaniques complexes (trains d'atterrissage, éjecteurs d'emport, ...), (voir références 3 et 4).

Cette base de modèles est construite par notre système de calcul de structure « ELFINI ». On en extrait les opérateurs condensés permettant le calcul rapide des réponses structurales pour toutes conditions de manoeuvre, statique ou dynamique, en tenant compte des effets d'aéroélasticité, dans tout le domaine de vol, et pour toutes les configurations d'emport (voir références 3 et 4); ces principaux « opérateurs condensés » sont :

- ▲ les coefficients aérodynamiques « avion souple », nécessaires au calcul des manoeuvres
- ▲ les opérateurs « indicateurs de sévérité des charges » reliant une sélection d'efforts internes, de contraintes ou déformations, considérés comme « pilotes » pour la sélection des cas de charges maximales (voir annexe), aux paramètres d'état de la mécanique du vol (pression dynamique, Mach, incidences, braquages des gouvernes,...)
- ▲ opérateurs de reconstruction sur le modèle Elément Finis des cas de

charges à partir des paramètres de mécanique du vol.

Pour les charges dynamiques ces opérateurs sont livrables sous forme de fonctions de transfert (analyses linéaires domaine fréquence) ou de modèles « rationnels » (équations différentielles) pour les analyses non linéaires domaine temps.

#### □ Sélection des cas de charges de dimensionnement.

Elle est menée par un balayage systématique de calculs de configurations de charge forfaitaire, principalement :

- ▲ de cas de manoeuvre reflétant les qualités de vol exigées, au départ des manoeuvres statiques simples combinant facteur de charge, vitesse ou accélération de roulis, braquages maximum de gouvernes ou efforts maximum de servocommandes.
- ▲ pour les charges atterrisseurs et pour tous les cas dont les conditions ne sont pas complètement déterminées par le Pilote et le S.C.V.E., simulations numériques avec balayage d'un domaine de conditions initiales et de conditions d'environnement probables, avec recherche systématique des conjonctions défavorables. Le S.C.V.E. est modélisé dans ces simulations.

Les cas majorants sont repérés automatiquement à partir des indicateurs de sévérité des charges avec la méthode détaillée en annexe.

#### □ Dimensionnement de la cellule :

Il est effectué avec l'aide de l'optimiseur mathématique de ELFINI (voir références 5 et 6) qui prend en compte :

- ▲ la résistance structurale sous tous les cas de charges statiques et dynamiques sélectionnés

précédemment et majorés du coefficient de sécurité charges extrêmes/charges limites (voir §3),

- ▲ la résistance structurale en fatigue pour les parties métalliques,
- ▲ les contraintes de qualité de vol liées à l'aéroélasticité statique, les contraintes de flutter, pour toutes les configurations d'emport.

#### □ Définition des limites de résistance structurale.

Ces valeurs sont dérivées du dimensionnement précédent, elles sont représentées par un vecteur « d'états limites » des indicateurs de sévérités des charges (voir annexe). Ces limites de résistance sont égales ou supérieures aux valeurs des indicateurs de sévérité des charges pour les cas de dimensionnement (ramenés au niveau « limite »)

#### □ Conception et dimensionnement du S.C.V.E.

Le S.C.V.E. est directement conçu pour satisfaire la contrainte de pilotage « care free ». La vérification est faite par des simulations de mécanique du vol (simulation numérique sur ordinateur et simulateur de vol temps réel) ; au cours de ces simulations les valeurs des indicateurs de sévérité des charges sont calculées en permanence et comparées à leurs valeurs limites. On mène avec ces simulations de pilotage une recherche systématique des configurations les plus sévères pour la résistance structurale.

Les cas de dépassements des limites structurales sont traités soit par la modification du réglage du S.C.V.E., soit par la modification des charges de dimensionnement.

La fonction de pilotage « care-free » du S.C.V.E. est sécurisée par l'architecture redondante du système, elle n'est pas affectée par les défaillances dites « probables », arrivant séparément au sens de la norme US - MIL-A-87221 § 3.2.22 ; les charges limites de

dimensionnement ne sont donc pas affectées non plus par ces défaillances « probables ».

#### • Phase de mise au point et de qualification

L'ensemble des modèles précédemment cités est vérifié et calibré sur les résultats d'essais au sol et en vol des avions de développement. En particulier les opérateurs de calcul des indicateurs de sévérité sont recalés et validés à partir de mesures extensométriques ; nous en avons présenté la procédure dans les références 7 et 8.

Les réglages des commandes de vol sont adaptés en conséquence.

Les chargements de l'essai statique général de la cellule sont dérivés des charges de dimensionnement de façon à envelopper au plus juste les limites des indicateurs de sévérité des charges.

Les marges dégagées après les essais statiques peuvent être consommées pour améliorer les qualités de vol en réglant le S.C.V.E. avec des valeurs limites augmentées des indicateurs de sévérité.

### 3. Coefficients de sécurité charges extrêmes/charges limites

Sachant que le système de commande de vol protège des dépassement de charges limites, un débat peut s'ouvrir pour une éventuelle modification du coefficient de sécurité (actuellement 1.5 pour le Mirage 2000 et le Rafale) ; la discussion butte sur de grosses difficultés :

- le coefficient de sécurité actuel couvre d'autres facteurs que la rencontre de conditions de charges plus sévères que les limites ; ce sont entre autre :
  - les défauts éventuels du modèle de calcul des charges (champs de forces appliquées à la cellule) en fonction des conditions de charges (paramètres de vol)
  - les différences inconnues entre la résistance des cellules en service et de

celle qui a été qualifiée (défauts de fabrication ou de matériau non détectés, dommages divers non détectés de corrosion, de fatigue, d'impact, etc...).

- Pour aucun de ces facteurs on ne dispose de modèles de probabilité vraiment probants donnant les distributions de dépassement de charges ou de résistance structurale ; on ne sait pas quantifier séparément ces facteurs à l'intérieur du coefficient de sécurité globale.
- Le coefficient de sécurité global de 1,5 ne se justifie quantitativement que par l'expérience, en constatant une résistance structurale globalement convenable des avions en service depuis ½ siècle, mais ce coefficient de sécurité n'est pas dissociable du reste de l'environnement de techniques utilisées, de construction, de méthodes d'analyse et de processus de vérifications. Les évolutions partielles de l'environnement technique doivent s'accompagner d'une démonstration de non régression de la sécurité par le point concerné (c.f. règles de qualification pour les matériaux composites) sans qu'on sache échanger l'éventuel gain sur un point contre une diminution de marge sur un autre point.

Un autre élément de débat porte sur les avantages à tirer d'une éventuelle réduction du coefficient de sécurité :

- pour un nouveau projet le gain potentiel de masse structurale est probablement faible, le taux d'échange coefficient de sécurité masse reste très en deçà de la proportionnalité (dimensionnement des parties métalliques par la fatigue, zones de minimum technologique, à contraintes d'aéroélasticité dimensionnantes,...).
- La discussion est plus ouverte si on considère pour une cellule existante l'amélioration ponctuelle ou circonstancielle des performances de manoeuvre.

#### 4. Conclusions

L'introduction des S.C.V.E. permettant un pilotage « care free », a demandé une évolution du processus de détermination des charges de dimensionnement pour les cas de manoeuvre.

Le principe directeur que les charges limites sont les charges « maximales » rencontrables en service est renforcé ; on doit d'ailleurs associer ce principe à une définition plus rigoureuse de la notion de charges « maximales » (voir annexe).

Il n'est plus besoin que les règlements définissent des cas de manoeuvre de dimensionnement, cette responsabilité est transférée au constructeur ; à charge pour lui de développer un S.C.V.E. garantissant le maintien de l'avion dans son domaine limite de résistance structurale, tout en obtenant les qualités de vol désirées.

Pour Dassault Aviation cette évolution s'est faite progressivement à partir des programmes Mirage 2000 puis Rafale ; elle s'est accompagnée d'évolutions correspondantes du processus de conception (interactions accentuées entre la conception structurale et celles des commandes de vol). Des développements spécifiques de méthodes et outils d'analyse ont été nécessaires, notamment :

- la définition « d'indicateurs de sévérité des charges », la construction de leurs opérateurs de calcul en fonction des paramètres de vol par notre outil ELFINI, l'intégration de ces opérateurs dans les simulations de mécanique du vol,
- l'utilisation de l'optimisation mathématique pour le dimensionnement qui fournit directement les taux d'échange entre la masse structurale et les performances de manoeuvre,
- les techniques d'identification de modèle aéroélastique sur les mesures en essais au sol et en vol, permettant de recalibrer et de valider les modèles mathématiques pour la démonstration de qualification.

Il est difficile de démontrer qu'il y ait possibilité de modifier le coefficient de sécurité charges extrêmes/charges limites en conséquence de ces évolutions; d'ailleurs les avantages à tirer d'une diminution de ce coefficient ne sont probablement que circonstanciels.

#### REFERENCES

1. **C. PETIAU, S. BRUN**  
Tendances actuelles de l'analyse aéroélastique des avions militaires AGARD conférence proceedings N° 403 - Athènes 1986
2. **C. PETIAU**  
Aéroélasticité et Vibration des Structures, Etat de l'Art et Tendances  
Forum International Aéroélasticité et Dynamique des Structures - AAAF - Strasbourg 1993
3. **C. PETIAU, A. CELIER**  
Méthode de simulation numérique du système avion - atterrisseur  
AGARD conference proceeding N° 326 - Bruxelles 1982
4. **Y. MARTIN - SIGFRIED**  
Calcul des interactions entre avion et train d'atterrissage  
Povoa de Varzim 1990, AGARD conference proceedings N° 484
5. **C. PETIAU, G. LECINA**  
Eléments finis et optimisation des structures aéronautiques, AGARD conference proceeding N° 280 - « The use of computer as a desing tool » - Munich 1978
6. **C. PETIAU**  
Structural Optimization of Aircraft  
Thin-Walled Structures 11 (1991) 43-64  
Elsevier Science Publishers
7. **C. PETIAU, M. DE LAVIGNE**  
Analyse aéroélastique et identification des charges en vol, AGARD conferences proceeding N° 375 - « Operational loads data » - Sienna 1984
8. **C. PETIAU, Ph. NICOT**  
A general method for Mathematical Model Identification in Aeroelasticity, International Forum on Aeroelasticity and Structural Dynamics - Royal Aeronautical Society, Manchester 1993

## Annexe

### Notion de cas de charge « maximale » et « d'indicateurs de sévérité des charges »

#### • Remarque

Un cas de charge correspond à un **champ de force**, généralement de pression et d'inertie, appliqué à l'avion, ce champ de force est approximé par un vecteur, lui-même fonction de la « grille » de discrétisation choisie. A ce niveau toute métrique est arbitraire, on ne peut donc stricto sensu, définir de cas de charge maximale sauf cas particulier.

**De façon générale les cas de charge ne peuvent être classés qu'en fonction de leurs effets sur la cellule.**

#### • Méthode de repérage des charges maximales

Elle comporte les opérations suivantes :

- Identifier l'ensemble des **modes de défaillance structurale** possibles sous chargements mécaniques (ruptures locales sous contrainte ou déformation, flambages locaux ou généraux, déformations d'ensemble inadmissibles,...)
- Attacher à chacun de ces modes de défaillance un **critère de résistance\* scalaire** calculable en fonction du dessin de la structure et des charges.

**Un cas de charge sera dit maximal quand il engendrera la valeur maximale d'au moins 1 critère de résistance de mode défaillance.**

\*Les critères de résistance peuvent prendre en compte les effets thermomécaniques et le vieillissement ; nous avons ainsi défini les états de sollicitations limites pour les thermostructures de la navette Hermès.

- Limiter, autant que possible le nombre de modes de défaillance à surveiller en sélectionnant des **indicateurs de sévérité des charges** (quelques dizaines à quelques centaines) ; ces indicateurs sont des scalaires qu'on peut considérer comme étant en relation monotone avec les critères de résistance d'une zone de structure, quel que soit le chargement. On choisit généralement comme indicateurs de sévérité :
  - ▲ des composantes de contrainte ou déformation locale en des points pilotes
  - ▲ des réactions internes (exemples : efforts aux paliers d'attache de voilure ou de gouverne)
  - ▲ des efforts « généraux » (effort tranchant, moment de flexion,...) sur des sections particulières.
  - ▲ La gestion des calculs est simplifiée si les indicateurs de sévérité restent des fonctions linéaires des charges ; ils sont alors calculables à très faible coût en fonction des paramètres de vol à partir d'une base de données **d'opérateurs indicateurs de sévérité** établie indépendamment du calcul des manoeuvres (voir références 1 et 2)
- L'implantation des capteurs extensométriques en essais en vol essaye de refléter le choix des indicateurs de sévérité des charges, ce qui permet la calibration et la validation des opérateurs et donc celle de l'ensemble du processus de calcul des charges (voir références 7 et 8).



## PROBABILISTIC APPROACHES - COMPOSITE DESIGN

Christos C. Chamis  
Structures Division  
NASA Lewis Research Center  
Structures Div., Mail Stop (5-11)  
2100 Brookpark Road  
Cleveland, Ohio 44135, U.S.A.

### ABSTRACT

Probabilistic composite design is described in terms of a computational simulation. This simulation tracks probabilistically the composite design evolution from constituent materials, fabrication process through composite mechanics and structural component. Comparisons with experimental data are provided to illustrate selection of probabilistic design allowables, test methods/specimen guidelines, and identification of in situ versus pristine strength. For example, results show that: in situ fiber tensile strength is 90 percent of its pristine strength; flat-wise long-tapered specimens are most suitable for setting ply tensile strength allowables; a composite radome can be designed with a reliability of 0.999999 and laminate fatigue exhibits wide spread scatter at 90 percent cyclic-stress to static-strength ratios.

**KEY WORDS:** Design methods, computer codes, design allowables, graphite fibers, test data, comparisons, in situ strength, testing guidelines, shear buckling, component reliability, laminate fatigue.

### 1. INTRODUCTION

Probabilistic composite design is simply the process required to evaluate the reliability of a specific design. The reliability of any specific design is determined by evaluating the probability that all structural design criteria are satisfied at pre specified levels of probability. Evaluation of the probabilities for the various structural responses to satisfy the pre specified design criteria requires quantification of uncertainty ranges for each response. To quantify those uncertainty ranges in composite structural design we need to have formal methods which trace the uncertainty ranges of all participating variables in the structural design. We, therefore, must start with the constituent materials and continue introducing uncertainties expected to be present as we progress through the higher scales (micro, macro, laminate and structure). Another important aspect in probabilistic composite struc-

tural design is verification. Substantial work has been reported for the predictive part of probabilistic composite structural design [1,2]. The objective of the present article is to describe a multiscale probabilistic composite design method and comparison with measured data.

A multiscale probabilistic composite design to be practical must be in the form of computational simulation. In order to be credible it must have appropriate verification at all scale levels. The procedure must be suitably illustrated to be in-structive. The design must be representative of typical designs to add confidence in the method and simulation scheme used. In this article we introduce probabilistic structural analysis/design with a simple component in order to identify the essential elements. We continue with the description of the formal methods and their respective computer codes. We follow these up with applications for setting and or deciding strength allowables for ply, laminate, and laminate with holes. We describe select extensions for fabrication implications, testing guidelines and laminate fatigue. We conclude with a sample probabilistic composite design. Select references are cited for complimentary information.

### 2. SOURCE OF UNCERTAINTIES IN COMPOSITES

We consider the schematic shown in Figure 1 in order to identify sources of uncertainties in composites and therefore primitive variables. The schematic in Figure 1 is a simplistic representation of composite fabrication process but contains most of the important variables for our purposes. All the items listed under the schematic constitute one or more primitive variables. For example, at any one point through the laminate thicknesses and for each ply in the laminate, there are as many primitive variables as there are constituent material properties but only single primitive variables for the other factors under the schematic. We will

discuss these primitive variables further in the verification and application sections. Identifying primitive variables at the lowest fundamental level and all other levels, and then let the mechanics propagate their respective scatter to the desired response accounts automatically for correlations among variables that may be present at higher scales.

### 3. COMPUTATIONAL SIMULATION METHOD

It is important to note that computational simulation methods are not unique. They very much depend on the experience of the researchers who develop these methods. The computational simulation method used to obtain the results to be presented later is shown schematically (Fig.2). This computational method is called (IPACS) for Integrated Probabilistic Assessment of Composite Structures.

IPACS was developed by merging two independent stand alone computer codes: (1) probabilistic composite mechanics and (2), probabilistic structural analysis. Probabilistic composite mechanics is simply the ICAN (Integrated Composite Analyzer) [3] computer code with provisions for uncertainties and Fast Probability Integration (FPI) [4] to generate the probabilistic distributions for composite or laminate properties at any scale. The details are described in references [5,6]. The reason to use proven deterministic codes is that the mean should be accurately predicted compared to measured data. Probabilistic structural analysis is simply, (1) A deterministic general purpose finite element analysis upgraded to account for uncertainties in the structural primitive variables and, (2) FPI to generate the probability distribution functions of the desired structural response with relatively small number of simulations. The details of the probabilistic finite element are described in reference [7]. It suffices to say that the deterministic finite element accurately predicts all the usual and not so usual, structural responses. It is very important to note that by using proven (credible) deterministic methods and codes, then the scatter ranges and probabilistic predictions for the desired response are also credible since the desired responses are obtained by repeated application of those deterministic methods/codes.

Returning to Figure 2, note that uncertainties are introduced and predicted everywhere there is a

probabilistic distribution schematic. On the syntheses part (left side) - uncertainties enter from the constituent materials and any successive upward scale up to the structural scale. On the decomposition side (right side), uncertainties are traced at any successive downward scale down to the constituent material where failure modes are easily identified and respective fracture criteria are readily implemented. Another important point to note is that the structural model can be relatively coarse but be inclusive of the whole structure - that is, the structural model must be inclusive of the boundary, loading and environmental conditions.

### 4. VERIFICATION

Verification results will be presented for unidirectional tensile and compressive strengths, strength of specimens with the hole, and panel shear buckling. The verification results were obtained by different researchers as noted in the acknowledgment.

The ground rules were: (1) predict the probabilistic distribution curve by including their knowledge of the scatter range and the mean values in all the primitive variables and (2), plot their experimental data on the respective predicted probability distribution. The composite system used in the verifications is graphite fiber/epoxy. Typical properties for the graphite fibers, the scatter and distributions used in the simulations are listed in Table 1. It is noted that some of the strengths were modified to match proprietary data. Those for the matrix are listed in Table 2. Note that Table 2 includes also typical fabrication variables. All the comparisons discussed subsequently are for simulation results obtained by using the information in Tables 1 and 2 and from composites made from the same or very similar constituent materials.

#### Ply Tensile Strength

One of the important properties in composite design is tensile strength. It is important to know how well probabilistic predictions compared with measured data. The comparisons are shown (Fig. 4) in terms of cumulative distribution function. Note the number of test data. Recall that the predicted curve was plotted first using information from Tables 1 and 2 and then the experimental data. Obviously, the comparisons are excellent throughout the scatter range. Also in Figure 3 are

plotted the sensitivity factors for two probability levels 0.001 (1 in 1000) and 0.999 (999 in 1000).

Several observations are in order from the information in Figure 3. (1) The scatter in the ply strength is considerable, spreading 1378 GPa (200-KSI) to 2412 GPa (350KSI) with a mean (0.5 probability) of about 2067 GPa (300KSI). This means that the probabilistic simulation captures, (a) the physics through the composite mechanics, (b) the scatter through the procedure described previously, and (c) the known and assumed information in Tables 1 and 2. (2), Any test value from that material within the scatter range is a legitimate data point and expected from the probabilistic simulation used. (3), We can limit the allowable for ply strength for robust designs to 1378 GPa (200 KSI) lower limit in the scatter with a reliability of one exceedence in 10,000. The lower limit allowable will definitely provide us with a robust design but heavy and expensive. (4), The sensitivity factors indicate that the fiber strength dominates, as is to be expected. Other factors including fiber misalignment (avg. Theta) and fiber volume ratio (FVR) are negligible. This information translates simply - we need only to control the fiber tensile strength and relax the quality control requirements on the others which are essential in fabricating reliable, cheap and fast products. (5), The order and magnitude of the sensitivity factors do remain practically constant throughout the scatter range. It further reinforces that fiber tensile strength dominates at all probability levels. The important conclusion is that probabilistically predicted ply strengths following the procedure described herein are credible and can reliably be used in composite design.

#### **Ply Compressive Strength**

Ply compressive strength is also important in composite design. Comparisons are shown (Fig. 4). The predicted curve was plotted first and then the test data. Inputs for the predictions were from Tables 1 and 2. The comparisons are excellent demonstrating that the probabilistic simulation captures both the physics and the scatter. The scatter range is from 1240 GPa (180KSI) to 2205 GPa (320KSI) with a mean of about 1722 GPa (250KSI). Several factors contribute significantly to ply compressive strength (Sensitivity, Factors Plot). The order of significance is fiber volume ratio (FVR), matrix compressive strength (SMC),

matrix shear modulus (GM) and fiber misalignment (Theta).

The multitude of these factors explain in part why it is difficult to interpret ply compressive strength test data as well as having a consensus on a deterministic model. The respectable magnitude of Theta (fiber misalignment) lends credence to the deterministic micromechanics models based on kink-bends of fiber. The other observations (except sensitivity factors) made for the ply tensile strength apply to compressive strength as well. The very important conclusion is that probabilistically predicted ply compressive strengths via the procedure described herein, are credible and can reliably be used in design. Two points make these predictions very important (1), The environmental (temperature and moisture) effects can also be reliably predicted since these effects influence the matrix only and since they are accounted for in the deterministic composite mechanics which are constituent level micromechanics based. Stated differently, temperature and moisture affect the matrix shear modulus and matrix compressive strength both of these are significant sensitivity factors. (2), We do not need to have the large number of experiments shown in Figures 3 and 4, for verification. The author contends that we can get by with at most three so long as they are within the probabilistically predicted scatter.

#### **Tensile Strength of Laminate with a Hole**

Laminate-with-a-hole tensile strength is a commonly used design allowable in tensile load bearing composite components. The tensile strength of a specific laminate with a hole predicted probabilistically is shown in (Fig. 5) in terms of cumulative probability distribution. Three data points are also plotted. The data fall on the predicted curve. This is very important because it collectively verifies the probabilistic simulation for (1), composite laminate behavior, (2) stress concentration via finite element and (3) laminate fracture and (4) the author's previous contention that three tests are sufficient for verification.

The important conclusions are, (1) probabilistically predicted laminate strengths with stress concentrations are credible and can reliably be used for design load bearing composite structures with defects and, (2) only limited data (3-points minimum) are enough to verify laminate behavior and even com-

posite component structural behavior provided that all three points fall on the predicted distribution. It is worth noting that the contention for three tests, mentioned in the previous section, was made long before the data in Figure 5 became available.

#### Panel Shear Buckling

It is well known that composite panel shear buckling is important in aircraft fuselage and wing skin designs. The importance of composite panel shear buckling increases in importance in view of the difficulties, costs and time, associated in performing the requisite tests for design concepts verification. Therefore, verifiable probabilistic predictions will go a long way to minimize the testing that may otherwise be required.

Probabilistically predicted results for shear buckling of a stringer reinforced composite panel are shown (Fig. 6) in terms of mean values and one and two standard deviations on either side of the mean. The predictions were based on the constituent material properties, the processing variables and their respective scatter ranges (Tables 1 and 2). The probabilistic simulation for the panel shear buckling was performed by using the IPACS computer code. Experimentally available data were plotted in terms of vertical bars in the same figure. All the test data are within the predicted two standard deviations scatter.

Ply thickness is by far the most sensitive factor to the panel's shear buckling. Stringer locations (bay width left and right) and ply orientation having relatively minor significance compared to ply thickness. The implication is that control the ply thickness and relax the criteria for stringer precise location and ply orientation during the fabrication of these types of structures. The important conclusions are, (1) probabilistically predicted complex structural responses are credible and can be reliably used when obtained by procedures described herein, (2) factors which influence these responses are identifiable and can be appropriately adjusted for cost and time benefits without sacrificing reliability and (3) probabilistically evaluated composite design concepts require relatively minimum testing. (The author will be presumptuous and call for only one test).

### 5. SELECT EXTENSIONS

Assuming that verification demonstration results

presented and discussed previously establish confidence in probabilistic simulation of composite, we proceed to describe three important extensions. These extensions are included as being representative of what can be done by using probabilistic simulation. Specifically, we will describe composite fabrication implications, testing guidelines and laminate fatigue.

#### Fabrication Implications

In composite structural design a commonly asked question is in situ strength versus pristine strength especially for fiber tensile strength. Herein we illustrate how probabilistic simulation can be used to identify whether the fabrication process degrades fiber tensile strength and how much. We illustrate the procedure with the aid of Figure 7 where two probabilistically predicted curves are plotted for ply tensile strength and the test data. Note the two curves are labeled as pristine and in situ. The pristine curve was obtained by using the fiber-supplier's fiber tensile strength of 3721 GPa (540KSI). The in situ fiber strength was obtained by degrading the fiber tensile strength by the difference in the means between the supplier of 3721 GPa (540KSI) and the data of 3307 GPa (480KSI). Even though the supplier may claim no processing degradation, the data shows otherwise.

The degradation of 413 GPa (60KSI) is believable because of the following. We note that the shape of the cumulative distribution functions is exactly the same for both the data and the predicted one using the pristine fiber tensile strength. This implies that the scatter is properly captured and the two can be made to coincide simply by a parallel shift. The amount of parallel shift required usually equals the mean in one of the dominant primitive variables - in this case, fiber tensile strength. Shifting is very important in performing and or verifying probabilistic simulations. For example, (1) missing a significant primitive variable will result in similar shift and, (2) probabilistic structural responses obtained from coarse mesh finite element models can be calibrated by using the respective mean results from fine mesh finite element models [8]. The important conclusion from the above discussion is that probabilistic simulation can be effectively used to pinpoint fabrication processing effects on dominant primitive variables which are identifiable from respective sensitivity factors.

### Testing Guide Lines

Minimum reliable testing is critical in setting material allowables for composite structural design. Probabilistic simulation is adaptable to identify contributing factors and respective testing ramifications. What can be done and how, is illustrated by the following specific example.

A single ply of about 12.7 mm (5 mills) thick and 0.6 fiber volume ratio will contain 15 fibers through its thickness. We probabilistically simulate the effect of the local fiber volume ratio on the ply tensile strength. The results obtained are shown (Fig. 8). As can be seen, the fiber volume ratio of fibers located near the quarter points of the thickness has negligible effect as compared to that at the outer surfaces and at the center.

The implications from these results are: (1) Tensile strength specimens should either be pin loaded, or fiber volume ratio graded through-the-thickness, or flat-wise long-tapered. The flat-wise long-taper is the most practical. It is interesting to note that type of specimen was used by the author and one of his colleagues about 20 years ago to obtain high strength with reduced scatter in tensile strength tests of boron/aluminum specimens (unpublished data). Neither the author nor his long-since-retired colleague, had the vaguest notion why it worked. The important conclusion is that probabilistic composite simulation can aid in identifying effective testing techniques and recommending guidelines.

### Laminate Fatigue

Laminate fatigue is indispensable for any practical composite structural applications. Having demonstrated that probabilistic simulation credibly and reliably predicts composite ply laminate and structural behavior, it is interesting to explore its extension to predict composite laminate fatigue. Herein we briefly describe how it can be done and show typical results obtained for a specific laminate. The details are described in [9].

In order to probabilistically simulate laminate tensile fatigue, we postulate that (1) laminate fatigue strength is limited by first ply failure and, (2) the respective ply strengths are degraded cyclic as determined by respective degradation in the constituent materials; (3) the degraded properties are used at preselected laminate stresses while the

laminate is loaded in tension and the number of cycles is increased until the first ply fails; (4) the number of cycles at first ply failure is taken as the laminate fatigue; and (5) the results are plotted as cumulative distribution functions. Results from this procedure are shown in Figure 9 for a specific laminate cycled at 90 percent of its first ply static strength.

The fatigue (number of cycles) scatter is from 20 percent to about 50 percent of infinite life which is assumed to be the mean number of cycles at 10 percent of first ply failure static strength. Note that the mean value is about 40 percent of the infinite life. The dominant sensitivities are in order of significance ply thickness, matrix tensile strength, fiber volume ratio, fiber and matrix modulus. Implications are: (1) laminate fatigue exhibits substantial scatter and, (2) several primitive variables affect fatigue therefore making it difficult to interpret test data and set design allowables. The important conclusion is that laminate fatigue can be simulated probabilistically by procedures described herein. Respective verification comparisons are still pending but the author conjectures it will be as successful as the comparisons for the static cases.

### 6. PROBABILISTIC COMPOSITE DESIGN

Probabilistic design is simply the evaluation of a composite structure for its probability of failure or its reliability. We described all the essentials that are required to perform a probabilistic design. In this section we illustrated the procedure with a specific example - the design of a composite radome.

The geometry and the finite element model are shown (Fig. 10). Note that the entire radome is modeled with a relatively coarse mesh. The laminate configuration selected is  $[0/\pm 45/90]_6$ . Some inputs to the probabilistic design are shown in Table 3 with their respective scatter. The remaining constituent properties and fabrication processing variables are from Tables 1 and 2. Using I-PACS, the reliability of the radome was predicted to be 0.999999 or one failure in one million. The sensitivity factors for stress and strength are shown (Fig. 11). For low probability of failure (high reliability) the dominant primitive variables are fiber volume ratio and fiber modulus. Interestingly the ply thickness and the applied pressure are

relatively insignificant at high probability of failure. (low reliability) while the fiber volume ratio dominates. See also reference 10.

Implications: (1) design for high reliability by controlling the dominate primitive variables at low levels of failure probability, (2) design for proof testing by controlling the primitive variables with dominant sensitivities at high levels of failure probability, and (3) each design needs to be evaluated individually for reliability and dominant sensitivities since results may not be transferrable. The important conclusion is that composite structures can be probabilistically designed by procedures described herein.

## 7. SUMMARY

Probabilistic methods and computer codes have been described for composite structural design starting from constituent materials and fabrication processing variables and tracking the design evolution to structural configuration. Verification comparisons were presented to lend credence to probabilistic design. The salient results are summarized as follows:

1. Probabilistic simulation has been verified for ply, tensile and compressive strength, for laminate with a hole tensile strength and for shear bucklang of a skin stringer reinforced panel. The experimental data is within the predicted distribution for all cases.
2. Dominant probabilistac primitive variables and sensitivity factors have been identified for all verification cases.
3. Probabilistic simulation is effective in identifying in situ strength and testing guidelines to minimize scatter - fiber tensile strength degrades by 10% and a flat-wise tapered specimen is most suitable for ply tensile strength.
4. Probabilistically evaluated laminate fatigue life has substantial scatter - 20 to 50 percent of respective infinite life when cycled at 90 percent of its static strength.
5. A composite radome was probabilistically designed with a reliability of 0.999999 or accepting one failure in one million.
6. Primitive variables with dominant sensitivities at low probability of failure must be controlled to assure high reliability designs; while those with dominant sensitivities at high probabilities of failure must be controlled for effective proof testing.

## 8. ACKNOWLEDGMENT

The author expresses his gratitude to Dr. Larry Sobel from Northrop-Grumman and to Dr. Steve Wanthel from McAir for their many helpful suggestions during the development of the IPACS computer code and for performing the verification comparisons presented in the text. He also expresses his gratitude to his NYMA colleagues for developing the IPACS computer code and for generating the computational simulation results included in the article.

## 9. REFERENCES

- [1] Shiao, M.C., Abumeri, G.H. and Chamis, C.C, "Probabilistic Assessment of Composite Structures," AIAA/ASME/ASCE/AHS/ASC, 34th Structures, Structural Dynamics and Materials Conference, 1993, pp. 1174-1186.
- [2] Shiao, M.C. and Chamis, C.C., "Probabilistic Design of Smart Composite Structures," 39th Int. SAMPE Symposium, California, 1994, Vol. 39, pp. 3112-3126.
- [3] Murthy, P.L.N. and Chamis, C.C., "ICAN: Integrated Composites Analyzer," Journal of Composites Technology & Research, Vol. 8, No. 1, pp. 8-17.
- [4] Thacker, B. and Wu, Y-T., "A New Response Surface Approach for Structural Reliability Analysis," AIAA/ASME/ASCE/AHS/ASC, 33rd Structures, Structural Dynamics and Materials Conference, Dallas, 1992, pp. 586-593.
- [5] Stock, T.A., Belline, P.X., Murthy, P.L. N., and Chamis, C.C., "Probabilistic Composite Micromechanics," AIAA/ASME/ASCE/AHS, 29th Structures, Structural Dynaeics and Materials Conference, Part 3, 1988, pp. 1289-1298.
- S6] Mase, G.T., Murthy, P.L.N. and Minnetyan,

- L., "Quantification of Scatter in Composite Properties Via Probabilistic Mechanics," *Composite Material Technology* PD-Vol. 45, ASME 1992, pp. 71-76.
- [7] Wu, Y-T, "NESSUS Structural Reliability Analysis Methods - Review and New Developments," AIAA/ASME/ASCE/AHS/ASC, 33rd Structures, Structural Dynamics and Materials Conference, Dallas, 1992.
- [8] Shiao, M.C. and Chamis, C.C., "Mapping Methods for Computationally Efficient and Accurate Structural Reliability," AIAA/ASME/ASCE/AHS/ASC, 33rd Structures, Structural Dynamics and Materials Conference, Dallas, 1992, pp. 433-443.
- [9] Shah, A.R., Murthy, P.L.N. and Chamis, C.C., "Effect of Cyclic Thermo-Mechanical Load on Fatigue Reliability in Polymer Matrix Composites," 36th AIAA/ASCE Conference, New Orleans, LA, April 1995, Part 3, pp. 1670-1682.
- [10] Shah, A.R. and Liaw, D.G., "Probabilistic Sizing of Laminates with Uncertainties," 24th Int. SAMPE Technical Conference, Toronto, Canada, 1992, Vol. 24, pp. T447-T460.

**Table 1 - Uncertainties in the Constituent Properties - Fiber**

Fiber	Mean		Scatter%	Distribution Type
Normal Modulus, $E_{f11}$	213.7	GPa	5	Normal
Normal Modulus, $E_{f22}$	13.8	GPa	5	Normal
Poisson's ratio, $\nu_{f12}$	0.20	-	5	Normal
Poisson's ratio, $\nu_{f23}$	0.25	-	5	Normal
Shear Modulus, $G_{f12}$	13.8	GPa	5	Normal
Shear Modulus, $G_{f23}$	6.9	GPa	5	Normal
Tensile strength, $S_{ft}$	3.3	GPa	5	Normal
Compressive strength, $S_{fc}$	3.0	GPa	5	Weibull

1.0 GPa = 0.145138 Mpsi

**Table 2 - Uncertainties in the Constituent Properties - Matrix**

Matrix	Mean		Scatter%	Distribution Type
Normal Modulus, $E_m$	3.47	GPa	5	Normal
Poisson's ratio, $\nu_m$	0.35	-	5	Normal
Tensile strength, $S_{mT}$	0.1	GPa	5	Weibull
Compressive strength, $S_{mC}$	0.24	GPa	5	Weibull
Shear strength, $S_{mS}$	0.09	GPa	5	Weibull
<b>Fabrication Variables:</b>				
Fiber volume ratio, $k_f$	60	%	2	Normal
Void volume ratio, $k_v$	2	%	5	Normal
Ply thickness, $t_i$	0.127	mm	5	Normal
Ply misalignment	0	Deg.	2	Normal

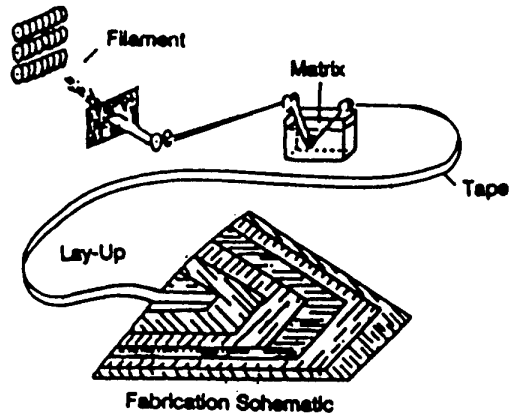
1.0 GPa = 0.145138 Mpsi

**Table 3 - Variables Used in the Composite Redome**

Random Variable	Mean Value	Coeff. of Variation	Distribution Type
Fiber Modulus ( $E_{f11}$ )	213.7 GPa	10%	Weibull
Fiber Volume Ratio (fvr)	0.6	10%	Lognormal
Thickness	12.7 mm	5%	Normal
Air Pressure	55.2 - 96.5 Pa	25%	Normal

1.0 GPa = 0.145138  
 1.0 mm = 0.394 mills  
 1.0 Pa =  $1.45 \times 10^{-4}$  psi





- Constituents
- Fiber Misalignment
- Fiber Volume Ratio
- Void Volume Ratio
- Ply Orientation Angle
- Ply Thickness

Figure 1 - Sources of Scatter - Fabrication Process

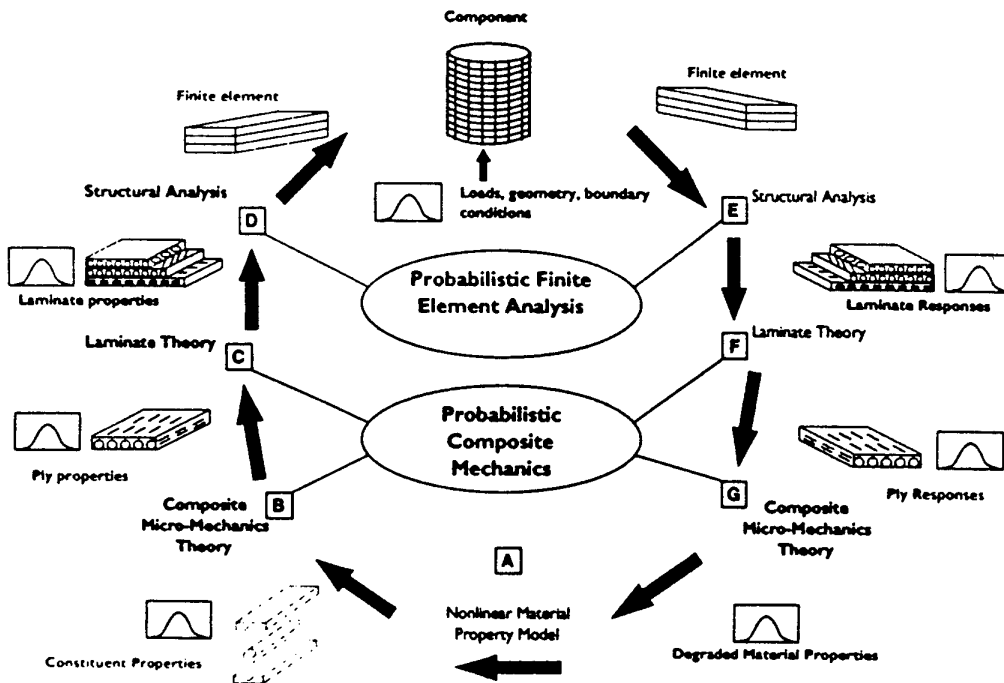


Figure 2 - Integrated Probabilistic Assessment of Composite Structures (IPACS)

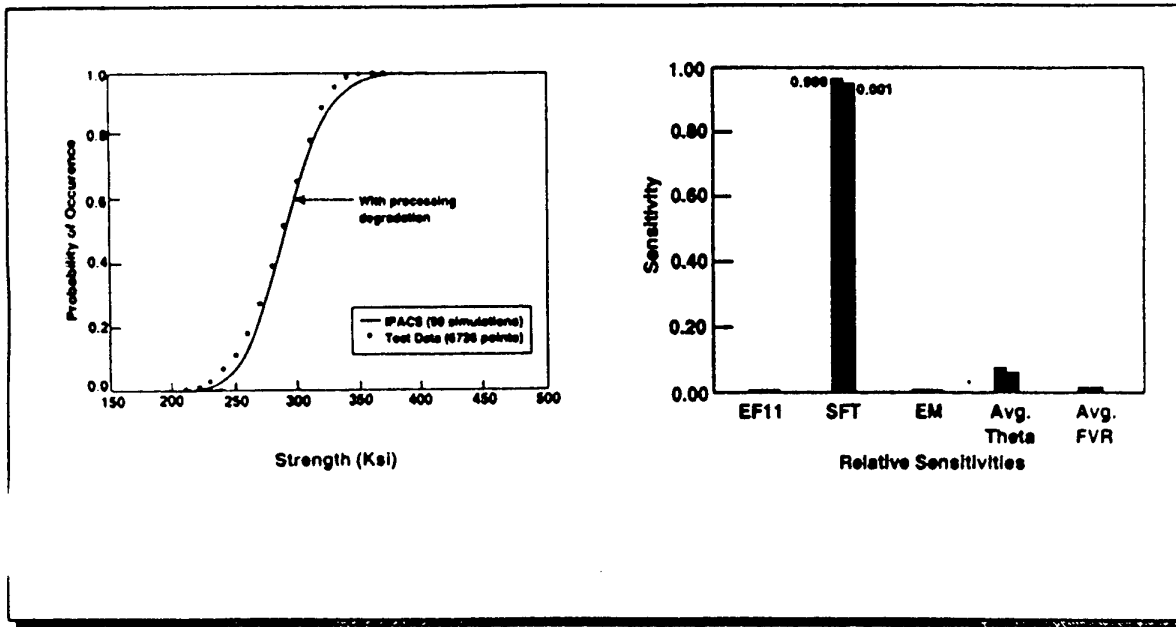


Figure 3 - Probabilistic Simulation Composite Strength and Respective Sensitivities (Graphite Fiber/Epoxy; 0.6 FVR)

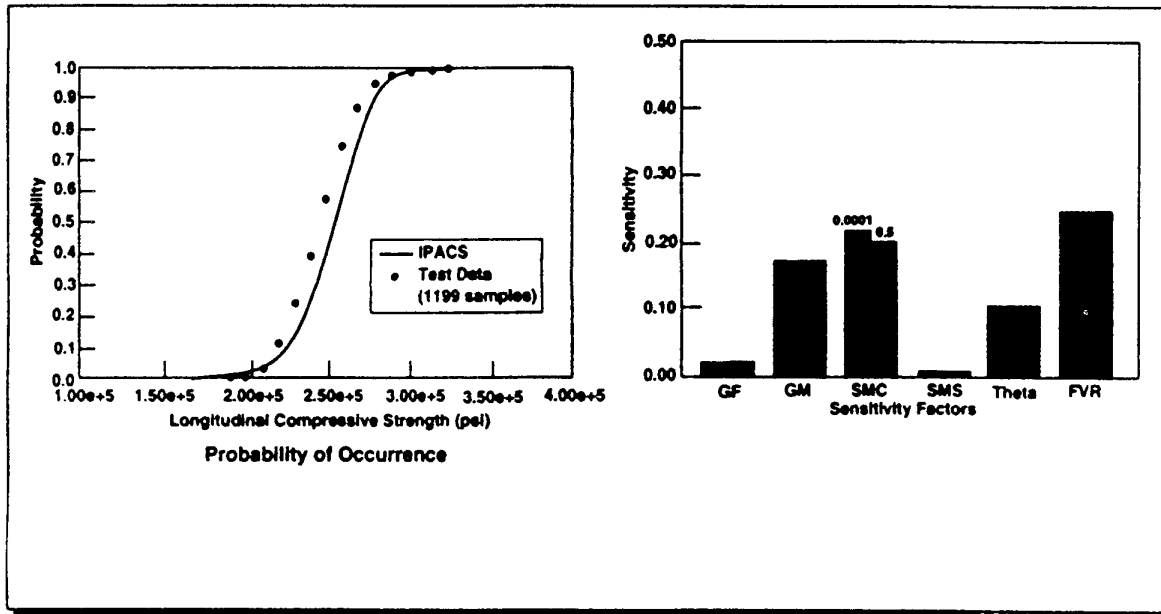


Figure 4 - Probabilistic Ply Longitudinal Compressive Strength (AS4/3501-6 Graphite/Epoxy at 0.6 FYR)



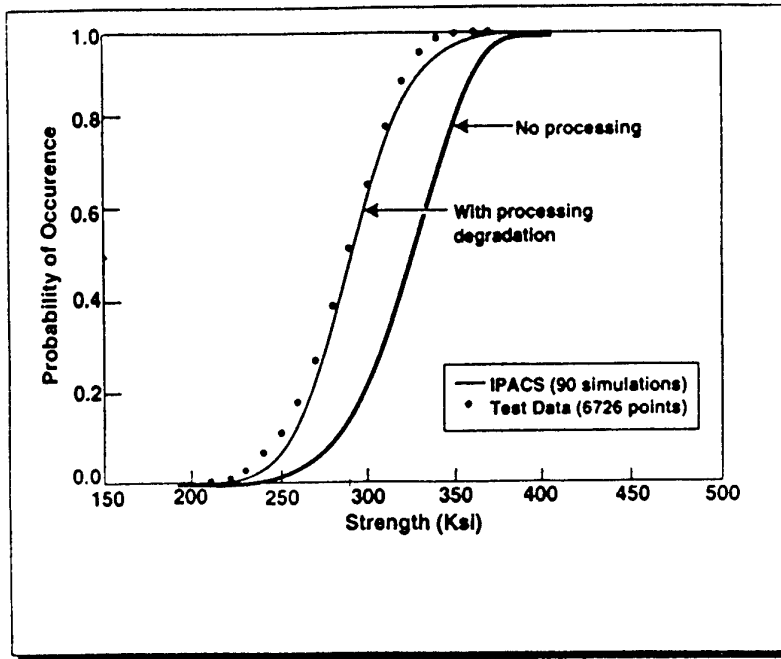


Figure 7 - Probabilistic Simulation of Longitudinal Tensile Strength Scatter in AS/E Composites.

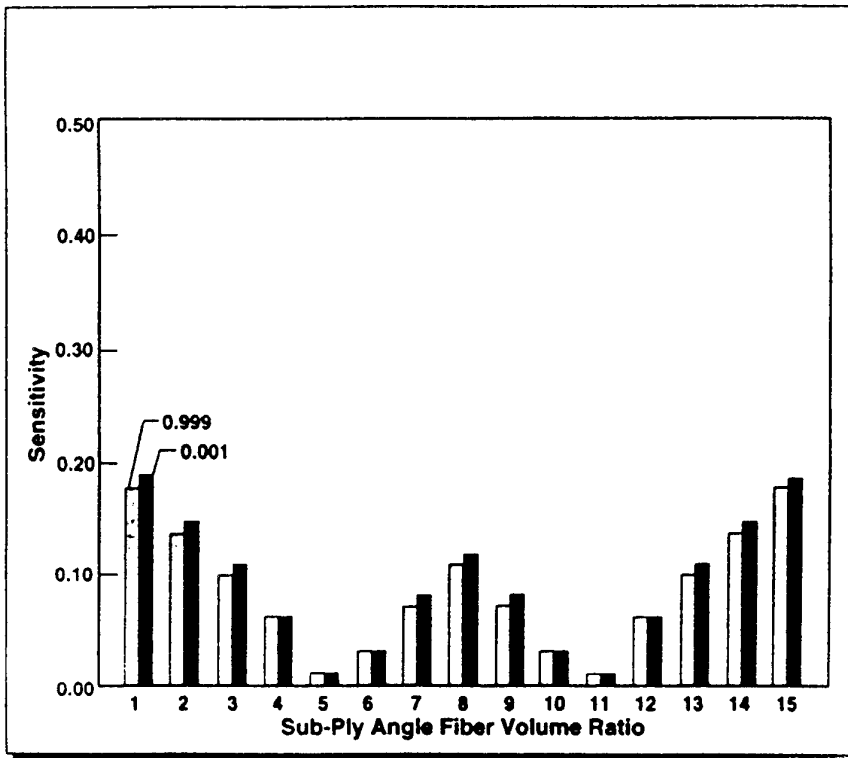


Figure 8 - Tensile Strength (AS4/3501-6 Graphite/Epoxy).

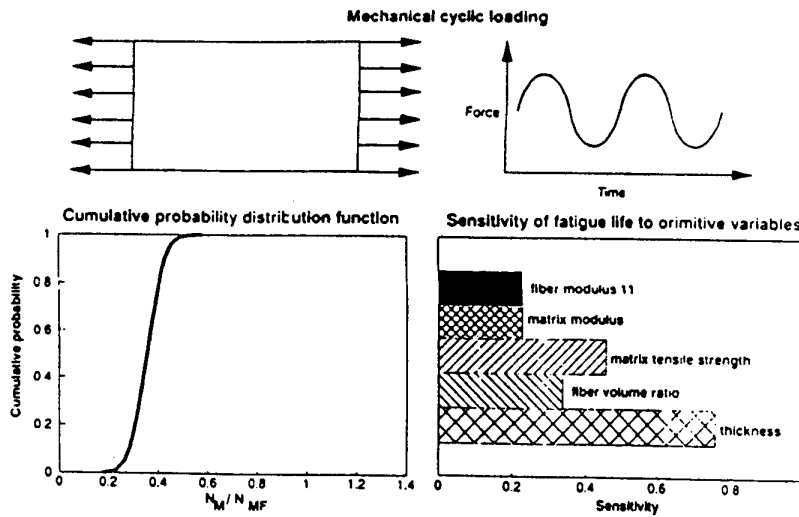


Figure 9 - Probabilistic Simulation of Fatigue Life Curve for Graphite/Epoxy (0/±45/90)<sub>10</sub> Laminate. Applied Stress/First Ply Failure Strength = 0.9.

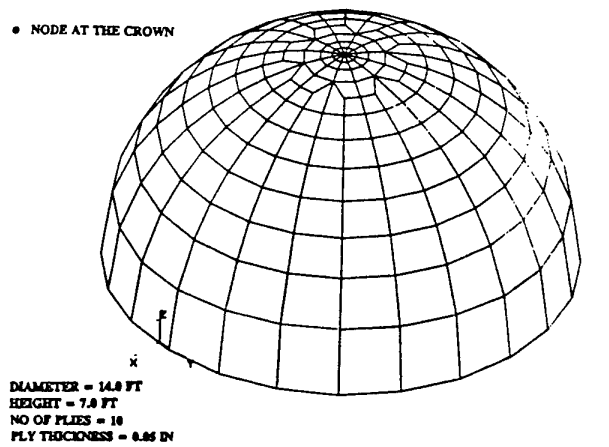


Figure 10 - Radome Structure Finite Element Model.

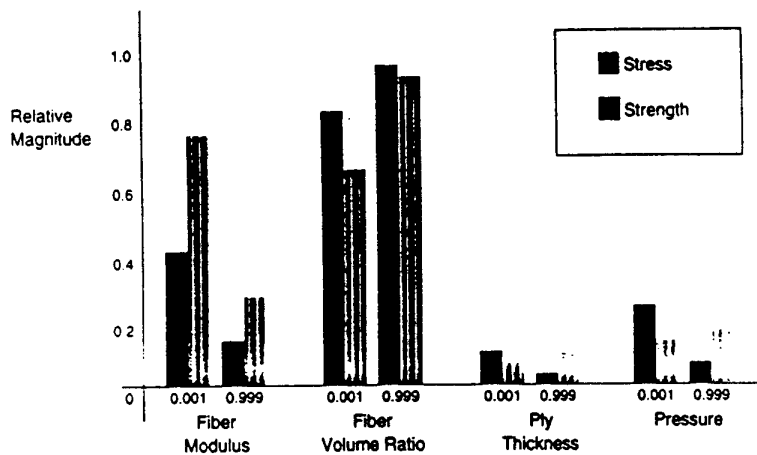


Figure 11 - Probabilistic Sensitivity Factors Affecting Stress and Strength of the Redome.

## Determination and Verification of Operational Maneuver Parameters and Time Histories

**J. Molkenthin**

Daimler-Benz Aerospace Airbus GmbH, EDA  
Hünefeldstraße 1-5  
28183 Bremen  
Germany

### SUMMARY

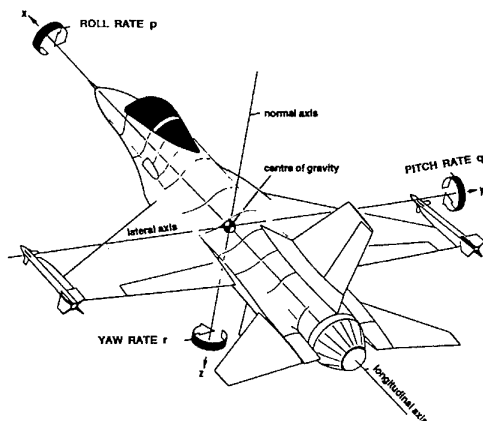
This paper describes a procedure for the evaluation of operational maneuver parameters and time histories, with the goal, to derive loads from operational flight parameters.

The basic assumption is that for each operational maneuver type performed in service or simulation as a set of normalized parameter time histories can be verified, called Standard Maneuver.

The Standard Maneuver is obtained by normalization of amplitudes and maneuver time to make the parameters independent of intensity of the maneuver, flight condition, flight control system, mass configurations and the aircraft type.

This paper outlines the determination of the operational maneuver parameters, the identification process of the maneuver types, the normalization procedure, the determination and verification of the Standard Maneuver time histories.

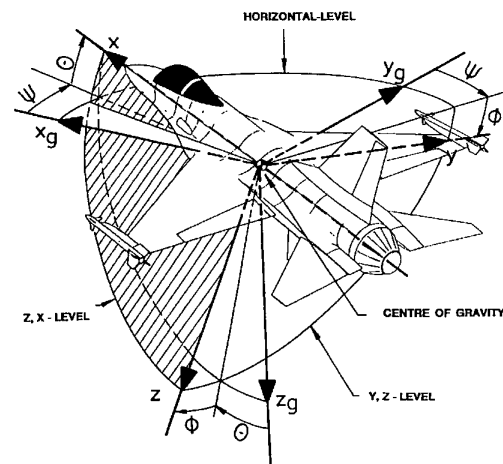
### SYMBOLS



$n_x$  = Longitudinal Load Factor  
 $n_y$  = Lateral Load Factor  
 $n_z$  = Normal Load Factor

$p$  = Roll Rate  
 $q$  = Pitch Rate  
 $r$  = Yaw Rate

Body - Axes System  
 $x$  = Longitudinal Axis  
 $y$  = Lateral Axis  
 $z$  = Normal Axis



Normal Earth, Axes System

$x_g$   
 $y_g$   
 $z_g$

Eulerian Angles

$\Phi$  = Bank Angle  
 $\Theta$  = Pitch Attitude  
 $\Psi$  = Heading

### 1. INTRODUCTION

The determination of the design maneuver loads is largely specified in regulations independently of the maneuvers or missions actually performed in operation.

For conventionally controlled Aircraft the regulations give the time history of the control surface deflections and numerically define several essential maneuver – load parameters for the determination of the design load level.

Obviously with the introduction of the fly-by-wire and/or active control technology, as well as care free maneuvering features, recent specifications no longer define the control surface deflections but rather provide the cockpit displacements of the controls in the cockpit.

This means that existing design load regulations and specifications based on conventional aircraft configurations, structural design concepts and control system technologies, may not be adequate to ensure the structural integrity of future military aircraft configurations using novel control methods, structural concepts and combat tactics.

In service, maneuvers, especially combat maneuvers, are flown in accordance with practiced rules that lead to specified motions of the aircraft. In Germany, an evaluation of operational flight maneuvers has been made for several aircraft types flown by the USAF, CF and GAF with the aim of deriving operational loads by applying parameters measured in operational flights.

This approach is based on the assumption that maneuvers trained and flown by the NATO Air Forces can be standardized. In practice, maneuvers, especially combat maneuvers, are flown in accordance with given, practiced rules that lead to a specified motion of the aircraft in the sky.

The standardized maneuver time history is the replacement as a quasi unit maneuver, for all operational maneuvers of the same type.

The Standardized Maneuver is obtained by normalization of amplitudes and maneuver time to make the parameters independent of mass configurations, intensity of the maneuver, flight condition, flight control system and of the aircraft type.

The goal is to find a standardized time history for each type of maneuver, which is independent of the extreme values of the relevant parameters and aircraft type.

**2. PROCEDURE OVERVIEW**

The flow chart in Figure 1 presents the general data flow and indicates the major phases of the procedure.

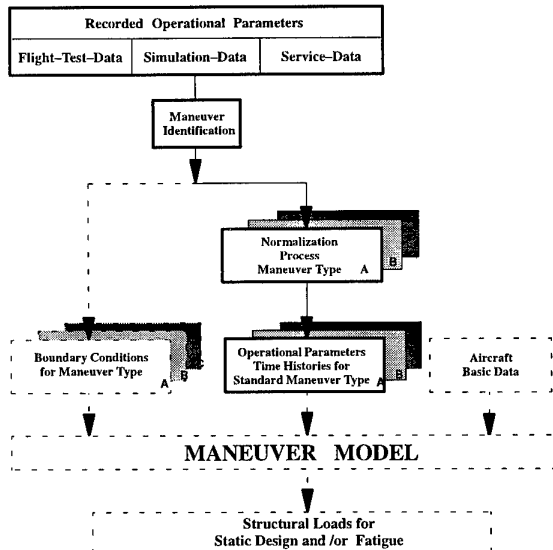


Figure 1 Procedure Overview

This paper describes the operational parameter part of a maneuver model to derive loads from operational parameters. The application of the maneuver model is based on three basic inputs:

- First: Standardized parameter time histories of different maneuver types, derived from operational maneuver types.
- Second: The boundary conditions of the selected maneuver types.
- Third: Basic aircraft data for the maneuver model calculation.

The MANEUVER MODEL is designed specifically to calculate the control deflection time histories from the specified motion of the aircraft in the sky. After a process of verification, the control deflection and response parameter data represents the model parameters for the structural load calculation. The loads for structural components are calculated in the conventional way.

The description and application of the Maneuver Model is presented by my colleague Horst Struck in paper 4 .

**3. OPERATIONAL PARAMETERS**

The number of parameters defining the aircraft motion should be chosen in such a way that recording and evaluation cause minimal expense.

This can be achieved by using parameters available from existing systems of the aircraft.

Each aircraft motion must be represented by a data set of relevant parameter time histories.

The following operational parameters are necessary:

- ma      Mach-Number,
- alt      Altitude,
  
- $n_x$       Longitudinal Load Factor,
- $n_y$       Lateral Load Factor,
- $n_z$       Normal Load Factor,
  
- p      Roll Rate,
- q      Pitch Rate,
- r      Yaw Rate,
  
- t      Maneuver Time,

the Eulerian angles, if available:

- $\Phi$       Bank Angle,
- $\Theta$       Pitch Attitude,
- $\Psi$       Heading

and additional parameters only for the verifications process:

- $\alpha$ (Alfa)      Angle of Attack
- $\beta$ (Beta)      Angle of Sideslip
  
- $\xi$  ( $X_i$ )      Aileron/ Flaperon Deflection
- $\eta$  (Eta)      Elevator Deflection
- $\zeta$  (Zeta)      Rudder Deflection

### 3.1. Maneuver Identification

The goal of the maneuver identification is to select the relevant maneuver segments from the recorded operational data base. A maneuver is identified by comparing the observed data with the predefined maneuver characteristics as described in Maneuver Type Description Figure 2.

<b>Turn</b>	:	$n_z \leq 2, p > \pm 20^\circ/\text{sec}, \phi \approx 40 \div 90^\circ$
		Roll steady to bank angle, pull, the bank angle is held as long as desired, opposite roll back to level
		Roll rates of opposite sign before and after g peak
<b>High g Turn</b>	:	Turn Maneuver
		$n_z > 2$
<b>Break</b>	:	High g Turn Maneuver with g peak during initial maneuver time
		$n_z > 3$
<b>Scissors</b>	:	A series of High g Turn Maneuvers
<b>Roll Reversal</b>	:	
		$n_z < 2, p > \pm 20^\circ/\text{sec}, \phi \approx 20 \div 90^\circ$
		Roll steady to bank angle, directly opposite roll back to level
<b>High g Rolls</b>	:	
		(Barrel rolls)
		$n_z > 1, 5, p > \pm 20^\circ/\text{sec}, \phi_{\text{max}} \approx 360^\circ$
		Roll steady in one direction
		Barrel roll over top $\ominus$
		rise to a positiv peak value
		Barrel roll under neath $\omin�$
		descend to a negativ peak value
<b>Pull sym.</b>	:	From $\sim 1g$ to g peak, back to $\sim 1g$
		$n_z > 1, 5, \Delta\Phi < 10^\circ$

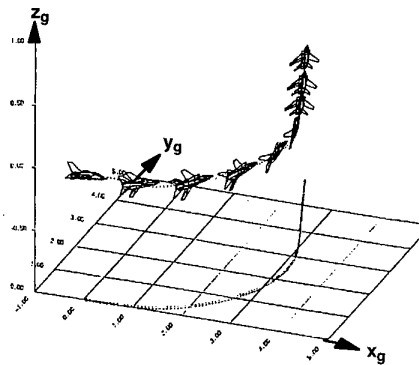
finally rolls it back to the wings level position. In parallel, the g rises to a peak value. The peak is held as long as desired. The g drops down from its peak as the aircraft is rolled back to the wings level.

The start and end of the maneuver are determined as follows: the maneuver starts when the first negative/ positive deflection of the roll rate trace starts and the maneuver finishes after recovering i.e. the opposite deflection of this trace, decreased to zero.

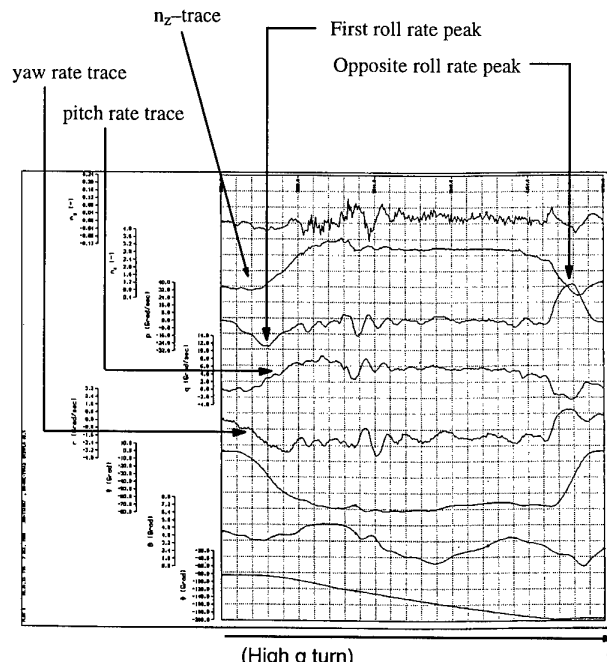
The Eulerian angles -  $\Phi, \Theta, \Psi$  give the aircraft orientation with respect to the earth's coordinate system.

The bank angle values indicate the type of maneuver as defined in Figure 2.

All recorded parameters are time related.



Movement projected on ground



(High g turn)

Figure 3 Identified Time Histories of Correlated Operational Parameters

Figure 2 Maneuver Type Description of Selected Maneuvers

The maneuver identification parameters are mainly load factor ( $n_z$ ), roll rate ( $p$ ) and bank angle ( $\Phi$ ).

- First: The data are checked for completeness and suitability for separating them into missions and maneuver types.
- Second: The start and end time of each maneuver type are identified when the roll rate is near zero and the g is approximately 1. The bank angle also indicates the type of maneuver, i.e. full roll  $\Phi \approx 360$  degrees, half roll  $\Phi \approx 180$  degrees, turn  $< 90$  degrees.







Figure 3. shows as an example for the identification of a high g turn maneuver. In this case the roll rate trace primarily defines the maneuver length.

The pilot first rolls the aircraft in the direction of the turn and



From the available data base, the data were broken down into different types of maneuver. A logic identification process is used to separate the recorded data into maneuver types, as described. The data base contains operational flight maneuver parameter data from modern fighter

of several NATO nations. The data were recorded during normal operations (service data), special flight tests and simulations of several maneuvers respectively for selected maneuvers. See table 1. Table 2 shows the type and number of identified maneuvers depending on the aircraft type.

RECORDED DATA AVAILABLE						
	GAF				USAF	CF
A/C Type	Alpha-Jet	F-4F	MRCA	JF-90	F-16	CF-18
Kind of Data						
Flight Test for Specific Maneuvers	7/33 *	7/46	6/20			7/49
Service Data					6/66	7/392
Simulation for Specific Maneuvers		6/25		6/47		
Recording System	Specific Flight-Test Recording System	Specific Flight-Test/ Simulation Recording System	Specific Flight-Test Recording System	Simulation Recording System	Crash Survivable Flight Data Recorder	Maintenance Signal Data Recording System

\*) Number of Maneuver Types /Number of single maneuvers evaluated

Table 1. Data Base

Nation	GAF					USAF	CF
	A-Jet	F-4F	F-4F Simulation	MRCA	JF-90 Simulation	F-16	CF-18
Break	5	1	3	5	6	-	-
Barrel roll	8	6	8	5	16	11	9
Full aileron reversal	-	10	-	-	5	-	-
High g roll	4	7	4	2	7	-	-
High g turn	4	7	4	2	7	21	15
Roll	-	-	-	-	-	-	131
Rolling entry a. pull out	4	7	-	-	6	-	183
Roll reversal	-	-	-	-	-	11	-
Scissors	4	2	4	4	-	13	-
Slice	4	-	2	2	-	-	-
Turn	-	-	-	-	-	7	45
Pull	-	-	-	-	-	3	6
Push	-	-	-	-	-	-	3

Table 2. Number of Identified Maneuvers

### 3.2 Normalization

Normalization is necessary because several maneuvers of the same type are different in roll direction, amplitude of motion and in maneuver time. For the calculation of loads from operational maneuvers it is not important to separate the maneuver types into different roll directions. Therefore, maneuvers of the same type are transformed into a unified roll direction. See Figure 4

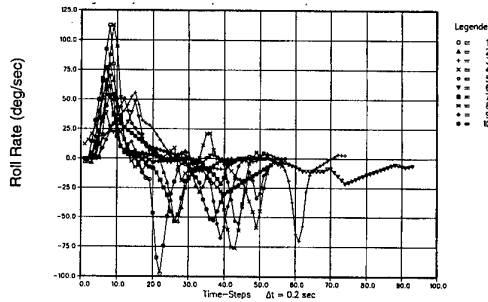


Figure 4 Unified Roll Directions

For a requisite comparison, a two-dimensional normalization is necessary.

In Figure 5 illustrates the basic procedure of normalization. The ordinate presents one of the parameters of motion ( $y = n_y, n_z, p, \dots$ ) for several maneuvers of the same type ( $y_1, y_2, \dots, y_n$ ).

These parameters are normalized by relating them to the maximum values (absolute derivation from zero) which have occurred. This means the maximum value of each normalized parameter becomes in this case:

$$Y = y_1 (\max) = y_2 (\max) = + 1.0$$

The time is presented by the abscissa ( $t$ ), where by the maneuver executing time is marked by  $t_1, t_2, \dots, t_n$  for several maneuvers. The normalization is accomplished in a way that:

- firstly, the maneuver time is chosen as the value 1.0 ( $t_1 = t_2 = T = 1.0$ )
- secondly, the extreme values of the relevant parameters is chosen at the same normalized time.

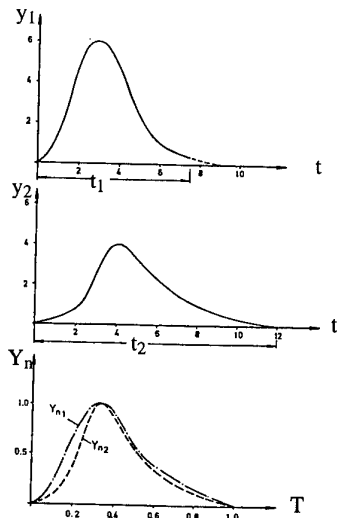


Figure 5 Normalization of Parameters

The time scale normalization factor for **all** correlated parameters ( $n_y, n_z, p, q, r, \Phi, \Theta, \Psi$ ) within, for example, a High g turn was derived from the roll rate trace. See Figure 6

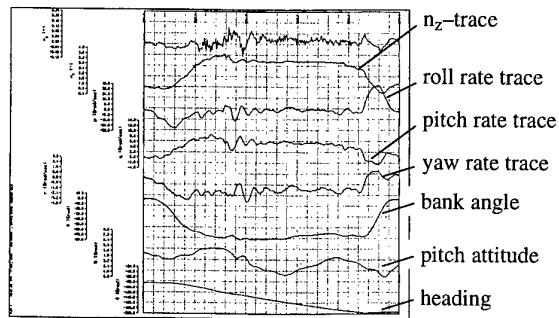


Figure 6 Correlated Parameters

In the normalized time scale,  $T = 0$  corresponds to the time when the roll rate trace first goes negative or positive (start of the maneuver), and  $T = 1$  corresponds to the time when the roll rate trace is back to zero after the opposite roll rate peak (finish of the maneuver). Figure 7 shows the normalized roll rate trace (positive roll direction).

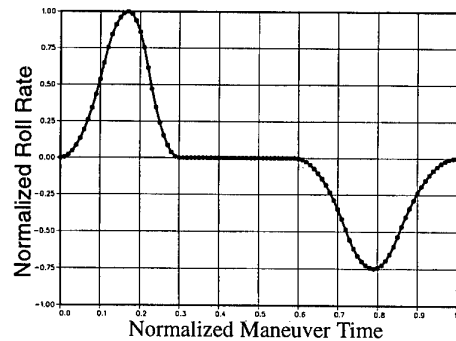


Figure 7 Normalized Roll Rate Trace

This normalization procedure is dependent on an accurate maneuver start value. ( $p \approx 0 \text{ deg/sec}$ )

In several cases the start values of the available time slices are very poor.

One reason is the low sample rate of e.g. 1 or 2/sec. Recordings from Flight tests are sampled 24 times per second.

An other reason is the selected parameter threshold values of the data reduction and maneuver identification process, combined with a low sample rate.

For these cases an upgraded normalization procedure, derived from the basic procedure, is used.

The estimated time of a high g turn ( $t_m$ ) had a very high correlation with the difference between the time of the first and the second roll rate peak. See Figure 7. This time ratio is very important for the normalization procedure.

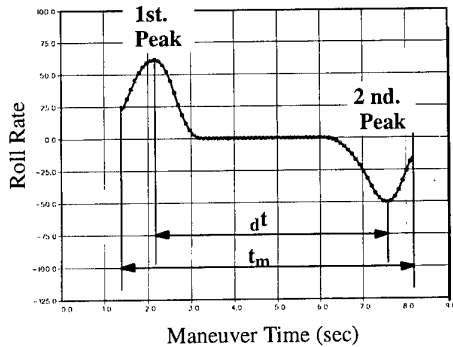


Figure 7 Time Ratio

The time transformation from real time into normalized time requires several steps:

**1<sup>st</sup>.** Determination of time ratio

The time ratio is defined by:

$$t'_1 = dt / t_m$$

**2<sup>nd</sup>.** Harmonization

For the comparison of the parameter traces, a harmonization of the maneuver time ratios is necessary.

$$t'_1 * sf_1 = t'_2 * sf_2 = t'_3 * sf_3 = \dots = t'_n * sf_n$$

sf = scale factor

**3<sup>rd</sup>.** Shifting

A new interpolation of a similar number of time steps for each of the correlated parameter for all maneuver of the same type is necessary.

Then the roll rate traces were shifted in a way, that all selected 1st peaks coincided at the same **time step**.

All correlated parameters are shifted parallel in the similar way. Figure 8 presents the comparison of the shifted roll rate traces versus normalized time for the selected high g turn maneuvers.

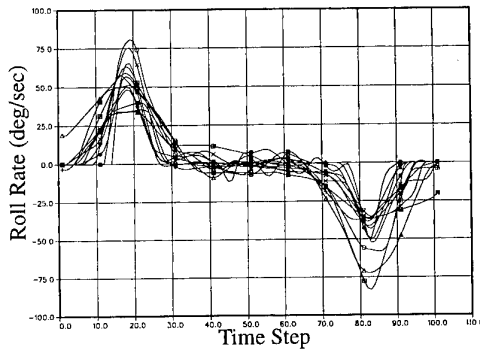


Figure 8 Shifted Roll Rate Traces

The amplitudes of the traces are normalized individually. Each value of the trace is divided by its absolute deviation value from zero, therefore, all normalized amplitudes will fall between  $\pm 1$ .

Figure 9 shows the results of the "peak to peak" normalization procedure.

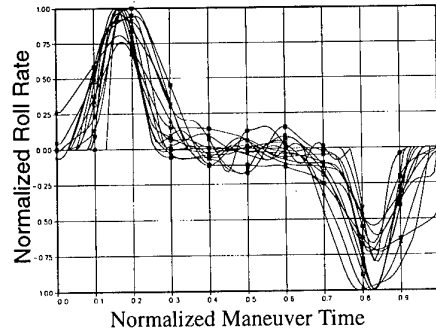


Figure 9 Comparison of Normalized Roll Rate Traces

The application of the two-dimensional normalization procedure is very helpful for the comparison of maneuver time histories. In this normalized form, all parameter time histories are independent of the aircraft type.

**3.3 Mean Values**

After normalization of the maneuver time, for all selected maneuvers of the same type, the typical values of the relevant parameters—in this case the peaks of the roll rate—coincide at the same normalized time. Each parameter time history contains the similar number of time steps, independent of its individual maneuver length. This is the basis for calculating the arithmetic mean values for each of the time steps.

Figure 8 presents the comparison of non-normalized roll rate traces versus normalized time for the selected high g turn maneuvers. The roll rate is a good example for all relevant parameters.

Note: The amplitudes for the mean value calculation are not normalized

The mean value is defined by:

$$Y_m(j) = \frac{\sum_{i=1}^n Y_i(j)}{n}$$

$n$  = number of maneuver of the same type

$j$  = time step

$Y_i(j)$  = relevant parameter

$Y_m(j)$  = mean value

The mean values of all parameters have been formed in combination by smoothing of the time history.

For the plot comparison, a normalization of the amplitudes is necessary.

The normalized values **cannot** be used for any calculations.

Therefore, a denormalization or reconstitution of the normalized parameters for amplitudes and time is necessary for use in loads calculations.

Figure 10 presents the comparison of normalized parameter traces and mean value versus normalized time for several high g turn maneuvers.

Table 3 shows the recorded extreme values of the selected high g turn maneuver parameters.

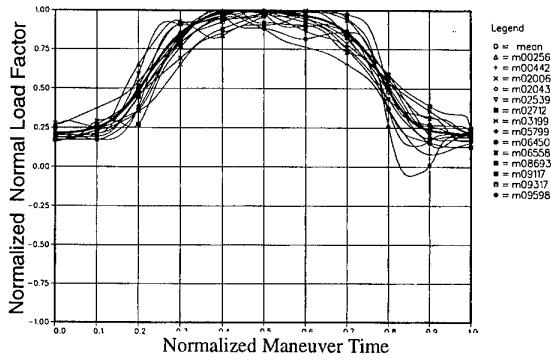


Figure 10.1

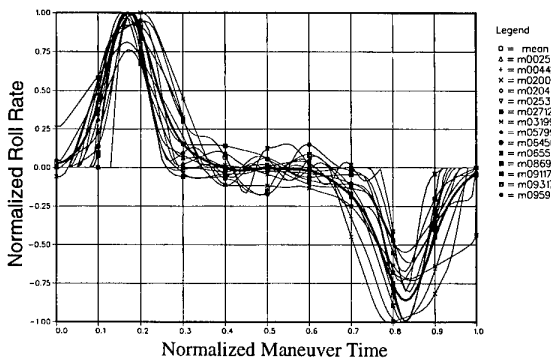


Figure 10.2

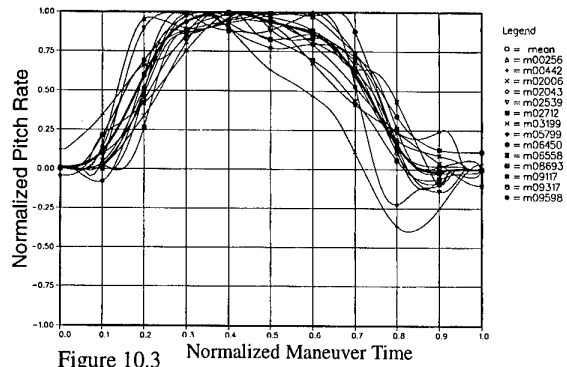


Figure 10.3 Normalized Maneuver Time

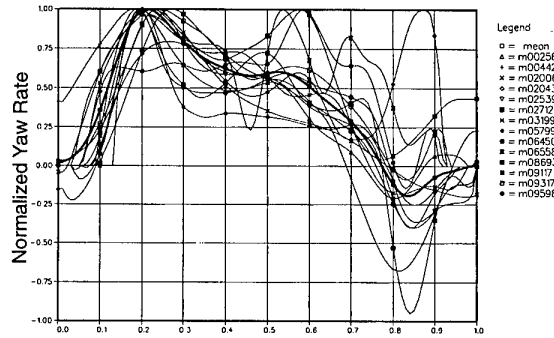


Figure 10.4 Normalized Maneuver Time

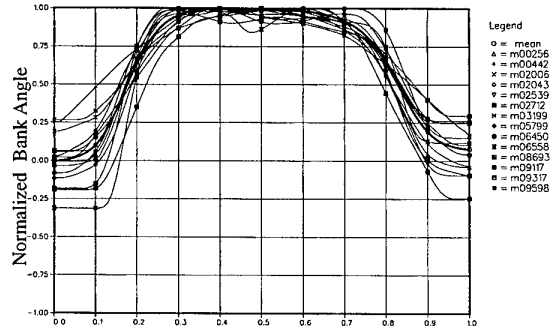


Figure 10.5 Normalized Maneuver Time

Figure 10 Comparison of Normalized Parameter Traces of one Aircraft Type

Maneuver Time (sec)	Normal Load factor $n_z$ (-)	Roll Rate (deg/sec)	Pitch Rate (deg/sec)	Yaw Rate (deg/sec)	$\Delta$ Bank Angle (deg)	Ma (-)	Alt (m)	Maneuver Identification Number
9.90	4.591	84.93	10.601	6.810	88.600	0.725	1102	m00256
6.60	5.216	73.78	13.487	6.493	92.542	0.645	371	m00442
8.60	4.470	37.67	9.921	3.500	78.001	0.641	692	m02006
10.10	6.057	76.68	13.000	6.492	86.224	0.757	644	m02043
11.90	5.331	55.16	12.545	3.498	77.005	0.656	1131	m02539
9.00	4.096	61.39	9.030	3.550	81.566	0.857	6788	m02712
6.90	5.727	51.99	14.118	7.497	85.818	0.712	770	m03199
10.70	5.227	53.91	10.678	2.501	80.559	0.906	6027	m05799
13.50	4.712	71.32	12.762	4.501	79.072	0.661	731	m06450
17.60	5.934	63.09	13.585	4.012	83.770	0.749	1261	m06558
11.00	5.067	41.43	11.494	4.510	84.414	0.721	673	m08693
8.90	5.905	89.16	10.866	3.697	88.201	0.797	712	m09117
10.80	5.370	97.92	10.584	3.508	87.612	0.786	585	m09317
11.10	4.858	45.46	9.828	2.473	75.891	0.774	1979	m09598
10.57	5.190	64.58	11.607	4.500	83.71			mean

Table 3 Recorded Extreme Values

The comparison of the mean value parameter time histories for the same aircraft type as shown in Figure 10 shows a good agreement for the correlated parameter time histories. For the demonstration of the independence of the aircraft type, the comparison of the correlated parameter time histories for several aircraft types are shown in Figure 11 .

The comparison of the normalized maneuvers for the several aircraft types has been done using mean values. The scatter band is about the same as that for the individual aircraft. This means that the normalized time histories can be considered as independent of the aircraft type.

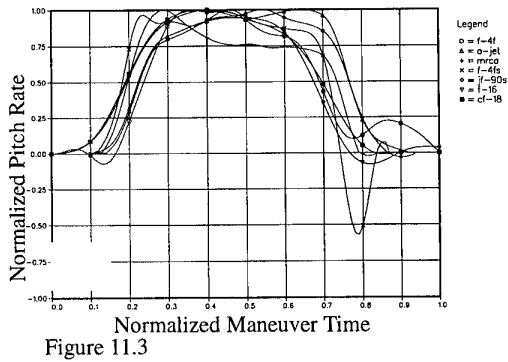
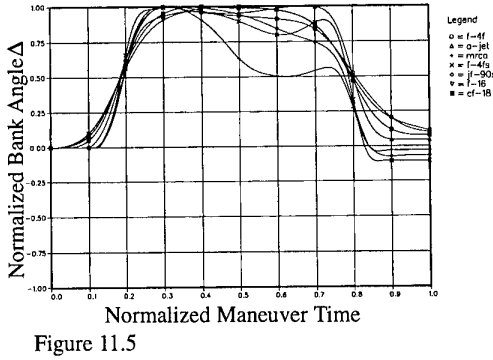
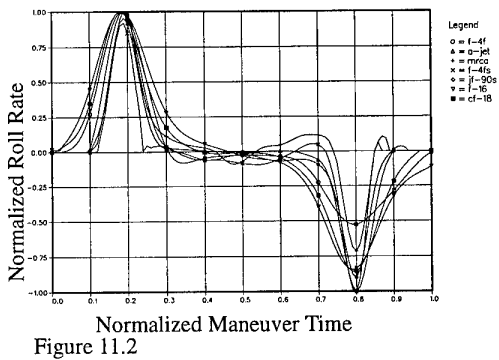
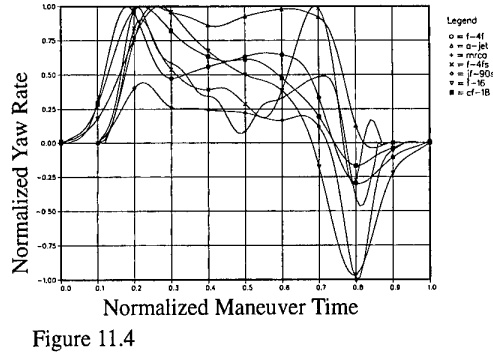
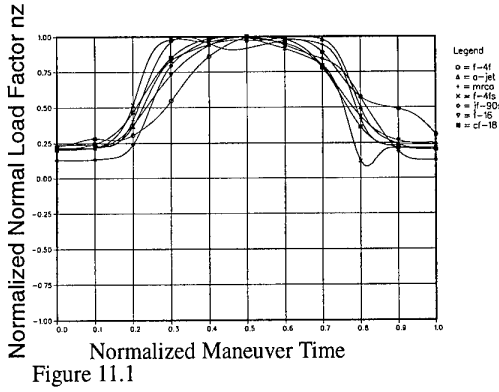


Figure 11 Comparison of Normalized Parameter Traces of Several Aircraft Types

### 3.4 Idealization

The mean value traces represent a good estimation of the relationship between the selected parameters during a maneuver (e.g. high g turn).

For the compensation of any minor errors by the mean value calculation and for reasons of compatibility, the mean values have to be idealized and tuned.

The Interpretation of "idealized and tuned" as follows:

To cover the most extreme peaks of the control surface deflections possible, the most extreme accelerations in roll (p), pitch (q) and yaw (r) are used.

These values are obtained by linearization of the acceleration time history in a way such that the same response of the aircraft is obtained.

For the idealization, the calculation is performed in three steps.

In the **first step**, the following parameters werecalculated: The three angular accelerations  $\ddot{p}$ ,  $\ddot{q}$  and  $\ddot{r}$  by differentiating the three angular rates p (roll), q(pitch) and r (yaw) with respect to maneuver time. The differentiation was given by:

$$\dot{y} = \frac{\Delta y}{\Delta x}$$

In the **second step**, the acceleration traces  $\ddot{p}$ ,  $\ddot{q}$ ,  $\ddot{r}$  were replaced by linearized traces with respect to the zeros of the traces and extreme values of  $\ddot{p}$ ,  $\ddot{q}$ ,  $\ddot{r}$  and the corresponding extreme values of roll-, pitch- and yaw rate.

Figure 12 presents the comparison of derived roll acceleration trace and idealized trace versus maneuver time for a high g turn maneuver.

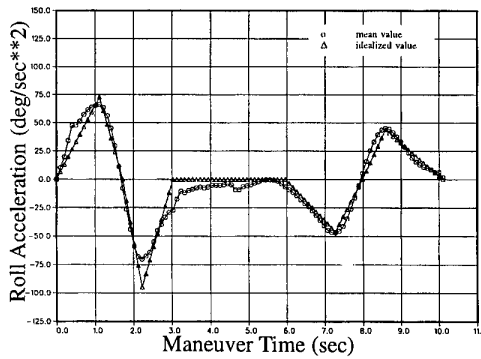


Figure 12 Idealization

In the **third step**, the three angular rates –roll, pitch and yaw were recalculated by integrating the idealized values of the three angular accelerations – $\ddot{p}$ ,  $\ddot{q}$  and  $\ddot{r}$ .

For the reasons of compatibility, the idealized data have to be tuned, that means the relation between the three Eulerian angles – $\Phi$ ,  $\Theta$ ,  $\Psi$  and the angular rates p, q, r is verified with the equations:

$$\begin{aligned} p &= \dot{\Phi} - \dot{\Psi} * \sin \Theta \\ q &= \dot{\Theta} * \cos \Phi + \dot{\Psi} * \sin \Phi * \cos \Theta \\ r &= -\dot{\Theta} * \sin \Phi + \dot{\Psi} * \cos \Phi * \cos \Theta \end{aligned}$$

The result is the standardized maneuver.

Figure 13 presents the idealized and tuned –standardized– traces of the three angular rates for a high g turn maneuver. (normalized)

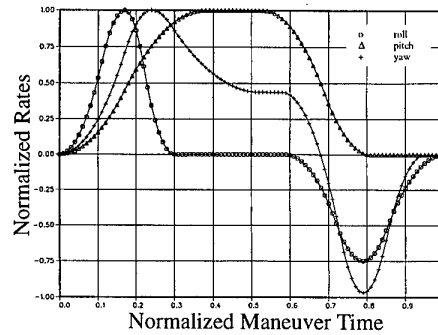


Figure 13 Standard Maneuver Traces

For each type of standardized maneuver the normalized motion parameters are independent of aircraft type, mass configuration and flight control system.

**4.0 STANDARD MANEUVER**

The whole evaluation is based on the assumption that it is feasible to standardize each maneuver type trained and flown by the NATO Air Forces.

This means it should be possible to find a data set of standardized time histories for each type of maneuver, which is independent of the extreme values of the relevant parameters. Figure 14 summarizes the overview of the standardization procedure.

Provided the operational parameter time histories of the basic parameter are available in correct units, this procedure includes several steps:

- (2) Normalization of relevant parameter time histories for a number of identified maneuvers of the same maneuver type for comparison
- (3) Determination of the mean values for each relevant parameter time history of the same maneuver type
- (4) Idealization and tuning of the parameter time histories
- (5) Determination of the standard maneuver time histories.

The result of this procedure is a data set of standardized parameter time histories. The parameter are roll rate, pitch rate and yaw rate of the selected maneuver type. See Figure 13 and Figure 14.

- (1) Maneuver type identification

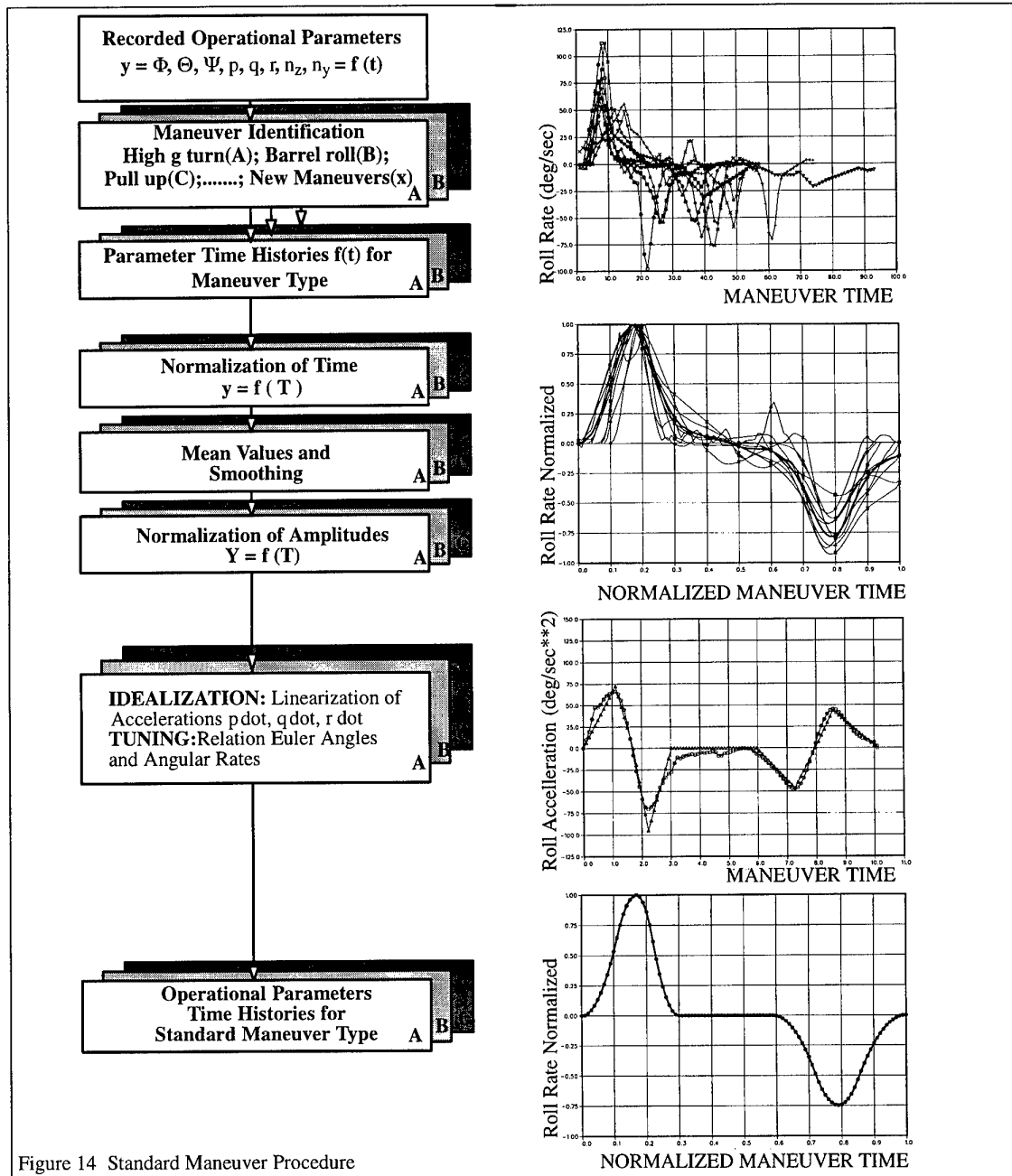


Figure 14 Standard Maneuver Procedure

In the normalized form the standardized parameter time histories are the maneuver input for the loads calculation process, called Maneuver Model. See Figure 1.

#### 4.1 Verification of Standard Maneuver Independent of Aircraft Type for the High g Turn Maneuver

The normalized Standard Maneuver time histories **cannot** be used for any calculations. Therefore, a denormalization or reconstitution of the normalized parameters for amplitudes and time is necessary for use in loads calculations.

For this paper, the verification process is limited to one maneuver type and two different aircraft. The High g turn maneuver was selected (m\_02043) for the demonstration of the reconstitution process of the Standard Maneuver time histories. The selected aircraft types are the USAF F-16 and the CF-18.

The application of the Standard Maneuver time histories and verification process is described as follows:

The Standard Maneuver Time History from the F-16 will be reconstituted to real time using the CF-18 performance data for one selected High g Turn maneuver of the CF-18 Service Data recordings.[4]

These reconstituted values will be compared to the existing recorded values of the selected maneuver.

In this case the reconstitution factors are the maximum values of the selected CF-18 High g Turn maneuver (m\_02043).

Figure 15 shows the reconstitution process.

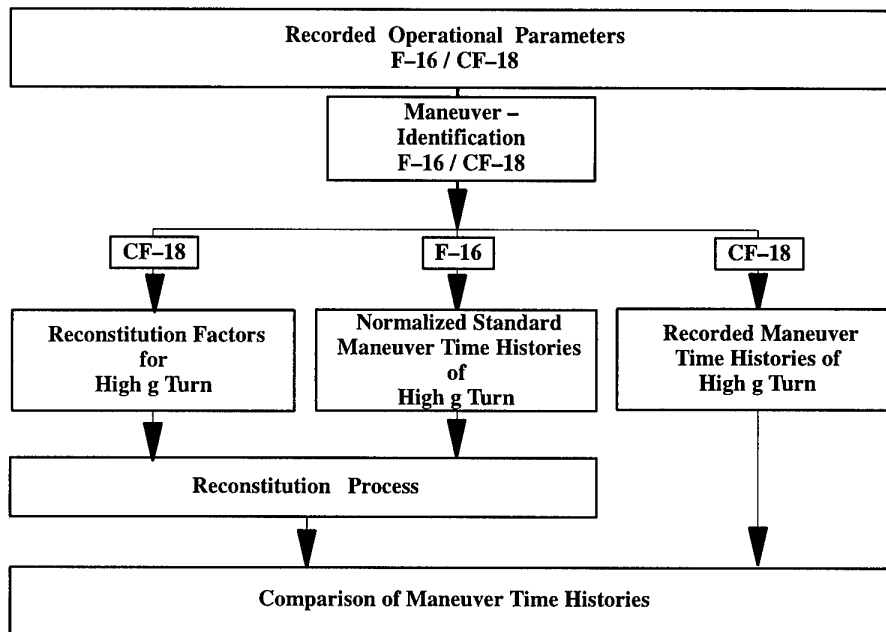


Figure 15 Reconstitution Process

The results of the verification process have been plotted for comparison. The plots are showing the comparison of the reconstituted F-16 Standard- and Mean Values- and the real time histories of the selected CF-18 Maneuver.

The comparison of the reconstituted parameter as plotted in Figure 16-21 shows a good agreement for the relevant parameters (roll and pitch). The exception is the lack of agreement for the yaw in the initiation phase which is explained by a start value different from zero.

It is concluded that the Standard Maneuver independent of the aircraft type is representative of the time histories of different aircraft in an normalized form and can be reconstituted using the reconstitution factors of the aircraft to be considered.



4.1 F-16 High g turn Standard Maneuver  
Reconstituted with CF-18-Maneuver Data  
(max  $n_z$ -level)

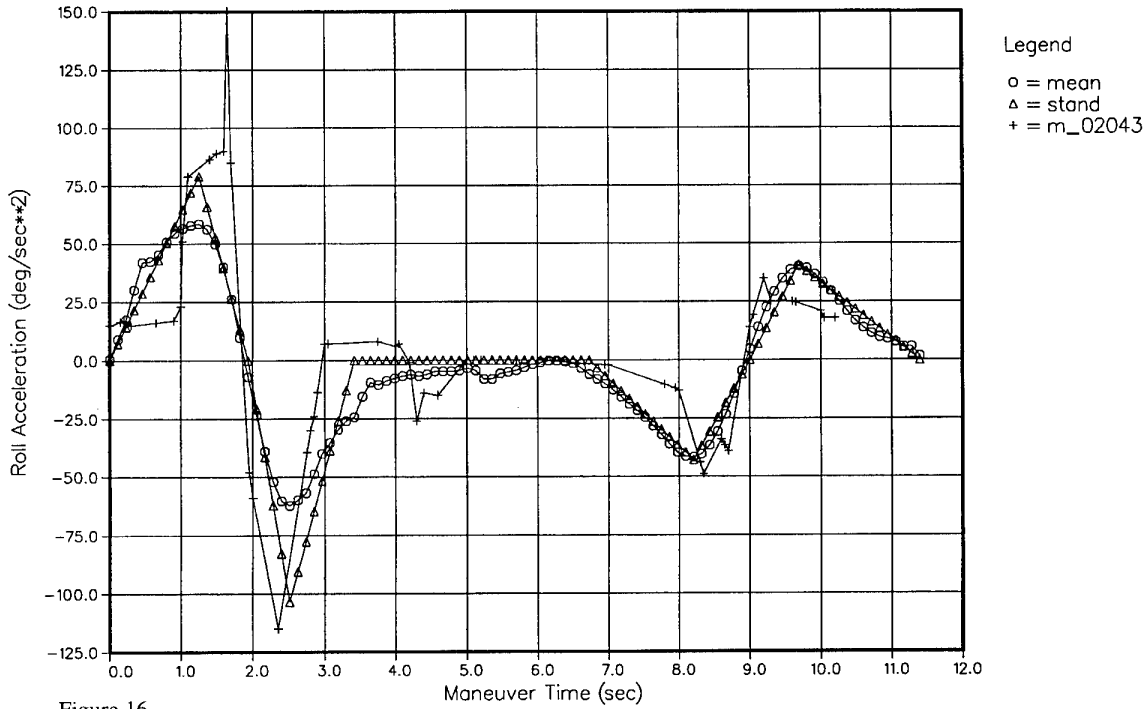


Figure 16

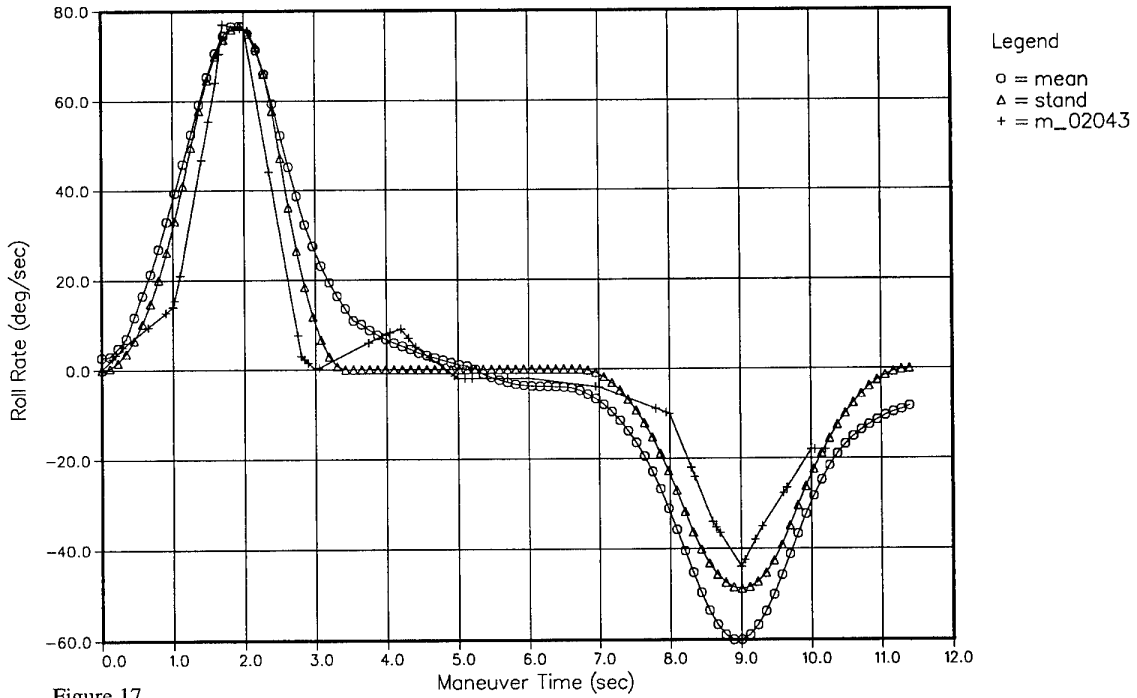


Figure 17

4.1 F-16 High g turn Standard Maneuver  
 Reconstituted with CF-18-Maneuver Data  
 (max  $n_z$ -level)

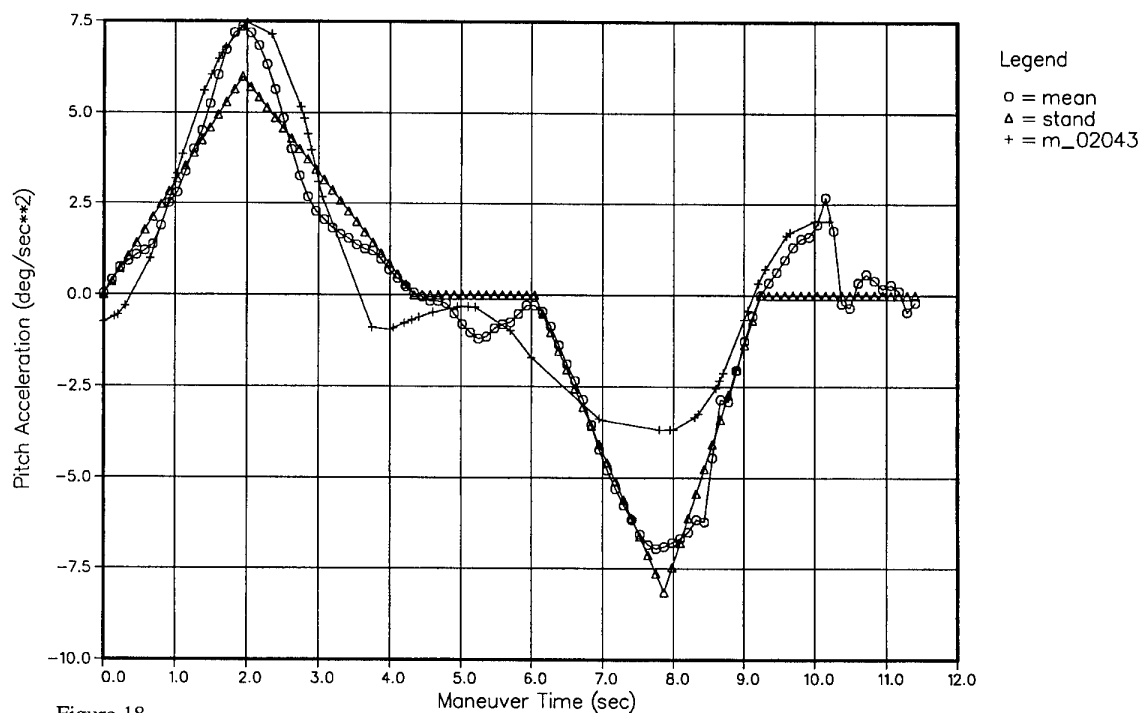


Figure 18

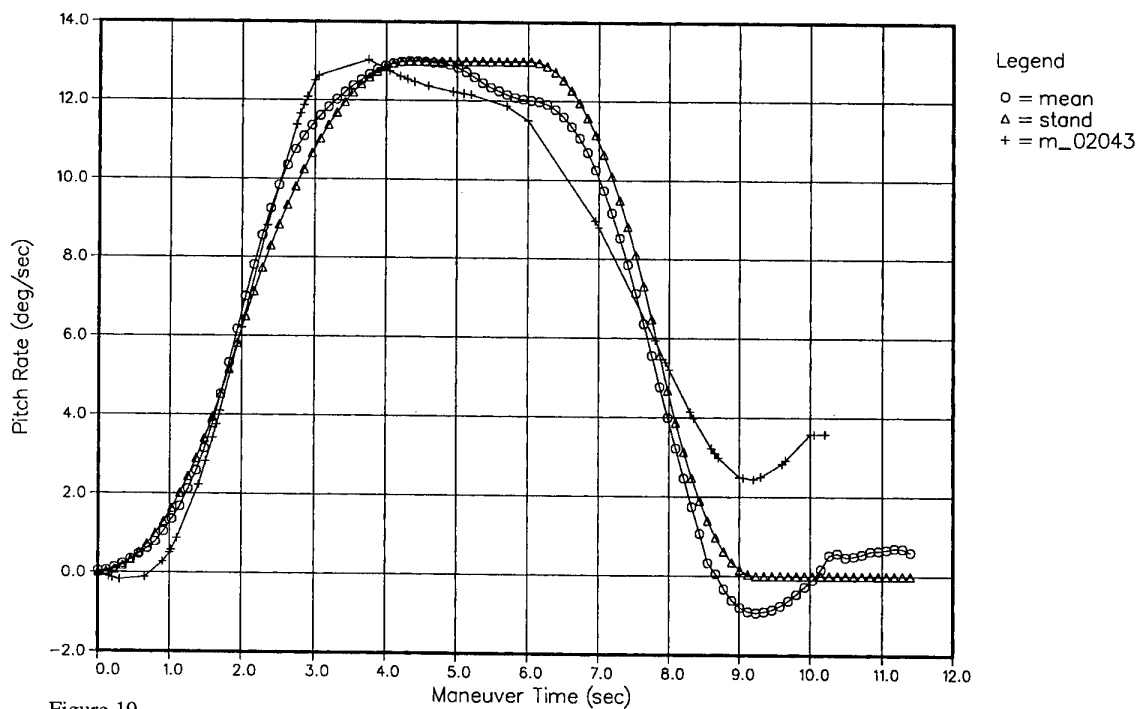


Figure 19

4.1 F-16 High g turn Standard Maneuver  
Reconstituted with CF-18-Maneuver Data  
(max  $n_z$ -level)

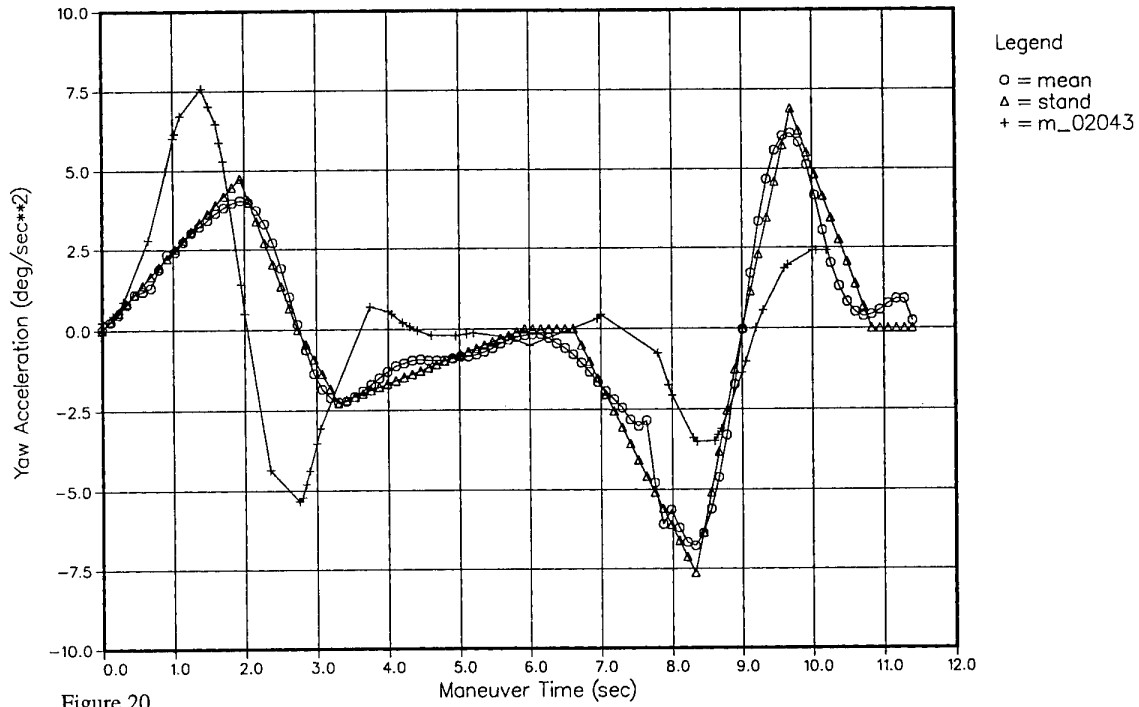


Figure 20

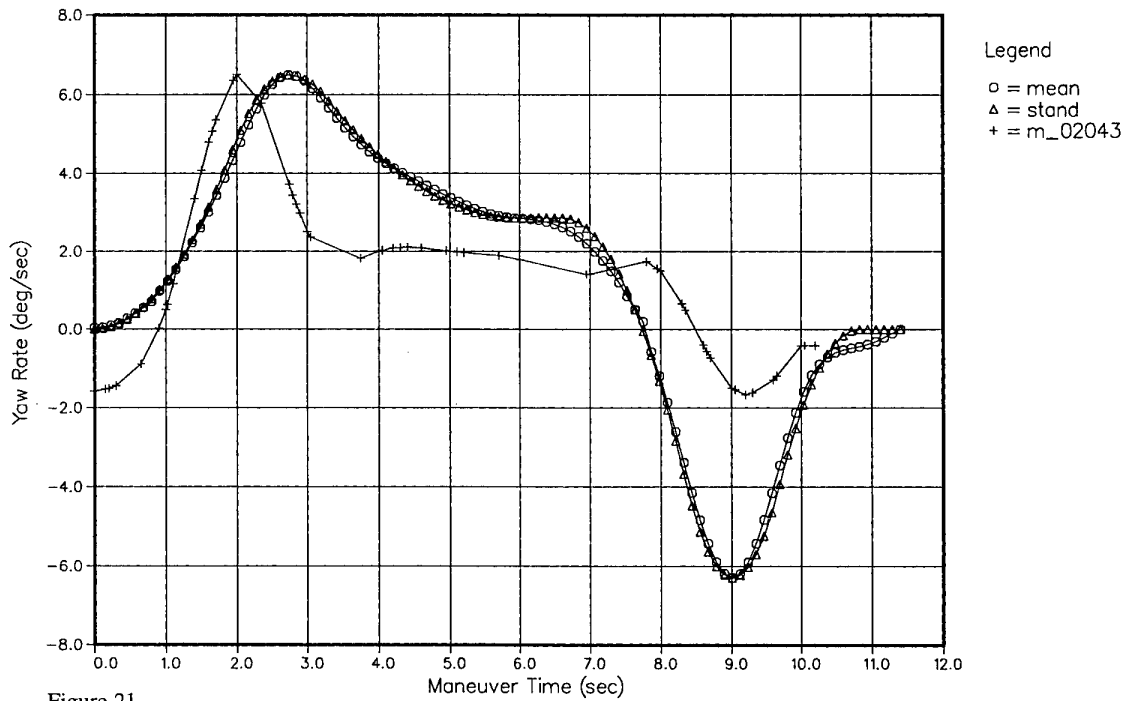


Figure 21

## 5. CONCLUSION

- For the evaluation of the operational parameters, the following data were made available and have been judged as applicable.
  - a) Flight test data by GAF Test Centre for specific operational maneuvers on three aircraft (Alpha Jet, F-4F, MRCA)
  - b) Data from simulations by GAF for specific operational maneuvers recorded on Dual Flight Simulator for two aircraft (F-4, JF-90)
  - c) Service data by USAF recorded on the F-16 (selected subset from over 300 sorties from 97 aircraft)
  - d) Service data by CF recorded on the CF-18 (selected subset of CF-18 fleet monitoring)

Taking all data available, which have been found to be suitable for separation into maneuver types, the data base is about 13 maneuver types. For two maneuver types, High-g-turn and Barrel roll, more than 60 maneuvers for each maneuver type have been considered as applicable for evaluation.

- The normalization procedure has been developed and applied to the data base for 3 GAF-aircraft in operation and one aircraft in development.
- For service data from the USAF for F-16 aircraft and from the CF for CF-18 aircraft, an identification of the maneuver types from the recordings was completed without any problems. These identified maneuvers have been normalized for forming mean values.
- The comparison of the normalized maneuvers for the several aircraft types has been done using mean values. The scatter band is about the same as that for the individual aircraft. This means that the normalized time histories can be considered as independent of the aircraft type.
- The actively controlled aircraft (MRCA, F-16, CF-18) fit in the same scatter band as the conventional controlled aircraft. This means the hypothesis that the operational maneuvers are performed in the same way, i. e. performing the same normalized parameter time history, can be considered as confirmed.
- For this paper, the determination of Standard Maneuver time histories has been limited to one maneuver type. The maneuver type chosen is the High-g-turn because of the sufficient data base i. e. includes all aircraft and has the biggest number of maneuvers. For the definition of Standard Maneuver independent of aircraft type, an idealization of the maneuver time history combined with load relevant criteria was performed.
- Also, the High-g-turn maneuver was selected for the demonstration of the reconstitution of the Standard Maneuver time histories. The reconstituted parameters have been compared with a specific High-g-turn maneuver selected from CF-18 usage data.

The comparison has been performed for the F-16 Standard Maneuver time histories

The comparison shows an acceptable agreement in the maneuver time histories for both aircraft.

- The result is, that the Standard Maneuver independent of the aircraft type is applicable as unit input for calculation of the movement of a specific aircraft by reconstitution of the real aircraft configuration and flight condition.

## 8. REFERENCES

1. AGARD ADVISORY REPORT 340  
Evaluation of Loads from Operational Maneuvers  
Final Working Group Report of WG 27  
April 1996
2. AGARD Report No. 746  
Workshop on Design Loads for Advanced Fighters  
April 1987
3. Presentation of 69. AGARD-SMP Meeting  
by C.A. Babisch and I.M. Slye  
**Study of F-16 Maneuvers**  
of Wright-Patterson AFB arranged by C.L. Petrin
4. AGARD CONFERENCE PROCEEDINGS 506  
FATIGUE MANAGEMENT  
**Ref. 7 : A Parametric Approach to Spectrum Development by**  
D.L. Simpson, R.I. Hiscocks and D. Zavitz  
May 1991

## Flight Loads Derived from Operational Maneuvers

**H. Struck**

Daimler-Benz Aerospace  
Airbus GmbH, ED03  
Hünefeldstraße 1-5  
28183 Bremen  
Germany

**C. Perron**

Bombardier Inc./ Canadair  
Defence Systems Divisions  
10000 Cargo Road A-4  
Montreal International Airport, Mirabel  
Mirabel, Quebec, Canada  
I7N 1H3

### SUMMARY

This paper describes the feasibility for the determination of operational loads applying an operational Maneuver Model. The essential input for the Maneuver Model is a set of Standard Maneuvers consisting of normalized operational parameter time histories.

Operational external loads can be determined for:

- extreme operational loads
- fatigue loads
- loads related to the operational parameters

by introducing aircraft basic data, flight condition and boundary conditions for the maneuver to be considered.

The application of the Maneuver Model is demonstrated for one aircraft. For some operational maneuvers the extreme operational loads are determined and compared with the design loads required by MIL-8861.

The application of Standard Maneuver independent of the aircraft type has been demonstrated by determination of the loads applying the Standard Maneuver time histories from F-16 reconstituted to real time using the CF-18 performance data. The calculation of the loads has been performed using a proven Canadian loads calculation methodology and compared against flight test data of CF-18.

### 1. INTRODUCTION

The determination of the design maneuver loads is largely specified in regulations independently of the maneuvers or missions actually performed in operation.

For conventionally controlled Aircraft the regulations give the time history of the control surface deflections and numerically define several essential maneuver - load parameters for the de-

termination of the design load level.

Obviously with the introduction of the fly-by-wire and/or active control technology, as well as care free maneuvering features, recent specifications no longer define the control surface deflections but rather provide the cockpit displacements of the controls in the cockpit.

This means that existing design load regulations and specifications based on conventional aircraft configurations, structural design concepts and control system technologies, may not be adequate to ensure the structural integrity of future military aircraft configurations using novel control methods, structural concepts and combat tactics.

One promising approach is to derive design loads from a careful analysis of operational maneuvers by current fighters to extract critical parameters and their range of values.

To investigate this approach, Working Group 27 "Evaluation of Loads from Operational Flight Maneuver" was formed, AGARD involvement was particularly relevant since it allowed the expansion of the types of aircraft and the control systems considered in the study.

The Working Group formulated a set of activities that addressed the fundamental premises of a method to generate operational loads from flight parameters by determination of Standard Maneuver independent of the aircraft type and the control system. These operational loads can be statistically evaluated for use in static design and for fatigue fracture assessment.

**2. DESIGN REQUIREMENTS**

**2.1 Design parameter specified in regulations**

Aircraft structures are designed in accordance with the relevant regulations and based on a philosophy defining the load level so as to cover all loads expected in service. The design loads are largely independent of the maneuvers actually performed in operation.

The design load conditions are determined by the main load parameters as limit values for:

- symmetrical maneuvers as load factor ( $n_z$ )
- unsymmetrical maneuvers as roll rate ( $p$ ) and bank angle ( $\phi$ ) combined with a specified load factor ( $n_z$ )

as shown in Table 1 and 2.

REQUIREMENT Basic Mission Symbol Category III	SYMMETRICAL FLIGHT LIMIT LOAD FACTOR					Time for abrupt control displacement $t_1 / t_2$ second
	Basic Flight Design Weight		All Weights	Max. Design Weight		
	Max	Min at $V_H$	Min at $V_L$	Max	Min at $V_H$	
MIL-A-008861 A						
A, F, TF (Subsonic)	8.0 <sup>▪</sup>	-3.0	-1.0	4.0	-2.0	0.2
A, F, TF (Supersonic)	6.5	-3.0	-1.0	4.0	-2.0	0.2
O, T,	6.0	-3.0	-1.0	3.0	-1.0	0.2
AIR 2004/E Category	$n_1$ corresponding to A/C Specification					0.2/ 0.3

- as required by Performance and Design Requirements (PDR)

Table 1 Symmetrical Design Parameters for Fighter

REQUIREMENT Unsymmetrical Maneuver	Initial Load Factor		Roll Rate [°/s]	Bank Angle [°]	Time for abrupt control displacement
	Max.	Min.			
MIL-A-008861 A					
Rolling Pull Out	$0.8n_z$ (max)	1.0	$\leq 270$	$2x$ value corresp. to $n_z$	0.1
Roll 180	1.0	-1.0	$\leq 270$		0.1
Roll 360	1.0	1.0	$\leq 270$		0.1
Yawing	1.0	1.0	-		$\leq 5$
AIR 2004/E					
Roll 360	$0.8n_1$	$0.2n_1$	$\leq 300$	360	0.2/0.3
Yawing	1.0	1.0		$\leq 5$	0.2/0.3

Table 2 Unsymmetrical Design Parameters for Fighter

**2.2 Procedures specified for design load determination**

The structural loads are determined by response calculations of the aircraft for defined cockpit control displacements, and thus the maneuver loads for the whole flight envelope are calculated. The cockpit control displacements are defined as time history for

In accordance with the former regulations MIL-A-8861 and AIR 2004/D the control surface deflection is specified and its time history has to be determined so as to produce the most critical load conditions. Application of these control surface movements permits to determine the most critical loads acting on the main structural components.

- pitching maneuvers
- rolling maneuvers
- yawing maneuvers

stated in MIL-A-008861A as shown in Fig. 1 and in AIR 2004/E as shown in Fig. 2

This means, this procedure, as far as the control surface deflection time histories are concerned, includes distinct load criteria that provide a load level which cannot be exceeded by any other control surface movements.

The introduction of the fly-by-wire and/or active-control technology makes this philosophy inadequate, though. The latest regulations MIL-A-008861 A and AIR 2004/E do no longer specify the control surface deflections but the cockpit control displacements, whereas the other load criteria are retained. That means, the time history of the control surface deflection results firstly from the cockpit command and secondly from the parameters fed back. If there is no similarity between the time history of the cockpit control and of the control surface deflection, the task of determining the critical cockpit control displacement time history and thus the extreme loads on the main structural components is very complex. [2]

This means that existing design load regulations and specifications based on conventional aircraft configurations, structural design concepts and control system technologies, may not be adequate to ensure the structural integrity of future military aircraft configurations using novel control methods, structural concepts and combat tactics.

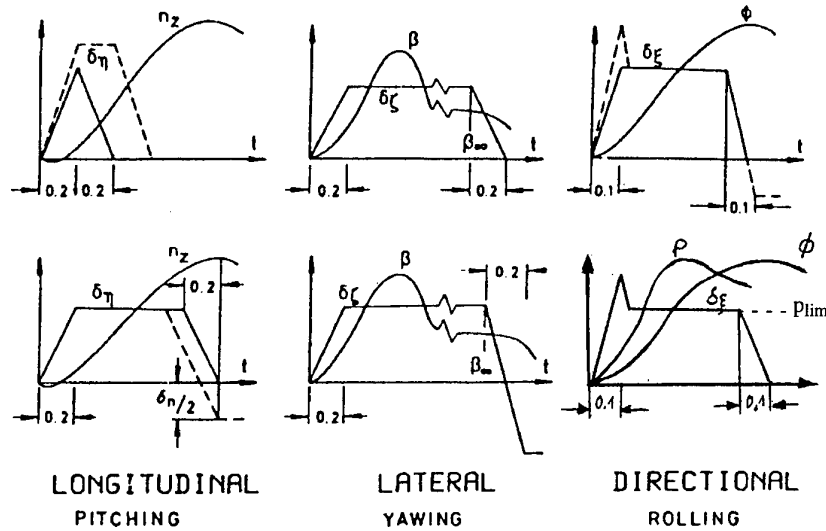


Fig. 1 COCKPIT CONTROL DISPLACEMENT MIL-A-008861A

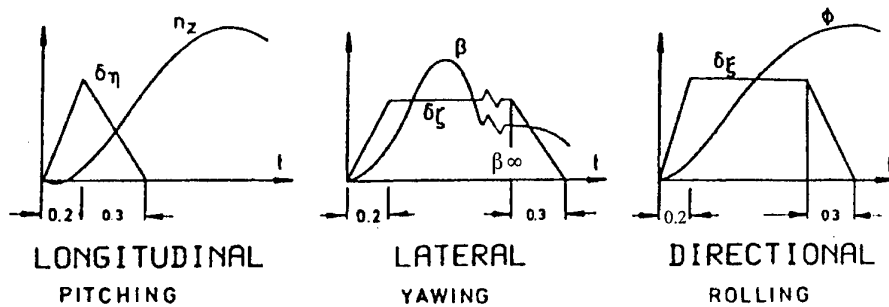


Fig. 2 COCKPIT CONTROL DISPLACEMENT AIR 2004/E

### 3. EVALUATION OF FLIGHT LOADS FROM OPERATIONAL MANEUVERS

#### 3.1 Operational Maneuver Parameters

In service, maneuvers, especially combat maneuvers, are flown in accordance with practiced rules that lead to specified motions of the aircraft. In Germany, an evaluation of operational flight maneuvers has been made for three aircraft types flown by the GAF with the aim of deriving operational loads by applying parameters measured in operational flights. This data was used as a data base. For the maneuvers evaluated, a normalization of the relevant parameters of motions was feasible, and the results could be verified in a maneuver model.

Within the scope of this evaluation, an attempt has been made to find a way of load analysis from operational maneuvers in addition to the applicable design specifications. The evaluation is based on the assumption that it should be possible to standardize the several maneuvers trained and flown by NATO Air Forces. Specifically, this means that it should be possible to find a standardized time history for each type of maneuver, which is independent of the extreme values of the relevant parameters. The determination and verification of operational maneuver parameter time histories is presented by my colleague Jürgen Molkenhain in paper 3 .

Based on this assumption, it was analyzed how the evaluation of structural loads could be realized after previous standardization of maneuvers taking into account the maneuver model for calculating the control surface deflections necessary for performing the maneuvers considered.

#### 3.2 Maneuver Model

The maneuver model process is shown in Figure 3. as a flow chart. As input, standardized parameters are used. First, the boundary conditions have to be determined. For example, for a high g turn, the following is required:

- maneuver time,  $T_{MAN}$
- load factors,  $n_y, n_z$
- bank angle,  $\Phi$

Using the standardized parameters the reconstitution into real time is performed. In order to perform the response calculation in the conventional manner, the control deflections are necessary and can be determined as follows:

- roll control  $\xi$  by applying roll- and yaw equations
- pitch control  $\eta$  using the pitch equation (taking into account the symmetrical aileron deflection: if existing)
- yaw control  $\zeta$  by applying sideslip- and yaw equations

The response calculation is done for real time conditions, but for the purpose of checking the results with respect to the standardized maneuvers, the response parameters are normalized. In a comparison of the parameters between input and output of the maneuver model, the standardization is checked. In the case of confirmation the conformity of the main parameters of the response calculation with the standardized parameters, the output parameters are considered to be verified. These verified data represent the model parameters for structural load calculation.

#### Application of the Maneuver Model

The application of the maneuver model is feasible for the determination of loads in general

- **for Extreme Operational Loads / Limit Loads** taking into account the boundary conditions for design
  - limits of flight control system
  - minimum of maneuver time  $T_{MAN}$
  - maximum of load factors  $n_z, n_y$
  - maximum of bank angle  $\Phi$  of the maneuver to be considered
- **for Fatigue Loads** by building a usage spectrum made up of reconstituted standardized maneuvers.
- **for Loads related to the recorded parameters** taking into account the recorded parameters directly without application of the standardization procedure (Normalization, mean values and smoothing, tuning idealization) and without boundary conditions.

Only for the calculation of the control deflection necessary to perform the maneuver



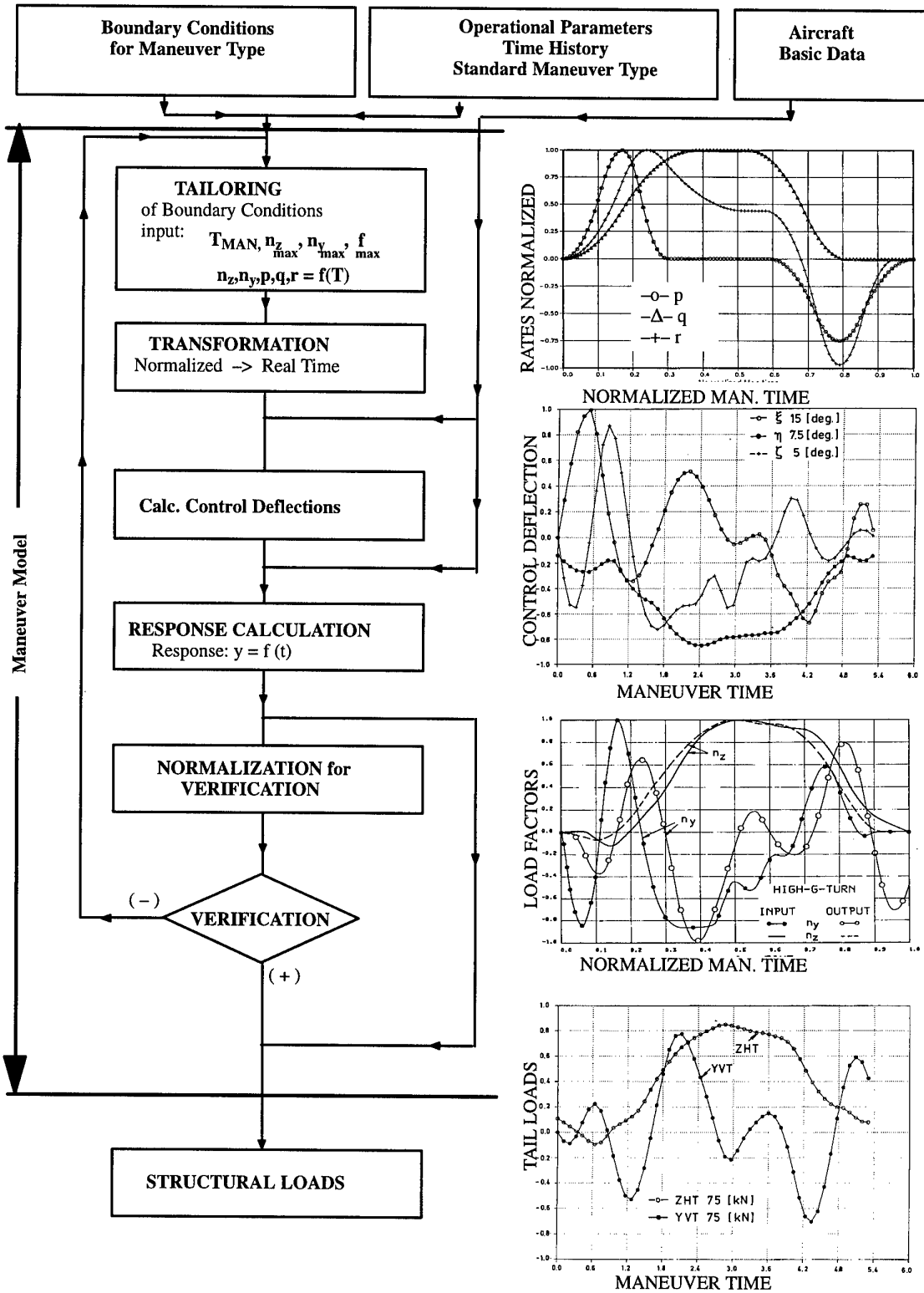


Figure 3. Procedure of the Maneuver Model

**3.2.1 Boundary Conditions**

Boundary Conditions have to be determined as the main input for the application of the maneuver model defining the load level. This is necessary for the determination of the extreme operational maneuvers and consequently for the verification of the design loads. For example, the parameters to be defined for a operational maneuver are:

- Design Maneuvers
  - a) the shortest maneuver time ( $t_{Man} = \min$ ) realizable by the control system and the aerodynamic limits
  - b) the maximum vertical load factor ( $n_z$ ) for the maneuver to be considered
  - c) the maximum lateral load factor ( $n_y$ )
  - d) the maximum bank angle ( $\Phi$ ) for the maneuver to be considered

These boundary condition parameters can be derived from spectra of main load parameters by applying extreme value distributions, an example is shown in Figure 4

If no spectra are available the main load parameters stated in the Design Requirements (MIL-Spec) e.g.  $n_z, \Phi$  can be applied.

- Fatigue Maneuvers

All the main load parameters can be taken from the related spectra available.

**3.2.2 Aircraft Basic Data**

Aircraft basic data is also the inputs for the maneuver model and is required to perform the reconstitution from the standardized maneuvers.

1. For calculation of the control deflections necessary to generate the parameter time history, the following aircraft basic data are needed:

- Aircraft configuration
  - geometric data
  - operational mass
  - inertia properties
- Aerodynamic data set for the aircraft
  - $C_L, C_m = f(\alpha), C_y, C_l, C_n = f(\beta, \alpha)$
- Flight Control System Data
  - for conventionally controlled aircraft mechanical gearings / limits
  - for active controlled aircraft Flight Control Law (EFCS)
- Engine Data
  - Thrust
- Flight Condition
  - airspeed, Ma
  - altitude

2. For calculation of structural loads on aircraft components, the following data are needed:

- aerodynamic data set for the components to be considered (Wing, Horizontal Tailplane, .....)
- mass data for the components to be considered

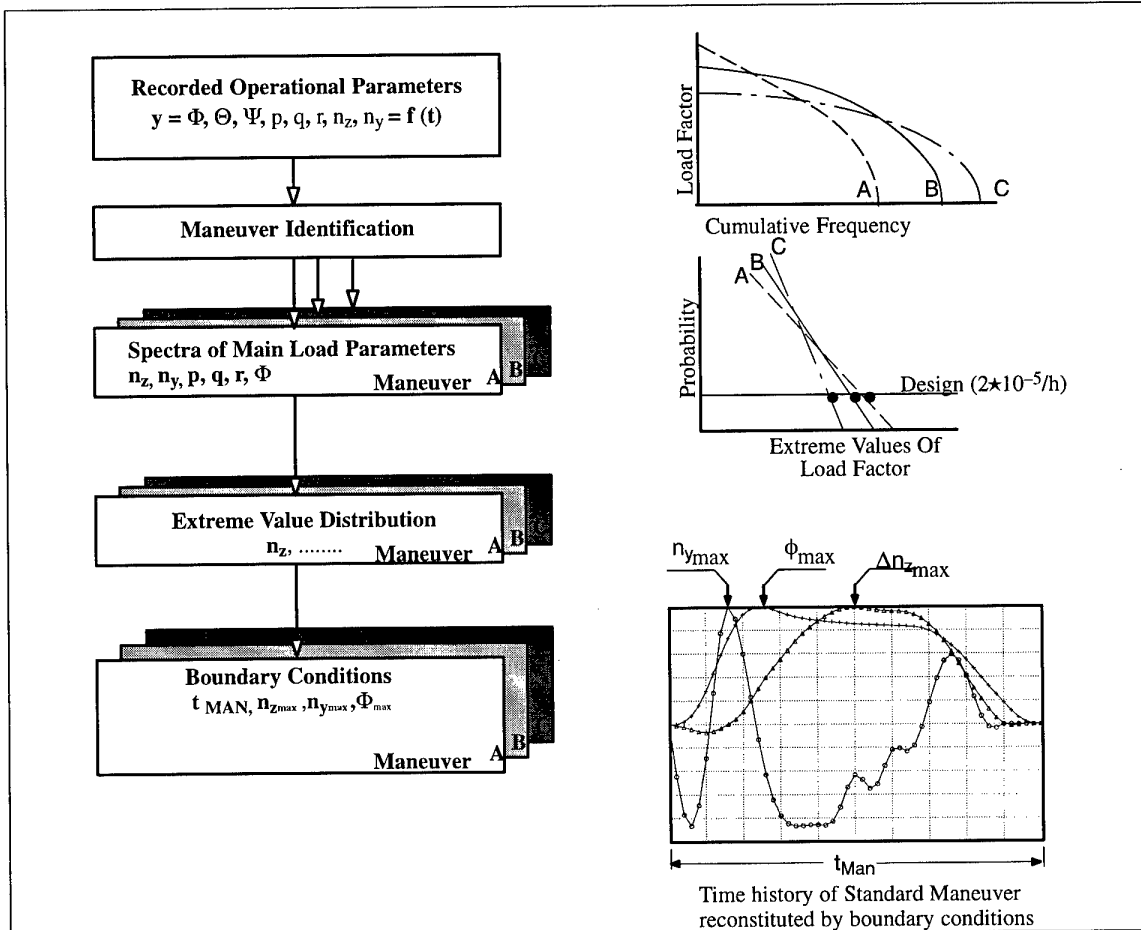


Figure 4 Boundary Conditions for Design Maneuvers

### 3.3 Application of the Maneuver Model

#### Determination of extreme operational loads GAF F-4F

The operational parameters of the standard maneuver are considered as mean parameters.

For deriving the extreme maneuvers, the main parameters of the standard maneuver are scaled up to the boundary conditions to be obtained. The values for the parameters of the boundary conditions ( $T_{MAN}$ ,  $n_z$ ,  $n_y$ ,  $\Phi$ ) can be derived from extreme value distributions or can be assumed with reference to design parameters required by specifications (MIL-Spec.). In the following example the boundary conditions were applied corresponding to MIL-A-008861 shown in Table 3.

#### Stations for load analysis

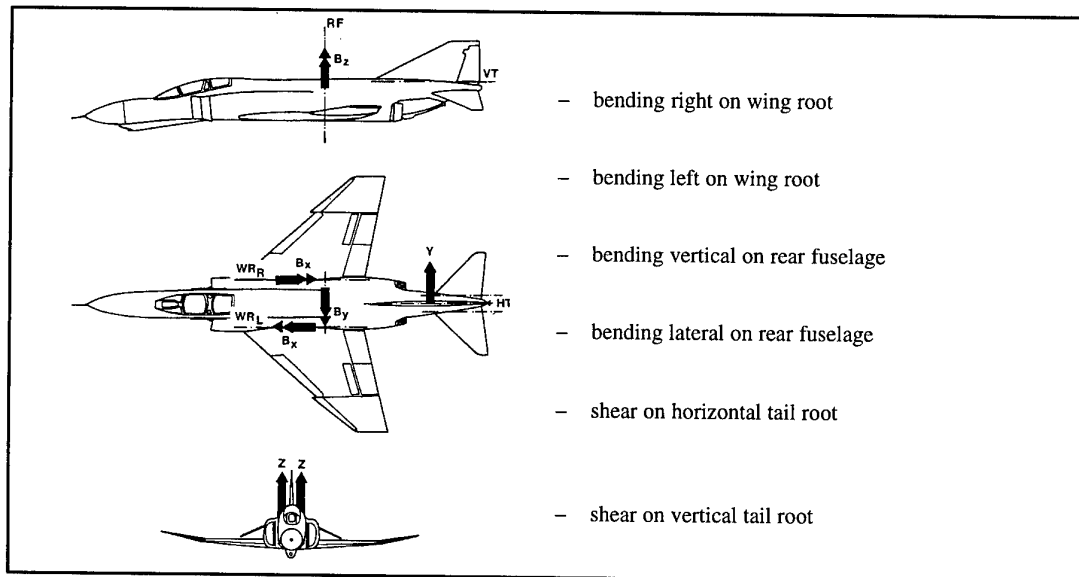
Table 1 shows the mean values and the assumed corresponding extreme values for the maneuver time ( $T_{MAN}$ ), load factors ( $n_z$ ,  $n_y$ ), the angles of bank ( $\Phi$ ).

For determination of the extreme values the maximum values of the mean parameters for the 5 analyzed maneuvers have been scaled up to the load factors required by MIL-8861. The determination of the extreme maneuvers is performed by the same procedure as for the mean maneuvers, but applying extreme boundary conditions.

OPERATIONAL MANEUVERS	$T_{MAN}$ (sec)		$n_z$		$n_y$		$\Phi$ [°]	
	mean	extr.	mean	extr.	mean	extr.	mean	extr.
FULL AILERON REVERSAL	11	11	5.0	6.5	0.4	0.6	100	100
HIGH-G-BARREL ROLL O.T.	20	5.6	4.0	5.0	0.12	0.3	360	360
HIGH-G-BARREL ROLL U.N.	20	6.8	3.5	4.5	0.12	0.4	360	360
HIGH-G-TURN	8	5.3	5.0	8.0	0.25	0.5	90	90
ROLLING ENTRIES + PULL OUT	17	7.5	5.0	6.5	0.15	0.4	100	100

Table 3 Model Parameters for Load Analysis

For the extreme maneuvers the loads on the following main structural components have been analyzed as shown the following sketch.



For the High-g-turn maneuver, the extreme operational maneuver parameters are plotted in Figure 5.1-5.4, the extreme operational loads in Figure 5.5-5.7, and the control deflections in Figure 5.8.

The parameters and loads are plotted as normalized values versus real time. For the normalization the values are related to the maximum values indicated in the diagrams.

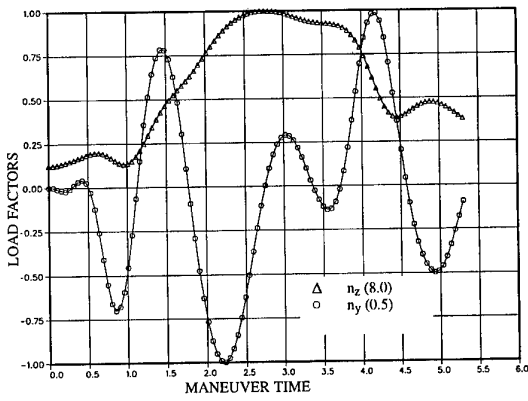


Figure 5.1  
EXTREME OPERATIONAL  
PARAMETERS HIGH-G-TURN

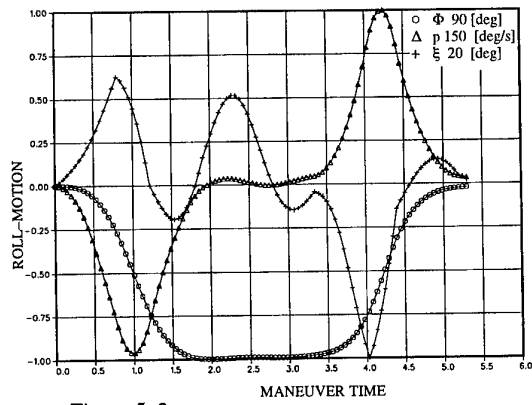


Figure 5.2  
EXTREME OPERATIONAL  
PARAMETERS HIGH-G-TURN

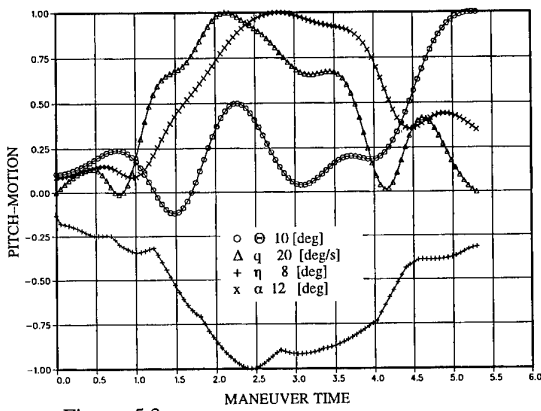


Figure 5.3  
EXTREME OPERATIONAL  
PARAMETERS HIGH-G-TURN

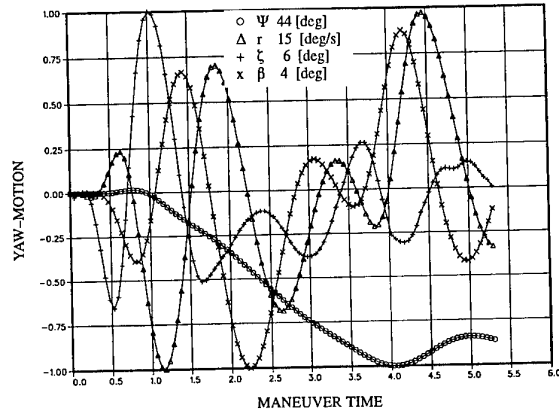


Figure 5.4  
EXTREME OPERATIONAL  
PARAMETERS HIGH-G-TURN

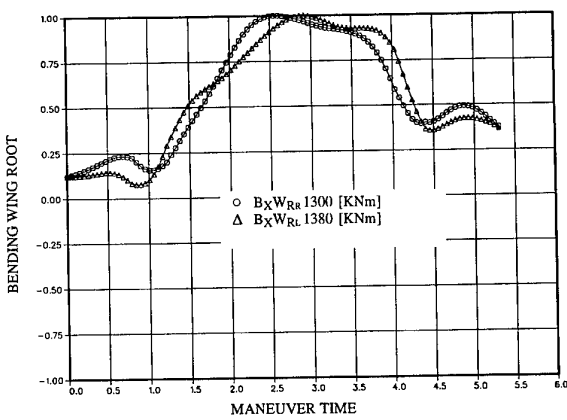


Figure 5.5  
EXTREME OPERATIONAL  
LOADS HIGH-G-TURN

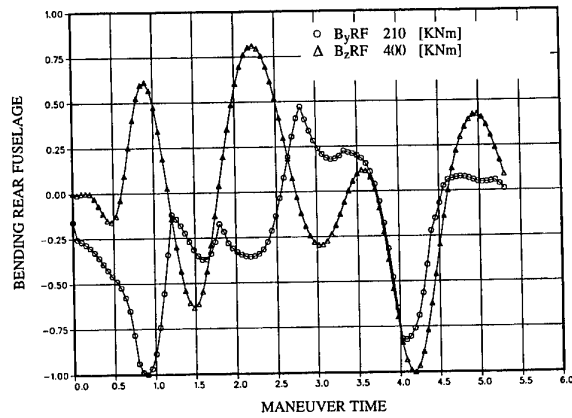


Figure 5.6  
EXTREME OPERATIONAL  
LOADS HIGH-G-TURN

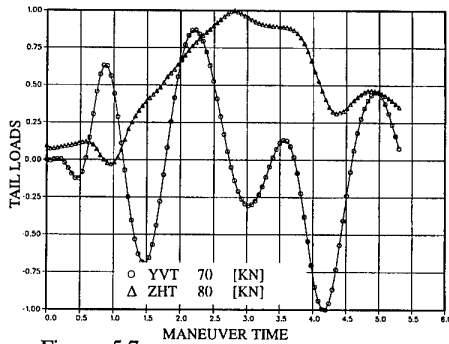


Figure 5.7  
EXTREME OPERATIONAL LOADS  
HIGH-G-TURN

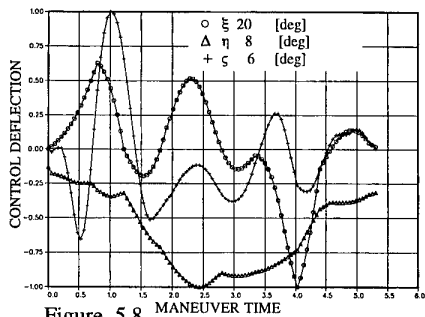


Figure 5.8  
EXTREME OPERATIONAL CONTROL  
DEFLECTIONS HIGH-G-TURN

As examples, the evaluation of operational maneuvers has been performed for the following 5 maneuvers:

- full aileron reversal
- high-g-barrel roll over the top
- high-g-barrel roll underneath
- high-g-turn
- rolling entries + pull out

The control deflections plotted in Figure 5.9–5.11 show an interesting course for the five individual operational maneuvers. In three of the maneuvers, alternating control deflections have been found, especially roll- and yaw controls.

In detail:

	aileron	rudder
high-g-turn	3	4
full aileron reversal	3	3
rolling entries	2	2

The pitch control deflections occurs in one direction only, alternating for the maneuvers full aileron reversal and rolling entries + pull out. For the other maneuvers the pitch control deflections show a moderate history.

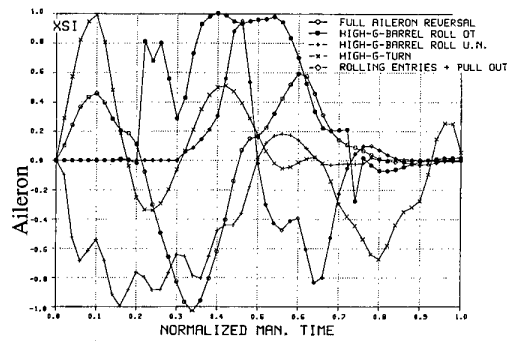


Figure 5.9

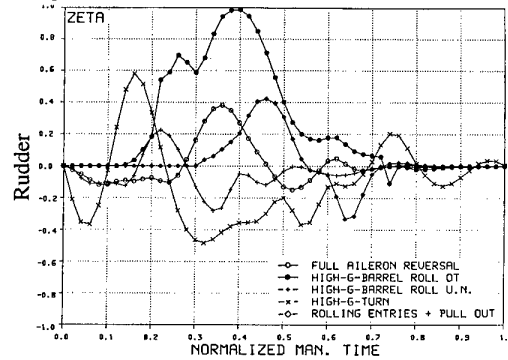


Figure 5.10

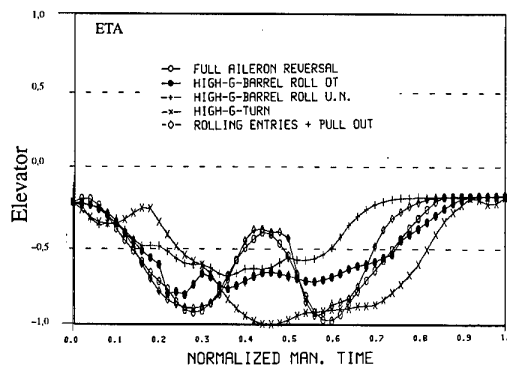


Figure 5.11  
EXTREME OPERATIONAL CONTROL DEFLECTIONS  
OPERATIONAL MANEUVERS

### Comparison of extreme operational loads with design loads required by MIL-8861

In the design requirements, several flight conditions are specified, distinguishing between

- symmetrical flight conditions
  - pitching maneuvers
- asymmetric flight conditions
  - yawing maneuvers
  - rolling maneuvers

For these maneuvers, the displacements of the cockpit control are specified as shown in Fig. 1 and 2 .

For comparison, the vertical load factor and the structural loads on the main components for all MIL-manuevers have been calculated. The results are plotted in the same manner as for the operational maneuvers.

In Figure 6.1, the load factors are presented. At a glance, a moderate variation of the load factor during all maneuvers is evident. Figure 6.2-6.6 show the loads on the wing, rear fuselage and the tail planes where the load factors and the loads have been normalized with the design values, i.e.  $n_z$  (design) = 8.0 equaling 1.0

In table 4 the maximum values of the main load parameters, the structural loads for MIL-manuevers, and the extreme operational maneuvers are presented. The main parameters are absolute values, but the loads have been normalized by the design loads.

This summary shows that in some cases the extreme operational structural loads are lower than the design loads specified by MIL-8861.

The load level is about the same for the symmetrical pitch maneuvers and about, 77% for the unsymmetrical rudder maneuver.

		$n_z$		$n_y$	P	$\beta$	$B_{xWR}$	$B_{yRF}$	$B_{zRF}$	ZHT	YVT
		max.	min.		[°/s]	[°]					
MIL-MANEUVERS	ROLL 180°	0.80	-3.2	0.53	203	3.6	0.22	0.37	0.62	-0.38	0.59
	ROLLING PULL OUT	6.50	+3.9	0.55	124	4.7	0.97	0.31	0.88	0.54	0.77
	ROLL 360°	1.30	-1.1	0.28	210	1.8	0.34	0.39	0.35	-0.18	0.27
	RUDDER KICK	1.10	+0.5	0.83	20	7.5	0.18	0.09	1.00	0.08	1.00
	ABRUPT PITCHING $\wedge$	8.0	+0.8	0	0	0	1.00	1.00	-	1.00	-
	ABRUPT PITCHING $\wedge$	8.0	+0.9	0	0	0	1.00	0.57	-	1.00	-
OPERATIONAL MANEUVERS	FULL AILERON REVERSAL	6.5	+0.5	0.60	150	5.1	0.81	0.26	0.77	0.53	0.75
	HIGH-G-BARREL ROLL O.T.	5.0	+0.6	0.25	177	2.0	0.60	0.21	0.48	0.44	0.40
	HIGH-G-BARREL ROLL UN.	4.5	+0.7	0.40	164	2.7	0.56	0.40	0.59	0.40	0.52
	HIGH-G-TURN	8.0	+0.3	0.50	132	4.2	1.00	0.37	0.60	0.70	0.58
	ROLLING ENTRIES+ PULL OUT	6.5	+0.5	0.40	139	1.9	0.81	0.27	0.52	0.57	0.48

Table 4 Maximum values of main load parameters and structural loads MIL- Maneuvers / extreme operational maneuvers.

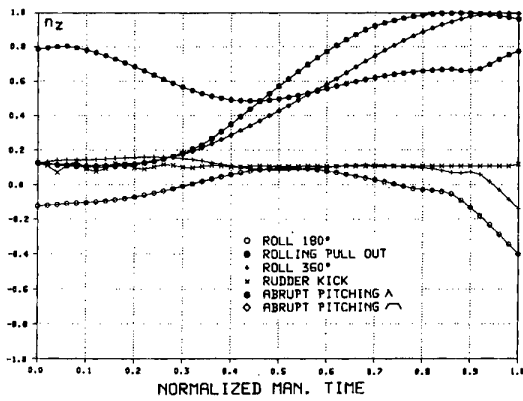


Figure 6.1 LOAD FACTORS-MIL-MANEUVERS

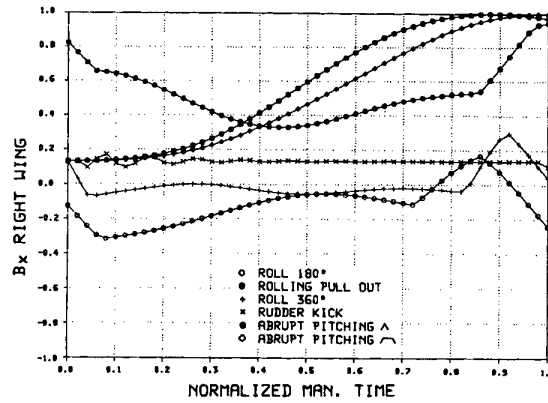


Figure 6.2 STRUCTURAL LOADS MIL-MANEUVERS

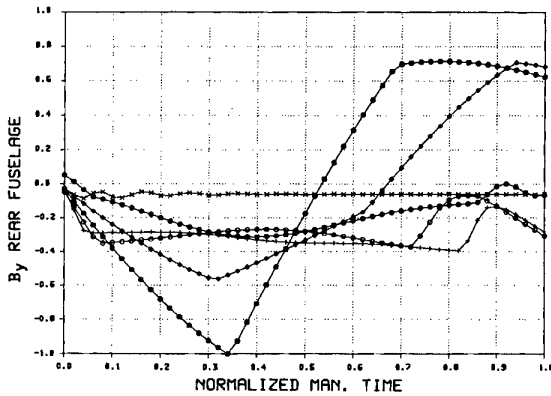


Figure 6.3 STRUCTURAL LOADS MIL-MANEUVERS

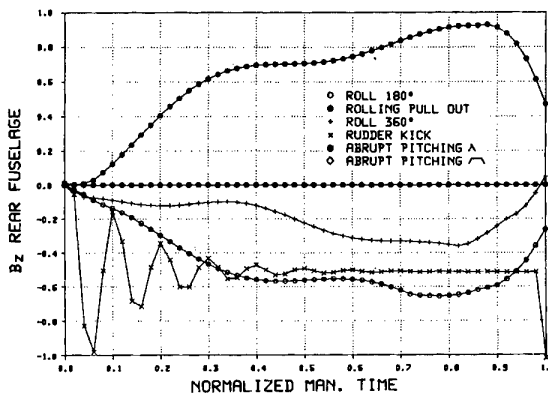


Figure 6.4 STRUCTURAL LOADS MIL-MANEUVERS

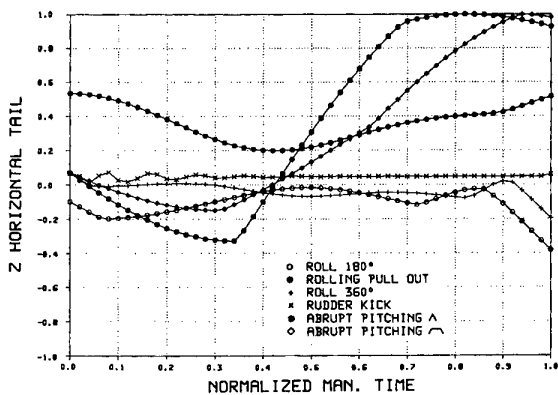


Figure 6.5 STRUCTURAL LOADS MIL-MANEUVERS

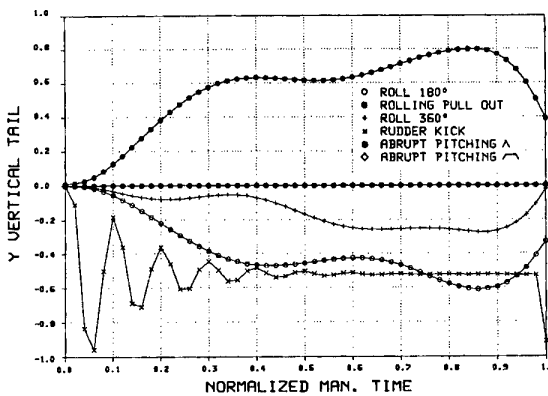


Figure 6.6 STRUCTURAL LOADS MIL-MANEUVERS

### Potential aspects for fatigue design

Fatigue load prediction and monitoring are only as good as the knowledge of the magnitude and the frequency, namely the load parameters expected and monitored in service. The potentiality of the maneuver model allows the realization and the evaluation of long-time measurements of the relevant parameters. The recording should include all fatigue-relevant data, such as mass configuration (weight, C/G, external stores) and the data describing the flight profiles (speed, altitude, flap setting).

For standardized maneuvers, the maneuver model provides

- the time history of the main parameters and the loads on the main structural components
- the correlation of the main parameters and the loads.

The spectra of relevant parameters for several operational maneuvers can be determined by systematic measurements made in service. Applying the maneuver model and the parameter spectra, the resultant load spectra for the expected mission of an aircraft can be established. This means the maneuver model can be applied for fatigue load prediction and for fatigue monitoring as well.

**4. VERIFICATION OF LOADS INDEPENDENT OF THE AIRCRAFT TYPE**

An essential activity of WG.27 was a limited demonstration study [1] which compared the loads calculated using the maneuver model from the reconstituted parameters to actual measured loads for a selection of maneuver types. The full process requires access to measured flight loads data and to aerodynamic and control system data for a selected aircraft type. Non-dimensionalized data for the maneuver types to be considered is also required. In practice, this was beyond the scope of WG.27 and an alternate approach that could be accomplished within the time restrictions of the WG.27 mandate had to be found.

A reduced program was defined which used available CF-18 loads data and a Bombardier/ Canadair Defence Systems Division (BI/CDS) loads calculation methodology. Canada was unable to release the CF-18 aerodynamic and control system data that would allow the use of the maneuver model.

The procedure used is shown in Figure 7.0 and is summarized as follows:

- Two maneuvers (one with higher symmetrical and the other with higher asymmetrical parameters) were chosen from the data set of maneuvers for which fully balanced loads had been determined and verified under the IFOSTP program as the basis of comparison. Also available were the time histories of the aircraft parameters.
- Using Standard Maneuver time histories as non-dimensionalized maneuver descriptions determined from F-16 data and the maneuver definition for the selected maneuvers, parameter time histories were determined for the maneuver.

To accelerate the loads comparison process, for the purposes of WG.27 these methodologies were used to calculate balanced loads conditions for the selected maneuvers based on the reconstituted parameters. These calculated loads were compared to "actual" (MSDRG) loads for the same maneuver which had been determined under the IFOSTP program. The comparison has been demonstrated only for the High g turn maneuver derived from F-16 and compared to CF-18 actual loads.

The comparison of the major section loads between "actual" (MSDRS) loads and loads based on reconstituted parameters is shown in Figure 7.1-7.4 .

**For Disparate Aircraft Type**

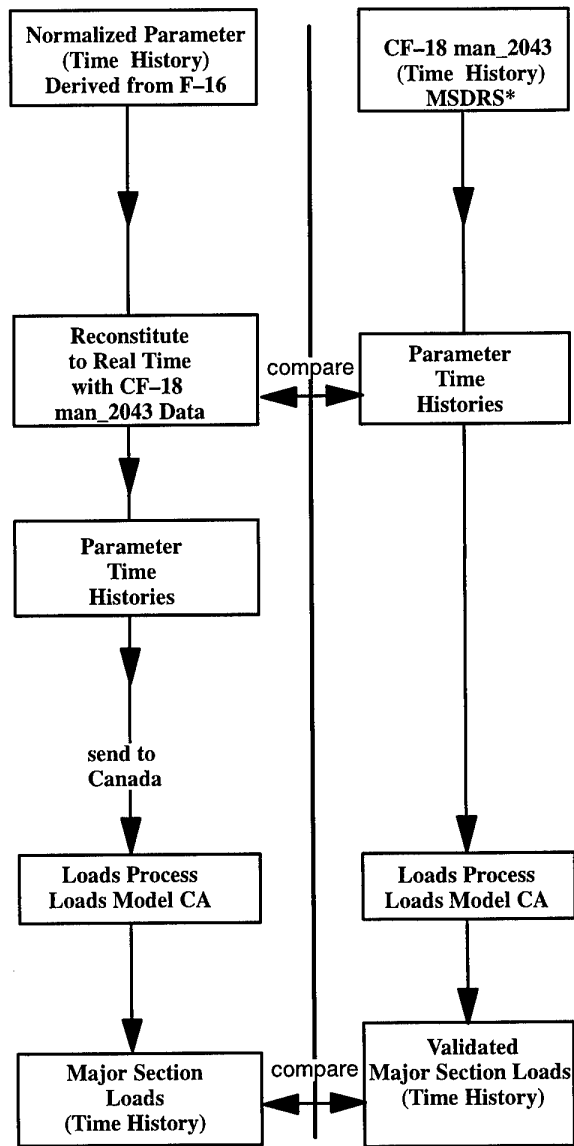
Demonstration of the application of the standard maneuver time histories process for a disparate aircraft has been performed as follows:

- Standard Maneuver Time History from the F-16 will be reconstituted to real time using the CF-18 performance data for one selected maneuver of the CF-Aircraft-Data recordings.

- For these reconstituted parameters in real time history the major section loads will be calculated applying the Canadian CF-18 loads model.

These calculated values will be compared to the existing recorded values of the selected maneuvers

- a) for maneuver parameters
- b) for major section loads



\* MSDRS: Maintenance Signal Data Recording System

Figure 7.0 WG.27 – Procedure



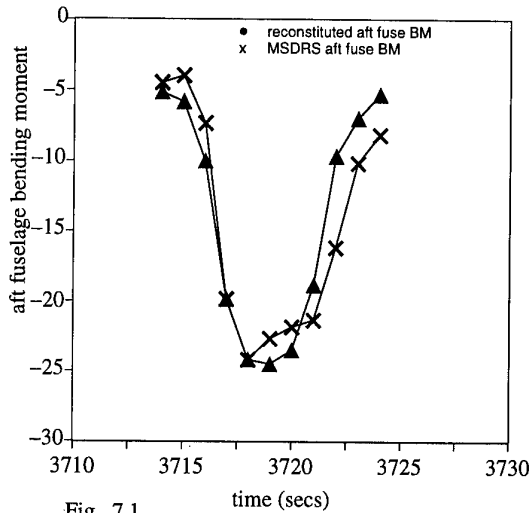


Fig. 7.1

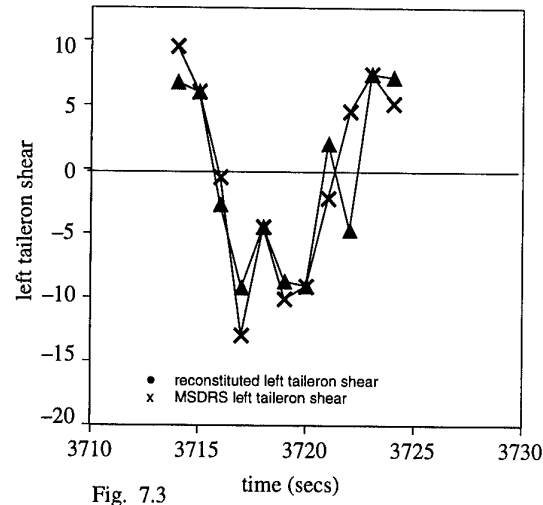


Fig. 7.3

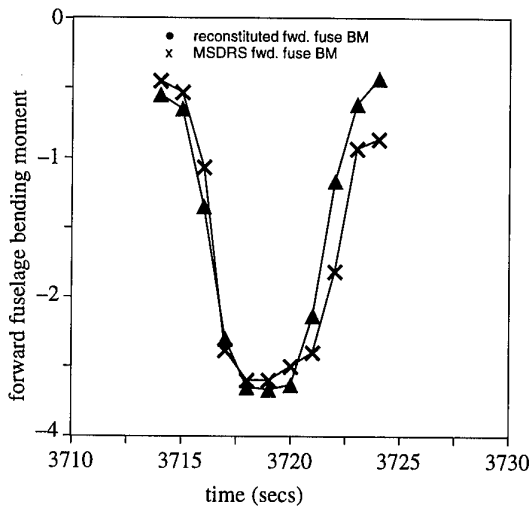


Fig. 7.2

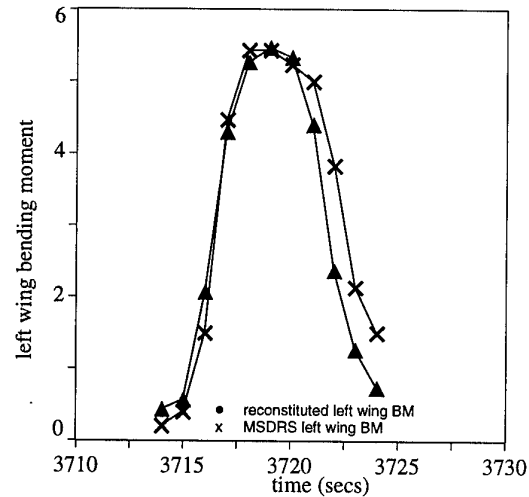


Fig. 7.4

### Comparison of Major Section Loads actual (MSDRS) and reconstituted Loads

In general, there is very good agreement for the peak and valley predictions. This means that the reconstituted loads histories are sufficiently accurate for use in static and fatigue assessments. There were some discrepancies noted in the time correlations between real and reconstituted maneuvers. This is an important issue since the full balance of the aircraft relies on coincident predictions. This issue was investigated and determined to be the result of the maneuver start-stop definition used during the formation of the non-dimensionalized data.

The issue is well understood and the methodology has been corrected. There was not however, sufficient time to recalculate the loads using the corrected data.

This exercise was limited to one maneuver and therefore only provides an indication of the performance of the technique. More maneuvers, both symmetrical and asymmetrical, must be studied. The effect of abruptness must also be addressed before the observation that the reconstituted loads histories are sufficiently accurate for static and fatigue purposes can be fully accepted. Unfortunately, this was beyond the scope of the WG.27 mandate [1].

Concluding that means the standard maneuver time history reconstituted to real time, using aircraft performance data to be considered is applicable independent of the aircraft type.

## 5. CONCLUSION

- Existing design load regulations and specifications based on conventional aircraft configurations and control systems may not be adequate to ensure structural integrity of military aircraft configurations using novel control methods, structural concepts and combat tactics.
- Evaluations of operational flight maneuvers has been made for several fighter aircraft types especially combat maneuvers are flown in accordance with practiced rules that lead to specified motions in the sky.
- Based on the assumption that all operational maneuvers performed in service can be verified as standard maneuvers (normalized parameter time histories for each maneuver type) one promising approach is, to derive design loads from careful analysis of operational maneuvers by current fighters to extract critical parameters and their range of values.
- The determination of Standard Maneuvers independent of the aircraft type has been demonstrated for two maneuver types by idealization of the maneuver time history taking into account load relevant parameters, as basic maneuvers for the calculation of loads, for use in static design and for fatigue assessment, applying the corresponding boundary conditions.
- The maneuver model has been applied for the determination of the extreme operational loads on the GAF F-4F aircraft for comparison with design loads required by MIL-8861.
- The verification of loads independent of the aircraft type for a Standard Maneuver time history is demonstrated by using a proven canadian load calculation methodology. The calculation of the loads has been performed for the reconstituted parameters of the Standard Maneuver of the F-16 and for the actual measured parameters. The calculated loads using the actual parameters have been validated against flight test data of CF-18.

## 6. POTENTIAL ASPECTS

The initial "Evaluation of Loads from Operational Flight Maneuvers" done by the working Group 27 has demonstrated the feasibility.

Further work is necessary to expand the scope of the investigation.

To cover more operational maneuvers in several NATO nations in the whole evaluation procedure and to extend the number of Standard Maneuvers in the reference database, the following activities are recommended:

- Establishment of a list of operational maneuvers in usage for NATO nations
- Obtain more operational maneuver recordings from service.
- Identify and verify more Standard Maneuvers.
- Establishment of spectra and extreme value distributions of relevant maneuver parameters ( $n_z$ ,  $n_y$ ,  $p$ ,  $q$ ,  $r$ ,  $\phi$ ) separated for maneuver types in order to determine boundary conditions.
- Apply and verify the Maneuver Model including calculation of control deflections and loads on major structural concepts for other aircraft.

### The result of the new maneuver approach can be used for:

- The judgement of the operational load level for aircraft already designed with regard to the design load level (static and fatigue) as specified in the regulations.  
  
That means the margin between design loads and the extreme operational loads is known.
- The determination of the load level for static and fatigue design due to operation for new aircraft to be developed.

## 7. REFERENCES

1. AGARD ADVISORY REPORT 340  
Evaluation of Loads from Operational Maneuvers  
Final Working Group Report of WG 27  
April 1996
2. AGARD Report No. 746  
Workshop on Design Loads for Advanced Fighters  
April 1987
3. Presentation of 69.AGARD-SMP Meeting  
by C.A. Babisch and I.M. Slye  
**Study of F-16 Maneuvers**  
of Wright-Patterson AFB arranged by C.L. Petrin
4. AGARD CONFERENCE PROCEEDINGS 506  
FATIGUE MANAGEMENT  
**Ref. 7 : A Parametric Approach to Spectrum  
Development by**  
D.L. Simpson, R.I. Hiscocks and D. Zavitz  
May 1991

A COMPARISON OF PRESSURE MEASUREMENTS BETWEEN A  
FULL-SCALE AND A 1/6-SCALE F/A-18 TWIN TAIL DURING BUFFET

Robert W. Moses\*

Ed Pendleton\*\*

**SUMMARY**

In 1993, tail buffet tests were performed on a full-scale, production model F/A-18 in the 80-by-120 Foot Wind Tunnel at NASA Ames Research Center. Steady and unsteady pressures were recorded on both sides of the starboard vertical tail for an angle of attack range of 20 to 40 degrees and at a sideslip range of -16 to 16 degrees at freestream velocities up to 100 knots (Mach 0.15, Reynolds number  $1.23 \times 10^7$ ). The aircraft was equipped with removable leading edge extension (LEX) fences that are used in flight to reduce tail buffet loads.

In 1995, tail buffet tests were performed on a 1/6-scale F-18 A/B model in the Transonic Dynamics Tunnel (TDT) at NASA Langley Research Center. Steady and unsteady pressures were recorded on both sides of both vertical tails for an angle-of-attack range of 7 to 37 degrees at freestream velocities up to 65 knots (Mach 0.10).

Comparisons of steady and unsteady pressures and root bending moments are presented for these wind-tunnel models for selected test cases. Representative pressure and root bending moment power spectra are also discussed, as are selected pressure cross-spectral densities.

**LIST OF SYMBOLS**

$A_j$	area of j-th tail element (ft <sup>2</sup> )
$A_F$	total planform area of tail (ft <sup>2</sup> )
$C_{MB}$	tail root bending moment coefficient
$C_{\Delta p}$	differential pressure coefficient
$\bar{c}$	wing mean aerodynamic chord (ft)
$F(n)$	nondimensional buffet pressure power spectral density function
$f$	frequency (Hz)
$M$	Mach number
$n$	frequency parameter, $f\bar{c}/U_\infty$
$p_{in(out)}$	pressure on inner (outer) tail surface (psi)
$\Delta p$	differential pressure, $p_{in} - p_{out}$ (psi)
$q_\infty$	freestream dynamic pressure (psi)
$t$	time (sec)
$U_\infty$	freestream velocity (ft/s)
$\bar{y}_j$	distance from root of tail to centroid of j-th tail area element (ft)
$\alpha$	angle of attack (degrees)

$\bar{\quad}$  indicates steady (mean) value

$(\quad)$  indicates root-mean-square value

$(\quad)''$  indicates power spectral density

**1. INTRODUCTION**

Buffet is a primary cause of structural fatigue of tails in many twin-tail fighter aircraft. The F/A-18, in particular, experienced fatigue problems due to tail buffet caused by breakdown of the vortices shed from the leading edge extensions (LEXs) at high angles-of-attack<sup>1,2</sup>. The severity of this problem was reduced by installing a trapezoidal vertical plate, which is known as the LEX fence, on each LEX just forward of the wing-fuselage junction<sup>1,2</sup>. Interaction of the LEX vortices with the LEX fence alters the characteristics of the unsteady forces imposed on the vertical tails, thereby reducing the severity of the buffeting response<sup>1,2</sup>.

The results of full-scale wind-tunnel tests, designed to quantify the pressure field that exists on the F/A-18 starboard tail in a buffet environment at various angles of attack and sideslip, are shown here. The resulting root bending moment coefficients are also illustrated. F/A-18 tail buffet has been studied intensively in both the experimental<sup>1-9</sup> and computational arenas<sup>10,11</sup>, but the full-scale tests described herein present a unique opportunity to explore several aspects of the tail buffet phenomenon without the model geometric scaling constraints present in most reduced-scale wind-tunnel studies.

The principal objectives of the full-scale tests were: (1) to quantify the steady and unsteady pressures that exist on the vertical tail in a buffet flow environment over a wide range of angle of attack and sideslip conditions, (2) to further quantify the effects of the LEX fence in reducing tail buffet, and (3) to provide detailed data for comparison with reduced-scale wind tunnel and computational results available from other sources<sup>12</sup>.

The results of the 1/6-scale wind-tunnel tests, designed to quantify the pressure field that exists on the F/A-18 starboard tail in a buffet environment at various angles-of-attack, are described herein.

The primary objectives of the 1/6-scale tests were: (1) to determine the effectiveness of the rudder, of piezoelectric actuators, and of other aerodynamic devices in alleviating buffeting, (2) to quantify the phasing of the differential

\* Program Manager, 1/6-Scale Study known as Actively Controlled Response Of Buffet Affected Tails (ACROBAT), Aeroelasticity Branch, MS 340, NASA Langley Research Center, Hampton, VA 23681-0001

\*\* Program Manager, Full-Scale Study, Wright Laboratory, Wright-Patterson Air Force Base, Ohio 45433

unsteady pressures that exist on the vertical tail in a buffet flow environment over a wide range of angle of attack, (3) to further quantify the propagation speed of the unsteady pressure as it moved down the tail, and (4) to provide detailed data for comparison with full-scale data from other sources<sup>12</sup>.

The purpose of this paper is to highlight the similarities and differences between the full-scale and 1/6-scale wind-tunnel data by comparing power spectra, cross spectra, and scaling relationships. Of primary interest is the phase reported in the cross spectral densities for differential pressures between leading-edge and trailing-edge stations.

## 2. EXPERIMENTAL SETUPS

### 2.1 80x120 Wind Tunnel and Full-Scale Test Article

The test article, supplied by the US Navy, was from the first F/A-18 model A production block. The engines and avionics were removed prior to shipment to the wind tunnel. For these studies, the test article was configured with flow-through inlets and the missile rails were left in place. The test article, installed in the 80- by 120-Foot Wind Tunnel at the NASA Ames Research Center, is shown in Figure 1.

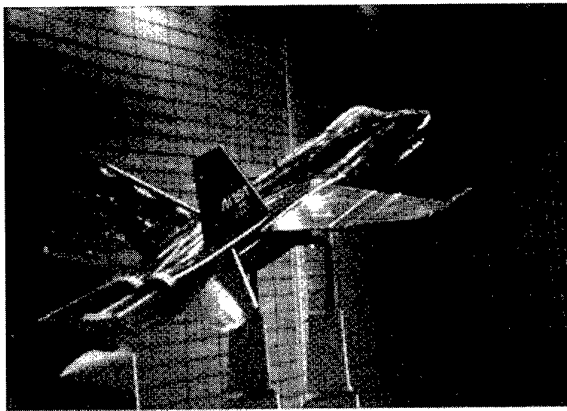


Figure 1. The F/A-18 in the 80'x120' Wind Tunnel at the NASA Ames Research Center

Geometric dimensions of the F/A-18 aircraft are: overall length (56.0 ft), wing span (37.42 ft), wing reference area (400 ft<sup>2</sup>), wing mean aerodynamic chord (11.52 ft), and vertical tail reference area (52.12 ft<sup>2</sup>). The leading-edge flaps were fixed at a deflection angle of 34 degrees down and the trailing-edge control surfaces were fixed at a zero deflection angle for all runs. These control surface settings are representative of the standard control-law scheduled deflections for angles-of-attack greater than 26 degrees. The rudders were fixed in their zero deflection position throughout the test envelope, and the horizontal stabilators were actuated to match the orientation of those on the High Angle-of-Attack Research Vehicle (HARV) for steady, trimmed flight at each angle of attack.

Pressures and tip accelerations were measured on the starboard vertical tail surfaces of the F/A-18 full-scale model.

### 2.2 TDT and 1/6-Scale Test Article

The test article was a 1/6-scale F-18 A/B drop model that was outfitted with interchangeable rigid and flexible vertical tails on both sides. The starboard vertical tails were configured with an active rudder for performing buffeting alleviation studies.

Likewise, the deflection angles of the leading-edge flaps, trailing edge flaps, rudder (when not actuated), and the horizontal stabilators were set identically to the F/A-18 aircraft as listed above.

Pressures, root strain, and tip accelerations were measured on the starboard and port vertical tail surfaces. The test article, installed in the TDT at the NASA Langley Research Center, is shown in Figure 2.



Figure 2. The 1/6-Scale F/A-18 model in the Transonic Dynamics Tunnel at the NASA Langley Research Center

### 2.3 Ground Vibration Test of Full-Scale Tails

A ground vibration test (GVT) was conducted in preparation for the full-scale tests to determine the modes and natural frequencies of the tail structure when the full-scale model was mounted on the wind-tunnel struts. Table 1 lists the resulting symmetric (S) and anti-symmetric (A) modes and natural frequencies of the vertical tails. Levrera et al<sup>13</sup> give further information on the dynamic characteristics of the vertical tails, including mode shapes.

Table 1. Full-Scale Vertical Tail Modes

Mode	Frequency (Hz)
1st bending (S, A)	15.4, 15.3
1st torsion (S, A)	44.2, 45.4
2nd bending (S, A)	61.3, 61.9

### 2.4 Ground Vibration Test of 1/6-Scale Tail

A GVT was conducted on the 1/6-scale model to determine the modes and natural frequencies of the tail structure when the 1/6-scale model was sting-mounted in the TDT. Table 2 lists resulting natural frequencies for the modes of the flexible tails.

During the GVT, a rigid vertical tail was mounted on the port side, opposite the flexible tail on the starboard side. The modes reported in Table 2 are for the starboard tail only.

Table 2. 1/6-Scale Vertical Tail Modes

Mode	Frequency (Hz)
1st bending	16.5
1st torsion	58.5
2nd bending	71.5

## 2.5 Instrumentation on Full-Scale Model

Seventy-two Kulite pressure transducers (model LQ-167-125-10SG) were mounted on the starboard vertical tail of the F/A-18 prior to installation of the test article in the wind tunnel. These sensors were located in a 6-by-6 grid on either side of the tail as illustrated in Figure 3.

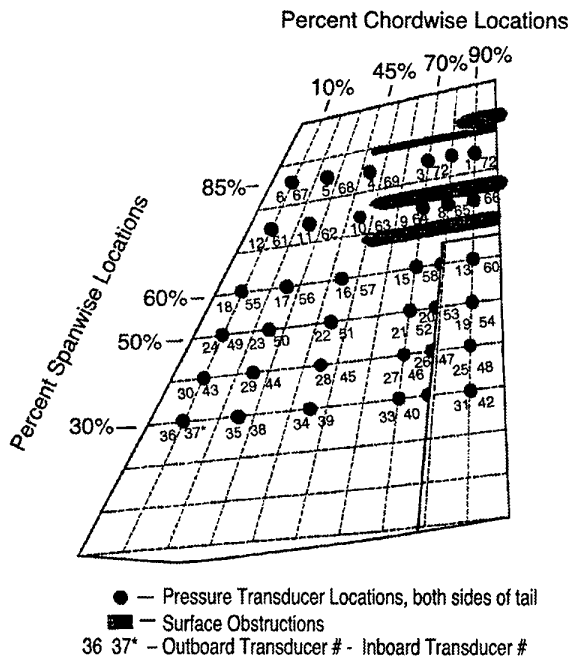


Figure 3. Pressure Transducer Locations on Full-Scale Starboard Vertical Tail

## 2.6 Test Procedure for Full-Scale Model

Steady and unsteady data were acquired for approximately 30 seconds at each test condition. Each channel was sampled simultaneously at a rate of 3.32 samples per sampling cycle. Each of the signals passed through an anti-aliasing, 6 pole butterworth filter with a nominal cut-off frequency of 500 Hz prior to digitization. The transducer signals then passed through one of five Aydin-Vector pulse code modulation (PCM) multiplexers (model SCU-700-16), which digitized the signals prior to their being recorded on magnetic tape.

## 2.7 Instrumentation on 1/6-Scale Model

Twenty-eight, thirty, and thirty Kulite pressure transducers (model LQ-167-125-10SG) were mounted on the starboard flexible vertical tail, starboard rigid vertical tail, and port rigid vertical tail, respectively, of the 1/6-scale F/A-18 model prior to installation of the test article in the wind tunnel. These sensors were located in the pattern on either side of the tail as illustrated in Figures 4 and 5 for the starboard flexible and starboard rigid tails, respectively. The pattern on the starboard flexible tail was chosen for investigating pressures created by the responses of the flexible tails to buffet. Therefore, the transducers are concentrated toward the tip of the tail.

The flexible tails' response to buffet was measured using a full-bridge strain gage at the root and two tip accelerometers (leading edge and trailing edge).

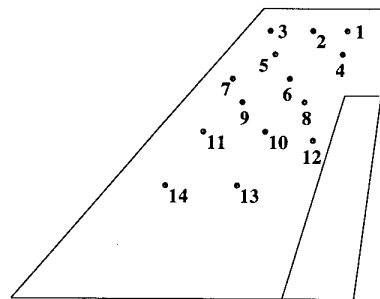


Figure 4. Pressure Transducer Locations on 1/6-Scale Starboard Flexible Vertical Tail

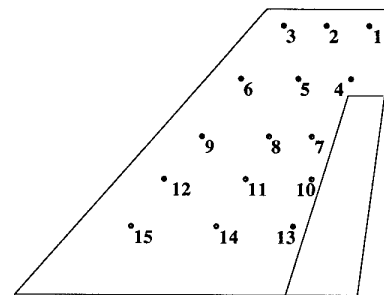


Figure 5. Pressure Transducer Locations on 1/6-Scale Starboard Rigid Vertical Tail

## 2.8 Test Procedure for 1/6-Scale Model

Steady and unsteady data were acquired for approximately 30 seconds at each test condition. Each channel was sampled simultaneously at a rate of 3.27 samples per sampling cycle. Each of the signals passed through an anti-aliasing, 6 pole butterworth filter with a nominal cut-off frequency of 2000 Hz prior to digitization. The transducer signals then passed through one of three Aydin-Vector pulse code modulation (PCM) multiplexers

(model SCU-700-16), which digitized the signals prior to their being recorded on magnetic tape.

This system is the same system used in the full-scale test except that a faster sampling rate was used. To resolve the propagation speed of the unsteady pressure wave as it moves past the vertical tail, a sampling rate higher than 500 Hz was necessary. Therefore, the only alternative sampling rate for the system, 2000 Hz, was chosen. Thus, time domain analysis in addition to frequency domain analysis could be used in characterizing the flowfield during buffet.

## 2.9 Full-Scale Test Conditions

A wind-off, baseline run was performed to record the null levels of the pressure transducer signals before the buffet tests were initiated.

Fifty-nine runs were conducted at a freestream velocity of 168 ft/s, which corresponded to a dynamic pressure of 33 psf, a Mach number of 0.15, and a Reynolds number of  $1.23 \cdot 10^7$  based on the mean aerodynamic chord. The four remaining runs were conducted at a freestream velocity of 102 ft/s and a dynamic pressure of 20 psf. Angle of attack was varied from 20 to 40 degrees for all runs.

## 2.10 1/6-Scale Test Conditions

Over sixty runs were completed during two TDT entries at various angles-of-attack without a LEX fence. Prior to and after each run, wind-off, baseline pressure signals were acquired to record the null levels of the transducers.

Most of the runs were conducted in atmospheric air at a freestream velocity of 110 ft/s, which corresponds to a dynamic pressure of 14 psf, and a Mach number of 0.10. This condition was chosen by scaling, using the Strouhal number, a full-scale condition of 340 psf at which severe buffeting occurs<sup>11</sup>.

## 3. Data Reduction

### 3.1 Full-Scale Model

Reduction of the pressure transducer signals initially involved subtracting the pressure values obtained during the baseline run from each of the subsequent pressure signals. This process ensured that all pressures were measured relative to the proper zero reference levels since the microphones could not be nulled in the tunnel.

Steady pressure differences at each transducer-pair station were computed by subtracting the mean of the outer surface transducer signal from the mean of the inner surface transducer signal. The unsteady, or buffet, pressures were assumed to be zero-mean, stationary random processes amenable to standard analysis techniques in the time and frequency domains. Differential pressure time histories were computed at each transducer-pair station for each test condition by subtracting the outer surface pressure reading from the inner surface pressure reading at each time step.

The differential pressure and acceleration time histories were converted to the frequency domain using Fast Fourier Transform (FFT) techniques. Approximately 15 seconds of

data from each test condition were divided into blocks, each containing 2048 samples. A Hanning window was applied to reduce bandwidth leakage, and an average of 22 transforms with 50% overlap was used to increase statistical confidence. The resulting frequency resolution was 0.8 Hz. Power spectral density (PSD) functions were computed from the Fourier transforms. Root-mean-square (RMS) values of unsteady pressures and accelerations were then computed from the PSDs via numerical integration.

The dimensionless form chosen for presenting the buffet pressure spectra normalized by the freestream dynamic pressure is suggested by Mabey<sup>14</sup>:

$$\left(\frac{p'}{q_\infty}\right)^2 = \int_{n=0}^{n=\infty} F(n) dn = \int_{\ln(n)=-\infty}^{\ln(n)=+\infty} nF(n) d(\ln n) \quad (1)$$

where  $F(n)$  is the nondimensional buffet excitation power spectral density in terms of the frequency parameter,  $n$ . The resulting fluctuations of the pressures, normal force, and bending moment are plotted as  $\sqrt{nF(n)}$  vs  $n$  from  $n=0$  to 8. For  $q_\infty = 33$  psf and  $\bar{c} = 11.54$  ft,  $n = 1$  corresponds to a dimensional frequency of 14.56 Hz.

### 3.2 1/6-Scale Model

The unsteady, or buffet, pressures were assumed to be zero-mean, stationary random processes amenable to standard analysis techniques in the time and frequency domains. Differential pressure time histories were computed at each transducer-pair station for each test condition by subtracting the outer surface pressure reading from the inner surface pressure reading at each time step.

The differential pressure and root strain time histories were converted to the frequency domain using Fast Fourier Transform (FFT) techniques. Approximately 16 seconds of data from each test condition were divided into blocks, each containing 8192 samples. A rectangular window was applied to reduce bandwidth leakage, and an average of 9 transforms with 75% overlap was used to increase statistical confidence. The resulting frequency resolution was 0.2 Hz. Power spectral density (PSD) functions were computed from the Fourier transforms.

The dimensionless form chosen for presenting the buffet pressure spectra normalized by the freestream dynamic pressure is:

$$F(n) = P(f) / q_\infty^2 \cdot (U_\infty / \bar{c}) \quad (2)$$

where  $P(f)$  is the power spectral density of the pressure. The resulting fluctuations of the pressures are plotted as  $\sqrt{nF(n)}$  vs  $n$  from  $n=0$  to 5 for a  $q_\infty = 14$  psf and  $\bar{c} = 1.92$  ft.

## 4. Results and Discussions

### 4.1 Full-Scale Model Root-Mean-Square Tail Buffet Loads

Time histories of the unsteady root bending moment coefficient were calculated from the unsteady differential pressures using:

$$C_{M_B}(t) = \frac{1}{q_{\infty} A_F \bar{c}} \sum_{j=1}^{36} \Delta p_j(t) A_j \bar{y}_j \quad (3)$$

where  $\Delta p_j(t) = [p_{in}(t) - p_{out}(t)]_j$  is the differential pressure time history at the j-th transducer-pair station,  $A_j$  is the area element around the transducer, and  $\bar{y}_j$  is the distance from the root to the centroid of the area element. The corresponding root-mean-square values of the unsteady bending moment coefficients are denoted symbolically by  $C'_{M_B}$ .

Figure 6 shows the variation of the RMS value of bending moment coefficient with angle of attack at zero sideslip. The LEX fence produced a considerable decrease in  $C'_{M_B}$  from 20 to 36 degrees angle of attack, but the fence-on and fence-off curves converge at an angle of attack of 40 degrees.

Dynamic pressure scale effects are also depicted in Figure 6, where results at 26 and 28 degrees angle of attack for a freestream dynamic pressure of 20 psf are overlaid on the results for 33 psf. For these two angles of attack, this result supports previous findings that the RMS values of the buffet pressures that were used to calculate the time histories of the root bending moment are linear functions of the dynamic pressure in the freestream.<sup>3</sup>

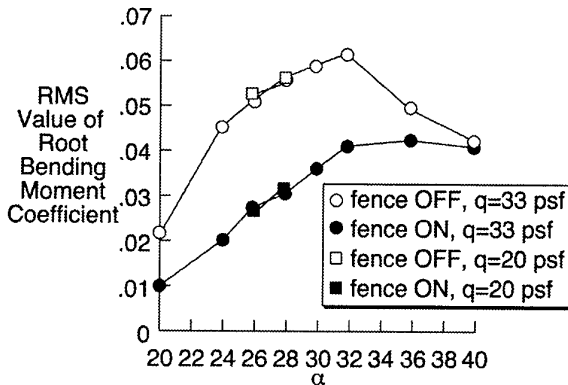


Figure 6. RMS Value of Root Bending Moment Coefficient vs. Angle of Attack in Degrees

#### 4.2 1/6-Scale Model Root-Mean-Square Tail Buffet Loads

The buffet loads on the 1/6-scale vertical tail were obtained more directly by computing the root-mean-square of the time history for the strain gage located at the root of the flexible tail.

Figure 7 shows the variation of the RMS root strain with angle of attack for a dynamic pressure of 14 psf. As shown in Figure 7, the peak buffeting occurs around 36 degrees angle of attack. Several factors could contribute to the peak occurring at 36 degrees rather than 32 degrees angle of attack which was the case for the full-scale model. These factors may include participation of other modes, angle-of-attack calibration for the sting in the TDT prior to the test, or a slightly different vortex trajectory off the LEX. To isolate

the factors due to other modes of the model, the PSD of root strain at the frequency of the first bending mode was computed. Presented as normalized values in Figure 8, the PSDs indicated that the maximum response in the first bending mode occurred around 34 degrees angle of attack.

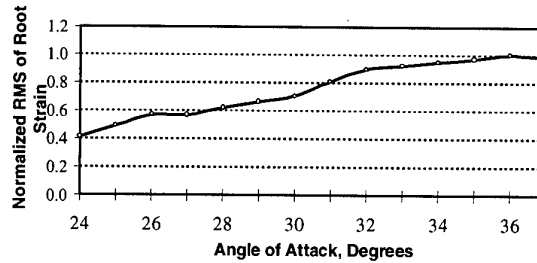


Figure 7. Normalized RMS of Root Strain on 1/6-Scale Vertical Tail

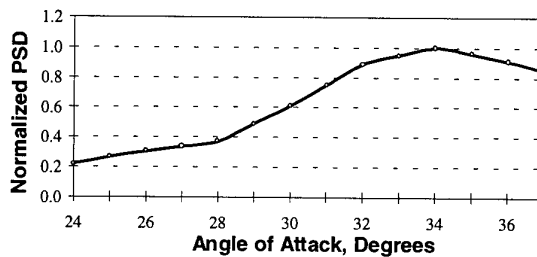


Figure 8. Normalized PSD of Root Strain (at Frequency of First Bending Mode) on 1/6-Scale Vertical Tail

#### 4.3 Full-Scale Model Buffet Pressures-Excitation Spectra

Figure 9(a) and 9(b) present spectra, RMS form, for the transducer-pair station located at 45% chord and 60% span, at two angles of attack. Both LEX fence-off and fence-on results are presented for comparison. At  $\alpha = 20^\circ$  in Figure 9(a), the peak of the curve for fence off is rather broad and centered about  $n=0.9$ ; however, the peak is considerably sharper at  $\alpha = 32^\circ$  and centered at  $n=0.6$  in Figure 9(b).

#### F-18 Tail Buffet Test: Q=33 Alpha=20 Beta=0

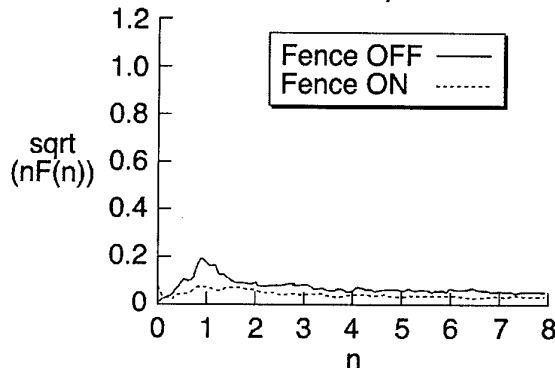


Figure 9(a). Excitation Spectra of Pressures on Full-Scale Tail,  $\alpha = 20^\circ$ ,  $q = 33$  psf



This concentrating of the buffet energy into a narrow frequency band with a higher peak as angle of attack is increased (up to the occurrence of maximum buffet) is typical for the F/A-18. This trend is also noted elsewhere.<sup>1,3</sup>

**F-18 Tail Buffet Test: Q=33 Alpha=32 Beta=0**

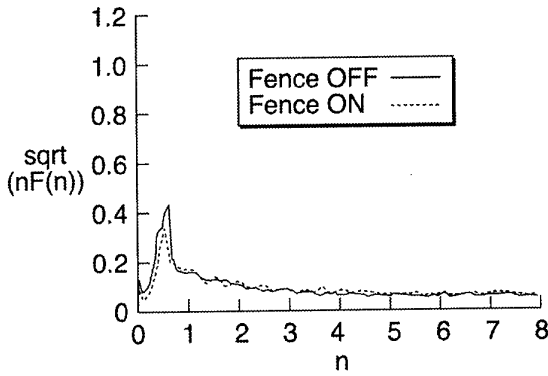


Figure 9(b). Excitation Spectra of Pressures On Full-Scale Tail,  $\alpha = 32^\circ$ ,  $q = 33$  psf

**4.4 1/6-Scale Tail Buffet Pressures - Excitation Spectra**

Figure 10(a) and 10(b) present spectra, RMS form, for the transducer-pair station located at 50% chord and 60% span, at two angles of attack. There is no LEX fence on the

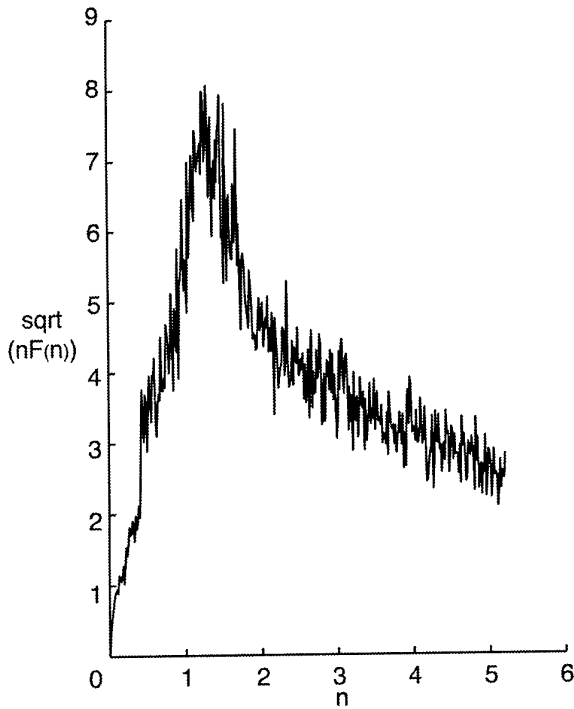


Figure 10(a). Excitation Spectra of Differential Pressures on 1/6-Scale Flexible Tail,  $\alpha = 20^\circ$

1/6-scale model. At  $\alpha = 20^\circ$  in Figure 10(a), the peak of the curve is rather broad and centered about  $n=1.2$ ; however, the peak is considerably sharper at  $\alpha = 32^\circ$  and centered about  $n=0.5$  in Figure 10(b). Like the F/A-18, this concentrating of the buffet energy into a narrow frequency band with a higher peak as angle of attack is increased (up to the occurrence of maximum buffet) is typical for the 1/6-scale model.

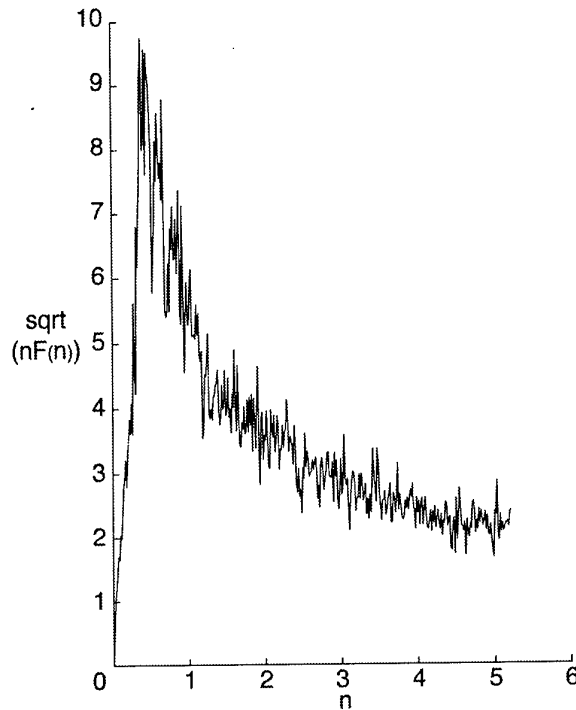


Figure 10(b). Excitation Spectra of Differential Pressures on 1/6-Scale Flexible Tail,  $\alpha = 32^\circ$

**4.5 Full-Scale Tail Buffet Loads-Power Spectral Densities**

Power spectral densities of the root bending moment coefficients were determined from the time histories defined by Equation (3) for each test condition. Representative bending moment coefficient PSDs are presented in Figure 11. Normally, these PSDs would have dimensions of  $\text{Hz}^{-1}$  since  $C_{MB}$  is dimensionless. Here, the normal force and bending moment coefficient PSDs have been made dimensionless through multiplication by  $U_\infty / \bar{c}$ .

Figure 11 depicts the root bending moment coefficient power spectral densities,  $C''_{MB}$ , for angles of attack of 20 and 32 degrees. As depicted in Figure 11, the frequency at which the peak bending moment was exerted on the tail decreased with angle of attack. This trend corresponds to the frequency shift with angle of attack discussed previously for the buffet pressures.

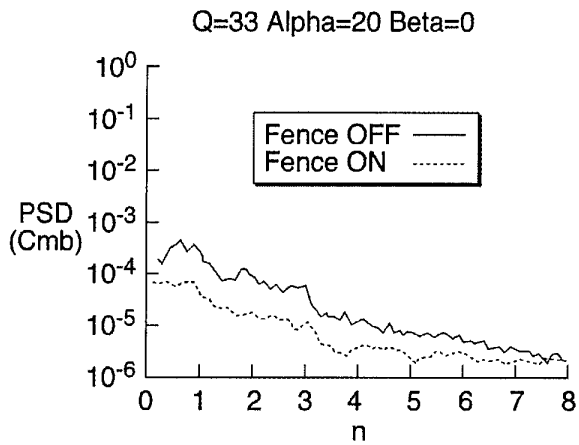


Figure 11(a). PSD of Full-Scale Root Bending Moment Coefficient,  $\alpha = 20^\circ$ ,  $q=33$  psf

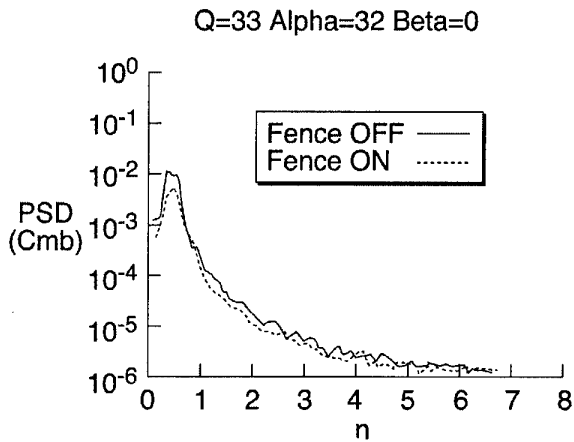


Figure 11(b). PSD of Full-Scale Root Bending Moment Coefficient,  $\alpha = 32^\circ$ ,  $q=33$  psf

#### 4.6 1/6-Scale Model Buffet Loads-Power Spectral Densities

Power spectral densities of the tail root bending moment were computed from the time histories of the root strain gage. PSDs of the tail root bending moment for  $\alpha = 20^\circ$  and  $\alpha = 32^\circ$  are presented in Figure 12.

In Figure 12, the peak value and the value at 58 Hz correspond to the first bending mode and first torsion mode of the tail, respectively. The response in the first bending mode has grown with the increase in angle of attack while the response in the first torsion mode has diminished slightly. This trend is related to the frequency shift of the excitation spectra with increased angle of attack illustrated in Figure 10.

In both the full-scale test and the 1/6-scale test, the maximum value of the PSD (corresponding to first bending)

grows by at least one order of magnitude at  $\alpha = 32^\circ$  from its original value at  $\alpha = 20^\circ$ .

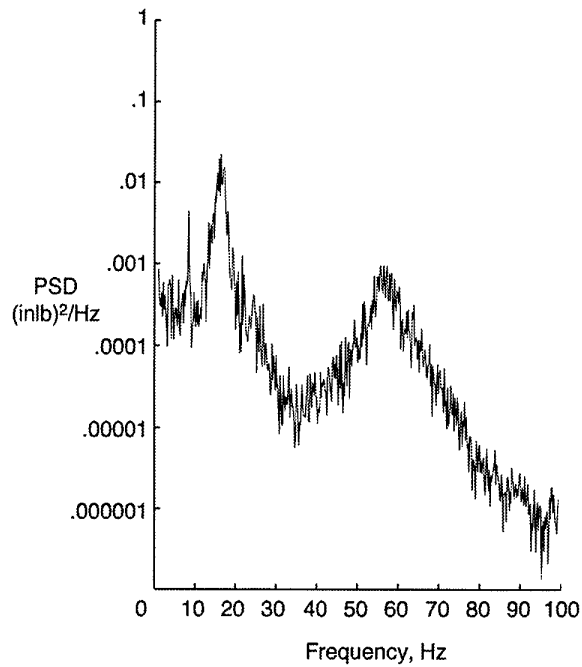


Figure 12(a). PSD of Tail Root Bending Moment, 1/6-Scale Model,  $\alpha = 20^\circ$ ,  $q=14$  psf

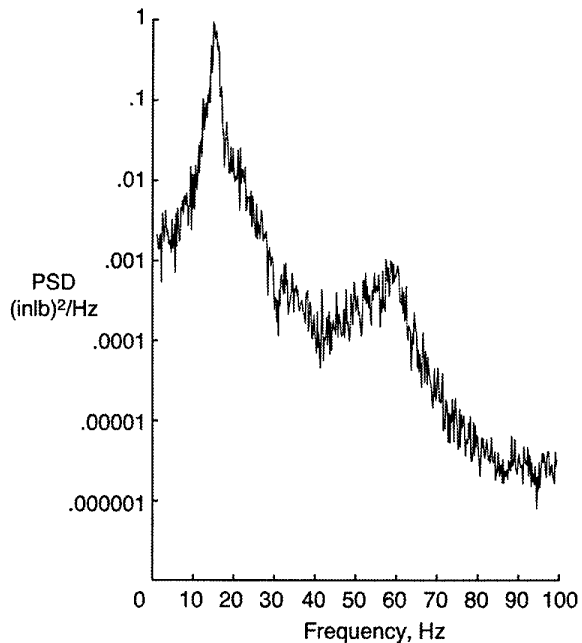


Figure 12(b). PSD of Tail Root Bending Moment, 1/6-Scale Model,  $\alpha = 32^\circ$ ,  $q=14$  psf

#### 4.7 Full-Scale Model Buffet Pressures-Cross Spectral Densities

Further insight into the tail buffet process was gained by computing cross spectral densities (CSDs) between the surface pressures acting on the inboard and outboard surfaces at selected locations on the tail. For a given transducer station  $j$ ,  $CSD[(p_{in}, p_{out})_j]$  was computed for both the LEX fence-off and -on test conditions at angles of attack of 20 and 32 degrees with zero sideslip. These CSDs are presented as coherence and phase angle functions, which are dimensionless. No effort was made to account for any artificial coherence in the pressures due to any response of the tail to the buffet.

CSDs of the unsteady pressure signals from transducer stations near the tip of the tail and along its leading edge generally displayed the strongest levels of buffet excitation. The coherence, magnitude, and phase functions in Figures 13 and 14 for the 40% span, 10% chord location were typical for the LEX fence-off case at 20 and 32 degrees angle of attack, respectively.

In Figures 13 and 14, the coherence levels are highest in the lower frequencies. Accordingly, the curves for the magnitude and phase are the smoothest at the lower

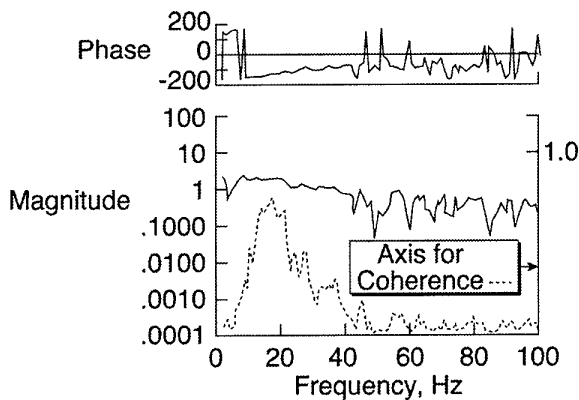


Figure 13. CSD Between Inboard and Outboard Pressures, Full-Scale Tail,  $\alpha = 20^\circ$ ,  $q = 33$  psf, LEX fence off

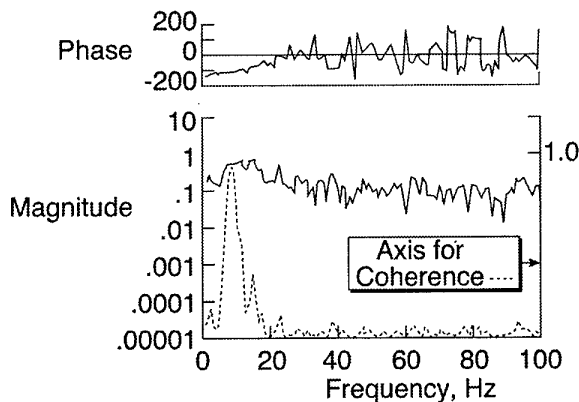


Figure 14. CSD Between Inboard and Outboard Pressures, Full-Scale Tail,  $\alpha = 32^\circ$ ,  $q = 33$  psf, LEX fence off

frequencies. Therefore, high coherences indicate high accuracy in the assumed linear input/output relationship between the two signals<sup>15</sup>. The frequency ranges of high coherence exhibited phase angles greater than 100 degrees. This implies that the pressures at a station on the inboard side opposite a station on the outboard side of the tail were not in-phase when tail buffet occurred, resulting in a net differential pressure at that station. This phase relationship would seem to be necessary to account for the net buffet excitation represented by the root bending moment PSDs in Figure 11.

Cross Spectral Densities of the differential pressures at the one station referenced to the differential pressures at another station were also computed. The phase indicated in the cross spectral densities of the differential unsteady pressures between leading-edge and trailing-edge stations offer significant insight into the application of the buffet loads. For instance, if, for some given flight speed, the differential pressures are applied to the tail in a torquing manner (at or near 180 degrees phase between leading-edge and trailing-edge stations), then the participation of the torsion mode in the fatigue of the vertical tail cannot be ignored. However, if this phase relationship is considerably less than 180 degrees, then the participation of the torsion mode in the fatigue of the vertical tail may be less significant.

The phase between the differential pressure at the leading-edge and the differential pressure at the trailing-edge is shown in Figures 15 and 16. As shown in Figure 15, at 20 degrees angle of attack, the phase around the frequency of the torsion mode at 45 Hz for the full-scale tail is approximately 400 degrees (360 plus 40). This value is far from 180 degrees; however, its significance will be illustrated below when presenting the CSDs for the 1/6-scale test. Similar phase relationships can be extracted from additional CSD plots provided in the reports on the full-scale test<sup>12</sup>.

As seen in Figure 16, the phase relationship between the leading-edge and trailing-edge stations at  $\alpha = 32^\circ$  in the vicinity of the 45-Hz torsion mode cannot be easily extracted. Typical of the pressure data for the full-scale

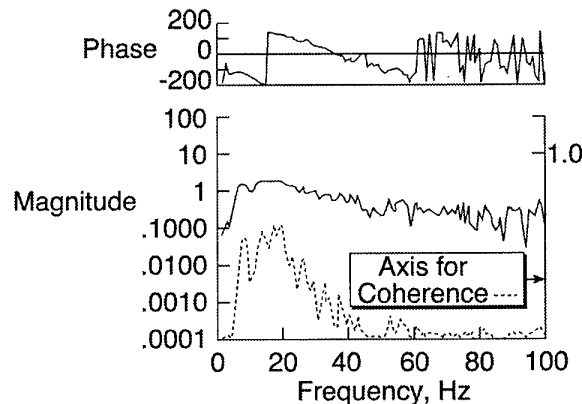


Figure 15. CSD Between Full-Scale Differential Pressures, Stations 1 and 5,  $\alpha = 20^\circ$ ,  $q = 33$  psf, LEX fence off

model at  $\alpha = 32^\circ$ , these low coherences at the higher frequencies are a result of the low dynamic pressure used in the 80x120 wind-tunnel. In general, by increasing the wind velocity in a tunnel for a given model, the magnitudes of the buffet pressures at the higher frequencies will increase, effectively shifting the peak of the spectra curve to a higher frequency.<sup>3</sup> Therefore, it is difficult, if not impossible, to determine the phase relationship in the vicinity of the torsion mode at the higher angles of attack for the full-scale model.

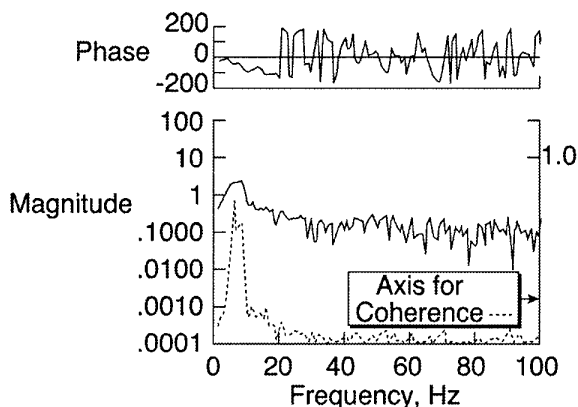


Figure 16. CSD Between Full-Scale Differential Pressures, Stations 1 and 5,  $\alpha = 32^\circ$ ,  $q = 33$  psf, LEX fence off

#### 4.8 1/6-Scale Model Buffet Pressures-Cross Spectral Densities

Cross spectral densities (CSDs) were computed between the unsteady pressures acting on the inboard and outboard surfaces and between the differential unsteady pressures at selected locations on the tail at angles of attack of 20 and 32 degrees. The CSD for the 40% span, 10% chord location at 32 degrees angle of attack is presented as magnitude and phase angle functions in Figure 17 for the flexible tail. Similar to the results shown for the full-scale model in Figure 14, the frequency ranges of high coherence exhibited phase angles greater than 100 degrees. As explained above, this phase relationship would seem to be necessary to account for the net buffet excitation represented by the root strain PSDs in Figure 12.

Cross Spectral Densities of the transducer pair at the leading-edge tip station referenced to the transducer pair at the trailing-edge tip station are shown in Figures 18 and 19 for the flexible tail. At 20 degrees angle of attack, the phase around the frequency of the 1/6-scale tail's torsion mode of 55 Hz is approximately 150 degrees. Therefore, the buffet pressure on the tail is applied in a torquing manner in addition to being applied at the frequency of the torsion mode.

To confirm that the motion of the tail is not producing this phase relationship seen in the pressures of the flexible tail, the same CSDs are plotted for the rigid tail. Comparing the data for the rigid tail in Figure 20 with the data for the flexible tail in Figure 18, the phase values reported on each figure for 55 Hz appear quite similar for 20 degrees angle of

attack. Therefore, the response of the tail to the buffet pressures at this angle of attack do not appear to effect the phase relationship around the torsion mode.

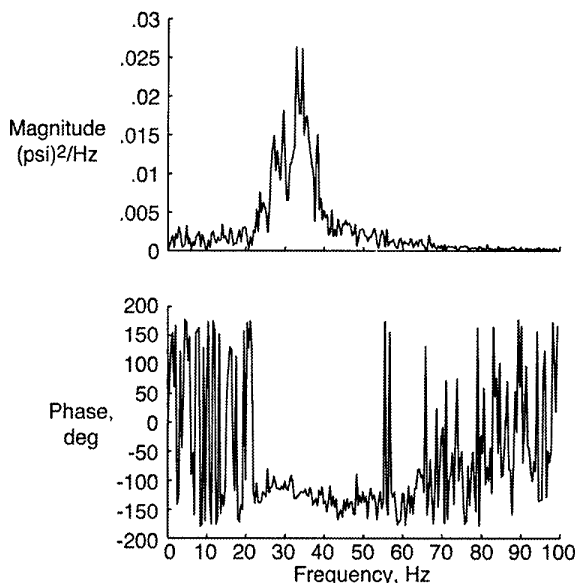


Figure 17. CSD Between Inboard and Outboard Pressures, 1/6-Scale Tail, 40% Span, 20% Chord,  $\alpha = 32^\circ$

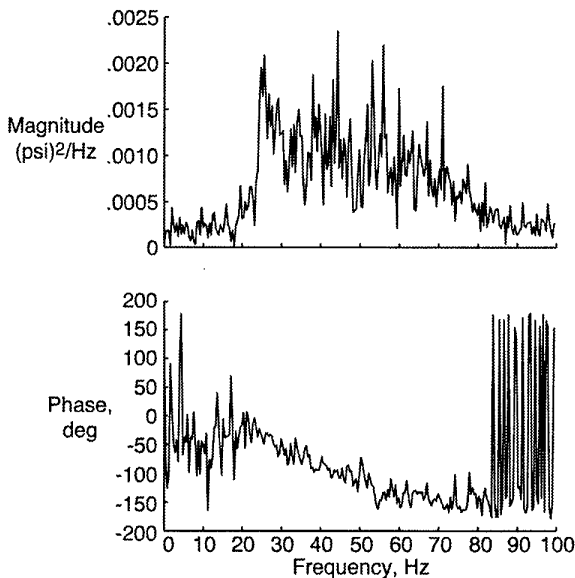


Figure 18. CSD Between 1/6-Scale Differential Pressures, Flexible Tail Stations 1 and 3,  $\alpha = 20^\circ$

At an angle of attack of 32 degrees, the phase relationship seen in Figure 19 has changed from the relationship seen in Figure 18 for an angle of attack of 20 degrees. The trajectory of the phase curve between the two stations at 32 degrees angle of attack appears lower than the trajectory of the phase curve at 20 degrees angle of attack, especially when comparing the phase values around 40 Hz on Figures 18 and 19. Although not illustrated but easily

supported by the steady root strains observed during the test, the trajectory of the vortex switched from the outboard side of the tail at the lower angle-of-attack to the inboard side of the tail at the higher angle of attack. Vortex position appears to have a direct effect on the phase relationship of the differential pressures between two stations along the vertical tail.

Comparisons of the phase characteristics of the 1/6-scale differential pressures to the full-scale differential pressures shows that a prediction of the full-scale phase can be made from 1/6-scale model data. From Figure 18, for the 1/6-scale tail, at an angle of attack of 20 degrees, the phase at the frequency of the torsion mode of 45 Hz for the full-scale tail is approximately 100 degrees. Again, from Figure 15, the phase measured on the full-scale tail at 45 Hz is approximately 400 degrees.

A scale factor between the phase of the 1/6-scale CSDs and the phase of full-scale CSDs can be derived from a relationship between angular velocity and time. Shown in Equation (4a), angular velocity can be converted to frequency, and time, t, may be obtained by dividing the distance, d, between two transducer stations by the velocity, v, of the freestream flow. The scale factor, shown in Equation (4b), is obtained by dividing the results of Equation (4a) for the 1/6-scale model by the results of Equation (4a) for the full-scale (aircraft) model.

$$\phi = \omega t = (2\pi f) \cdot \left(\frac{d}{v}\right) \quad (4a)$$

$$\left(\frac{\phi_{model}}{\phi_{aircraft}}\right) = \frac{f_m d_m v_a}{f_a d_a v_m} = 0.255 \quad (4b)$$

Using data presented earlier for both models and wind-tunnel conditions, the phase scale factor between the 1/6-scale and full-scale tails, for a frequency ratio of one, is 0.255. The ratio of the two values of phase stated above for 45 Hz is 0.25.

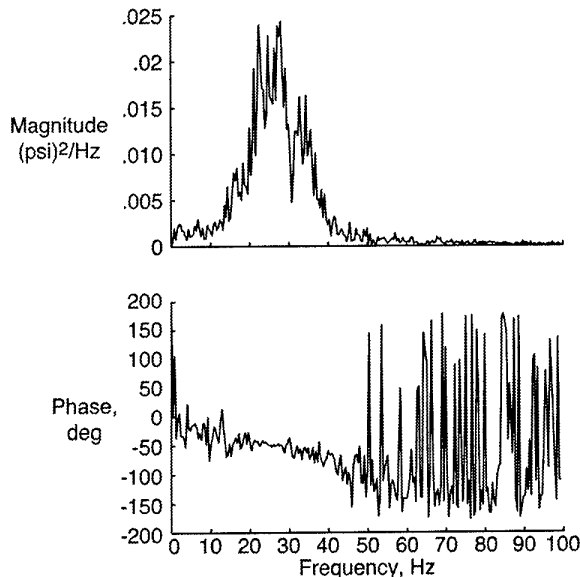


Figure 19. CSD Between 1/6-Scale Differential Pressures, Flexible Tail Stations 1 and 3,  $\alpha = 32^\circ$

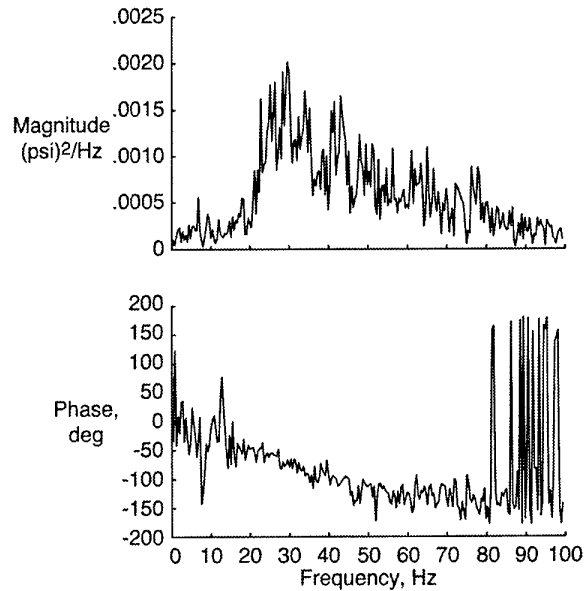


Figure 20. CSD Between 1/6-Scale Differential Pressures, Rigid Tail Stations 1 and 3,  $\alpha = 20^\circ$

Comparisons were made for the phase of the differential pressures at other stations on the full-scale and 1/6-scale with similar results. Rough estimates of the phase relationship for any two stations on the full-scale tail can be extracted from the CSDs of the 1/6-scale tail using equation (4). In addition, by using equation (4), one may predict the phase of the differential pressures at the frequency of any tail mode for other flight conditions. Since the first bending and first torsion mode are the only two modes that affect the fatigue life of the vertical tails on the F/A-18, the phase relationships of interest would be at the frequencies associated with these two modes.

Because the dynamic pressure used for the 1/6-scale model is the (scaled) equivalent of 340 psf for the full-scale aircraft, the magnitudes of the buffet pressure are higher at the higher frequencies for the higher angles of attack than seen in the full-scale data<sup>1,12</sup>. This is confirmed by comparing the data in Figures 14 and 19. In Figure 19 for the 1/6-scale model at 32 degrees angles of attack, the phase at 40 Hz is well below 100 degrees. Therefore, the buffet pressures are not being applied to the tail in a torquing manner at the higher angles of attack.

The loss in response of the tail in its torsion mode around 58 Hz at the higher angle of attack, as seen by comparing Figures 12(a) and 12(b), confirm two aspects of the buffet pressures at the higher angles of attack: 1) the buffet pressures are no longer being applied to the tail as a torque; and 2) the magnitudes of the buffet pressures around 58 Hz are significantly lower at the higher angles of attack than the magnitudes associated with the lower angles of attack.

The effects of the response of the flexible tail to the buffet in the first bending mode around 16 Hz can be seen in the magnitude and phase plotted in Figure 19. To confirm this, the CSD between the same two stations on the rigid tail

at the same conditions are provided in Figure 21. In Figure 21, the magnitude and phase around 16 Hz for the rigid tail is not as pronounced as shown in Figure 19 for the flexible tail.

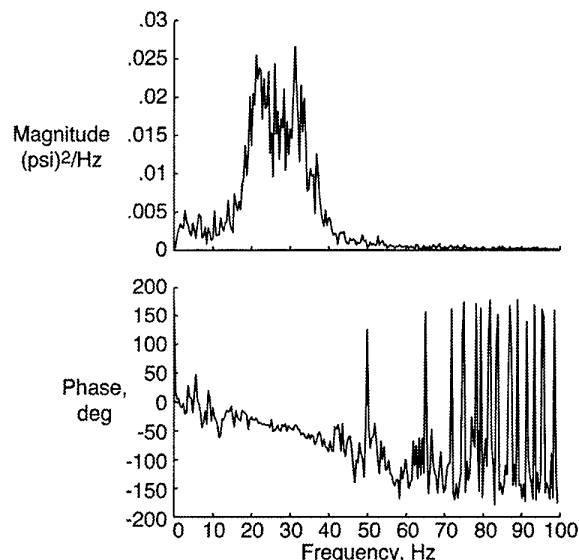


Figure 21. CSD Between 1/6-Scale Differential Pressures, Rigid Tail Stations 1 and 3,  $\alpha = 32^\circ$

## 5. Concluding Remarks

Full-scale wind tunnel tests were conducted to quantify the pressures responsible for inducing tail buffet on the F/A-18. The resulting tail-tip accelerations were also measured. The LEX fence was shown to effectively reduce the RMS root bending moments, as well as the corresponding spectral levels, up to 32 degrees angle of attack at zero sideslip. Higher angles-of-attack reduced the benefits of the LEX fence. Higher angles-of-attack caused the buffet pressures to be concentrated in a narrow, low frequency band. Dynamic pressure scale effects on the RMS root bending moment were found to be minimal under the current test conditions.

For the full-scale model, cross-spectral densities between the buffet pressures on the inside and outside surfaces of the starboard tail showed strong coherence and phase relationships at the lower angles of attack.

Wind tunnel tests of a 1/6-scale F/A-18 model were conducted at the Transonic Dynamics Tunnel to determine, among other aspects, the phase relationship of the unsteady pressures on the outboard and inboard surfaces (as well as differential) of flexible and rigid vertical tails on both sides of the model.

Comparison of the 1/6-scale data to the full-scale data reveal similarities in the trends of the spectral content as a function of angle of attack. The phase between inboard and outboard transducers at one station was nearly identical for both models. The phase of the differential unsteady pressures between two stations on the 1/6-scale model may be scaled up to identically located stations on the full-scale vertical tail using the scaling relationship in equation (4).

Equation (4) may also be used to predict the phase of the differential pressures at the frequency of any tail mode for other flight conditions.

## 6. Acknowledgements

The authors wish to acknowledge the cooperation of the NASA Ames and the NASA LaRC F/A-18 Wind Tunnel Test Teams especially. The authors also wish to acknowledge the technical advice provided by Dr. Holt Ashley of RANN Corporation and Dr. Marty Ferman, formerly of McDonnell Douglas Corporation.

## 7. References

- Pettit, C. L., Brown, D. L., and Pendleton, E., "Wind Tunnel Tests of Full-Scale F/A-18 Twin Tail Buffet: A Summary of Pressure and Response Measurements," AIAA-94-3476, proceedings of the AIAA Atmospheric Flight Mechanics Conference, Scottsdale, AZ, August 1994.
- Lee, B. H. K., Brown, D., Zgela, M., and Poirel, D., "Wind Tunnel Investigation and Flight Tests of Tail Buffet on the CF-18 Aircraft," in *Aircraft Dynamic Loads Due to Flow Separation*, AGARD-CP-483, NATO Advisory Group for Aerospace Research and Development, Sorrento, Italy, April 1990.
- Zimmerman, N.H. and Ferman, M.A., "Prediction of Tail Buffet Loads for Design Application," NADC-88043-60, July 1987.
- Shah, G.H., "Wind-Tunnel Investigation of Aerodynamic and Tail Buffet Characteristics of Leading-Edge Extension Modifications to the F/A-18," AIAA Paper 91-2889, August 1991.
- Meyn, L.A. and James, K.D., "Full Scale Wind Tunnel Studies of F/A-18 Tail Buffet," AIAA Paper 93-3519, August 1993.
- Lee, B.H.K. and Brown, D., "Wind-Tunnel Studies of F/A-18 Tail Buffet," *Journal of Aircraft*, Vol. 29, No. 1, Jan.-Feb. 1992.
- Lee, B.H.K. and Tang, F.C., "Buffet Load Measurements on an F/A-18 Vertical Fin at High-Angle-of-Attack," AIAA-92-2127-CP.
- Lee, B.H.K., Brown, D., Tang, F.C., and Plosenski, M., "Flowfield in the Vicinity of an F/A-18 Vertical Fin at High Angles of Attack," *Journal of Aircraft*, Vol. 30, No. 1, Jan.-Feb. 1993.
- Lee, B.H.K. and Tang, F.C., "Unsteady Pressure and Load Measurements on an F/A-18 Vertical Fin," *Journal of Aircraft*, Vol. 30, No. 5, Sept.-Oct. 1993.
- Rizk, Y.M. and Gee, K., "Numerical Prediction of the Unsteady Flowfield around the F-18 Aircraft at Large Incidence," AIAA Paper 91-0020, January, 1991.
- Ferman, M.A., Patel, S.R., Zimmerman, N.H., and Gerstenkorn, G., "A Unified Approach to Buffet Response of Fighter Aircraft Empennage," from *Aircraft Dynamic Loads due to Flow Separation*, AGARD-CP-483, 1990.
- Pettit, C.L., Banford, M., Brown, D., and Pendleton, E., "Pressure Measurements on an F/A-18 Twin

Vertical Tail in Buffeting Flow," Volume 1-4, WL-TM-94-3039, August 1994.

13. Levraea, V.J., Henderson, D.A., Pacia, A.P., and Banford, M.P., "Modal Survey of a Full-Scale F-18 Wind Tunnel Model," WL-TM-92-350-FIBG, September 1992.
14. Mabey, D.G., "Some Aspects of Aircraft Dynamic Loads due to Flow Separation," AGARD-R-750, 1987.
15. Bendat, J. S., and Piersol, A. G., Random Data, Wiley-Interscience, New York, 1986.

# THE IMPACT OF DYNAMIC LOADS ON THE DESIGN OF MILITARY AIRCRAFT

W. Luber, J. Becker, O. Sensburg  
Daimler Benz Aerospace AG  
Military Aircraft LMT2  
Postfach 80 11 60  
81663 München

## ABSTRACT

The layout of military aircraft structures is strongly influenced by dynamic loads from the early development phase onwards up to final design and clearance phase. Different dynamic loads have to be considered, namely dynamic gust loads, buffet loads on wing, fin, fuselage and also buffet loads from airbrakes, cavities and blisters, gunfire loads mainly at attachment frames and panels, Hammershock loads for air intake, bird strike and ammunition impact, acoustic loads for outer air intake and missile bays. Also dynamic loads from landing, jettison, brake chute and rough runway induced loads as well as wake induced loads may be designing. Dynamic loads resulting from flight test excitation like bunker input, stick jerks and control surface sweeps also have to be considered.

For some of the designing dynamic loads examples are given to explain their derivation and significance both for design of aircraft structural parts and related clearance aspects.

Methods to derive dynamic design loads for different application by using analytical and experimental tools will be presented.

Validation methods for various design loads using dynamic model test results, windtunnel model and flight test results are mentioned.

Main purpose of this presentation is to indicate where dynamic loads would be dimensioning structures of future high performance combat airplanes and how to approach the problem of integrating all aspects into an optimum design.

## 1. INTRODUCTION

Experience of in service modern fighter aircraft has shown many problems due to the fact that dynamic loads had not been considered with care during design and early flight clearance phase. Very well known are problems due to wing buffet and outer wing redesign after flight testing, known are also vibration problems and connected local structural fatigue of fin structure especially for aircraft with double fins. Acoustic fatigue is known for outer intake structure and in missile bay structure. Gunfiring effects if not considered from the beginning have created often

redesign of frame structures and requalification of equipment.

Therefore the combat aircraft design approach was to include dynamic loading from the beginning to avoid costly redesign phases.

Some examples of dynamic load derivation and application in military aircraft design are described and validation methods of dynamic loads are outlined.

## 2. GENERAL DESIGN CONSIDERATIONS

### 2.1 Structural design criteria

Combinations of gust design speeds and aircraft speeds are considered following MIL-A-8861A for the discrete 1-cosine gusts to the limits:

Gust intensity [ fps ]	Aircraft speed [ KEAS ]	Description
25	$V_L$	Design Dive Speed
50	$V_H$	Design Cruise Speed
66	$V_G$	Design Gust Speed

Gust encounter to be applied at 1g level flight, covering all gust lengths between 5 and 25 wing chord reference length.

A 25 fps vertical gust up to  $V_H$  shall also considered at  $0.6 \cdot n_{zmax}$

### 2.2 Requirements

A robust design shall be achieved through variation of mass distribution at the extremes of the aircraft in a conservative manner and full consideration of the all worst flight conditions.

Flexible aircraft gust loads from discrete tuned gust analysis have fully to be considered for structural design.

## 3. EXAMPLES OF DYNAMIC LOAD CALCULATIONS AND VALIDATION

### 3.1 Dynamic gust loads

Methods are well established for the calculation of the flexible aircraft in turbulence, see Ref. 1-4.





also for the derivation of the  $L_{EE}$ ,  $L_{RE}$ ,  $L_{ER}$ ,  $P_R$  and  $P_E$  matrices.

### Examples of aircraft response prediction

Some typical results of gust response calculations on a flexible aircraft investigation are listed here in order to demonstrate the importance of arising problems.

The investigated aircraft is a delta canard configuration with wing tip mounted stores. The first example shall illustrate the prediction of vibration levels on external stores and resulting dynamic wing loads due to discrete gusts (Fig. 1).

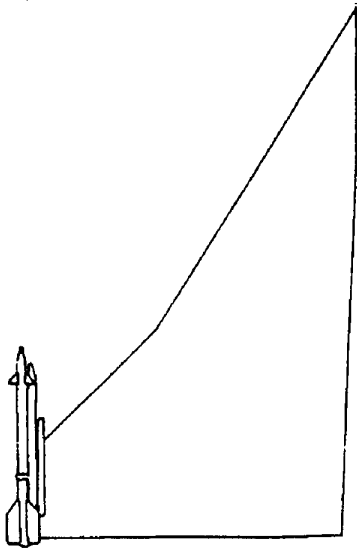


Fig.: 1 Wing with tip mounted missile

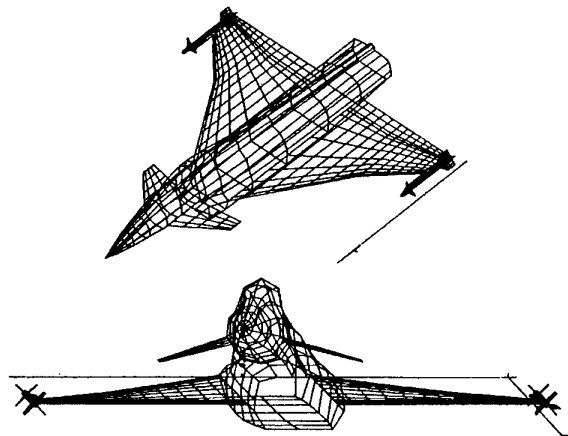
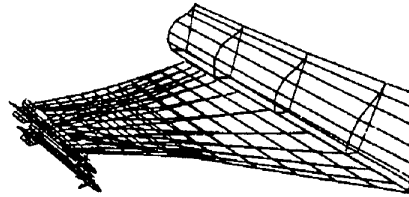


Fig.: 2 Aerodynamic Grid (Idealisation)

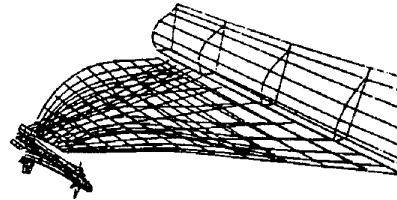
The total aircraft configuration is idealised for unsteady aerodynamic force calculation by the grid shown in Fig. 2. The unsteady aerodynamic derivatives and generalized forces together with load distributions on subcomponents are calculated with the programs

(Ref. 9-13) for the degrees of freedom aircraft angle of attack, rotation around centre of gravity, canard deflection, flap deflection and wing elastic normal modes shown in Fig. 3.

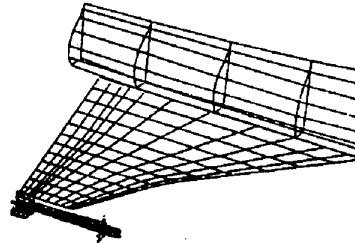
first wing bending



second wing bending



missile pitch



first wing torsion

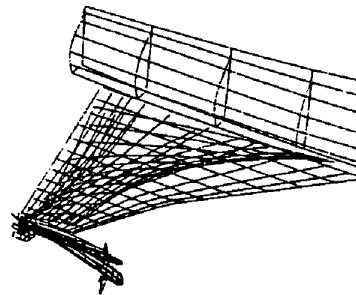


Fig.: 3 Vibration Modes

Fig. 4 documents very high accelerations on the tip mounted missile due to discrete gust caused mainly at short gust length (18 m) by the second elastic mode of the wing and also shows alleviation effect of the elastic wing on the response at long gust length (144 m) compared to the rigid response (full line).

The discrete gust response of the flexible aircraft results in wing shear and bending distributions as depicted in Fig. 5 and 6.

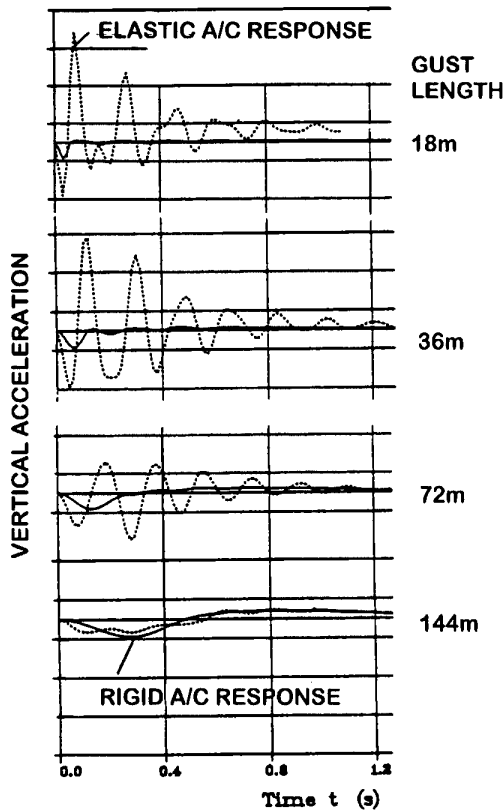


Fig.: 4 Discrete Gust Analysis: Acceleration at Missile Nose

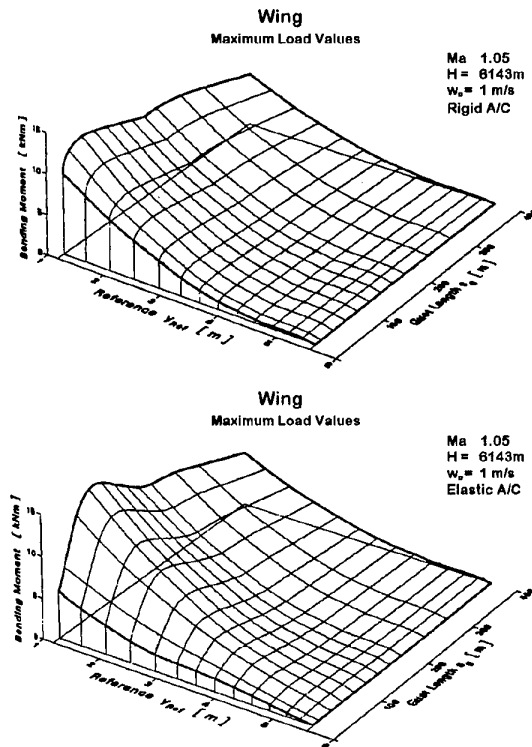


Fig.: 6 Design Gust Calculation: Wing Bending Moment

Very high wing loading is observed especially at wing outboard stations for different gust length compared to rigid response. Flexible aircraft gust loads from discrete tuned gust analysis have fully to be considered for structural design.

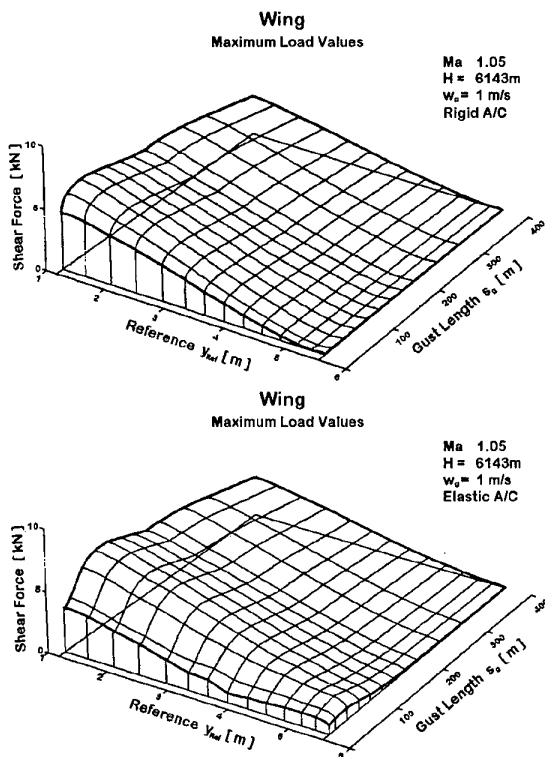


Fig.: 5 Design Gust Calculation: Wing Shear Force

### 3.2 Dynamic buffet loads

During the design of a highly manoeuvrable fighter aircraft, buffeting characteristics at high angles of attack have to be considered, Ref. 5. Buffeting defines dynamic loads for design as well as structural fatigue loads and vibration levels for equipment qualification. Vibration levels may for instance impose limits to the effectiveness of installed missiles, guns and of the radar. The general aim during the development phase is to predict the buffeting for wing, fin and fuselage by semiempirical procedures, which enable the approximate calculation of aircraft vibrations and dynamic loads of its substructures. The method which can be applied is based on experimental results of unsteady pressures on a windtunnel models. Fluctuating pressures due to flow separation have to be measured to derive excitation forces and unsteady motion dependent pressures due to harmonic oscillations in order to investigate the flow separation effects mainly on aerodynamic damping of elastic modes. Correction methods for the unsteady forces of arbitrary elastic modes of the aircraft structure have to be based on windtunnel measurements, Ref. 7.

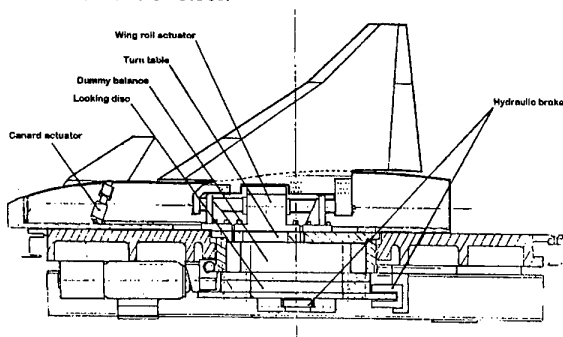
Assumptions for the prediction method are constant flight condition (constant incidence, Mach number, Reynolds number), small rigid and elastic amplitudes of vibration together with the assumption of decoupled fluctuating and motion induced forces. With these assumptions the buffet dynamic response problem is treated similar as the small perturbation gust response problem.

A description of the windtunnel models of wing and fin, the tests and test results of unsteady pressures and buffeting prediction results for wing tip and fin accelerations are described. The prediction method is tested using measured model response, and the predicted aircraft buffeting was compared to results of Mabey's method, Ref. 6.

### Outline of the Model Testing

#### Experimental set-up of wing model, Ref. 8, 14

The windtunnel tests were performed on a 1/7 scaled half model of an predesign aircraft configuration. The model configuration included a delta wing, a foreplane and half a fuselage installed at the windtunnel wall (Fig. 7). The wing and foreplane were very stiff, machined out of steel.



**Fig.: 7 Windtunnel Model Set Up**

The fuselage was fixed to the turn table by means of a large rigid cylindrical part locked when incidence was reached by a set of hydraulic brakes (Fig. 7). The fuselage contained two hydraulic actuators. The first one aligned with the foreplane axis, allowed to give static foreplane deflections while the second one aligned with the fuselage centre line provided roll excitation of the wing. Furthermore the wing actuator had to bear the very large steady moment of the wing at high Mach number and high angle of attack.

The different measurements performed were: steady and unsteady pressure fields, steady and unsteady moments and accelerations on the wing. The model was equipped with 67 pressure pick-ups, 67 steady pressure tapping, 7 accelerometers, 3 strain gauge bridges. The steady and unsteady pressure pick-ups pairs were distributed along four wing sections on the upper surface and, in a smaller number, along three wing sections on the lower surface.

Some of the unsteady pressure signals were recorded several times in order to get correlation both chordwise and spanwise. The signals were filtered in a frequency range of 5-150 Hz.

In the case of roll excitation of the wing, tests were performed using sinusoidal excitation. After conditioning and switching, amplifying and filtering at a cut-off frequency chosen between once and twice the excitation frequency, the signals were digitalized at a sampling rate of eight times the excitation frequency. Fourier analysis was performed on line, modules and phase of each signal, normalised to the amplitude of the roll oscillation were computed at the excitation frequency, giving unsteady pressure and moment coefficients.

Acceleration responses were also computed, allowing to check elastic deformations of the model.

Tests were performed for different Mach numbers and angles of attack including buffeting situations. The Mach number ranged from 0.6 to 0.95 incidence ranged from 0 to 12 degrees, decreasing as Mach number increased: 10 degrees at  $Ma = 0.85$  and  $0.9$  and 8 degrees at  $Ma = 0.95$ . The effect of the foreplane deflection on buffeting was investigated. Furthermore some measurements were performed without foreplane.

#### Experimental set up of fin model

Two methods are applicable for fin buffet predictions:

- unsteady flow measurements in the region of fin using a complete aircraft windtunnel model, see Ref. 15,16.

The Technical University Munich has developed a new method based on measured unsteady flow components from separated wing/fuselage flow at high incidence. The measured unsteady flow components can be transformed into unsteady pressures. The advantage of the method is in the early design phase, because high windtunnel model costs for direct unsteady pressure measurements can be avoided.

- unsteady pressure measurements on the fin of a complete aircraft windtunnel model.

A total aircraft windtunnel model (scale 1:15) with transducer fin for buffet (unsteady pressures) measurement was tested in the CALSPAN 8\*8 ft transonic windtunnel. 24 unsteady pressure pick ups on each side, 4 accelerometers and one bending moment sensor were installed. The tested incidence range was from 0 to 35 degrees, side slip from 0 to 10 degrees, foreplane incidence -10, 0, 5 degree and Machnumber range between 0.5 and 1.2, including also 0.95.

### The Buffet Prediction Method

The method is divided into two parts to evaluate

- the rigid aircraft response
- the elastic wing or fuselage response

where the total response consists of the rigid aircraft and the local elastic response.

The dynamic response calculation is performed for the longitudinal, symmetric and the lateral, antisymmetric motion of the aircraft using linearized equation of motion.

The rigid aircraft response is calculated from the normal, lateral force and pitch, roll and yaw moment equations. Here the wing buffeting calculation is demonstrated.

$$mV \cos \alpha_0 \dot{\alpha} - mV \cos \alpha_0 \omega_y + mg \sin \alpha_0 \theta - \frac{\rho}{2} V^2 S c_{z\alpha} \alpha - \frac{\rho}{2} V^2 S \frac{\bar{c}}{V} c_{z\alpha} \dot{\alpha} - \frac{\rho}{2} V S \frac{\bar{c}}{V} c_{zq} \omega_y = \tilde{Z}(t) \quad [3]$$

$$I_y \omega_y - \frac{\rho}{2} V^2 S c^2 c_{m\alpha} \alpha - \frac{\rho}{2} V^2 S \frac{c^2}{V} c_{m\dot{\alpha}} \dot{\alpha} - \frac{\rho}{2} V^2 S \frac{\bar{c}^2}{V} c_{mq} \omega_y = \tilde{M}(t) \quad [4]$$

$$\dot{\theta} = \omega_y$$

The excitation due to wing flow separation,  $\tilde{Z}(t)$  and  $\tilde{M}(t)$  are the fluctuating normal force and pitch moment due to flow separation, they are derived by integration of the measured fluctuating pressures  $\tilde{p}(x, y, t)$  for each condition of steady incidence and Mach number.

The dynamic response of rigid aircraft can be calculated in time domain and in frequency domain by use of PSD analysis. The assumptions made for the measured random pressures are stationary, ergodicity and zero correlation between the different pressure signals.

Therefore the response at a constant incidence can be corrected in order to eliminate windtunnel turbulence effects by subtraction of the  $\alpha=0^\circ$  response at the same Mach number.

$$\ddot{z}_{pc}(\alpha, t) = \ddot{z}_p(\alpha, t) - \ddot{z}_p(\alpha = 0, t) \quad [5]$$

The structural dynamic response is calculated using a linear system of generalised equation of motion with the assumption of relatively small oscillations, so that the motion dependent system forces are linearly

dependent on the deformation  $u$  and the exciting forces are independent of the structural motion, Ref. 5,7.

The deformation  $u(x, y)$  of the structure at a point  $(x, y)$  and the time  $t$  is represented by the superposition of natural modes shapes  $u_r(x, y)$  where the factors are the unknown generalised co-ordinates  $q_r(t)$ .

$$u(x, y, t) = \sum_{r=1}^R q_r(t) u_r(x, y) \quad [6]$$

$$M_r \ddot{q}_r(t) + \sum_{i=1}^J D_{rj} \dot{q}_j(t) + M_r \omega_r^2 q_r(t) + \sum_{j=1}^J A_{rj}(\alpha_0, Ma, t) q_j(t) = \tilde{Q}_r(t) \quad [7]$$

$u_r$	normal mode shapes
$u$	deformation vector
$q_r$	generalised co-ordinates
$\omega_r$	eigenfrequencies of the natural modes
$M_r$	generalised masses of the natural mode $r$
$D_{rj}$	generalised structural damping terms
$A_{rj}(\alpha_0, Ma)$	generalised aerodynamic motion dependent system forces
$\tilde{Q}_r(\alpha_0, Ma)$	the generalised aerodynamic exciting forces due to fluctuating pressures

Both, the generalised aerodynamic motion dependent forces  $A_{rj}$  and  $\tilde{Q}_r$  are functions of the steady incidence and of Mach number.

Transformation of equation [7] into the frequency domain gives the following relationship.

$$-\omega^2 M_r q_r + \omega_r^2 M_r (1 + i\chi_r) q_r + \sum_{j=1}^J A_{rj}(\alpha_0, Ma, \omega) q_j = \tilde{Q}_r(\alpha_0, Ma, \omega) \quad [8]$$

$\chi_r$  is structural damping coefficient

This set of equations is there used to calculate the dynamic response in frequency domain.

The generalised buffet excitation forces  $\tilde{Q}_r$  in eq. [8] are directly evaluated from the windtunnel measurement of unsteady pressures  $\tilde{p}(x, y, t)$  in time domain.

$$\tilde{Q}_r(t) = \int_S \tilde{p}(x, y, Ma, \alpha_0, t) \cdot u_r(x, y) ds \quad [9]$$

and in frequency domain the corresponding complex generalised spectra of the buffet excitation forces

$S_b(i\omega)$  are derived from the Fourier transform  $F_b(i\omega)$  of the integrated generalised pressures at finite surface elements  $\Delta S$  for the normal modes  $r$  and  $j$ .

$$S_{B_r,j}(i\omega) = F_{B_r}(i\omega) \cdot F_{B_j}(-i\omega) \quad [10]$$

$$F_{B_r}(i\omega) = \int_{S=-\infty}^{\infty} \int \tilde{p}(x, y, t) \cdot u_r(x, y) e^{-i\omega t} dt \cdot ds \quad [11]$$

The complex generalised cross spectra of the normal modes  $r$  and  $s$  may reduce to generalised auto spectra  $S_{B_{rs}}(\omega)$  if the generalised correlation  $R_B$  between pairs of pressures is negligible, as shown for the Delta wing results.

$$R_{B_r,j}(\tau) = \lim_{T \rightarrow \infty} \frac{1}{T} \int_0^T \int_S u_r \tilde{p}(x, y, t) \cdot ds \cdot \int_S u_j \tilde{p}(x, y, t + \tau) \cdot ds \cdot dt \quad [12]$$

$$S_{B_r,j}(i\omega) = \int_{-\infty}^{+\infty} R_{B_r,j}(\tau) \cdot e^{-i\omega\tau} d\tau \quad [13]$$

$$R_{B_r,j} = 0; R_{B_{rr}} \neq 0$$

The calculation of the generalised aerodynamic motion dependent forces  $A_{ij}(\alpha_0, Ma, k)$  is performed by a modification of linear unsteady aerodynamic theory, the 3d Doublet lattice method, using both measured steady pressure distributions and the measured unsteady pressure distribution of the wing roll oscillation. The problem consists here mainly in the prediction of the diagonal terms  $A_{rr}$  for more than one mode and naturally in the derivation of the cross coupling terms  $A_{rj}$  at separated flow condition if only one measured mode is available (due to high model and windtunnel costs).

The corrected generalised aerodynamic motion dependent forces  $A_{ij}(\alpha_0, Ma, k)$  are calculated as follows for given Mach number  $Ma$  and reduced frequency  $k$ .

$$A_{rj} = \iint_S \left\{ \Delta c_{pr}^*(\alpha_0, k) + \left[ \Delta \bar{c}_{p_{rc}}(\alpha_0, k) - \Delta c_{p_i}^*(\alpha_0, k) \right] \right\} u_j \cdot ds \quad [14]$$

The corrected unsteady pressure distribution  $\Delta c_{p_i}^*$  of the measured vibration mode  $u_i(x, y)$  is calculated by using a modified kinematics boundary condition.

$$\Delta c_{p_i}^* = [D' + iD'']^{-1} \cdot \alpha^* \quad [15]$$

$D' + iD''$  matrix of aerodynamic influence coefficients

$$\alpha^* = \frac{U_\infty + \bar{u}_0}{U_\infty} \cdot \frac{\partial u_j}{\partial x} + ik\bar{u}_i \quad [16]$$

The local velocity is calculated from local Mach number and speed of sound.

$$U_\infty + \bar{u}_0(x, y) = a(x, y) \cdot Ma(x, y) \quad [17]$$

$$Ma(x, y) = \left\{ \frac{2}{\kappa - 1} \left[ \frac{1 + \frac{\kappa - 1}{2} Ma_\infty^2}{\left( 1 + \frac{\kappa Ma_\infty^2}{2} c_p \right)^{\frac{\kappa - 1}{\kappa}}} - 1 \right] \right\}^{\frac{1}{2}} \quad [18]$$

The local speed of sound  $a(x, y) = \sqrt{\kappa RT}$  is derived from adiabatic compression.

From the difference between measured and corrected unsteady pressure distribution of the measured vibration mode an additive correction term

$$\left[ \Delta c_{p_i} - \Delta c_{p_i}^* \right]$$

is known, which for the formulation of arbitrary vibration modes is assumed to be independent of the mode.

The corrected pressure distribution for arbitrary mode shapes  $u_j$  are then calculated by

$$\Delta \bar{c}_{p_j} = [D' + iD'']^{-1} \cdot \alpha_j^* + \left[ \Delta \bar{c}_{p_{jc}} - \Delta c_{p_i}^* \right] \quad [19]$$

In general the measured motion induced pressure contains a contribution of the fluctuating pressure at the reduced frequency of the harmonic oscillation  $k$ . The contribution  $\Delta c_{p_i}^*(k)$  maybe approximately extracted from the static measurement. Therefore the measured unsteady pressure can be corrected.

$$\Delta \bar{c}_{p_{ic}}(k) = \left[ \Delta \bar{c}_{p_i}(k) + \Delta \tilde{c}_{p_i}(k) \right] - \Delta \tilde{c}_{p_0}(k) \quad [20]$$

Having established all coefficients of the equations of motions, the response calculation of the rigid aircraft is performed directly in time domain using a matrix notation of equation [3] and [4]

$$\dot{x}(t) = Fx(t) + P(t) \quad [21]$$

where the vector  $X(t) = \{ \alpha, \omega_y, \chi \}^T$   
 $u(t) = \{ Z(t), M(t) \}^T$   
 by the z-transformation of equation [21]

$$x_{k+1} = A_{x_k} + Cu_k \quad [22]$$

the response is known at discrete time steps. The response calculation of the elastic structure is performed in frequency domain with the assumption of no cross correlation of the fluctuating pressures. Therefore the spectral density of the deflection  $S_u$  at a point of the elastic structure is computed by the relationship

$$S_u(x, y, \alpha, Ma, \omega) = |H(i\omega)|^2 \cdot S_{B_r}(\omega) \quad [23]$$

with the generalised power spectral density of the forces  $S_{B_r}$  from equation (8) and the admittance of the system.

$$H(i\omega) = \begin{bmatrix} -\omega^2 M_r + \omega_r^2 M_r \\ +i\chi\omega^2 M_r \\ +A_{rj} \end{bmatrix}^{-1} \begin{bmatrix} \cdot \\ \cdot \\ \cdot \\ I \\ \cdot \\ \cdot \end{bmatrix} \quad [24]$$

Using an approximation of the motion induced aerodynamic forces at the frequency of each elastic mode also the dynamic response of the elastic structure due to buffeting can be performed in time domain.

**Results**

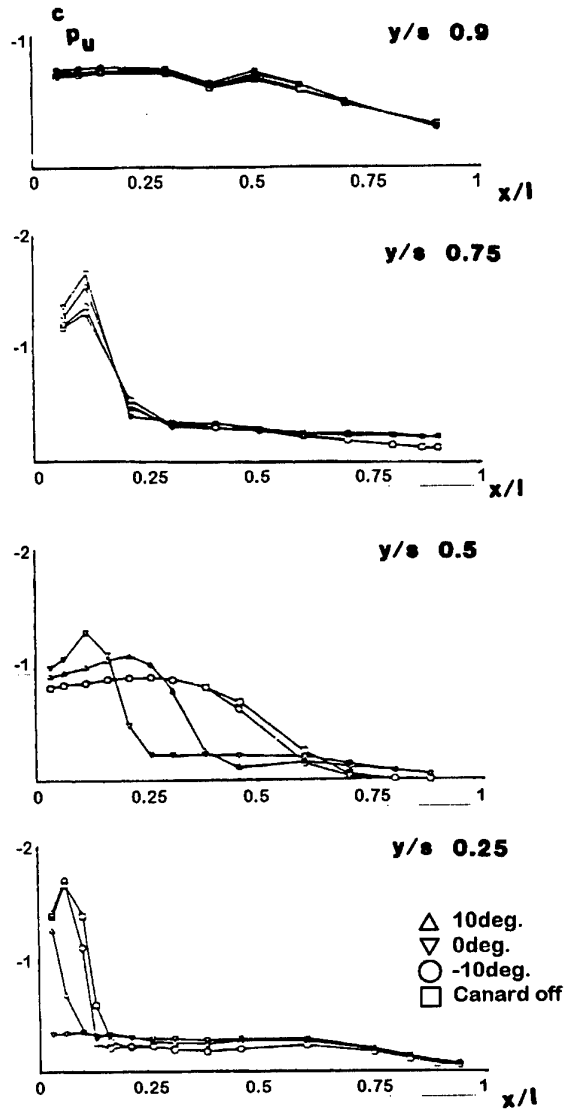
**Wing:**

Wing results are demonstrated for steady and unsteady fluctuating and roll motion induced pressure fields, model response prediction and aircraft buffeting prediction for the pilot seat and wing tip acceleration. Some examples of the effects of leading edge (i.e. vortices and flow separation on steady and unsteady pressure distributions are presented in the Figs. 8, 9. The prediction of the acceleration on a wing with tip missile are shown in Fig. 12.

Steady Pressure Distributions

Strong non-linear effects caused by leading edge vortex flow are apparent at the main parts of the wing with the indication of inner wing area reattached flow

up to incidences of about  $\alpha = 8$  deg. depending on Mach number or dynamic pressure and outer wing trailing edge flow reattachment up to  $\alpha = 6$  deg. Wing tip flow separation effects are observed starting at 6 to 8 degrees, the negative pressure at the outer wing section decreases then with increase of incidence. The inner wing pressure distributions are strongly affected by the interaction with the canard, whereas the flow and flow separation at the wing tip region is hardly affected by the static canard deflection. An example is illustrated in Fig. 8 for Ma 0.6 and 8 degrees.



**Fig.: 8 Steady Pressure Distribution**

Fluctuating Pressures

Fluctuating pressures at constant static incidence are of interest for the prediction of the structural dynamic response for the buffeting prediction. The power spectral density of exciting forces and its dependency

of the static incidence and of Mach number in Fig. 9 demonstrates time histories of two pressure signals at  $M = 0.8$  and 10 degrees, with peak values  $c_p = 0.12$ .

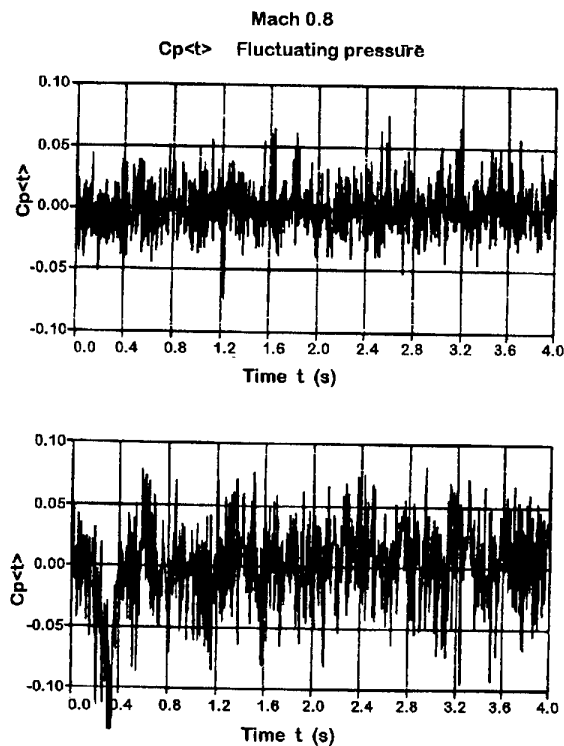


Fig.: 9 Fluctuating Pressures

Fig. 10 shows a typical example of the PSD of integrated fluctuating pressure distributions generalised for the first wing model bending mode at Mach 0.6.

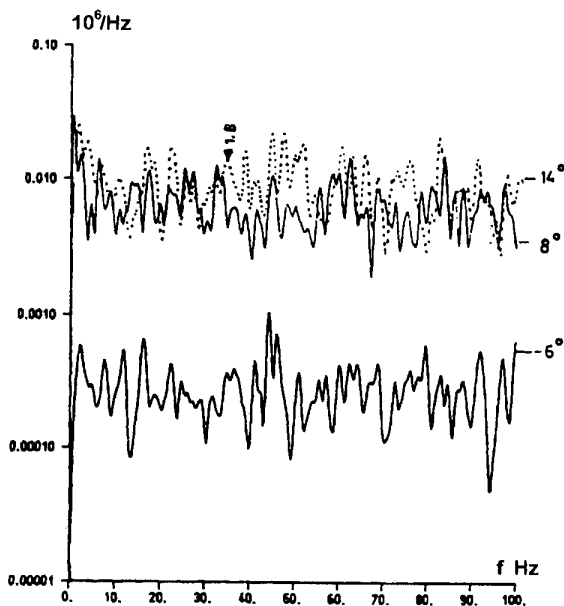


Fig.: 10 Fluctuating Forces PSD of First Bending Buffet Force

The major features of the buffeting excitation forces are:

- broadband characteristic of the PSD in the frequency region 0 - 100 Hz with no decay at incidences 6, 8 and 14 deg. and no specific peaks at the frequency of the first bending at 35 Hz.
- Strong increase in the amplitude from 6 to 8 degrees of static incidence followed by smaller increase with incidence.
- Effect of Mach number on the PSD is small, the modulus of the PSD is similar for  $Ma = 0.3$  and  $Ma = 0.6$  and is less to some small amount at  $Ma = 0.9$ .
- RMS values of pressures reach maximum values of  $c_p < 0.08$ , as shown for example in Fig.11.

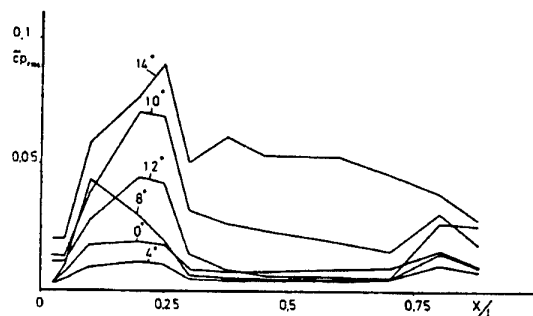


Fig.: 11 Fluctuating Pressure RMS Values

#### Elastic Wing Response Prediction

Flight experience on existing fighter aircraft often revealed unexpected high vibrations levels on the wing, especially on wings with wing tip mounted stores at high  $\alpha$  manoeuvring conditions at specific flight conditions. For these configurations in practice structural modifications or unwanted limitations of the flight envelope are necessary due to the fatigue loads or the defined limitations of weapon systems, for instance the limitations of the search head of a sidewinder.

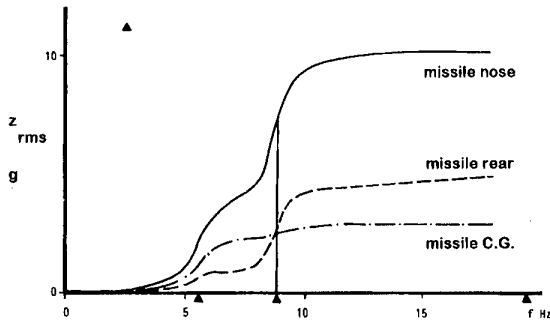
In a first step the existing wind tunnel results had been extrapolated to a wing with tip mounted missile assuming that the buffet forces and motion induced forces on the clean wing are valid also for the wing store configuration to investigate the vibrations levels on the store.

Since the evaluation of measured unsteady pressure distribution of the harmonically oscillating model showed maximum effects due to flow separation at  $Ma = 0.8$  in the incidence region 8 to 10 degrees in the



wing tip region the wing tip missile problem is investigated at  $Ma = 0.8$  and  $\alpha = 10$  degrees.

The described correction method of the unsteady forces at flow separation conditions was applied and the corrected forces were introduced in the stability calculation of the elastic wing.



**Fig.: 12 RMS Accelerations of Tip Missile as a Function of cut off Frequencies.**

The result of PSD analysis of the tip missile dynamic response for the vertical missile nose acceleration shows mainly the contribution of the excited first wing bending at 6 Hz and of the missile torsion mode at 11 Hz due to the excitation spectra. The corresponding rms values of the acceleration of missile nose, C.G. and rear are shown as function of cut off frequency in Fig. 12. Through the application of Mabey's buffet excitation parameter method for the prediction of wing tip vertical acceleration the missile C.G. acceleration was found to be almost identical.

Elastic Fin Response Prediction

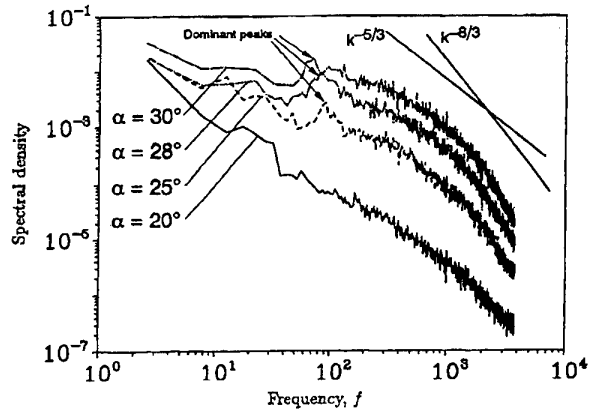
- Unsteady flow field prediction method:

Fig. 13 shows the result from measurements performed at the Technical University Munich (TUM). Spectral densities of lateral wind component in region of fin are demonstrated for high incidences up to 20 to 30 degrees. Corresponding unsteady pressures are very well documented in Ref. 15, 16.

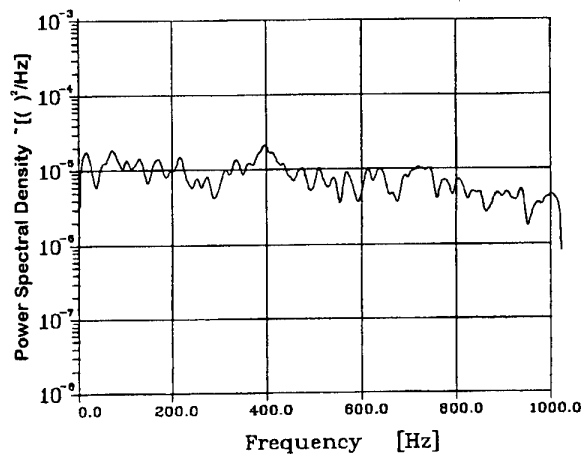
- Unsteady pressure measurements:

Fig. 14 shows a typical PSD of a non dimensional unsteady pressure at a middle fin location. At 400 Hz a peak was found which corresponds to 20 to 24 Hz for the real aircraft fin. Tuning of fin modes for this Strouhal effect is avoided in design by putting fin torsion mode to higher frequencies. Fig. 15 demonstrates the predicted dynamic response of fin tip, reaching 150 g's for Mach 0.8, incidence 30 degrees, 20000 ft. Fig. 16 shows the strong increase of fin tip lateral acceleration response with increasing incidence.

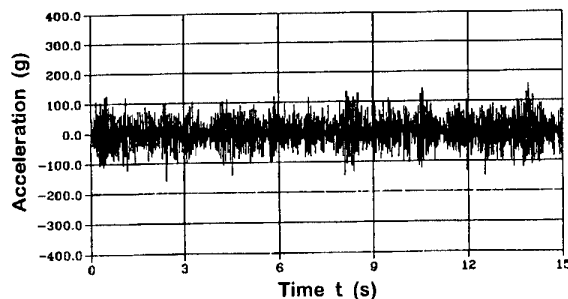
Resulting high dynamic fin loads have been considered in fin design.



**Fig.: 13 Spectral Density of Lateral Velocity**



**Fig.: 14 Power Spectral Density of Unsteady Pressure; Mach=0.9;  $\alpha=28^\circ$ ; Clean Configuration**



**Fig.: 15 Prediction Fin Acceleration**

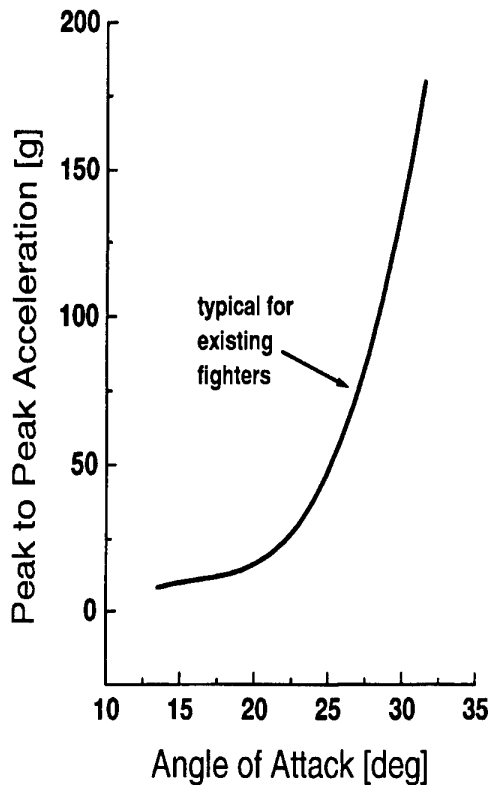


Fig.: 16 Fin Vibration Characteristics

#### Conclusion dynamic buffet loads

##### Wing buffet:

A semi-empirical method for the prediction of buffeting has been evaluated. The verification was performed by comparison with measured model response for the wing buffeting and with Mabey's excitation parameter for the aircraft buffeting.

##### Fuselage buffet:

The light to moderate buffeting conditions predicted for the pilot seat should be repeated including the elastic fuselage effects.

##### Fin buffet:

Dynamic buffet loads have to be fully considered in the design phase. Verification will be performed via model and flight test results.

### 3.3 DYNAMIC HAMMERSHOCK EFFECTS ON THE AIR INTAKE DESIGN OF SUPERSONIC AIRCRAFT

The design of an intake structure for supersonic aircraft is highly dependent on assumptions to be defined in the early design phase and in the subsequent check stress and structural clearance phases, see Ref. 17.

The assumptions to be made are related mainly to the dynamic hammer shock pressure wave and its dynamic behaviour in terms of magnitude depending on pressure at the engine face, the shape of the intake / duct, the flight condition, the change of magnitude during its travel from the air intake to the engine along the duct to the forward intake and the effect of surge interaction in case of two engine intake / ducts. The assumptions have to be based on the extrapolation of known data from other existing projects and a statistical approach has to be chosen with respect to the probability of occurrence of the hammer shock for flight hour and aircraft missions. Secondly the effect of dynamic response of the intake duct structure has to be carefully estimated during design.

The design philosophy can be based on the concept that the structure is able to carry for the limit load case a static loading consisting of flight manoeuvre loads, steady-state pressure and a maximum positive and negative hammer shock pressure factorized by a dynamic factor and that the structure withstands ultimate loading resulting from steady-state pressure and manoeuvre loads with the allowance for plastic deformation due to ultimate hammer shock pressure.

For both concepts it is essential during the different design and clearance phases to verify the assumptions made from the beginning using comparisons of different methods, experimental results from model tests, on aircraft ground surge interaction tests and flight test results.

The careful consideration of all dynamic aspects allows for a design without bigger weight penalties.

Hammer shock loading and different calculation tools for dynamic response due to hammer shock, and results from calculation and validation of results is described.

#### 3.3.1 Hammer shock loading

Aircraft with supersonic flight capability require an intake / duct in front of the engine because the engine cannot operate in supersonic flow conditions. Therefore the intake / duct has to be designed for subsonic flow conditions at the engine face (Fig. 17).

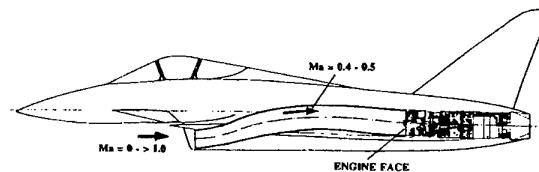


Fig.: 17 Scheme of Intake / Duct of Supersonic Aircraft

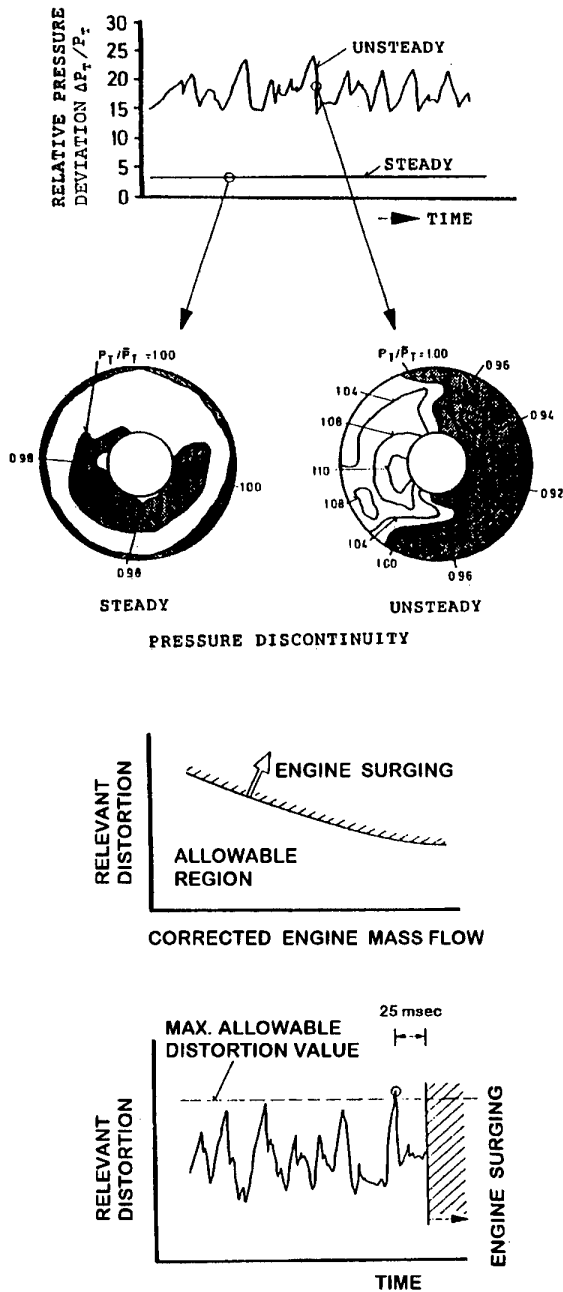


Fig.: 18 Origin of Hammershock

Origin of hammershock (H/S)

From the compressor region up to the combustion chamber a strong steady pressure increase occurs (Fig. 18). Near limit engine performance conditions a short-time pressure wave, called hammershock, can occur which advances in opposite direction of the airflow with high velocity ( $V_{HS} = 300$  to  $400$  m/s). Under normal distortion free conditions there is a steady pressure increase of the air up to the combustion chamber of the engine. If a high unsteady pressure

difference occurs which is caused by distortion of the air flow at limit engine performance conditions, an engine surge will occur, Fig. 18. This surge causes a very short pressure wave, which travels in opposite direction of the flow direction. The shock like wave - called hammershock (H/S) - produces a pressure up to 3 times of the steady state pressure.

Effect of engine bypass ratio and compressor overall static pressure ratio on H/S peak pressure

Increasing the compressor overall pressure ratio in general increases the ratio peak H/S pressure to steady-state pressure at engine face and a decrease in engine bypass ratio leads to an increase in hammershock peak pressure.

Assumption of design H/S pressure

The extrapolation of air intake H/S peak pressures from existing engines has to be based upon the evaluation of the root mean square value added to the mean pressure as function of the overall static compressor pressure ratio.

The peak H/S pressure is then chosen as 3 times or 2 times of the root mean square value added to the mean value pending design assumptions.

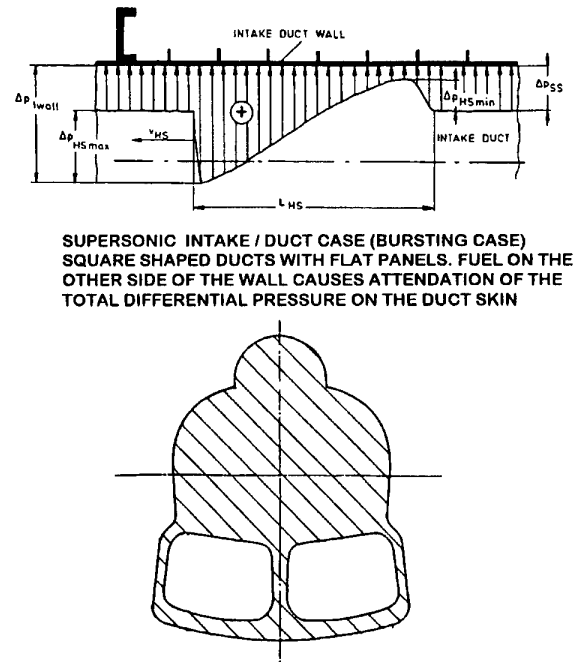
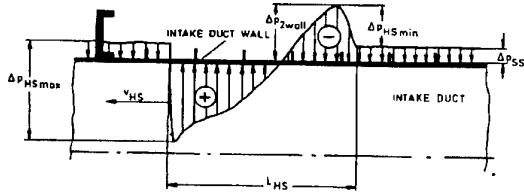


Fig.: 19a Influence of Intake/Duct Shape on Total Pressure Including Hammershock

Description of dynamic hammershock wave

The definition of the design hammershock wave is in general derived from experimental on ground surge - and flight test surge tests. Measurements performed on different aircraft in the engine face show typical time histories of the pressure at A.I.P. (air intake pressure), see for example Fig.20. The general evaluation of a set of time histories will allow a definition of the H/S

pressure time history for subsonic and supersonic flight condition as demonstrated in Fig. 21. Important for dynamic response is, besides the magnitude of the peak value, the rise time to the positive peak value (values from 5 msec's down to 0.6 msec's have been measured) and the rise time to the negative peak value. It has to be noted that the negative H/S pressure wave resulted from the reflected H/S at the forward intake.



SUBSONIC INTAKE DUCT CASE (BUCKLING CASE) CIRCULAR SHAPED DUCTS, FUEL ON THE OTHER SIDE OF THE WALL CAUSES AN INCREASE OF TOTAL DIFFERENTIAL PRESSURE ON THE DUCT SKIN

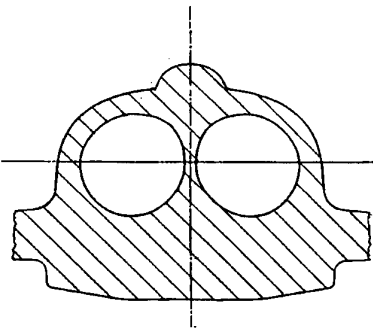


Fig.: 19b Influence of Intake/Duct Shape on Total Pressure Including Hammershock

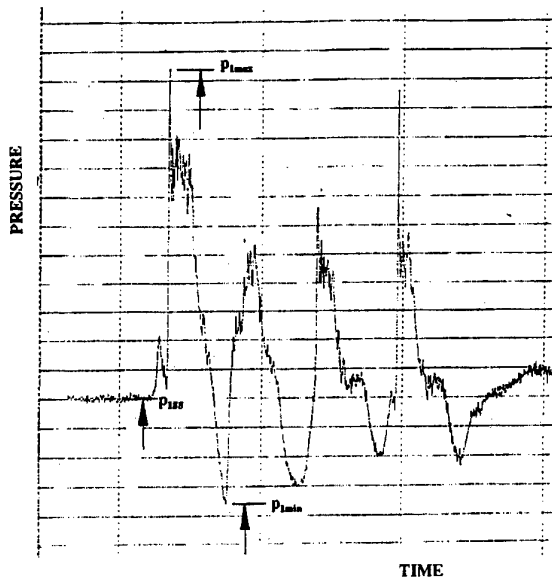


Fig.: 20 Inflight measured Time History of Hammershock at Engine Face, Subsonic

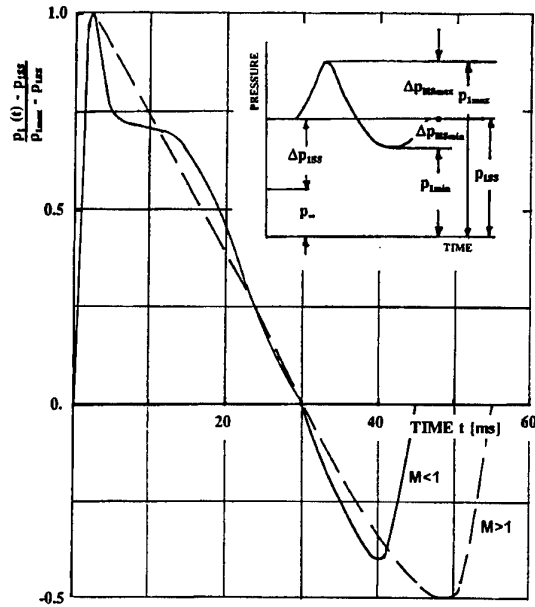


Fig.: 21 Hammershock Wave Shapes For Supersonic and Subsonic at Engine Face Derived From Experience

Effect of duct cross section on design

Different duct cross section shapes lead to different design conditions (Fig. 19)

- supersonic intake duct case in the square shaped duct membrane stresses are critical for the more flat panels. In the tank region additional tank hydrostatic and tank system pressures ( $p_{TH}$  and  $p_{TV}$ ) cause an attenuation of the total differential pressure on duct skin.
- subsonic intake duct case in the round shaped duct stability requirements design the panels. In the tank region additional tank hydrostatic and tank system pressures ( $p_{TH}$  and  $p_{TV}$ ) cause an increase of the total differential pressure on duct skin.

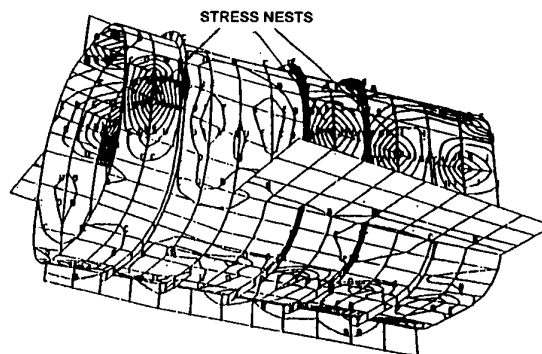


Fig.: 22 Stress Distribution at Timestep t According to Dynamic Load Case

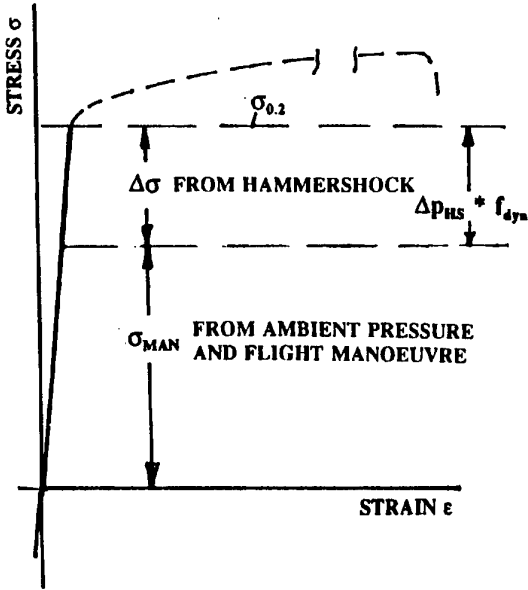


Fig.: 23a Air Intake/Duct Design Stress/Strain Relation for Limit Load Case

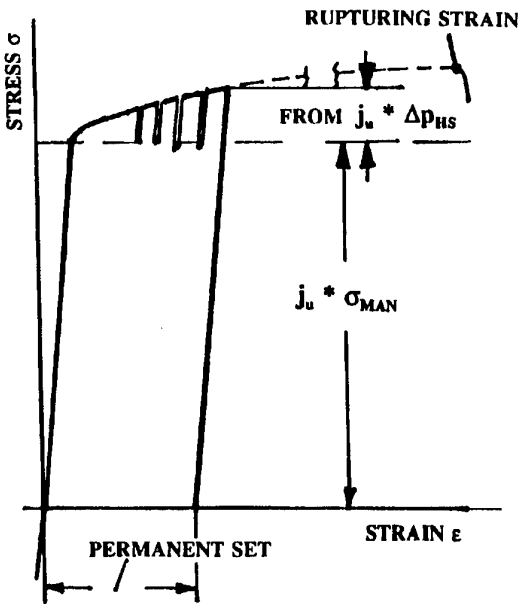


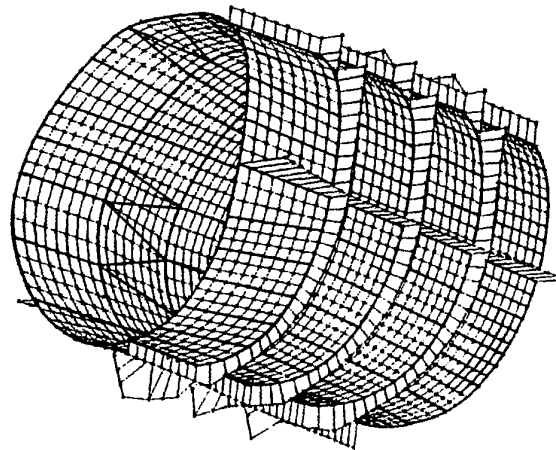
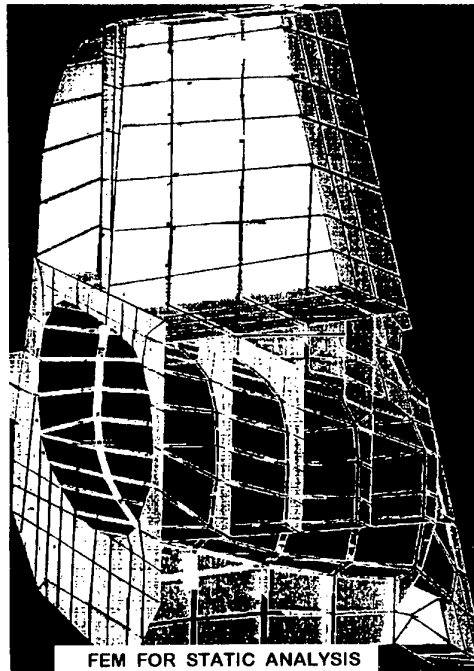
Fig.: 23b Air Intake/Duct Design Stress/Strain Relation for Ultimate Load Case

3.3.2 Analytical procedure

The intake / duct structure has to be analysed in the different design steps in order to calculate the resulting stresses on the intake / duct panels and frames due to a total loading from manoeuvre 'g' loads, steady-state pressure, hydrostatic pressure from fuel and dynamic hammershock pressure.

In order to perform dynamic calculations a finite element model (FEM) has to be established which is able to describe local structural responses up to 5 kHz, i.e. to cover essential panel vibration modes and which has the capability to introduce the static loads or displacements from manoeuvres and steady-state pressures.

In general for dynamic calculations an existing static FEM is modified by subdividing each of the original elements according to the frequency resolution requirement, see Fig. 24.



FEM FOR DYNAMIC ANALYSIS

Fig.: 24 Finite Element Models of Intake/Duct Structures

A full structural idealisation of the total intake / duct structure which would fulfil this requirement is not

feasible at the moment due to the enormous complexity of the model leading to computer capacity and computer time problems which would hinder a practicable approach. Therefore different structural sections of the duct have to be treated.

#### Calculation tools for limit load and ultimate load case

Different tools are applied in the dynamic investigations. In the first step, the natural frequencies and elastic mode shapes are calculated using NASTRAN SOLUTION 63 for model vibration analysis. In the second step for the investigation of the stresses and dynamic displacements in the limit load case NASTRAN SOLUTION 109 is applied for transient response analysis, with and without static preload using a dynamic hammershock load as described in para. 3.3.1, Fig. 21. The properties of the geometry and of the elastic materials are linear.

During the dynamic calculation local concentrations of high displacements and corresponding stress nests occur, see Fig. 22, which change in magnitude and position with the travel of the hammershock wave. The maximum stresses may remain for limit load case within the stress limit  $\sigma_{02}$  with the effect of the dynamic response covered by a dynamic factor on hammershock pressure in static design required the design philosophy. For this case the verification of the static design can be performed with NASTRAN SOLUTION 109, assuming that geometrical nonlinearities are not significant. For the ultimate load case the design philosophy might be based on the assumption that the duct structure is designed to ultimate loads from flight manoeuvres including steady state duct and hydrostatic pressures only, where the stress pulse from the ultimate hammershock pressure increment is covered by the plastic deformation capability of the duct material, see Fig. 23b. For this approach, a non-linear dynamic calculation with DYNA3D including non-linear plastic material description and non-linear geometrical properties is necessary for verification.

#### 3.3.3 Results - Validation of Tools and Comparison of different methods

Dynamic hammershock calculations have been performed on supersonic squared shaped and subsonic circular shaped duct sections using NASTRAN SOL 109 and DYNA3D software in order to verify analytical tools and to verify dynamic factors used in the static design. Fig. 24 demonstrates that the original FEM for static calculations has to be refined for dynamic calculations from the frequency resolution point of view. A typical example of a dynamic model was a FEM consisting of 2348 grids, 12164 degree of freedom, 2073 QUAD elements, 785 triangular

elements, 631 bar elements and 608 rod elements. Fig. 25 demonstrates that the local response of the stress on outer and inner side of the duct skin varies from element to element, i.e. the dynamic factors are different. The verification of an assumed dynamic factor in static design is demonstrated in the comparison of a static calculation with increased hammershock load and a dynamic calculation using SOLUTION 109 with a hammershock acting from 0 to 10 ms on the structure in Fig. 26 and 27.

The comparison of static and dynamic calculation results resulted in an almost equivalent ratio of maximum stress to allowable stress  $(\sigma/\sigma_A)_{static} = 0.57$   $(\sigma/\sigma_A)_{dyn} = 0.58$ . Fig. 27 shows in addition that large structural portions have smaller stress levels than seen from the static calculation, Fig. 26.

The comparison of the different methods SOLUTION 109 with DYNA3D resulted in excellent agreement for limit load case investigations.

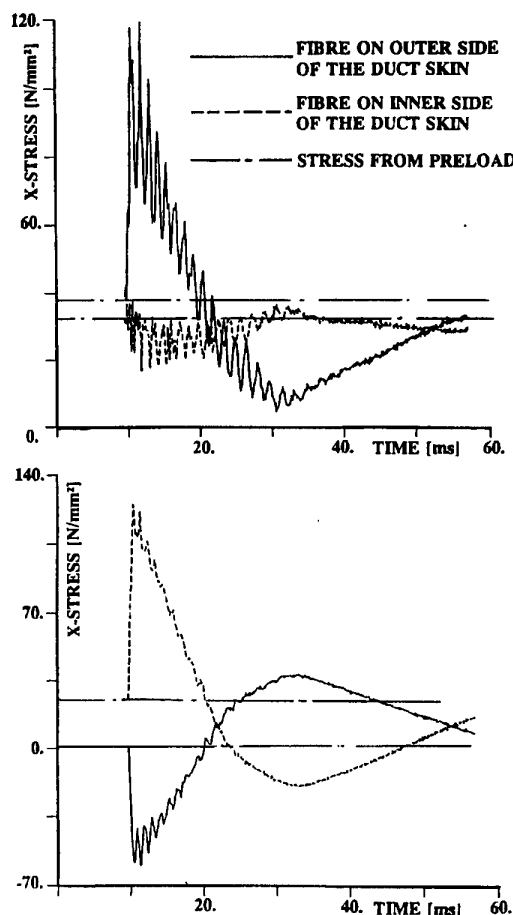


Fig. 25 Typical Response of Different Duct Skin Elements on Hammershock Excitation

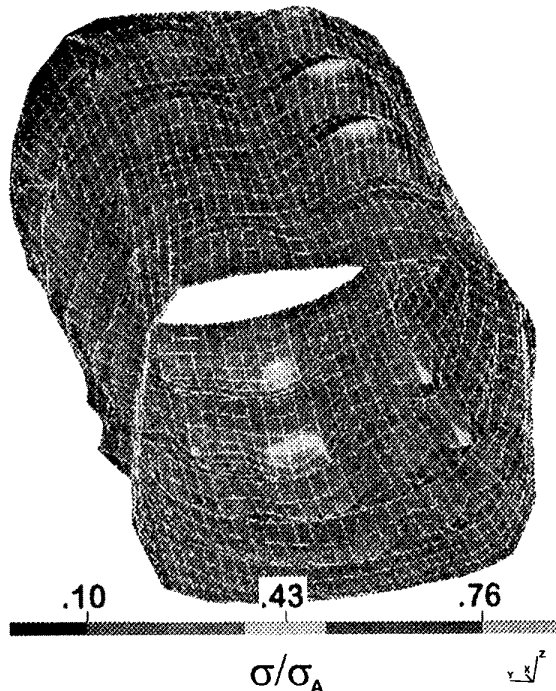


Fig.: 26 Increased Static Hammershock Load Displacement and Stresses; Max Stress/Allowable Stress  $\sigma/\sigma_A=0.58$ .

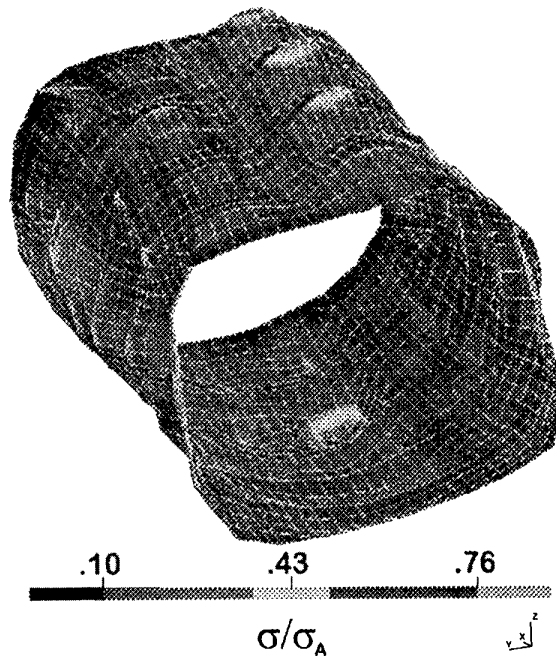


Fig.: 27 Increased Dynamic Hammershock Load Displacement and Stresses; Max Stress/Allowable Stress  $\sigma/\sigma_A=0.57$ .

#### Comparison with experimental results

The dynamic response was measured in terms of strains on a duct test section. A finite element model of the test section was used for calculation of strains with

the DYNA3D model using an input the experimental pressure pulse. The comparison of measured and calculated strain was reasonable good to validate the calculation.

#### 3.3.4 Conclusions Hammershock Loads

- There is sufficient evidence for the application of software tools from the performed comparisons of calculated results using NASTRAN SOLUTION 109 and DYNA3D and from the comparison from calculated and measured dynamic strains for dynamic hammershock response and stress calculation in the process of the verification of air intake - duct structure.
- Comparison of local dynamic stress calculations to static stress calculations with assumed constant dynamic load factors (based on identical FEM) indicate that the dynamic tools could be applied not only for verification but also for the design to minimise structural weight. The dynamic design approach is relatively more complex and time consuming. The profits of local dynamic design might be reduced by manufacturing constraints.
- The verification of the assumed magnitude of the hammershock pressure and its risetime for a given shape of duct is the most important step for structural clearance.

### 3.4 GUNFIRE LOADS

#### Response Calculation for Gunfire Vibration of the Total Aircraft

A dynamic FE model of the total aircraft, Fig. 33 was used which also include the IMU location. This model is valid up to about 80 Hz for total aircraft vibration modes. The model has been validated by ground resonance and structural coupling test and is believed to be accurate enough also for the gunfiring response prediction in the frequency range from 3 to 80 Hz.

With the known properties of the dynamic model, namely the generalized mass matrix  $M$  and stiffness matrix  $K$  and the normal modes  $\phi$  a dynamic response calculation due to gunfiring on ground can be performed in time domain using time histories of measured forces from gun rig testing.

$$[-\omega^2 M_j + (1 + ig_j) K_j] q_j(t) = P_j(t) \quad [25]$$

$$P_j(t) = \Sigma (X_1(t) \phi_{x_1}(x_1) + Y_1(t) \phi_{y_1}(x_1) + X_2(t) \phi_{x_2}(x_2) + Y_2(t) \phi_{y_2}(x_2) + Z_2(t) \phi_{z_2}(x_2) + Y_{blast}(t) \phi_{y_{blast}}(x_{blast}) + Z_{blast}(t) \phi_{z_{blast}}(x_{blast}))$$

$g_j$	structural damping of mode j
$M_j$	generalized mass of mode j
$K_j$	generalized stiffness of mode j
$q_j(t)$	generalized co-ordinate of mode j
$P_j(t)$	generalized gunfire force for mode j

$X_1(t)$	time history of x forces, gun rig measurement
$Y_1(t)$	time history of y forces, gun rig measurement
$X_2(t)$	time history of x forces, gun rig measurement
$Y_2(t)$	time history of y forces, gun rig measurement
$Z_2(t)$	time history of z forces, gun rig measurement
$Y_{blast}(t)$	time history of y forces, gun rig measurement
$Z_{blast}(t)$	time history of z forces, gun rig measurement

$x_1$	aircraft gun attachment station
$x_2$	aircraft gun attachment station
$x_{blast}$	aircraft gun attachment station

The time histories of the rig measurements are blast pressure location.

With this formulation in time domain the IMU-tray response, i.e. accelerations in x, y, z, the tray rates  $\Phi$ ,  $\Theta$ ,  $\Psi$  and angular accelerations  $\dot{\Phi}$ ,  $\dot{\Theta}$ ,  $\dot{\Psi}$  can be calculated using the  $\sigma$  component vector of the IMU normal modes  $[x, y, z, \Phi, \Theta, \Psi]$  of all modes j.

With the solution  $q_j(t)$  from the above equation the response is derived from and in addition the rates and accelerations are calculated

$$\begin{Bmatrix} \ddot{x}(t) \\ \ddot{y}(t) \\ \ddot{z}(t) \\ \ddot{\Theta}(t) \\ \ddot{\Phi}(t) \\ \ddot{\Psi}(t) \end{Bmatrix} = \begin{Bmatrix} \sum \Phi_x \\ \sum \Phi_y \\ \sum \Phi_z \\ \sum \Phi_\Theta \\ \sum \Phi_\Phi \\ \sum \Phi_\Psi \end{Bmatrix} \cdot \ddot{q}_j(t) \quad [26]$$

in the same way but using  $\dot{q}_j(t)$  and  $q_j(t)$ .

### 3.5 General Vibration and equipment tray loads

The equipment of military aircraft has to be designed and qualified to high dynamic environment, resulting mainly from landing impacts, buffet, turbulent aerodynamic flow, flight maneuvers, engine noise and gunfiring.

For a military aircraft typical safety critical equipment namely the inertia measuring unit (IMU), the design and qualification procedure of its tray is described. The design is based upon a finite element model and a subsequent modal analysis applied to define from dynamic response calculation the dynamic design loads, which result from general vibration covering buffet, aerodynamic turbulence, dynamic landing and gunfiring reaction loads.

The validation of the design loads is performed using results from shaker qualification tests and from gunfiring ground test on aircraft. It could be demonstrated that the application of structural optimization techniques based upon structural dynamic tools is absolutely necessary in order to achieve the performance requirements.

The equipment within a military aircraft is exposed to a wide variety of static and dynamic environment during ground- and flight operations. The equipment and the tray have to be designed and qualified, taking into account all these manifold conditions, in the full operational life.

It is necessary to define two categories of equipment: Category I: Equipment very important to the safety of the aircraft. The equipment's would be tested at the flight vibration levels for a considerable life time. Category II: Equipment less important to the safety of the aircraft, where the intention is to demonstrate the ability of the equipment to function within specification limits when subjected to representative flight vibration levels, and the equipment is sufficiently robust.

This paper presents a design procedure for a equipment tray carrying an equipment of category I, based upon MIL-STD-810D requirements and special equipment dynamic design criteria.

In detail the analytical structural dynamic modeling based on a finite element idealization of equipment and tray is described. The dynamic response analysis for general vibration and gunfiring excitation is outlined for the case of environmental control at the equipment attachment. Static and dynamic loads are predicted and the structure of the tray is modified iterative in order to withstand the loads. Different modifications are described with respect to their dynamic behavior.

A clearance test procedure is described which shows the benefits of the modification in terms of fatigue life.

#### 3.5.1 Design Procedure for Equipment Trays

##### Design Requirements

##### **General Vibration:**

The equipment shall meet the full requirements of the specification and suffer no degradation when subjected to the test requirements of MIL-STD-810D, Method 514.3, Procedure I with:

$$\begin{aligned} W_o \text{ (functional)} &= 0.10 \text{ g}^2/\text{Hz} \\ W_o \text{ (endurance)} &= 0.42 \text{ g}^2/\text{Hz} \end{aligned}$$

and with the vibration test spectrum of Fig. 28 (MIL-STD-810D, Method 514.3, Fig. 514.3-26) and the vibration reduction factor for mass loading as per Fig. 29 (MIL-STD-810D, Method 514.3, Fig. 514.3-27).



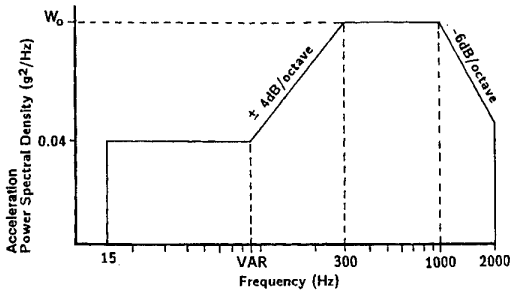


Fig.: 28 General Vibration Test Spectrum

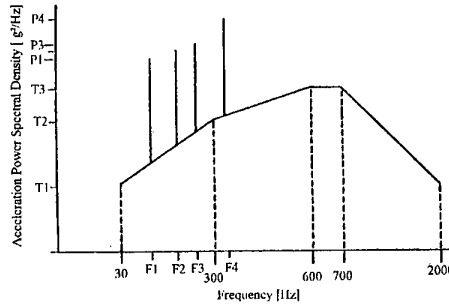


Fig. 30: Gunfire Induced Vibration Test Spectrum

**Acceleration:**

The equipment shall meet the full requirements and suffer no degradation when tested in accordance with Method 513.3, Procedures I and II of MIL-STD-810D. The levels of acceleration are given in Table 2 below:

Direction	Procedure I [g <sub>r</sub> ]	Procedure II [g <sub>r</sub> ]
Fore	3.3	2.5
Aft	6.9	5.3
Lateral	5.5	4.2
Up	12.5	9.6
Down	8.5	6.5
$g_r = 9.81 \text{ m/s}^2$		

Table 2: Acceleration Levels

**Special Equipment Dynamic Requirements:**

Since the requirement behavior is sensitive to special frequency the equipment supplier has sometimes specified additional requirements which are shown in Fig. 31 below and should indicate the frequency regions.

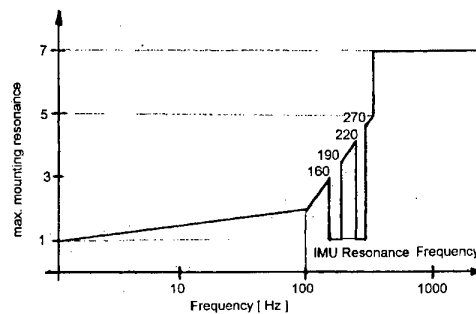


Fig.: 31 Special Equipment Vibration Limitations

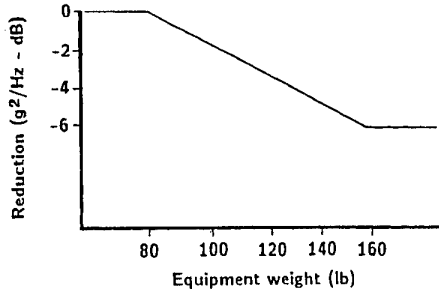


Fig.: 29 Vibration Reduction Factor

In addition, a vibration survey test shall be performed by varying the frequency of applied vibrations slowly through the 0 to 2000 Hz range at low level but with sufficient amplitude to excite the item, in order to determine the resonance frequencies of the equipment in the three orthogonal axes.

**Gunfire Vibration:**

The vibration resulting from repetitive gun blast pulses is two orders of magnitude above normal flight vibration levels. The equipment shall meet the full requirements of the specification when subjected to the vibration test of MIL-STD-810D, Method 519.3, Procedure I, test spectra in accordance with Fig. 30 and the following Table 1.

T <sub>1</sub> (g <sup>2</sup> /Hz)	0.0278
T <sub>2</sub> (g <sup>2</sup> /Hz)	0.1500
T <sub>3</sub> (g <sup>2</sup> /Hz)	0.4200
F <sub>1</sub> (Hz)	28.3
F <sub>2</sub> (Hz)	56.6
F <sub>3</sub> (Hz)	84.9
F <sub>4</sub> (Hz)	113.2
P <sub>1</sub> (g <sup>2</sup> /Hz)	0.1040
P <sub>2</sub> (g <sup>2</sup> /Hz)	0.1132
P <sub>3</sub> (g <sup>2</sup> /Hz)	0.1333
P <sub>4</sub> (g <sup>2</sup> /Hz)	0.1713
$g_{rms}$	19.15

Table 1: Gunfire Vibration Levels

**3.5.2 Definition of Static and Dynamic Design Loads**

The static loads are defined using the acceleration definition in chapter 2.1.

This approach to have a total aircraft idealization and a separate tray idealization has been adopted due to practical engineering handling. The tray segment is part of the total aircraft structure and preloaded with displacements from total aircraft calculation.

The dynamic loads are predicted using the analytical model of the total aircraft and an analytical model of the equipment on tray. Starting point for the models is a structural finite element model of total aircraft and of the equipment plus tray.

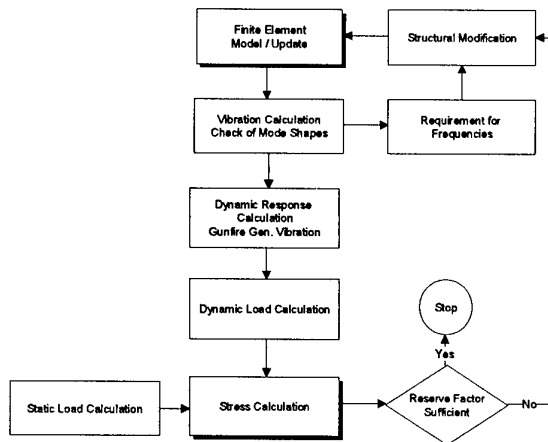


Fig.: 32 Optimization Process Tray Design

### Structural Modeling

During the design phase a set of different FE models are necessary due to the stepwise improvement of the structural dynamic behavior via structural changes. A flowchart, Fig. 32 explains the different steps to be performed during the optimization process.

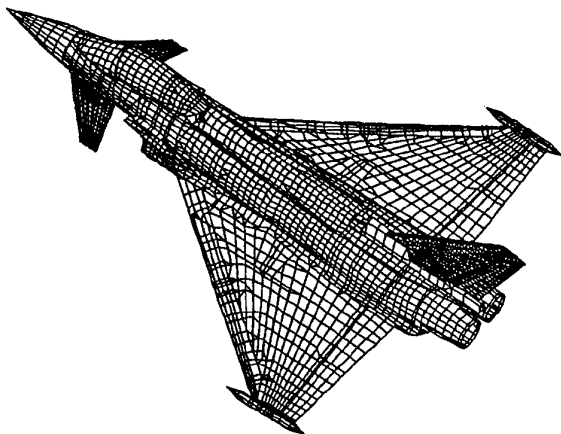


Fig. 33: Finite Element Model Total A/C Structure Idealization

A typical finite element (FE) model of total aircraft is shown in Fig. 33. The full aircraft is idealized for dynamic investigations with 968 residual nodes in three levels of substructures. For analysis the aircraft is divided into two half structures on the line of symmetry with symmetric and antisymmetric degrees of freedoms.

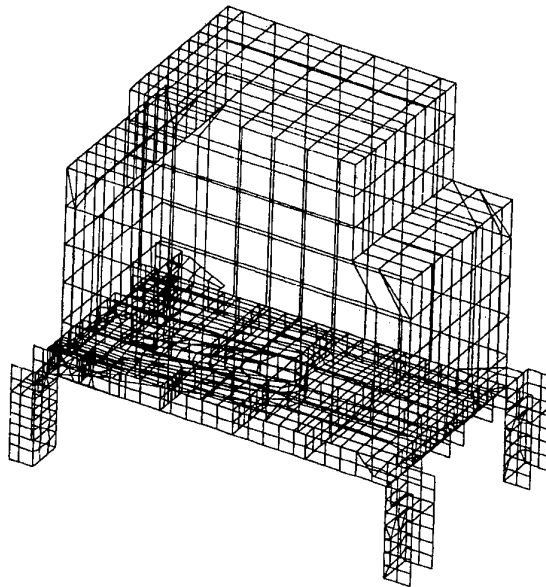


Fig.: 34 Finite Element Model IMU and Tray

Fig. 34 shows the FE model of the tray plus equipment. For dynamic investigations the static model of the tray and the housing of the equipment has been adapted. The tray including the housing was idealized for NASTRAN calculations with up to 4507 grids, 94 ROD elements, 107 ELAS elements, 3008 QUAD elements, 328 BAR elements, 304 TRIAX elements and 778 HEXA elements. The housing idealization was just a box without connection to the inside facilities. The IMU itself was idealized as one point (GENEL element) with six degree of freedoms at the c.g. and attached to the foot point of the tray. All calculations have been performed using MSC - NASTRAN SOL 63, Version 68.

### Vibration Calculation

#### Vibration Calculation of Total Aircraft

Typical example of frequencies and mode shape is presented in Table 3. The symmetrical and the antisymmetrical calculations are presented.

The analysis of total aircraft vibration calculation show a maximum reliable frequency up to 100 Hz.

Mode # sym/anti	Description of the Mode	Frequency [Hz]
S - 01	1st sym. wing bending	7.53
A - 01	1st antim. wing bending	8.27
A - 02	1st fin bending	10.61
S - 02	1st vertical fuselage bending	12.35
A - 03	1st lateral fuselage bending	13.33
S - 03	radome vertical mode	16.42
A - 04	engine pitch antimetric	17.35
A - 05	engine fore and aft	19.42
S - 04	engine pitch symmetric	19.63
S - 05	2nd sym. wing bending	20.33
A - 06	flap rotation	21.10
S - 06	tip pod pitch symmetric	21.54
A - 07	tip pod pitch antisymmetric	22.61
A - 08	1st foreplane bending	23.42
S - 07	1st wing torsion	23.88
S - 08	engine lateral	25.04
A - 09	1st wing torsion antisym.	26.81
A - 10	foreplane bending	27.09
S - 09	chordwise wing bending sym.	29.97

Table 3: Mode Shapes - Total A/C

**Vibration Calculation of the IMU with Tray**

Example of frequencies and mode shapes is depicted in Table 4 for the last tray design (with longerons).

Mode #	Description of the Mode	Frequency [Hz]
1	IMU housing x-translation	140.4
2	IMU housing y-translation	170.8
3	IMU housing z-translation	173.1
4	Tray & Ventral Duct Floor z	176.4
5	Tray x-translation	182.7
6	IMU housing & Tray y-tran.	194.9
7	Tray bending & Ventral Duct	206.1

Table 4: Mode Shapes Tray with IMU

**3.5.3 Dynamic Response Calculation**

The dynamic response calculation was performed with an analytical model describing the dynamic behavior of the IMU as well the IMU tray with different longerons up to 350 Hz. The dynamic models were formulated using the result of the vibration calculation of the different IMU trays i.e. the generalized masses and stiffness' and the mode shapes and eigenfrequencies of the tray up to 22 eigenmodes have been used in the calculation.

Fig. 42 demonstrates the results of the vibration calculation, showing three dimensional views of the mode shapes together with the mode frequencies for different trays.

There are low frequency modes which correspond first to modes of the bottom structure. The bottom structure is connected to the longerons. These vibration modes are considered to be minor importance to the IMU response since there are practically no elastic mode influences at the IMU tray and the IMU c.g. namely the mode shape at about 75, 112, 155 and 160 Hz for the short leg tray.

Due to the high frequency mode the amplitude of the IMU c.g. caused by vibrations of the IMU tray and for the vibration of the fittings together with the longerons, high dynamic loading has to be expected when the excitation have contributions in these mode frequencies.

**Excitation of the IMU Tray and IMU**

The IMU tray excitation due to aircraft responses results from different sources like engine noise, A/C ground operations, turbulent gust, buffeting on wing and fin, hammer shock, landing impacts, missile firing, in flight structural coupling, flutter frequency bias inputs, acoustic noise and. gunfiring.

The main effects results from buffeting and from turbulent gust and gunfiring. The non-aerodynamic excitations are comparatively small, i.e. the excitations due to engine runs, low and high speed taxiing are negligible. The non aerodynamic excitation are known from measured vibration levels during ground runs. The buffeting excitation is known from wind tunnel measured unsteady pressures and their introduction in total aircraft response calculations. The gust induced vibrations are known from dynamic gust calculations. In a first approach all these different excitations are described by the general vibration spectrum as defined in MIL-STD-810D.

For the dynamic response calculation this conservative approach has been used. The Environmental Handbook definition of acceleration power spectral densities of the equipment's in the center fuselage region has been applied for general vibration which is applicable for equipment functional tests.

0.04 g<sup>2</sup>/Hz for 0 up to 150 Hz

and the function level W<sub>0</sub>

W<sub>0</sub> = 0.100 g<sup>2</sup>/Hz for full envelope

W<sub>0</sub> = 0.025 g<sup>2</sup>/Hz for reduced envelope.

**Response Calculation for General Vibration**

The dynamic response calculation was performed using a set of 22 modal equations

$$[- \omega^2 M_j + (1 + i g_j) K_j ] q_j (f) = P_j(f) \tag{27}$$

$$P_j(f) = \Sigma ( m_i \phi_{ij} | x_i (f) | + m_i \phi_{ij} | y_i (f) | + m_i \phi_{iz} | z_i (f) | )$$

$g_j$	structural damping of mode j
$M_j$	generalized mass of mode j
$K_j$	generalized stiffness of mode j
$q_j(f)$	generalized co-ordinate of mode j
$P_j(f)$	generalized external forces for mode j for the environmental acting on the IMU foot

The module of  $|x_i|$ ,  $|y_i|$ ,  $|z_i|$  were introduced as the square root values of the power spectral densities of the defined environment versus frequency.

The equations were solved for unknown general co-ordinates  $q_j(f)$ .

With the unknown generalized co-ordinates the dynamic response of all IMU points can be calculated in each direction versus frequency.

$$\begin{aligned} x_i(f) &= \sum \phi_{ixj} q_j(f) \\ y_i(f) &= \sum \phi_{iyj} q_j(f) \\ z_i(f) &= \sum \phi_{izj} q_j(f) \end{aligned} \quad [28]$$

$\phi_{ixj}$ ,  $\phi_{iyj}$ ,  $\phi_{izj}$  being the eigenmode in each mode j in x-, y- and z-direction.

### Foot Point Control of the Environment

During calculation the foot point acceleration spectra were controlled. The worst case of acceleration out of the 6 IMU to IMU-tray attachments has been used for control in the following manner. Two different procedures were considered.

- Excitation in x-, y- and z-direction separately.

Calculation of the acceleration in x-, y- and z at the IMU attachments. Comparison of the power spectral densities of x-, y- and z-accelerations with the Environmental Handbook number.

In case of exceeding the specified level in a frequency band, the excitation level was reduced to the specified level in the frequency band (notch out of exceedance as in a shaker test). The vibration levels which were predicted to be below of the specified level remained unchanged.

- Excitation in x-, y- and z-direction separately.

The calculation was performed in the same manner as described in the above paragraph with one exception. Not only the exceeding the specified level was controlled, in addition also the vibration level predicted below the specification were controlled in such way that the IMU attachment experienced the full specified level.

### Response Calculation based on Measured Transfer-function

In general the transferfunction between excitation and location (gun attachment) and the IMU tray location may be based on FE modal calculation technique as far as the dynamic system behaves linearly. The prediction of vibration levels at IMU can also be performed using the measured transferfunction between gun attachment input force and IMU location acceleration in all three axis. Using the measured gun loads as described before the response can be calculated with the assumption of a linear system.

$$\begin{Bmatrix} \ddot{x}(i\omega) \\ \ddot{y}(i\omega) \\ \ddot{z}(i\omega) \end{Bmatrix} = H(i\omega)_{x,y,z} \cdot \begin{Bmatrix} X(i\omega) \\ Y(i\omega) \\ Z(i\omega) \end{Bmatrix} \quad [29]$$

$X(i\omega)$	Fouriertransform of measured gun loads $x(t)$
$Y(i\omega)$	Fouriertransform of measured gun loads $y(t)$
$Z(i\omega)$	Fouriertransform of measured gun loads $z(t)$
$H_{x,y,z}$	measured transfer function in x-, y- and z-direction between IMU accelerations in x,y,z-defined impulse hammer force at gun attachment

### 3.5.4 Structural Modification

In order to protect the IMU as a safety critical equipment against excitation due to the coupling of the attachment and tray with the aircraft it was necessary to optimize the elastic structure of the tray. The task was to optimize the tray including the attachments on the aircraft structure in that way that the eigenfrequencies of the tray are higher as the first eigenmodes of the IMU itself.

The design started conventional and the following modification were considered:

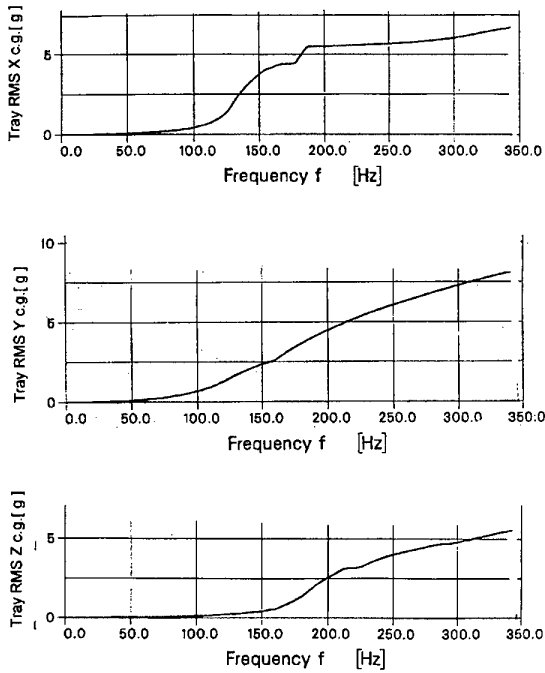
- tray with two short brackets and one movable assembly adjuster (toggle)
- tray with four short brackets, fixed mounted
- tray with four short brackets including pads
- tray with four extended brackets
- tray with four extended brackets including new longerons, for attachments to the A/C structure

### 3.5.5 Prediction Methods using FE-Models

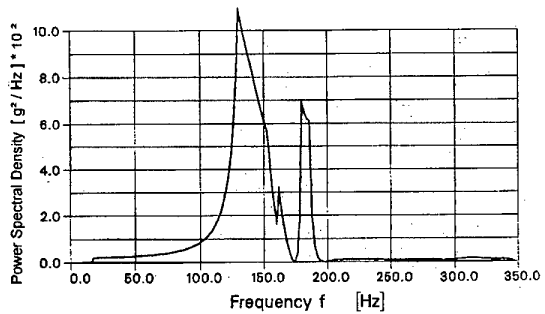
#### **Results from General Vibration Excitation IMU-Tray FE-Model**

Results of the response calculation at IMU c.g. due to general vibration input are demonstrated in Fig. 35 in terms of rms values for the three orthogonal axis. The excitation was always applied in the same direction as

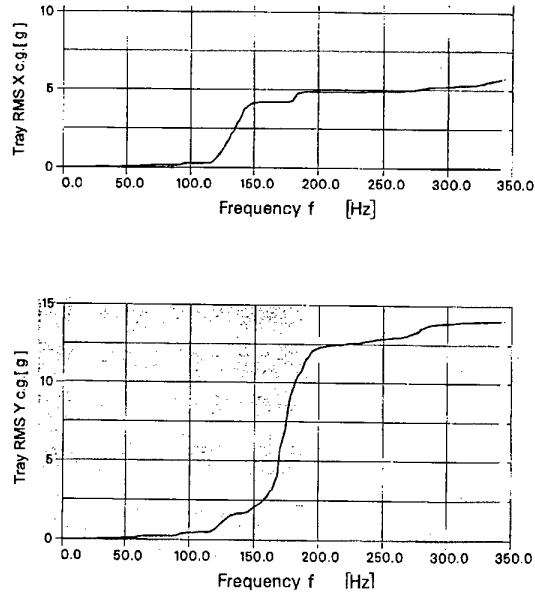
the response. The corresponding Power Spectral Density (PSD) in x-direction is shown in Fig. 36.



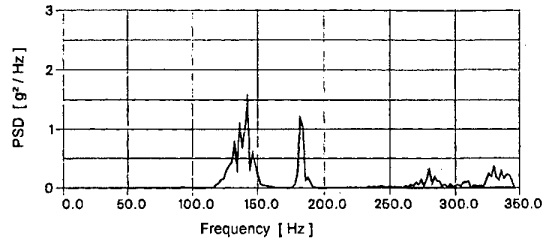
**Fig.: 35 Response due to general vibration at IMU foot at IMU c.g. position (IMU-Tray FE model)**



**Fig.: 36 X-acceleration at IMU c.g. from general vibration (IMU-Tray FE model  $f_{max} = 350$  Hz)**



**Fig.: 37 Response due to gunfiring input at IMU foot at IMU c.g. position (IMU-Tray FE model  $f_{max}=350$  Hz)**



**Fig.: 38 PSD of x acceleration at IMU c.g. due to buttfiring (x-excitation)**

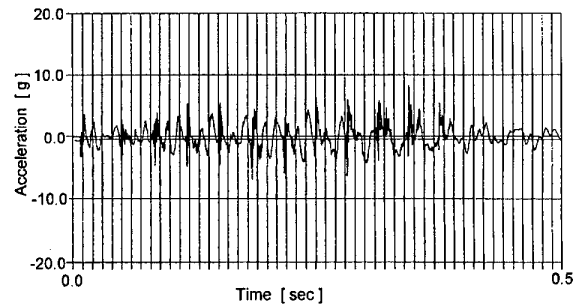
**Results from buttfiring response calculation.**

The results of the response calculation are depicted in Fig. 37 for Root Means Square (RMS) values and a Power Spectral Density (PSD) for x acceleration is shown in Fig. 38.

It should be noted that the gunfire results show two order higher levels compared with the general vibration results.

**Prediction from Total Aircraft FE-Model**

Results are demonstrated in Fig. 44 for defined gunfire input at the gun attachments. Fig. 39 illustrates the gunfire input and response in z-direction.



**Fig. 39: IMU acceleration in z due to gunfire (Total aircraft FE model  $f_{max} = 80$  Hz)**

### Prediction using Measured Transfer Function

In addition to the prediction using the total aircraft model and the IMU + tray FE model a prediction based on measured impulse hammer transfer functions from an aircraft test where the impulses were introduced in x-, y- and z-direction at the main gun attachment location was performed. The impulse hammer method was mainly introduced to predict responses beyond the frequency range of FE model.

### Comparison of the different prediction for gunfiring on ground.

The following Table 5 shows the comparison of rms values for the different prediction methods. The comparison is performed for the frequency ranges of 6-80 Hz and 6-2000 Hz. The MIL-SPEC based prediction shows for the IMU + tray model lower values since this model is evaluated only up to 350 Hz. The impulse hammer measured transferfunction is based on low force input at low frequencies and might have non-linear effects not included in the total aircraft model. The comparison of predictions to an aircraft test results show Table 5 which results in good correlation in x-, y- and z-direction.

	$\ddot{x}$	$\ddot{y}$	$\ddot{z}$
MIL-SPEC prediction			
impulse hammer pred.	1.61	1.19	0.94
total A/C response pred.	3.40		1.40
Aircraft gun test			

Table 5a: IMU rms accelerations, 6-80 Hz

	$\ddot{x}$	$\ddot{y}$	$\ddot{z}$
MIL-SPEC prediction	2.36	1.77	2.24
impulse hammer pred.	3.80	2.55	4.40
total A/C response pred.			
Aircraft gun test	2.62	2.94	3.85

Table 5b: IMU rms accelerations, 6-2000 Hz

### 3.5.6 Modal Validation

The design of the tray is performed with the use of the structural analytical model. The procedure of the validation of design by test results is demonstrated in Fig. 40.

According to the design procedure two analytical models namely the total aircraft model and the tray component model has to be verified by test results.

#### Ground Vibration Test of Equipment Tray.

A full scale dynamic model of the IMU + tray was built and tested. The test was performed to validate the prediction itself see Fig. 41.

A response search and a vibration test was performed. and the mode shapes and mode frequencies were

compared. Fig. 42 shows the first elastic mode comparison. The predicted IMU housing pitch mode was confirmed by the test.

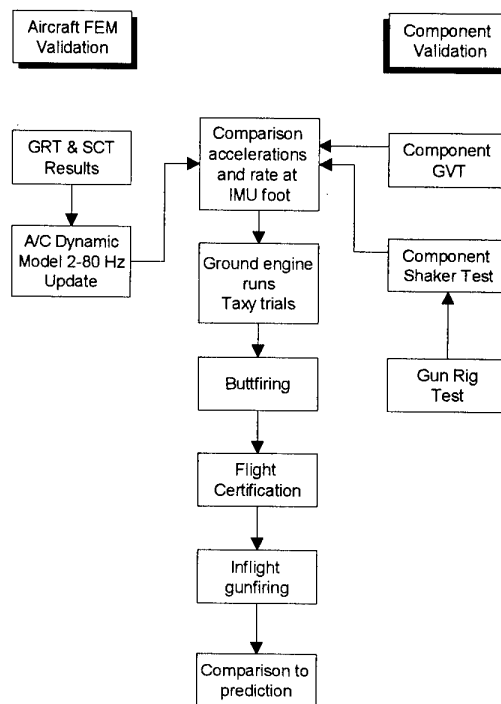


Fig.: 40 Modal Validation

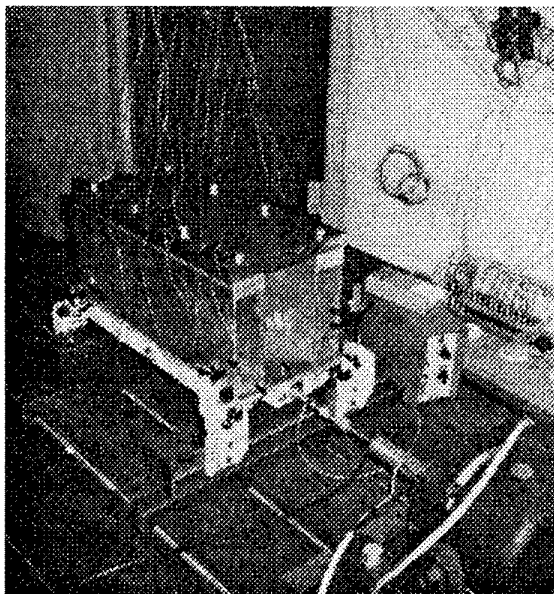


Fig.: 41 Ground Vibration Test Set Up

#### Tray Shaker Tests and Results

A shaker test has been performed with the final version of the IMU-tray after all design iterations on a shaker to validate the dynamic design loads which were derived from model prediction. Table 6 shows a

comparison of predicted and measured rms values of accelerations (0-300 Hz) for shaker excitation in x-, y- and z-direction. Reasonable agreement in the diagonal terms could be found.

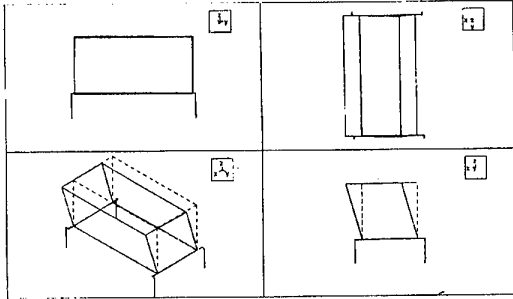


Fig.: 42a Measured Mode Shape; f = 51.66 Hz

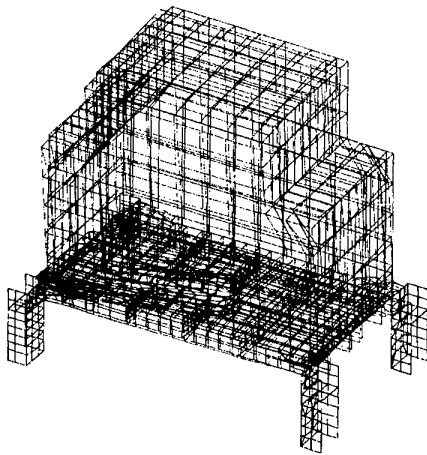


Fig.: 42b Calculated Mode Shape; f = 50.93 Hz

Excitation in x	rms x [g]	rms y [g]	rms z [g]
test result	9.2	1.22	2.5
prediction	6.8	0.13	1.4
Excitation in y	rms x [g]	rms y [g]	rms z [g]
test result	0.72	7.0	2.5
prediction	0.1	8.2	0.3
Excitation in z	rms x [g]	rms y [g]	rms z [g]
test result	1.4	1.7	8.0
prediction	1.1	3.0	5.6

Table 6: RMS Acceleration at IMU c.g. due to general vibration

### 3.5.7 Gunfire Tests and Results

#### Gun Rig Tests

Gun rig tests were conducted and during the tests the time histories of the gunfire response at the gun attachment points in x-, y- and z-direction and the blast pressure in front of the gun were measured. Time

histories are shown in Fig. 43 for the x-, y- and z- load at the main attachment and in Fig. 44 for z-load at the front attachment. The time history were used for a subsequent prediction of IMU response using the total aircraft dynamic model.

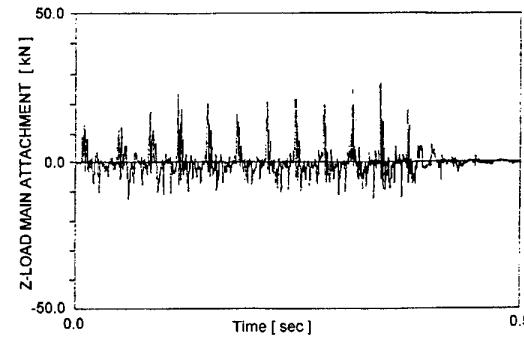
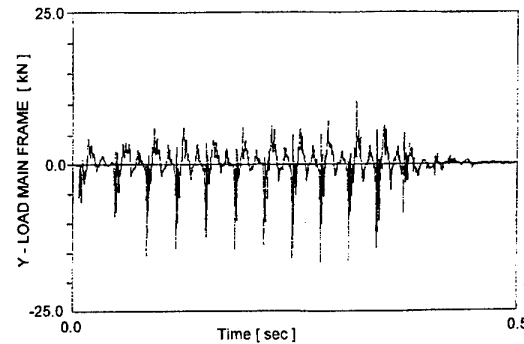
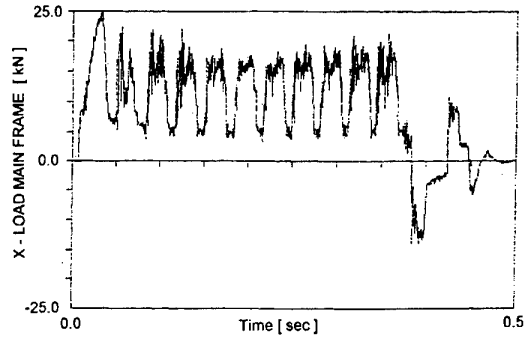


Fig.: 43 Time History from Gun Rig Test (Main gun attachment)

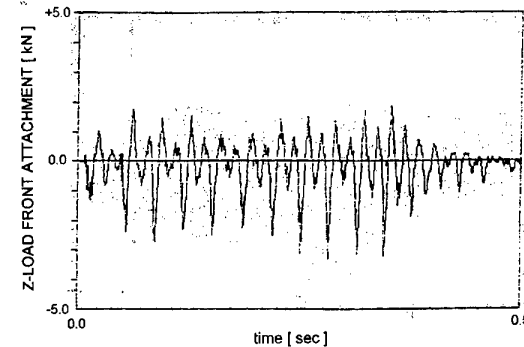
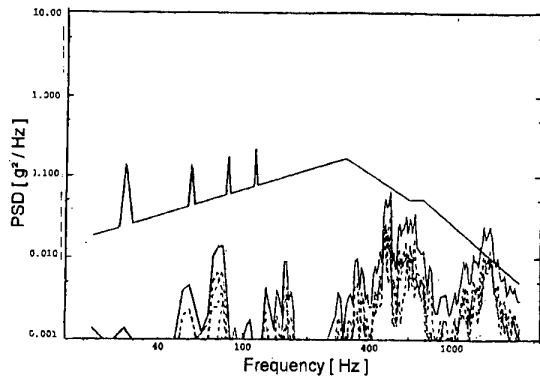


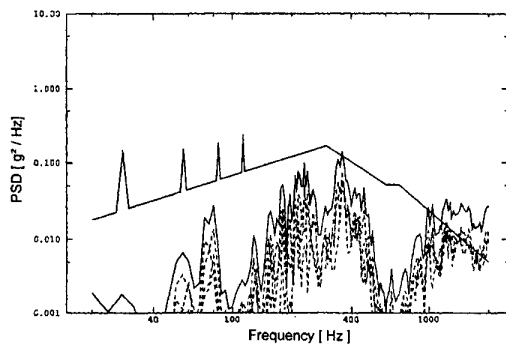
Fig.: 44 Time History from Gun Rig Test (Front gun attachment)

### Aircraft Buttfitting Tests

Results of measured and predicted power spectral densities are demonstrated in Fig. 45, good correlation was found for the low frequency harmonic gun excitation. Above 1 kHz the measurement exceeds the predicted values.



**Fig.: 45a Power Spectral Density - Aircraft Buttfitting x-acceleration**



**Fig.: 45b Power Spectral Density - Aircraft Buttfitting z-acceleration**

#### 3.5.8 Conclusion Equipment Tray Loads

The demonstrated optimization procedure for equipment trays under general vibration and gun fire environment could be verified using shaker test results of the final designed tray and on aircraft gun fire test results.

The iterative design of the tray leading to different stiffer structure of the tray is mainly controlled via the check stress calculation, where the IMU design constraints (minimum frequency at IMU resonance frequencies) are covered via the vibration calculation and the response calculation which also defines the dynamic design loads.

The tray design was performed with different computer tools for vibration calculation, dynamic response, dynamic load and stress. It is recommended to couple different tools in an overall structure optimization program.

Concerning the specifications of general vibration in MIL-STD-810D is believed to be very conservative in the application for structural design. The physical relevant vibration environment for a special aircraft can be defined after sufficient flight test experience which would be demonstrate in longer fatigue life.

#### 4. INTEGRATION INTO FUTURE STRUCTURAL OPTIMIZATION

During military aircraft structural development dynamic loads have been introduced which resulted from predictions of the flexible aircraft up to high frequencies. Dynamic gust loads, dynamic wing and fin buffet loads, Hammershock dynamic loads have been applied using different tools. In future an integrated design shall be be folloed which shall include the main dynamic effects as described here.

#### 5. CONCLUSIONS

Table 7 demonstrates the consequences of all existing dynamic load predictions due to the different origins of loads. It is recommended for future structural aircraft design to consider the different sources and the locations as shown in the Table 7.

#### 6. REFERENCES

- /1/ Sensburg O., Becker J., Lusebrink, H., Weiss F. Gust Alleviation on Airbus A300 B Contribution to the 13th Congress of the International Council of the Aeronautical Sciences (ICAS), Seattle/USA, Aug. 1982
- /2/ Becker J., Weiss F., Sensburg O. Compatibility of active control technologies with aircraft structure design. International Symposium on Structural Control University of Waterloo/Ontario (Canada), July 1985
- /3/ Becker J., Weiss F., Cavatorta E., Caldarelli C. Gust Alleviation on a transport aeroplane FDP-FMP Meeting of AGARD at Göttingen, May 1985
- /4/ Becker, J. Gust load Prediction and Alleviation on a fighter Aircraft



AGARD-R-728 SMP Conference, Oberammergau, Germany on 8-13 September 1985

/5/ Försching H.

Introductory survey of aeroelastic problems in separated and transonic flow

Von Karman Institute for Fluid Dynamics Lecture Series 1981-4

/6/ Mabey D.G., Cripps B. E.

Some measurements of buffeting on a flutter model of a typical strike aircraft

Royal Aircraft Establishment AGARD Flight Mechanics Conference, Paper 13, Oct. 1982

/7/ Becker J.

Bewegungsinduzierte Luftkräfte bei abgelöster Strömung und ihre Übertragung auf die Ermittlung der Strukturresponse

MBB/S/PUB/116/1982

/8/ Gravelle A., Destuynder R.

Methodes Nouvelles D'Excitation, D' Acquisition Et De Traitement Concernant Des Essais Instationnaires En Soufflerie AGARD-CPP-348, AGARD-Conference Preprint No. 348

/9/ Laschka B.

Interfering lifting surfaces in subsonic flow

Zeitschrift für Flugwissenschaften 181 Heft 9/10. 1970

/10/ Rodden W. P., Giesing J. P.

New Developments and Applications of the Subsonic Doublet-Lattice Method for Nonplanar Configurations AGARD-CP-No. 80, 1971

/11/ Bennekens B.

Description of the computer programs for the calculation of aerodynamic loads on oscillating wing-body configuration in subsonic flow (NLRI-Method)

NLR-TR-76120 C

/12/ Roos F. R., Bennekens B., Zwaan T. R..

Calculation on unsteady subsonic flow about harmonically oscillating wing/ body configurations

Journal of Aircraft Vol. 14. No. 5. May 1977

/13/ Hounjet M.H.L.

An improved potential gradient method for the prediction of aerodynamic loads on non-planar lifting surfaces oscillating in supersonic flow

NLR TR 81086 L, 7 June 1981

/14/ Becker, J.; Gravelle, A.

Some Results of Experimental and Analytical Buffeting Investigations on a Delta Wing

Second International Symposium on Aeroelasticity and Structural Dynamics; April 1-3 1985 Aachen, Germany

/15/ Breitsamter Ch. and Laschka B.

Turbulent Flow Structure Associated with Vortex-Induced Fin Buffeting.

Journal of Aircraft, Vol. 31 (No. 4) pp. 773-781; July-August 1994

/16/ Breitsamter Ch. and Laschka B.

Velocity Measurements with Hot-Wires in a Vortex-Dominated Flowfield. In Wall Interference, Support Interference and Flow Field Measurements.

AGARD-CP-535; Brussels, Belgium, Oct. 4-7 1993, pp. 11-1 - 11-13, 73<sup>rd</sup> Meeting of the AGARD Fluid Dynamics Panel

/17/ Becker J., Bergmann H., Luber W.

Dynamic Hammershock effects on the air intake design on supersonic aircraft

Structures under Shock and Impact; Third International Conference; Madrid, Spain, 1<sup>st</sup>-3<sup>rd</sup> June, 1994

/18/ Military Standard: **MIL-STD-810D**

Environmental Test Methods and Engineering Guidelines

/19/ British Standard Institution: **BS 3G.100 Part 2**

General Requirements for Equipment in Aircraft

/20/ Green C.

Vibration Manual

George C. Marshall Space Flight Center Report

NASA TMX - 64669

/21/ Harris Cyril M.

Shock and Vibration Handbook

McGraw-Hill BOOK COMPANY

/22/ Luber W., Becker J.

Design and Qualification of Equipment Trays in high dynamic Environment

International Forum on Aeroelasticity and Structural Dynamics; Manchester, UK, 26-28 June, 1995

type of dynamic load	Wing	Fin	Fuselage	Foreplane	engine mount	intake	store attachment	landing gear attachment	equipment tray	actuator attachment
<b>gust</b> • discrete • turbulent	outer wing upper / lower side wing attachment	upper fin fin attachment	front and rear	foreplane attachment			outer wing spigot pylon		outer wing upper fin front fuselage flap	foreplane rudder flap
<b>buffet</b>	outer wing	upper fin fin attachment	front and rear		forward, rear	attachment of fwd air intake inner duct structure	outer wing stations		fuselage, wing fin, front fuselage, radar frame	rudder o/b wing flap
<b>buffet due</b> • airbrakes • cavities		fin buffeting	fuselage skin panels						fuselage	
<b>gunfire</b>			gun attachment panel due to blast			gunfire induced Hammershock			fuselage	
<b>birdstrike</b>	leading edge	leading edge	canopy radome	leading edge		leading edge intake				
<b>landing</b>			front fuselage				o/b wing	fuselage		
<b>acoustic</b>						outer air intake missile bays			fuselage	
<b>rough runway</b>			front fuselage					attachment		
<b>flight test</b> • bunker • frequency sweep	attachment	attachment		attachment						all actuators

Table 7: Overview Influence of Dynamic Loads

# DYNAMIC LOADING CONSIDERATIONS IN DESIGN OF MODERN COMBAT AIRCRAFT

R. CHAPMAN  
AERODYNAMICS DEPARTMENT  
BRITISH AEROSPACE - MILITARY AIRCRAFT DIVISION  
WARTON AERODROME, PRESTON, LANCs. PR4 1AX  
UNITED KINGDOM

## SUMMARY

The design and clearance for flight of recent aircraft has provided new challenges in the field of loads prediction and validation. Traditionally during the initial design phases of an aircraft project, dynamic loading effects have been covered by uncertainty tolerances applied to static loads. Only when structural or equipment qualification problems emerge during development testing, or worse in-service, have dynamic loading problems been fully addressed.

The approach at BAe is to include dynamic loading at the design and development stage to a much greater extent than formerly. This is with the intention of reducing or eliminating the need for costly post-design investigations and/or structural re-design.

This paper outlines the effects considered and some examples of the challenges encountered with respect to project constraints/criteria, methods maturity and flight clearance procedures.

As validation of dynamic loading predictions is essential to aircraft qualification and certification, examples comparing predicted and flight measured data are presented.

## 1 INTRODUCTION

First a definition. The dynamic loading effects referred to here are the loading actions which cause an aerodynamic and structural response of the airframe in the frequency range 2Hz to 100Hz approximately. This is not a hard definition, but generally loading at a frequency below the range is held to be quasi-static and above that range there is not usually a major component problem; more often the concern here is related to localised acoustic effects and stores/equipment environmental qualification.

Basic trends in design specifications dictate that new aircraft projects are expected to have much more highly optimised structure. This in turn implies that, given sufficient definition of its proposed role in life, the aircraft can be optimised for specific activities. Therefore, so can the structure in order to withstand the loads generated by those activities, and meet any given mass targets.

Traditional approaches to developing design loads do not fully account for oscillating loads sufficiently to optimise the structure, from both a strength and fatigue point of view. With modern designs we have to account for dynamic loading effects much earlier in the design process than was previously the case.

This raises some fundamental questions, namely :

- What are the applicable criteria ?
- Precisely which effects should be addressed ?
- What methods and tools are available ?
- How can they be validated ?

## 2 CRITERIA

In the early stages of a project, searches are made for applicable criteria. Prior to the mid-1980's dealings with dynamic loading had generally been of the problem solving type, rather than prediction. This still forms a significant proportion of the work relating to older projects. So whilst there was experience of certain dynamic effects, design practices and criteria did not fully address all aspects of dynamic loads. This was compounded by the lack of suitable prediction tools and methods.

Hence, knowledge of related design criteria was sparse. The items with significant formal coverage were

- gust loads
- undercarriage loads

## ATMOSPHERIC GUSTS/TURBULENCE

Illustrated in table 1 is an item which was compiled during the 1980's to compare three sets of criteria relating to gust loading. At that time, changes were taking place. Established standards were being revised or replaced, which produced a variety of potential criteria.

The main thrust of the exercise was to compare the different approaches to discrete gust calculations (all had similar provision for continuous turbulence analysis). The main debate centred on the severity of the gust to be applied. A brief examination shows that, whilst the intensities (velocities) of the gusts were similar, the length of the assumed gusts was significantly different. For instance, when related to the Experimental Aircraft Project (EAP - a one-off technology demonstrator aircraft of foreplane-delta configuration first flown in 1986) the Def-Stan 00-970 document can be interpreted to require a 5c length gust whereas the Mil-Standards require a 25c length gust. Both have the same peak intensity.

The apparent mis-match reflects the differing emphasis in practice between the UK and US. The US approach places greater emphasis on the continuous turbulence analysis, to exercise the structure, whereas the UK relies on the discrete gust.

The Def-Stan discrete gust requirement is severe due to the potential for tuning with fundamental wing structural response modes. That is, the implied frequency of excitation provided by the short gust can be nearly coincident with the fundamental wing bending or torsion modes (given worst case combinations of aircraft speed, altitude and configuration assumed for calculation purposes).

At the risk of stating the obvious, if you excite a structure at or near its resonant frequency you will get a large response and consequently high loading. The implications of this approach are that parts of a highly manoeuvrable, supersonic, combat aircraft can be designed by gust induced loading rather than manoeuvre induced loads!

Discussions have taken place with colleagues, partners, customer nations and associated certification authorities to try and establish an agreed approach. Questions considered covered items such as alleviation of gust intensity at the shorter gust lengths for minimisation of the

'tuning' effects, could we use the then current civil aviation standards which did seem to offer this alleviation, what was the basis of the requirements and was it a realistic possibility to experience these gust characteristics during the service life of an aircraft, etc., etc..

Hard answers were initially few and far between, but eventually resolved. The short gust lengths combined with high intensities were felt to be severe, but proper clarification and understanding of the criteria provided a sound basis for design purposes. If the limit loading concerns the worst case that can occur during the lifetime of an aircraft, and probability analysis suggests that such a severe gust can occur during that lifetime, then it is reasonable to use that gust case for design. When applying criteria, it is essential to understand the design aims.

## UNDERCARRIAGE LOADS

Turning to the criteria related to undercarriage design, these were mostly applicable to the design of the units themselves. However, they did mention the possibility of a whole aircraft dynamic structural simulation, **if thought applicable**. This isn't usually necessary because combat aircraft usually have relatively short, stiff fuselages where interaction between landing gear and aircraft structure is not a problem; rigid fuselage assumptions usually being adequate. Given a moments consideration you can see the need for this with larger aircraft, and serious consideration needs to be given to this phenomenon. However, with ever increasing computing power available this type of analysis is more feasible than previously.

An example where this type of analysis would have been useful was a UK project of the early 1960's called TSR2. A problem was caused by significant interaction between the undercarriage and fuselage, immediately after touchdown. The loading problems associated with this were being addressed, when the project was cancelled.

## CERTIFICATION/FLIGHT CLEARANCE

This principle of **if thought applicable** appeared several times in the standards for several other areas, but major criteria are lacking. This can lead to lengthy discussions with Certification Authorities concerning which phenomena are to be fully covered.

There is an extensive range of dynamic phenomena which could merit closer examination,

and some of these will be dealt with in the next section. Experience shows that there are a few dominant phenomena, but open-mindedness is encouraged at the design stage in order to prevent problems occurring later in the project life due to omission. It is good practice to positively demonstrate why a phenomena need not be investigated further.

The next section deals with what we do consider when deciding precisely which effects should be examined, despite the lack of formal criteria.

### 3 DYNAMIC EFFECTS CONSIDERED IN COMBAT AIRCRAFT DESIGN

Where there is significant mass carried on a relatively flexible structure, structural dynamic response to excitation (or forcing) can be a significant contribution to load levels. Effects can be on major airframe structures or more localised, eg. store or undercarriage attachments.

Experience shows that the list of possible areas for consideration is large. In our experience, the following list shows the most important sources of excitation which affect major airframe components

- gust/atmospheric turbulence  
(already discussed in the criteria section)
- hammershock  
(locked-in surge - intake duct and external to the intake)
- flutter test excitation  
(during development flying only)
- buffet  
(wing, foreplane/tailplane, fin, airbrake, excrescences)
- store release and jettison  
(impulsive loading at several areas on the airframe)
- missile firing  
(impulsive loading and plume effects)
- ground operations  
(anything the pilot can conjure up during take-off, landing and taxiing)

These are all effects which should be considered in design.

### HAMMERSHOCK

Taking the example of hammershock, it is necessary to examine the effects forward of the intake because on aircraft like EAP the foreplanes are situated nearby. On EAP, the frequency of the hammershock pulses was predicted to be almost co-incident with that of the foreplane fundamental bending mode, giving the potential for serious consequences. Mass balancing was applied to the foreplanes to reduce the fundamental bending frequency so that 'tuning' was unlikely to occur. In the event, this was not a problem because the dissipation of the pressure pulses once they had left the intake was greater than predicted or measured in wind tunnel tests.

### FLUTTER TEST EXCITATION

A further item which has to be cleared for development flight testing, is the method of excitation for flutter testing. This has been reported elsewhere (ref. 1). Our favoured method on modern fly-by-wire combat aircraft is basically a series of sine sweep commands injected into the flight control system (FCS) signals to the control surface actuators. By definition it is intended to create a structural response large enough to be clear of potential background vibration levels (due to buffet and turbulence usually) and sufficiently exercise the structure for measurement and analysis of structural modes and their associated damping levels. Operation of the system can create high loading levels. Hence, it requires a significant amount of loads clearance and fatigue analysis work, due to the many combinations of ways that the system can be operated.

### BUFFET AND BUFFETING

More traditionally, excitation of the airframe by separated flow (buffet) and the associated response (buffeting and buzz) are of concern to the Dynamic Loads engineer.

The opportunities for this to happen are many and can, and indeed do, constitute a major area of study in their own right. It is not my intention to repeat all that here. Rather to point out, from the design point of view, that there are instances where the traditional quasi-static manoeuvre loads are not the designing case. For example, fin buffeting. It is possible to obtain high dynamic loading levels when the manoeuvre loads are low eg. at high incidence with zero sideslip.

Separated flow from wing leading edge root

extensions (LERX), foreplanes, wing etc. can have severe effects on the fin. The exciting flow (discrete vortex or combination of vortices) possesses characteristic frequency content depending upon its source. The source or sources may not always be clear, and the excitation frequency spectra may not actually contain discrete peaks at specific frequencies. However it is unlikely to be a 'flat' spectrum.

Several aircraft types have suffered this effect. On Tornado, for example, the excitation spectra show a 'humped' profile. The centre frequency of the 'hump' matches almost exactly with the fin fundamental torsion mode! This is illustrated in figure 1. At the worst case conditions, the response of the fin is almost entirely limited to this one modal frequency. In the tip region the response, and hence the loads, can be very large.

With Tornado, the phenomenon of fin buffeting was not encountered until well into the development phase and after initial service deliveries. A post-design modification was required to ensure structural integrity

In addition to our Tornado experience, there is much published material relating to twin-finned designs; notably F-18. It is clear that fin buffeting must be examined in the early stages of design for combat aircraft with significant angle of attack capability.

#### STORES RELEASE

For stores release and jettison (and missile firing) it is noted here that, whilst there may not be a design case due to this activity, it is essential to search for the possibilities. Particularly where the project specification calls for combined manoeuvring and release, loading levels can be significant. Development of existing designs for improved flight clearance envelopes can increase the problems here.

#### GROUND OPERATIONS

Whilst not an aerodynamic phenomena, touchdown during landing can significantly excite the airframe. It must be assessed for design purposes. Characteristics to look for are large masses mounted on relatively flexible structure. An example of this type would be a store or pod mounted in the wing tip region. Again, these cases are often covered by other dynamic phenomena such as gusts or buffeting, but local structural design can be influenced. This problem can be increased where high touchdown sink rates

are required, for example on carrier-borne aircraft.

#### LOCALISED AND SECONDARY EFFECTS

In addition to the sources of airframe excitation above, the following items relate to modification of the response and hence the loads.

Related to carriage of stores on pylons, one of our longer established approaches to pylon design and clearance has been to include an allowance for dynamic overswing. This is dominated by store inertia and pylon structural characteristics, and can yield factors of 2 or more on static loads!

Another loading related issue, particularly for clearance rather than design, is that of the potential effect of the FCS on the structural and aerodynamic response. In other words, structural coupling or aero-servo-elasticity. Due to the phased approach adopted for the implementation of a FCS, there is typically more than one version flown before the end of development. Each version has to be assessed for its effect on the aero-structural response characteristics and how these may affect any loading predictions.

A summary of the major dynamic loading effects covered here can be found in table 2. It shows the principal items for examination during design and clearance. It is not exhaustive, and the dynamics engineer is encouraged to investigate whether other phenomena should be addressed.

#### 4 LOADING PREDICTION METHODS

It is a fact that methods used to date cannot be considered highly accurate, in all cases. They are based on well established routines but with limited aerodynamic capabilities. eg NASTRAN aeroelastics suites or their equivalent. Some of their dis-advantages are

- linear structural and aerodynamic theories
- aerodynamics applicable to simple configurations or even lifting surfaces only
- no accurate transonic aerodynamic capability
- aerodynamic excitation usually derived by wind tunnel testing or semi-empirical methods

The principle adopted is that of caution. If doubt exists as to the validity of a prediction, then a pessimistic approach is adopted. This ensures a safe design, but may be unduly restrictive when formulating a clearance recommendation.

This means that a significant validation programme linked to flight testing is necessary before issue of final clearances. Take the case of figure 2. Wind tunnel testing is essential for prediction of some of the aspects illustrated. Whilst most of the effects shown would concern fatigue and environmental qualification issues, if advanced time-accurate unsteady computational fluid dynamics (u/s CFD) methods were available at a production standard for these phenomena then the ability to calculate major surface dynamic loading effects would be a considerable fall-out benefit. This is on the assumption that if the detailed localised flow can be predicted then prediction of major areas of separated flow (and characteristics) providing excitation to the airframe should be attainable.

#### CFD

Use of advanced u/s CFD methods is already possible but limited. Localised, specific problems have been tackled using such methods. However, they are not yet available for production standard use on complex configurations - ie not yet cheap and easy to use. However, research and development programmes are in progress to address this and should receive encouragement.

#### EMPIRICISM

An example of the successful use of an empirical approach is that of designing EAP to account for fin buffeting. Figure 3 illustrates how an initial prediction of structural response can be carried out. From Tornado measured characteristics, an estimate of EAP fin response was made. Using this approach requires making assumptions (true in this case) that EAP fin will have similar mass and structural characteristics to Tornado, and that the dominant parameters are wing sweep, incidence, and dynamic pressure. It would not of course be applicable to twin fin designs, or if the structure is radically different, but there does exist a large amount of publicly available information to derive such an approach.

It goes without saying, that this is not the only method used, merely a first indication. Extensive wind tunnel testing relating to fin buffet has yielded good results, but is not generally applicable for quick feasibility studies in the early stages of a project design.

The use of wind tunnel testing is necessary when no other methods are available, but does prove impractical for initial design purposes due to the time scales involved. The effects of scale, and

whether a rigid or flexible model should be used are important. Amongst other considerations are the density of instrumentation to be used and data analysis techniques which both affect how useful any testing can be.

#### FLIGHT TESTING AND VALIDATION

The authorities may require, as part of the clearance approval that, where the aircraft is undertaking manoeuvres causing buffeting, the structural response must be monitored in real time. Once it can be shown that there is no loading problem then those particular manoeuvres cease to need monitoring.

To satisfy this requirement, a simple real-time monitoring system has been developed and commissioned at Warton. This system monitors accelerometer output against predicted magnitudes and trends which are developed during the loads clearance process. It provides quick visibility of the quality of the predictions. This approach increases safety over traditional monitoring of pen-traces. It also reduces the need for post-flight analysis of data and thereby contributes to rapid progression of flight testing if predictions prove adequate.

Post-flight data analysis is still a vital part of operations in order to obtain validation of the predictions. As mentioned above, the existing methods are not accurate in all cases and prediction model matching may be necessary for progression of flight clearance work.

#### THE WAY AHEAD

Assuming the need for ever more rigorous structural optimisation, and thereby intensive design loads case development, design of future projects will need advanced methods to cut costs and design time scales by providing more extensive, more accurate predictions quickly.

A thought occurs that, whilst current projects are extensions of well established practices which have had similar aerodynamic design constraints on the external shape and structure for decades, the new criteria being developed to incorporate stealth technology mean that aerodynamic performance criteria are not the only ones affecting the external shape of the aircraft.

Hence, where with a certain amount of caution and application of experience, existing simple aerodynamic methods could be used in the design process, this is not now necessarily the case.

Research is on-going to establish what is valid from existing tool sets and what needs development for future projects. This approach applies equally to materials and structures. Of course, if the configurations chosen in future are very novel, then even experience may prove inadequate and a new database must be compiled!

In conclusion ,

- We do have some prediction methods but know them to be inaccurate, and they are used with caution.
- Wind tunnel testing is carried out to provide higher quality aerodynamic information, but we have to accept scaling effects and time-scale constraints.
- We have to analyse flight data extensively to validate the predictions made, and underwrite any clearance recommendations beyond development testing.
- Research and development is necessary to improve accuracy, shorten time-scales, and prove methods are suitable for use with airframe shapes dictated by considerations other than aerodynamic and structural performance criteria.

## 5 EXAMPLES OF PREDICTIONS AND FLIGHT DATA

The final section serves to illustrate two examples of how the predictions match with flight measured data. This is the first stage of the validation process.

Figure 4 shows a composite picture made up from a pen plotted time history and a screen plot from the monitoring system mentioned earlier. The pen trace is the traditional approach for this type of monitoring. The output being monitored is accelerometer signals from the wing tip region during a wind-up-turn manoeuvre. The left hand box is showing acceleration levels for three parameters, of which the pen trace is one, plotted as a percentage of their maximum expected values at that flight condition. The right hand box is plotting one of these but divided by  $q$  (dynamic pressure), against aircraft incidence. The solid lines represent predicted trends. As can be seen the measured data follow the predicted trends very well. The magnitudes are lower than expected.

A point worth mentioning here is that this example of flight measured data is very 'clean' -

there is not much evidence of spurious background vibration effects. This is not always the case, which makes the engineer's job of interpretation potentially much harder.

However, this is just one test point. A far larger set of flight measured data would need to be examined before reaching a conclusion concerning the accuracy of the predictions. In this case, using the combination of wind tunnel data, semi-empirical formulae and a good standard of structural modelling, an acceptable set of trend predictions has been produced. The magnitudes tend to be over-predicted.

A second example is shown in figure 5. This compares the predicted and measured data for a flutter test point. The flutter excitation was mentioned earlier. This case consists of a swept sine input to the trailing edge flaps (inboard and outboard simultaneously). It moves from 2Hz to 30Hz over 60 seconds. The accelerometer response measured is at the wing tip.

Again we have a pen plot showing what we see in 'real time' at the ground monitor station. Comparison with the predicted time history shows an extremely good match in terms of shape. The magnitude is not so good. In this example, the prediction is 50% greater. This is certainly the 'right side' as far as a safe clearance is concerned.

However, if this were typical, the implication is that we may unduly restrict the activities of the aircraft if we base any clearance recommendations on the predictions alone without taking into account increasingly available flight measured data from development test flying.

Like the buffet example, this is just one point in the flight envelope so before reaching any conclusions we need to consider a far wider sample of data. This example of prediction includes a specific part where the flap actuator characteristics are modelled. We know that these were 'pessimised' because of a sparse database relating to actuator characteristics in the early stages. This was addressed in subsequent analyses.

In conclusion, we have the ability to carry out predictions, but because we know that the methods available are not particularly accurate in predicting magnitudes, we tend to err on the pessimistic side throughout the modelling assembly. In some cases, these 'pessimisms' will produce potentially restrictive over-predictions,



but it can be difficult quantifying this until flight measured data are available.

## 6 CONCLUSIONS

This paper has outlined the dynamic loading effects which need consideration in design and clearance for modern combat aircraft.

Formal design criteria are sparse, with the exception of gust loading and undercarriage loads. When applying criteria, it is essential to have clear design goals. The decision to include a particular loading action is left to the experience of the Engineer, in consultation with the Project, but requires justification of inclusions and omissions to the certification authorities.

Examples of the major dynamic loading effects have been discussed, and these are summarised in the accompanying table. There are 7 categories identified for consideration in any new project - atmospheric turbulence/gusts, buffet and buffeting, stores release and jettison, missile firing, hammer shock, and ground operations. It is emphasised that this is not an exhaustive list and that the dynamics engineer should be prepared to think around the subject.

Prediction methods have been briefly addressed. Most aerodynamically induced dynamic effects are still predicted using wind-tunnel testing and analysis of existing databases. Semi-empirical formulae and rules have been developed, and will continue to play an important role. Some advanced theoretical aerodynamic prediction tools (u/s CFD) are becoming available, but have some way to go before use can be made of them on a 'production' basis for complex configurations. Some have been used to examine localised effects. Continued development of these tools is encouraged.

Validation of predictions is essential. Whilst improving, the present standard of prediction accuracy is good for trend identification, less so for magnitudes. Examples have been given to illustrate this. Over-prediction of magnitudes can lead to undue pessimism when developing clearance recommendations.

## ACKNOWLEDGEMENTS


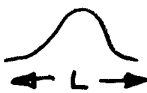
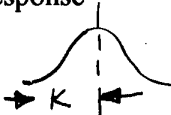
Whilst no specific individuals are singled out for mention, the author wishes to acknowledge the support of colleagues at BAe Military Aircraft Division and the Defence Research Agency at

Farnborough, UK. It is also noted that work on various aircraft projects produced for the UK Ministry of Defence has provided a breadth of experience which has contributed to this paper.

## 7 REFERENCES

1. RB RAMSAY  
In-Flight Structural Mode Excitation System for Flutter Testing.  
AGARD-CP-519, Paper no. 15, 1992

**TABLE 1 - REGULATIONS CONCERNING ANALYSIS OF DYNAMIC LOADING DUE TO GUSTS AND TURBULENCE**

REQUIREMENT	MIL-A-8861A	MIL-A-8861B	DEF.STAN 00-970 (Amdt. 5)
<b>Discrete '1-cos' gust</b>	YES or turbulence in accordance with contract  Para 3.22 & 3.22.1.1.1	YES but depends on contract  Para 3.5 & 3.5.1.1	YES  Chapter 204 Para 5.1
<b>Gust Length</b>	L = 25c    Para 3.22.1.1.1	L = 25c    Para 3.5.1.1	K > 15.2m (50 ft)  Varied to find peak of response   Chapter 204 Para 5.1
<b>Gust Intensities at V<sub>G</sub></b>	66fpsEAS up to 20kft  Between 20kft and 50kft linear variation between 66fps and 38fps EAS.  Above 50kft use ratio $\frac{\sqrt{\sigma_{alt}}}{\sqrt{\sigma_{50k}}}$	66fpsEAS up to 20kft  Above 20kft use ratio $\frac{\sqrt{\sigma_{alt}}}{\sqrt{\sigma_{50k}}}$	66fpsEAS up to 20kft  Between 20kft and 50kft linear variation between 66fps and 38fps EAS.  Above 50kft constant
<b>Gust Intensities at V<sub>H</sub></b>	As for V but 50fps and 25fps EAS	As for V but 50fps EAS	As for V but 50fps and 25fps EAS
<b>Gust Intensities at V<sub>L</sub></b>	As for V but 25fps and 12.5fps EAS	As for V but 25fps EAS	As for V but 25fps and 12.5fps EAS
<b>Gust Intensities at V<sub>LF</sub></b>	50fps EAS	50fps EAS	
<b>Gust Intensities</b>	25fps EAS	25fps EAS	25fps EAS
<b>Low altitude V<sub>H</sub> with manoeuvre of 0.6*max.g</b>	Para 3.22.1.1.4	Para 3.5.1.2	Chapter 204 Para 3.4

**TABLE 1 - REGULATIONS CONCERNING ANALYSIS OF DYNAMIC LOADING  
DUE TO GUSTS AND TURBULENCE**

<b>Continuous turbulence</b>	YES or discrete gust in accordance with contract  Para 3.22	YES but depends on contract  Para 3.5	Only if considered appropriate by Project Director  Chapter 204 Para 5.1
----------------------------------	---	--	---

**TABLE 2 - SUMMARY OF DYNAMIC LOADING EFFECTS RECOMMENDED  
FOR CONSIDERATION DURING DESIGN AND CLEARANCE**

<b>SOURCE OF LOADING</b>	<b>COMPONENTS AFFECTED</b>	<b>TYPES OF AIRCRAFT / COMMENTS</b>
ATMOSPHERIC TURBULENCE / GUSTS	WING FORE / TAIL PLANE FIN FUSELAGE CREW EQUIPMENT STORES & PYLONS SENSORS & PROBES	HIGH SPEED AIRCRAFT WITH RELATIVELY LOW WING LOADING
BUFFET / BUFFETING/ BUZZ	WING FORE / TAIL PLANE FIN STORES & PYLONS LOCALISED EFFECTS eg. Excrescences Panels Sensors & Probes Airbrake	ALL TYPES, BUT PARTICULARLY THOSE WITH SIGNIFICANT AoA AND MANOEUVRING CAPABILITY  Bluff shaped excrescences mounted on large panels
STORES RELEASE & JETTISON	WING FUSELAGE PYLONS ATTACHMENTS & BACK-UP STRUCTURE	ALL TYPES
MISSILE FIRING	As above + PLUME EFFECTS on local panels control surfaces tailplane etc.	ALL TYPES
HAMMERSHOCK	INTAKE & DUCT FOREPLANES FRONT FUSELAGE SENSORS & PROBES	CANARD CONFIGURATIONS WITH CHIN INTAKES AFT OF FOREPLANES
GROUND OPERATIONS	WING FORE / TAIL PLANE FIN FUSELAGE CREW EQUIPMENT STORES & PYLONS	ALL TYPES BUT WORSE FOR CARRIER-BORNE & VSTOL  Any extreme action that can be achieved by the pilot

FIGURE 1

# FIN BUFFETING

SKETCH OF FIN BUFFET EXCITATION AND RESPONSE  
POWER SPECTRA

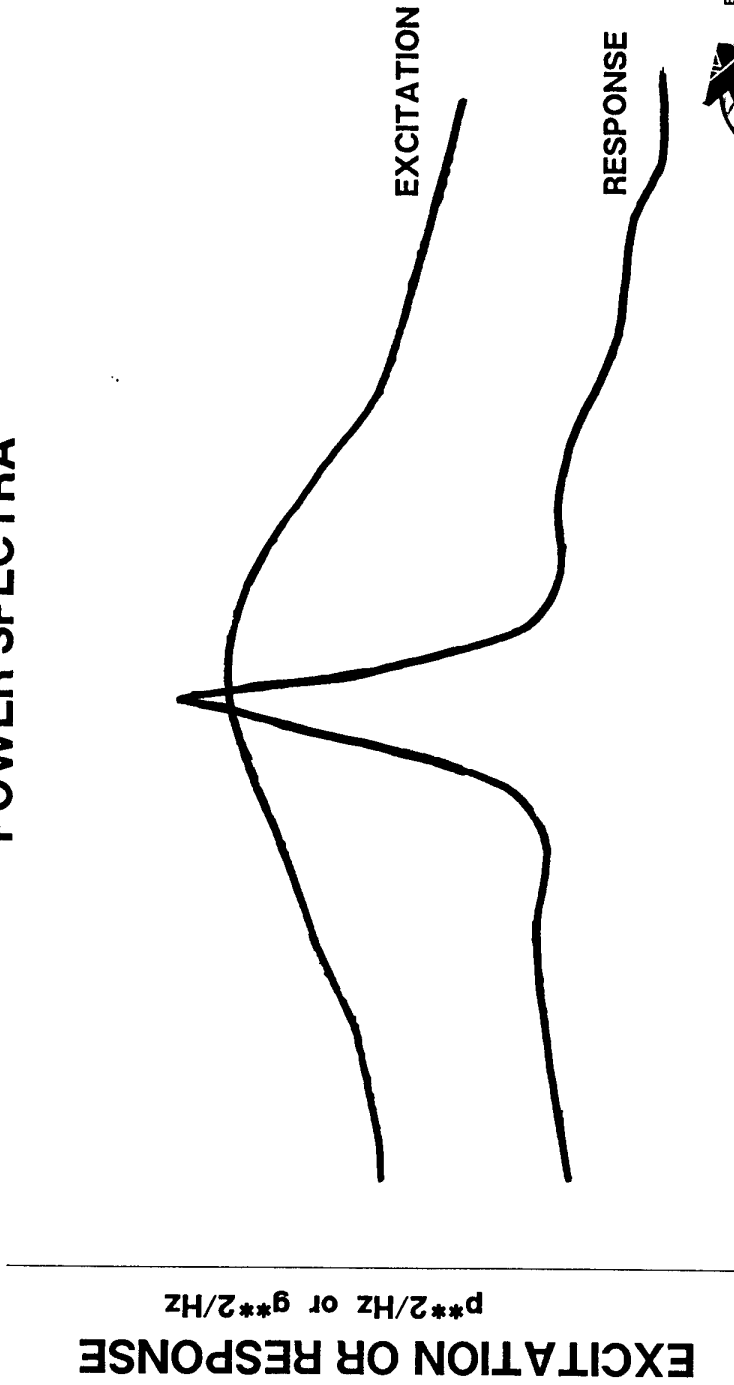
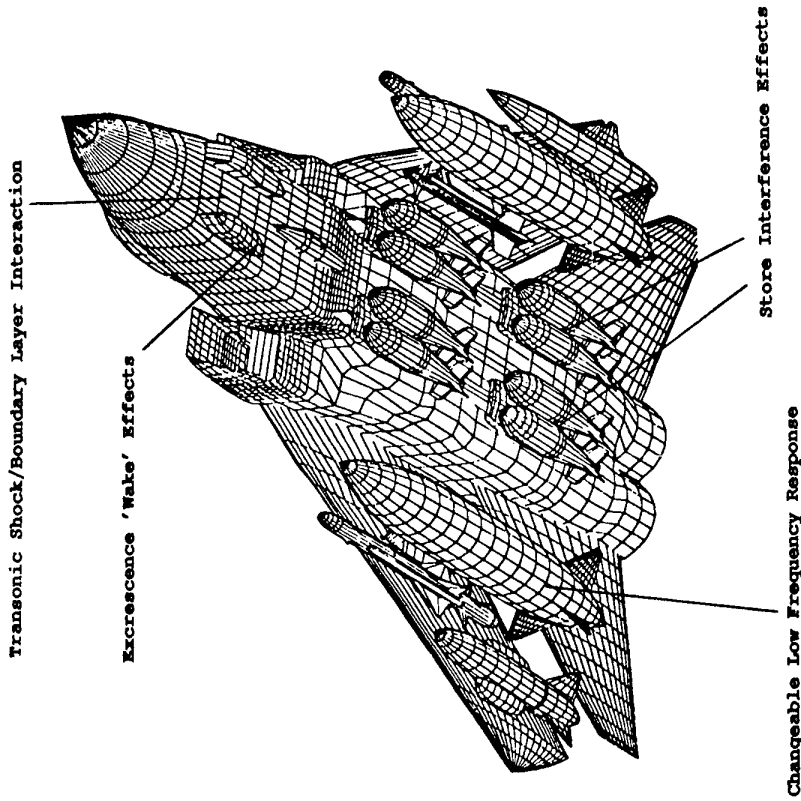


FIGURE 2

# UNSTEADY CFD



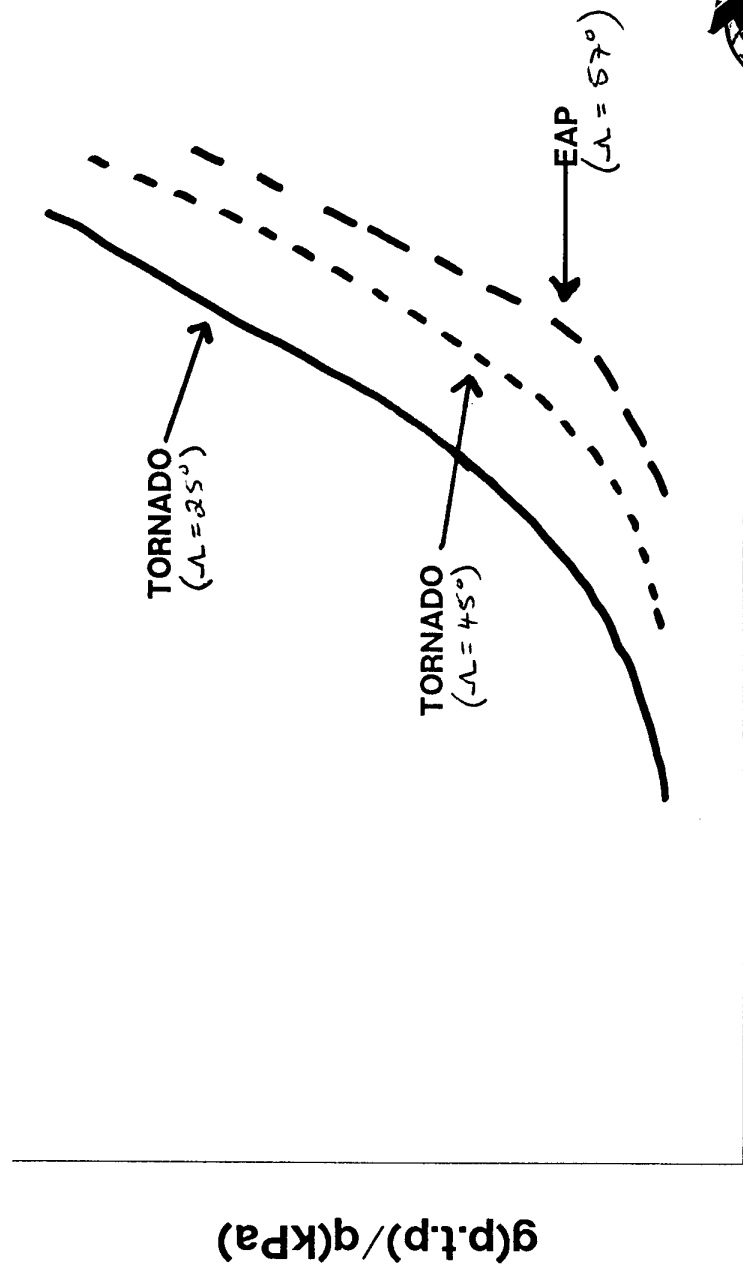
ENVIRONMENTALIST'S NIGHTMARE !!



FIGURE 3

# EMPIRICISM

## FIN VIBRATION CHARACTERISTICS

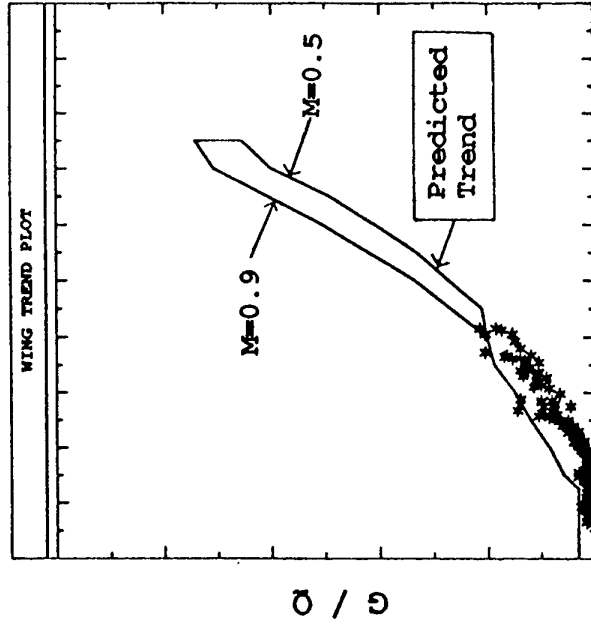
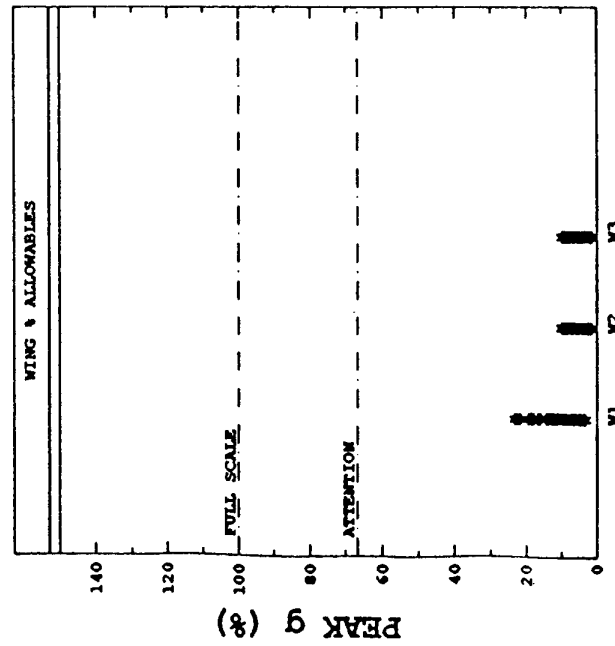


Incidence (AoA)



FIGURE 4

# VALIDATION OF PREDICTIONS - EXAMPLE 1



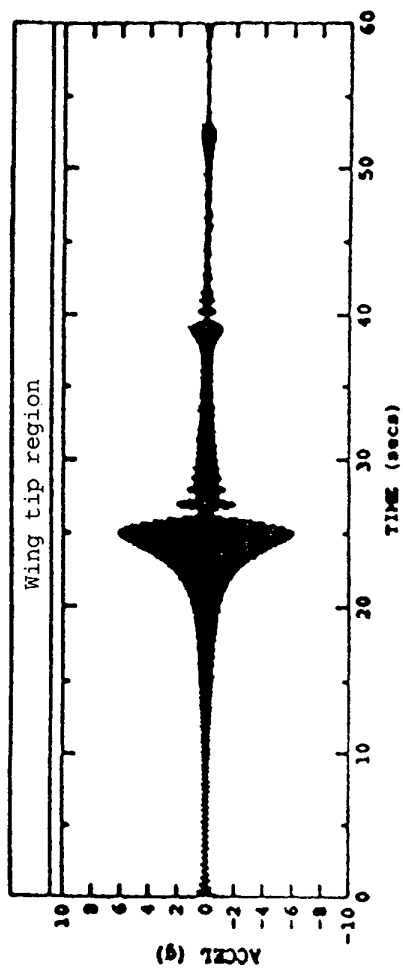
WING ACCELEROMETERS

α

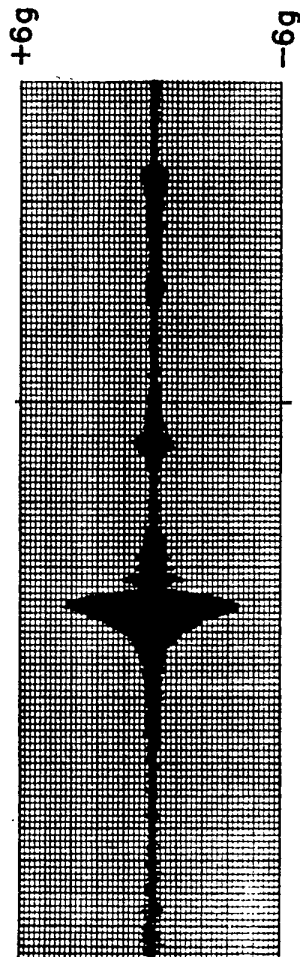


FIGURE 5

# VALIDATION OF PREDICTIONS - EXAMPLE 2



Prediction



Flight  
Measured



BRITISH AEROSPACE  
**DEFENCE**  
**MILITARY AIRCRAFT**

**LES CHARGES AU SOL LORS DES PHASES DE ROULAGE :**  
**LES SPÉCIFICATIONS CIVILES ET MILITAIRES**  
 par G.SQUEGLIA-O.REGIS  
 AÉROSPATIALE - 316 Route de Bayonne - 31060 TOULOUSE - FRANCE

**RÉSUMÉ.**

Cet article présente une étude comparative des normes militaires américaines, anglaises, françaises et des spécifications civiles (JAR/FAR) appliquées aux cas de roulage au sol. Les résultats obtenus avec des bosses discrètes, les pistes réelles et les travaux réalisés dans le cadre de l'harmonisation des règlements civils sont présentés. L'influence de ces différentes règles est explicitée en prenant pour exemple un turbopropulseur civil certifié pour les opérations sur des pistes semi-préparées.

**INTRODUCTION.**

Les charges de roulage au sol sont aujourd'hui critiques pour le dimensionnement statique des avions, ceci pour les atterrisseurs mais également pour certaines parties de la cellule si les effets dynamiques sont importants. En ce qui concerne les charges de fatigue, les charges de roulage présentent un extrême du spectre sol-air-sol sur de nombreuses parties avion et sont donc particulièrement importantes. Il faut donc dimensionner les avions sur la base de spécifications et de normes établies sur de bons critères de façon à ne pas limiter l'utilisation opérationnelle de l'avion même si celle-ci diffère légèrement des spécifications de départ. Un turbopropulseur civil certifié dans un premier temps pour les pistes préparées puis pour des opérations sur des pistes semi-préparées a été utilisé dans le cadre de cette étude. Les résultats présentés permettent de comparer les différentes normes et spécifications appliquées à cet avion.

**I - Normes militaires**

**I.1 - Normes américaines**

**I.1.1 - MIL-A-8863C.-->**

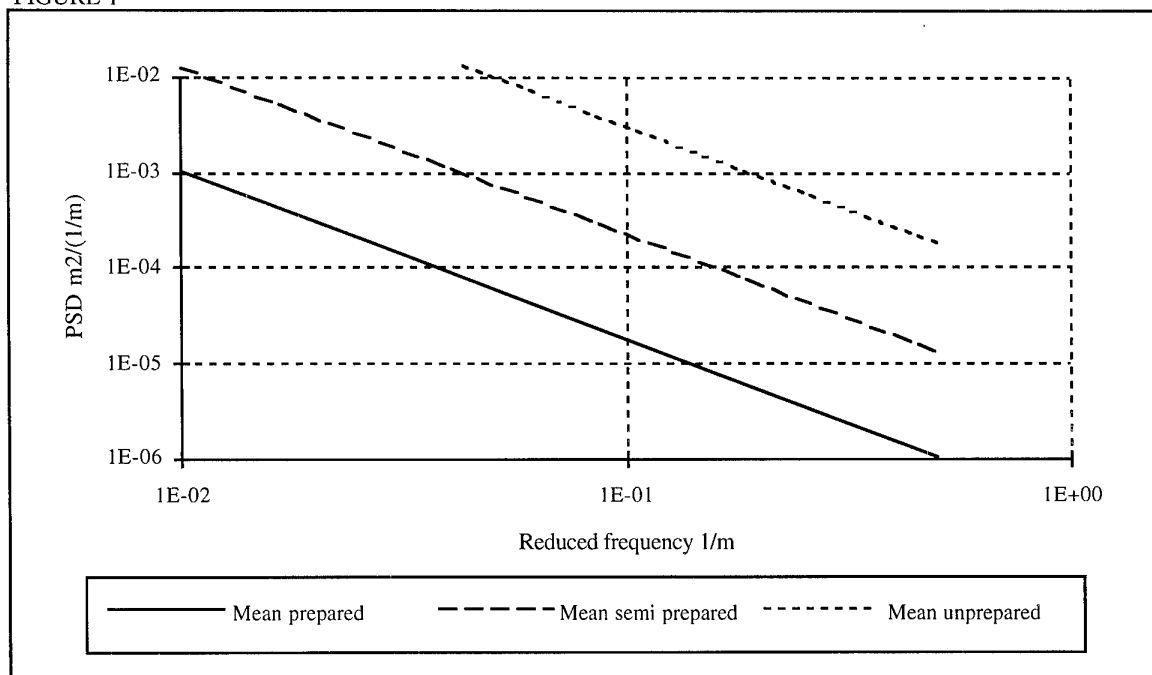
Roulage au décollage. La rugosité du sol est représenté sous la forme d'ondulations infinies de type (1-cosinus) de longueurs d'ondes constantes. A chaque décollage, l'avion doit accélérer jusqu'à la vitesse de rotation. Toutes les combinaisons de hauteur de bosses, de longueur d'ondes et de CBR doivent être simulées.

Roulage après l'atterrissage. Le même type de piste que précédemment doit être modélisé. L'avion doit pouvoir ralentir en utilisant toutes les combinaisons possibles, c'est à dire l'inversion de poussée, les freins, aérofreins et les autres systèmes éventuellement existant sur l'avion. Toutes les combinaisons de hauteur de bosses, de longueur d'ondes et de CBR doivent également être simulées.

L'avion doit aussi pouvoir traverser chacun des profils décrits ci-dessus pendant son ralentissement à toutes les vitesses, avec un angle entre l'axe fuselage et l'axe du profil allant jusqu'à 45°. Tous les angles doivent être parcourus.

Roulage à faible vitesse sur les taxiway. La somme des efforts verticaux au sol doit être égale à deux fois le poids de l'avion. Séparément, pour le train avant seul, la somme des efforts verticaux doit être égale à trois fois le poids de l'avion.

FIGURE 1



**I.1.2 - La dernière norme américaine, la MIL-A-87221** fait des demandes en terme de densité spectrale de puissance pour les pistes préparées, semi-préparées et non-préparées (Figure 1). Elle utilise également l'approche bosses et trous en faisant une différence entre les vitesses de taxiage et les vitesses supérieures. En dessous de 50 noeuds, la hauteur des obstacles rencontrés est supérieure (Figure 2 et 3). Les effets de masse, de distribution de masse, de position de centre de gravité et les caractéristiques des atterrisseurs

doivent être modélisés. Les réparations de piste ne sont plus mentionnées, les obstacles discrets non plus.

Le freinage après un décollage interrompu sur les pistes préparées et semi-préparées doit être étudié à toutes les vitesses jusqu'à la vitesse de décollage  $V_{LO}$ . Le freinage après l'atterrissage doit être étudié à toutes les vitesses jusqu'à la vitesse d'atterrissage  $V_{TD}$ .

FIGURE 2

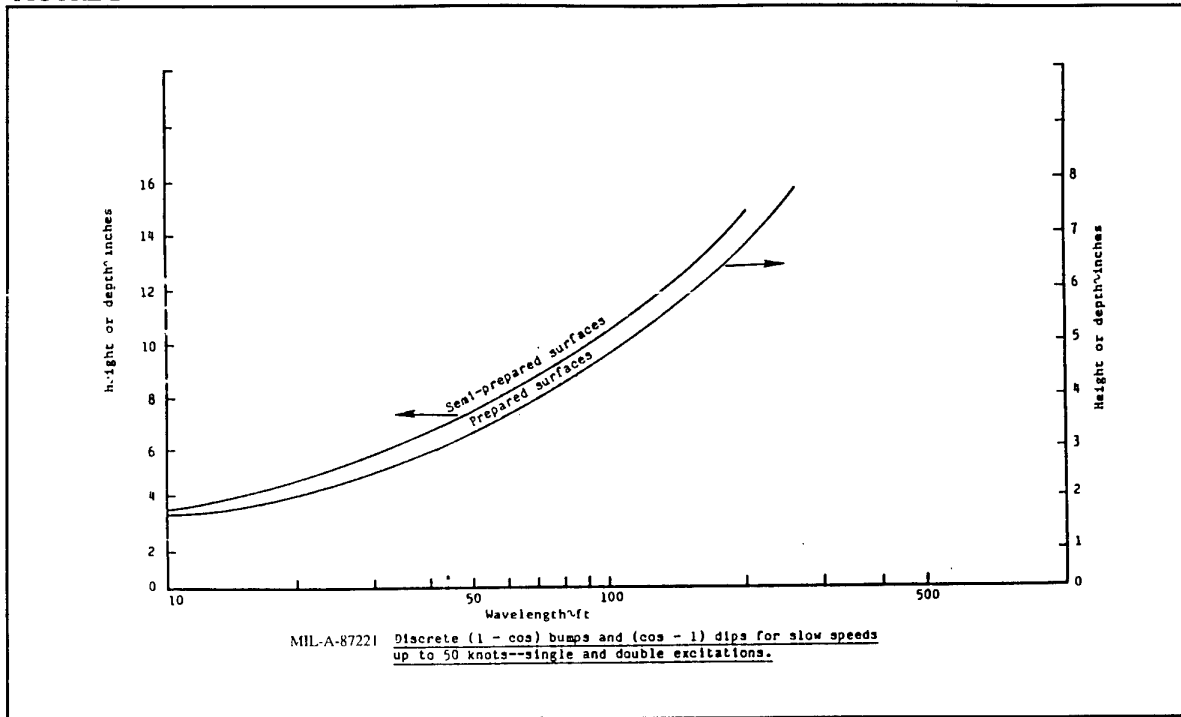
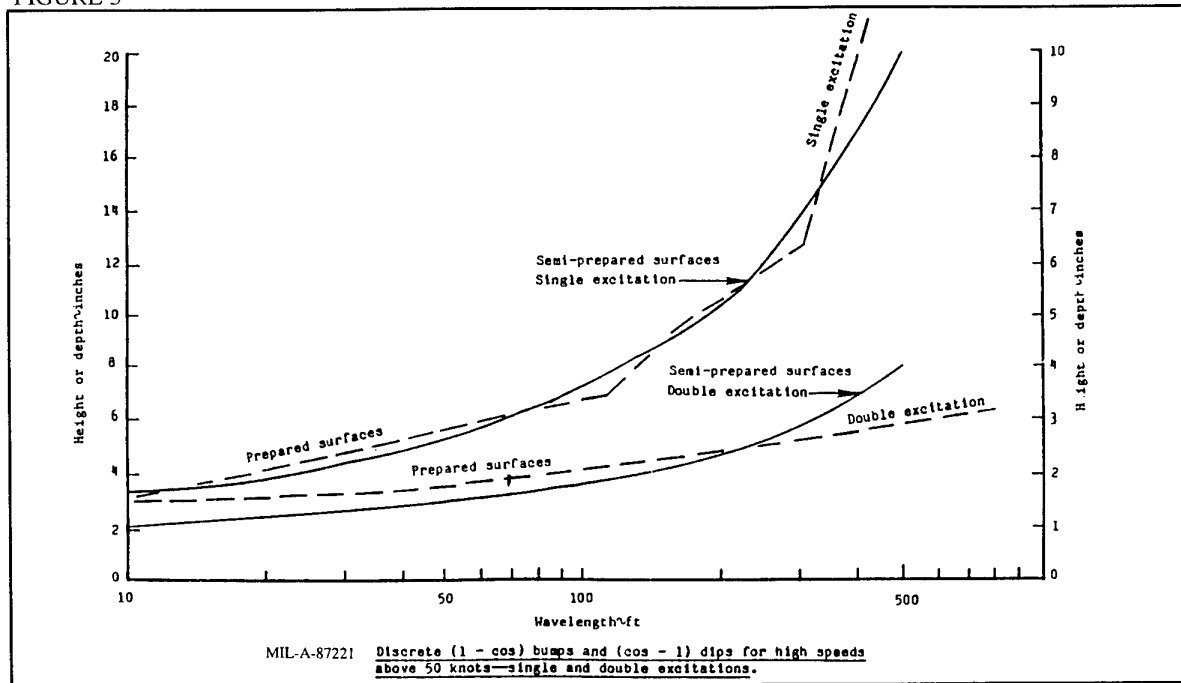


FIGURE 3



### **I.2 - Norme britannique.**

La spécification britannique est la DEF STAN00-970 Volume 1, Part 3. L'approche ondulatoire (1-cosinus) est reprise mais également complétée par

--> un obstacle unique de longueur faible applicable à un atterrisseur seulement.

--> un profil continu de 1500m de long.

--> un profil de réparation est également défini mais il s'agit d'une bosse unique. (pas de répétition)

### **I.3 - Norme française**

La norme AIR 2004E indique la compression du pneu associée à une piste revêtue, une piste en herbe préparée ou peu préparée pour des cas symétriques et asymétriques.

Ces spécifications concernent donc uniquement l'obstacle discret.

### **I.4 - Norme pour un nouvel avion de transport militaire.**

Il n'existe pas de spécifications communes pour les divers pays de l'OTAN. Rien n'est en préparation, ce sont en fait les cahiers des charges des armées qui évoluent avec le temps. Lorsque différentes armées sont impliquées, il faut que leur cahier des charges soit commun.

Nous allons voir que les différentes normes citées ci-dessus conduisent à un dimensionnement différent des atterrisseurs, et ceci particulièrement pour l'atterrisseur avant.

Une évaluation sera également effectuée en termes de coût de calcul.

## **II - Spécifications pour la certification des avions civils.**

### **II.1 - ACJ 25.491-**

a/ Pour des assiettes allant de la position 2 (level landing ) à la position 1 (tail down landing), 150% de la masse maximale à l'atterrissage sont appliqués sur les deux atterrisseurs principaux, 20% de l'effort vertical résultant sont également appliqués longitudinalement et latéralement sur chacun des atterrisseurs principaux.

b/ Avec le train avant et le train principal en contact avec le sol, un chargement vertical de 1,7 fois les réactions statiques doit être calculé à la masse maximale au décollage pour les conditions les plus pénalisantes en terme de répartitions massiques, en prenant en compte la poussée des moteurs.

### **II.2 - FAA-25.491**

Les systèmes amortisseurs ne doivent pas endommager la structure de l'avion lorsque l'avion est au sol, sur la surface possédant la rugosité la plus

élevée qu'il est raisonnablement possible de rencontrer dans les conditions normales.

La piste connue comme étant la plus dégradée correspond à un relevé de piste effectué à San Francisco avant réparation (28R). Elle est utilisée dans les deux QFU pour le calcul des charges statiques.

Lors de la certification d'un avion, la piste la plus dégradée sur laquelle il est susceptible d'opérer est bien sûr inconnue. La qualification d'une piste vient donc toujours après la certification d'un avion.

Pour les deux certifications, à ce jour aucune simulation n'est effectuée en prenant en compte les effets aérodynamiques, les effets de poussée ou d'inversion de poussée moteurs, les effets de freinage etc....

### **II.3 - Présentation des travaux réalisés dans le cadre de l'harmonisation JAR/FAR**

Les deux approches étant différentes, le temps de travail et les coûts sont augmentés. Des discussions sont en cours entre les autorités et les constructeurs afin de déterminer une règle commune.

L'approche basée sur le calcul des densités spectrales de puissance (PSD) à été rejetée. Cette approche est correctement adaptée pour les systèmes linéaires mais difficilement interprétable pour des systèmes non linéaires. En effet pour des systèmes non linéaires, seule une solution dans le domaine temporel est possible. Cette approche est utilisée dans le cadre militaire mais il est recommandé de déterminer un nombre de pistes important pour un même niveau spectral. Cette méthode donne de bons résultats pour des calculs de fatigue (faibles variations donc linéarisation possible) mais les valeurs extrêmes dépendent du tirage aléatoire permettant de générer la piste.

La densité spectrale de puissance représente une moyenne de la rugosité sur l'ensemble de la piste calculée. Il n'y a pas de différence pour une fréquence donnée entre quelques bosses d'une hauteur importante et un grand nombre de bosses de faibles hauteurs. L'espacement entre les bosses et les séquences de bosses ne sont également pas pris en compte.

De plus, pour pouvoir comparer correctement les pistes entre elles, il faut utiliser une méthode de calcul de la PSD qui soit unique.

#### **II.3.1 - Première proposition pour une certification commune**

Une première approche, non agréée, inclut toujours l'utilisation du relevé de piste de San Francisco (28R) comme une méthode acceptable de certification. Il est également établi que seuls des calculs symétriques doivent être effectués si l'avion ne possède pas un système particulier pouvant amener à des charges asymétriques particulièrement importantes.

Les charges de dimensionnement de l'avion doivent être déterminées pour les conditions de taxiage, décollage et roulage après atterrissage les plus critiques. Le modèle mathématique d'analyse doit inclure les modes rigides et les modes souples significatifs de

l'avion, ainsi que les caractéristiques des atterrisseurs et des pneus.

Les effets d'aérodynamique stationnaire doivent être inclus dans le modèle à moins que les charges produites sans les prendre en compte soient conservatives. Les effets d'aérodynamique instationnaire peuvent être négligés.

Les calculs doivent être effectués aux conditions de masses maximales avec les répartitions de masses fuel et de charges marchandes les plus critiques, et aux extrémités de la plage de centrage. Pour les avions possédant un empennage horizontal réglable, les cas de décollage doivent être simulés dans la plage verte et les cas d'atterrissage au réglage correspondant à l'approche.

La gouverne de profondeur est supposée rester immobile pendant toute la phase de décollage ou d'atterrissage, à moins qu'une procédure particulière soit indiquée dans le manuel de vol de l'avion.

Une série de roulages à vitesse constante doit être simulée dans les deux directions par pas de 20 noeuds jusqu'à la vitesse maximale en opération normale. ( $V_R$  pour le décollage,  $1,25V_{L2}$  pour le roulage après l'atterrissage.) L'analyse doit prendre en compte les variations de positions normales des becs, volets et spoilers, le freinage après l'atterrissage avec un coefficient de frottement de 0,3 et la poussée. (y compris la poussée des reverses après l'atterrissage)

### II.3.2 - Deux présentations ont été faites dans le but d'améliorer cette première suggestion.

La première présentation montre que les conditions définies ci-dessus sont couvertes par l'approche utilisée jusqu'à aujourd'hui par certains constructeurs.

Les positions extrêmes de centre de gravité sont utilisées à la masse maximale au décollage.

Les simulations sont réalisées à vitesse constante sur la piste de San Francisco par pas de 20 noeuds jusqu'à la vitesse de rotation dans les deux directions, mais la poussée, le freinage et l'aérodynamique ne sont pas pris en compte.

En effet, la prise en compte de l'aérodynamique soulage les atterrisseurs principaux, les charges maximales sont couvertes par celles de la JAR. (1.7). De même, le train avant est suffisamment soulagé pour compenser les effets du freinage, la masse à l'atterrissage est également plus faible. Au décollage, si la position du compensateur dans la plage verte est la plus pénalisante, alors les charges sont augmentées, mais pour un réglage normal, les charges calculées sans aérodynamique sont conservatives.

La seconde présentation cherche à remplacer la piste de San Francisco (28R) par une approche discrète du type des normes MIL. Cette méthode utilise toutes les hypothèses décrites précédemment pour une double bosse de type (1-cosinus) pour deux longueurs d'onde seulement.

Ces longueurs sont celles de l'empattement avion 'L' et celles du double empatement '2L'. Ces deux longueurs sont choisies ainsi parce qu'elles sont couplées avec les modes de pompage et de tangage de l'avion (Figure 4).

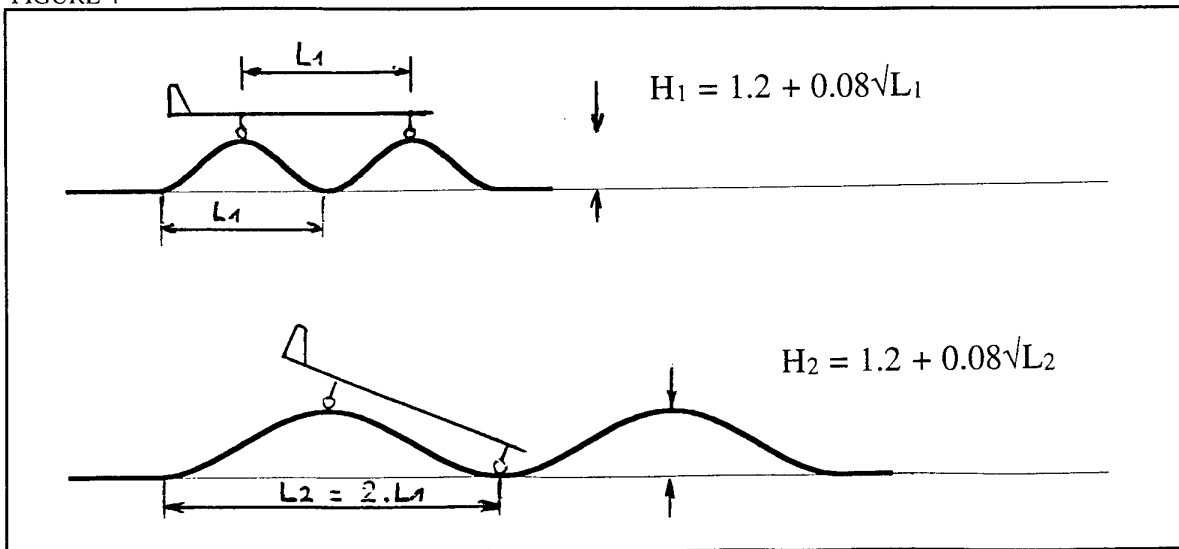
Les hauteurs des bosses sont sensiblement en accord avec les spécifications militaires 'H' en inch =  $1,2 + 0,08 \text{ SQRT}(L)$  (ou L est en pieds, attention les unités sont croisées)

Cette double bosse de forme (1-cosinus) est une alternative à l'utilisation du profil de San Francisco.

La variabilité des résultats de simulation (fonction de l'avion) sur San Francisco provient pour beaucoup des conditions initiales de l'avion lorsqu'il arrive sur une bosse. Cette méthode est plus stable. Le fait de n'utiliser que 2 longueurs de bosse ne diminue pas les charges avions même sur les éléments accrochés (moteurs, réservoirs sous voilure) pour les avions testés. (à condition d'utiliser les cas massiques les plus critiques).

Ces deux méthodes donnent un niveau de charges équivalent (légèrement plus conservatif) pour un coût de calcul plus faible.

FIGURE 4



**III - Études des différences opérationnelles entre un avion de transport civil et un avion de transport militaire. Les différences peuvent porter sur l'état des pistes utilisées et sur l'utilisation de l'avion.**

**III.1 - Niveau général de rugosité des pistes**

Les critères de dimensionnement des atterrisseurs civils sont identiques quelque soit l'avion, subissent très peu d'évolution dans le temps et couvrent une grande partie des opérations réelles des avions. Néanmoins avec l'ouverture récente du marché à l'ex U.R.S.S et aux pays de l'est, les avions civils sont amenés à opérer sur des pistes "dégradées". Une validation opérationnelle des avions a donc été réalisée.

(Ref1-->) A l'opposé, les critères de dimensionnement des atterrisseurs militaires dépendent largement du cahier des charges défini pour chaque avion. Une difficulté majeure est de définir correctement le niveau de dimensionnement longtemps avant d'avoir une flotte opérationnelle. Après développement, fabrication des avions, et détermination des marges structurales existantes, il faut que les conditions opérationnelles de la flotte soient toujours en adéquation avec le niveau de dimensionnement des atterrisseurs, celui-ci ayant été défini environ 10 ans auparavant dans le cahier des charges.

Dans tous les cas, Il faut trouver un juste milieu entre une spécification ne pénalisant pas exagérément l'avion en terme de masse et l'utilisation opérationnelle qui va être faite de l'avion.

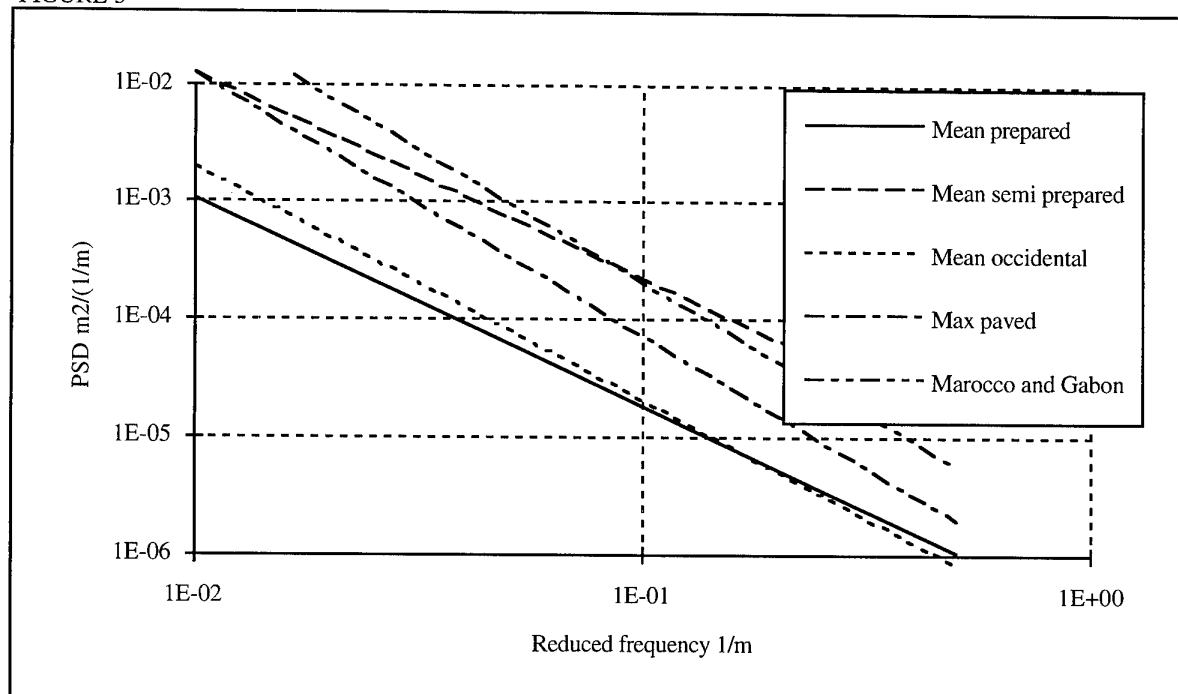
La question principale reste de définir des spécifications qui soient en accord avec l'environnement réel lorsque la flotte est opérationnelle.

Dans un premier temps, une comparaison du niveau moyen des pistes "militaires" et "civiles" a été effectué en utilisant la densité de spectre de puissance. Sur la figure 5, sont comparées les PSD des normes MIL pour les pistes pavées et semi-préparées (niveau maximum ) avec les PSD obtenues pour les pistes civiles occidentales et celles obtenues pour les profils semi-préparés de certains aéroports marocains et gabonais. Dans la cadre de la qualification de pistes, la comparaison des densités spectrales de puissance reste valable.

Les niveaux moyens des pistes civiles sont sensiblement identiques à ceux des pistes militaires notamment pour des longueurs de bosses correspondant aux modes de pompage et de tangage. Les différences existantes pourraient provenir de la méthode de calcul des PSD. Cependant, on peut noter qu'il y a environ un rapport 10 entre chaque niveau de piste de la norme MIL, ce qui correspond à un rapport de hauteur de bosse de  $\text{SQRT}(10) = 3$ . Cela correspond également au rapport existant pour les pistes civiles. Si l'on regarde les creux et bosses spécifiés dans la norme MIL (figure2) pour les vitesses supérieures à 50 kts ce rapport reste inférieur à 2 pour des longueurs de bosse inférieures à 70ft. Pour les vitesses inférieures à 50 kts, (figure3) il n'atteint jamais 3. Si l'on compare les PSD des pistes semi-préparées à celles obtenues pour les plus mauvaises pistes préparées, le rapport de PSD est beaucoup plus faible et environ égal à 3. Cela donne un rapport de hauteur de bosse égal à 1,7 qui correspond bien au rapport existant sur la figure2 (>50kts) entre les pistes préparées et les pistes semi-préparées.

Dans la suite de l'étude, on a cherché à quantifier les niveaux de charges obtenus pour des roulages sur les bosses de la norme MIL et sur les relevés des pistes civiles.

FIGURE 5



### III.2 - Problèmes ponctuels (réparations)

En dehors du niveau général de rugosité des pistes, les avions civils sont également confrontés à un type d'accident local que sont les intersections de pistes. Les réparations effectuées sur les pistes civiles ne correspondent en rien avec celles effectuées sur les pistes à usage militaire. Pour répondre à ce type de sollicitations, les pays occidentaux se sont fixés des règles, qui si elles sont bien suivies ne posent pas de problèmes particuliers. Mal suivies, certains problèmes de fatigue et de confort peuvent apparaître mais en aucun cas, l'avion ne se rapproche des charges limites.

C'est la principale différence entre ces deux types d'avions et c'est pour cela que l'aspect opérationnel reste beaucoup plus important pour un avion militaire. Pour un avion de transport militaire, il est également nécessaire dans les spécifications initiales de correctement prendre en compte les réparations de piste afin que l'avion construit ait une capacité suffisante pour les conditions opérationnelles rencontrées.

Côté militaire, il est cependant envisageable de définir des recommandations aux pilotes pour le passage d'obstacles ou de réparations.

Avec dix ans d'avance, il est difficile de prévoir correctement, les techniques de destruction et donc les profils des pistes réparées. De même, les techniques de réparation sont elles aussi susceptibles d'évoluer. La simulation de certaines doubles ou triples bosses de faible longueur (6,5m, 12,5m) provient de l'évolution du profil avec le trafic (figure 6), cette évolution pouvant se réduire très fortement si la qualité de la réparation s'améliore. De même, les profils et les catégories de réparation (A à E) définis dans les différentes normes MIL ou DEF STAN ont à la fois une forme et un temps de mise en oeuvre qui sont susceptibles d'évoluer.

Le problème consiste à trouver à la fois la hauteur maximale, la longueur d'onde et la séquence la plus pénalisante pour l'avion. Cette solution serait très sévère. En effet, dans la réalité, ce n'est pas cela. Les séquences de réparations proviennent de l'affaissement d'une réparation initiale, la longueur d'onde et la hauteur à utiliser sont donc différentes. La hauteur ainsi déterminée pour une séquence est inférieure à celle obtenue pour une bosse simple. Combien de réparations successives faut-il utiliser ? Trois réparations successives donnent à 1% près les charges obtenues pour une infinité de réparations, avec deux réparations, l'influence sur les charges est limitée à 5% mais le niveau de charges obtenu sur une réparation simple est inférieure de 35%. La figure 7 montre l'évolution de la charge sur un atterrisseur au passage d'une bosse simple, double, triple et quadruple. La vitesse et la longueur de la bosse choisie maximisent les efforts sur l'atterrisseur.

FIGURE 6

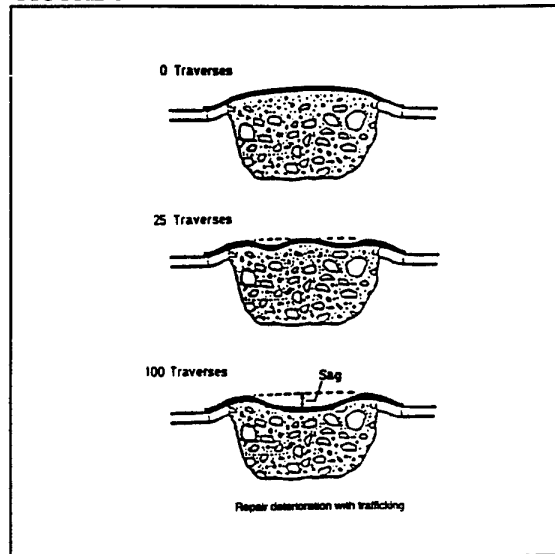
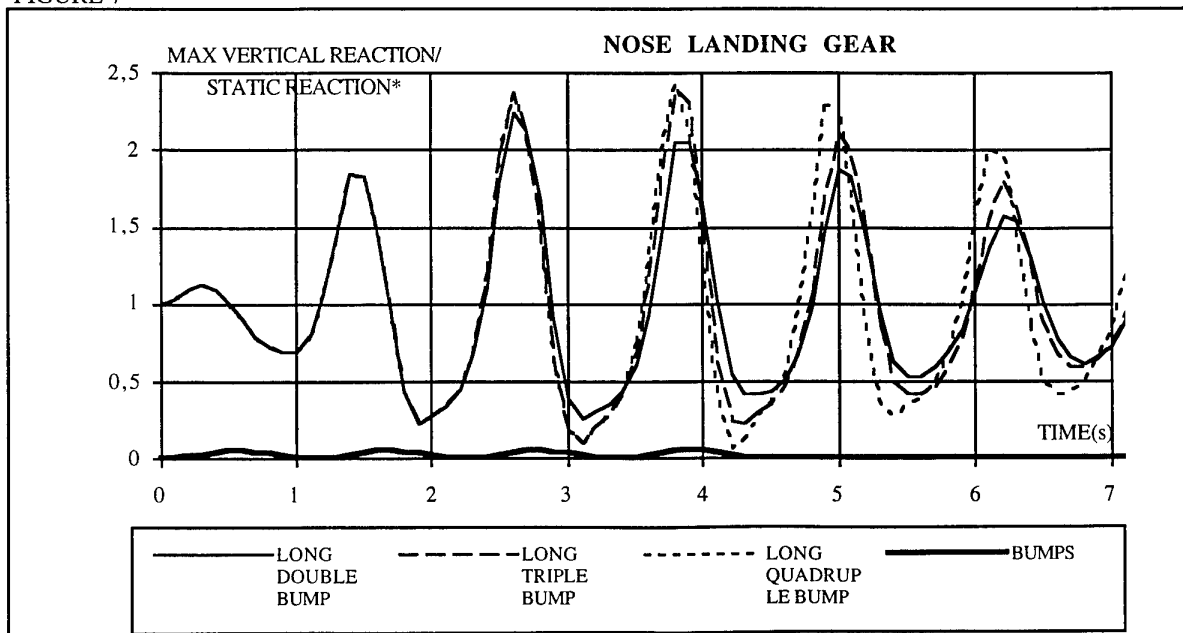


FIGURE 7



Si l'on suppose que les doubles ou triples bosses proviennent d'un affaissement des réparations causé par les passages successifs, alors il devient logique de diminuer la hauteur des bosses doubles par rapport aux bosses simples. Si l'on calcule pour une piste existante les hauteurs de bosses simples, doubles et triples, le type de résultat obtenu est donné sur la

figure 8. Sur ce type de piste, ce sont les hauteurs des bosses simples et non celles des bosses doubles qui vont créer les charges les plus élevées sur l'avion. Pour la norme MIL, les charges obtenues avec les bosses simples sont supérieures ou égales à celles obtenues avec les bosses doubles (fig 9).

FIGURE 8

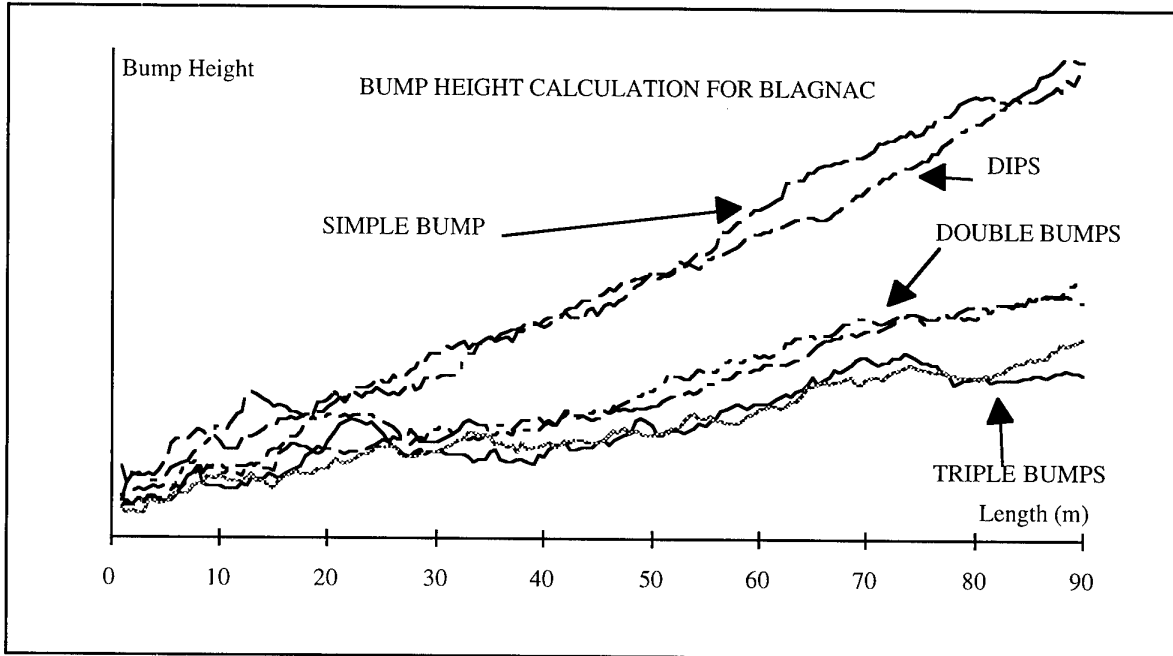
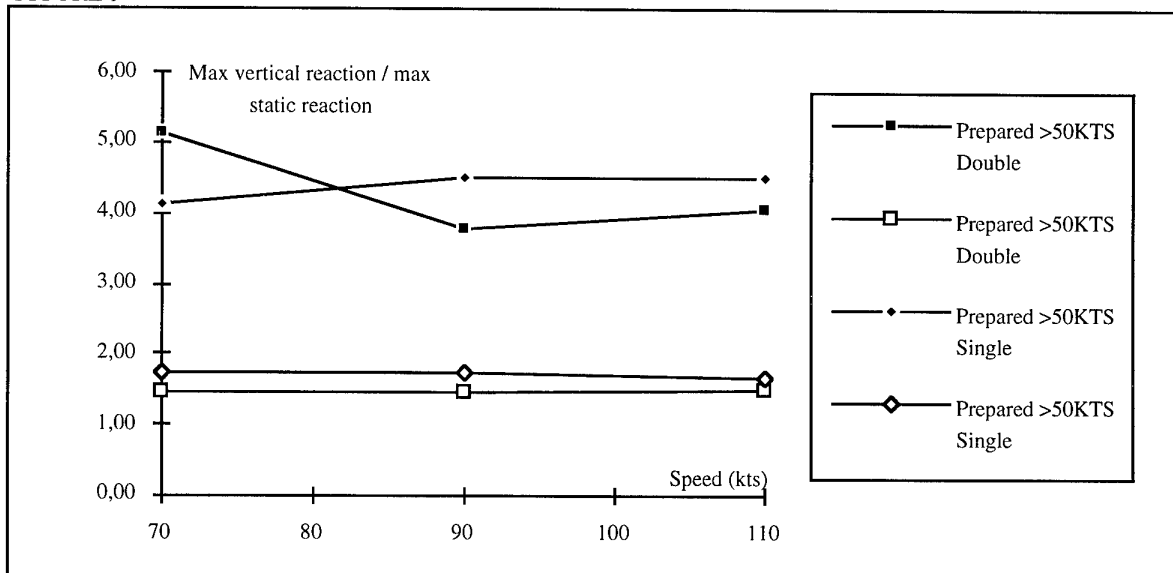


FIGURE 9



Les réparations à prendre en compte pourraient donc se limiter à des bosses simples seulement comme le définit la norme britannique. Une façon de ne pas pénaliser l'avion consiste à préciser le type de réparations dont l'avion est capable après dimensionnement. Sur la figure 10, on peut noter que les bosses proposées par les normes MIL pour les

pistes semi-préparées couvrent toutes les propositions existantes de réparations (fig 11).

Il convient non seulement de correctement modéliser les types de réparations que l'on sait réaliser mais aussi de connaître la réponse de notre avion pour des réparations ayant été effectuées par un autre maître d'oeuvre.



FIGURE 10

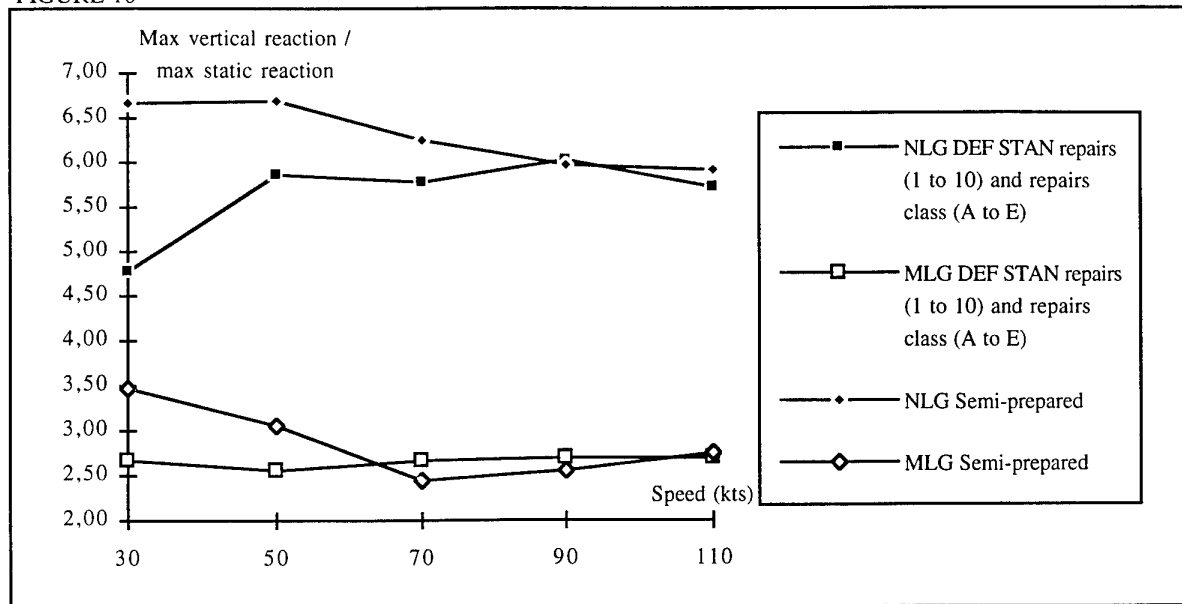
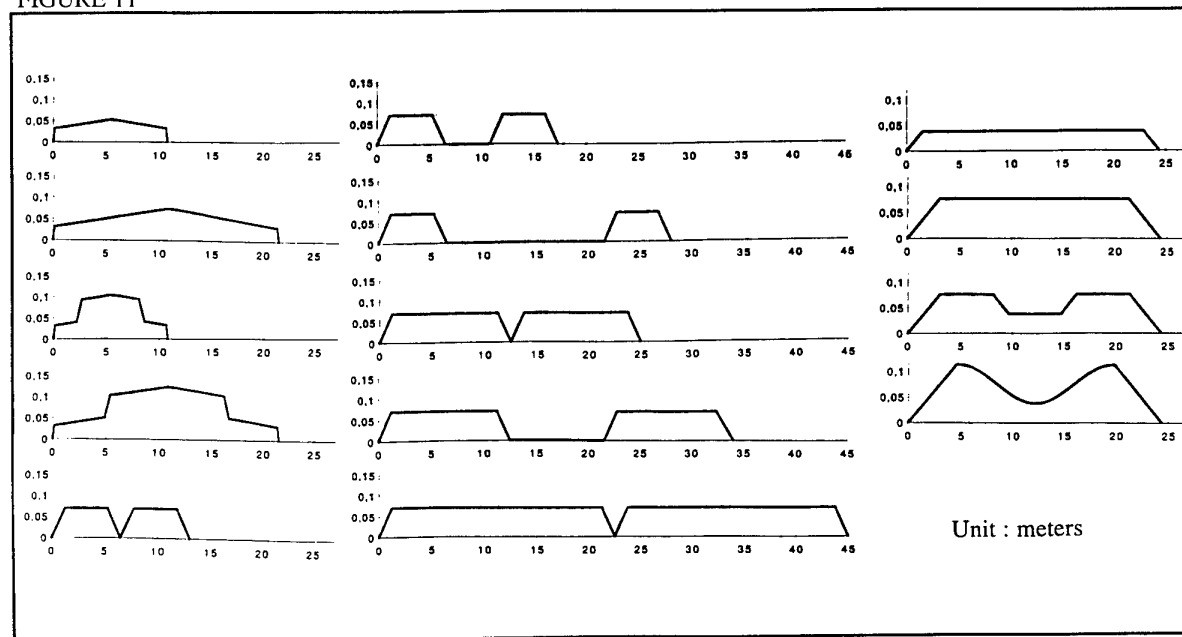


FIGURE 11



**III.3 - Obstacle discret**

Pour les avions militaires, le problème de l'obstacle discret existe également. Les obstacles discrets sont souvent dimensionnant pour la sélection du pneu (taille et pression). L'influence de la modélisation du contact pneu et piste (taille et forme de l'empreinte de contact) a une influence primordiale sur les résultats des simulations pour le franchissement d'un obstacle isolé. C'est pourquoi, cette sélection est généralement basée sur l'expérience. Le calcul de l'endommagement de la piste, et la hauteur de la marche pouvant être franchie (crash à la marche, sortie de piste) par l'avion n'est pas une contrainte du cahier des charges mais souvent le résultat des choix effectués au

préalable, dictés par des contraintes d'encombrement et de masse ou de concurrence.

**III.4 - Excitation asymétrique**

Une réponse avion à une excitation symétrique où tous les atterrisseurs passent sur le même profil est plus sévère qu'une réponse asymétrique où une partie de l'avion rencontre un profil moins sévère. Sur de multiples pistes, les relevés topographiques ont été effectués pour plusieurs profils plus ou moins éloignés de l'axe de la piste. Il est donc possible de calculer des charges asymétriques. Les résultats obtenus montrent des charges atterrisseurs inférieures aux résultats obtenus sur chacun des profils lorsqu'ils sont considérés comme symétrique.

### III.5 - Variabilité des réglages amortisseurs et pneus

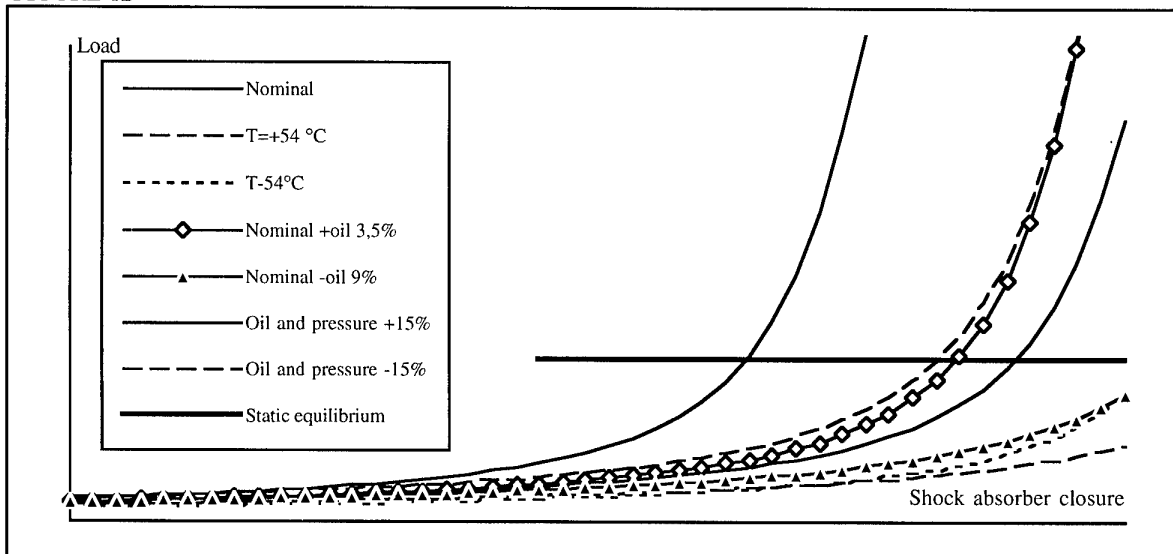
Les avions civils sont certifiés sur des bases précises et invariables. Les performances avion sont calculées au niveau de la mer, pour une température de 15° C, un vent nul et une piste à altitude constante, pour un état de surface donnée. La prise en compte d'écart par rapport à ces conditions nominales est également calculée pour les performances avion et dans le domaine structure, on tient compte de la rugosité de la piste pour éventuellement limiter l'avion en termes de masse et/ou de centrage.

Le réglage des atterrisseurs et la pression de gonflage des pneus doivent être nominaux pour les avions civils. Les avions sont certifiés de -54°C ou

-45°C à +55°C. Certains réglages atterrisseurs, voire des limitations avion peuvent également exister en fonction des températures rencontrées en opération.

La norme MIL-A-8863C permet des écarts de 15% à la fois sur le volume d'huile, la pression de gonflage de l'amortisseur et 20% sur celle des pneus. Cela va engendrer des différences considérables à la fois sur le confort, le niveau des charges et la possibilité d'arriver en butée de course des amortisseurs. Si l'on prend les deux solutions extrêmes, la raideur de l'amortisseur pour l'équilibre statique et l'effort à appliquer pour arriver en butée de l'atterrisseur vont varier de 1 à 10. Ces différences doivent couvrir les effets de variation de la température.

FIGURE 12

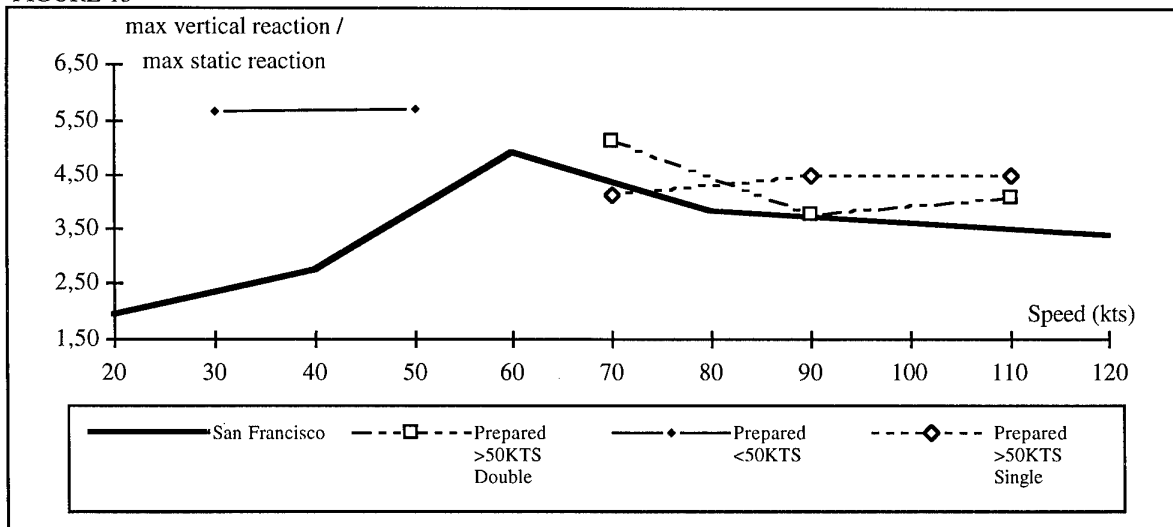


La figure 12 montre les courbes extrêmes de la certification civile et les écarts possibles pour le domaine militaire. Ces écarts couvrent très largement les effets de température, ils représentent donc une contrainte bien supérieure. La prise en compte d'une variation possible du volume d'huile des atterrisseurs

dans le calcul des charges avion constitue donc un point primordial à déterminer en début de programme.

La contrainte température correspond sensiblement à une variation du volume d'huile de plus 3,5% ou moins 9% dans l'exemple utilisé.

FIGURE 13



**IV - RÉSULTATS**

**IV.1 - Résultats pour un Turbopropulseur.**

Les figures 13 à 15 montrent les résultats obtenus dans le cadre d'une comparaison des règlements civils et militaires pour un turbopropulseur certifié pour des opérations sur des pistes semi-préparées. Cet avion est autorisé sur les pistes sommaires du Gabon et les pistes en latérite au Maroc.

Les premiers calculs ont concerné les roulages sur San Francisco dans les deux sens à MTOW sans

freinage, sans aérodynamique pour des vitesses constantes variant de 20 kts jusqu'à la vitesse maximale de rotation. Ensuite, la plupart des possibilités des différentes normes MIL sur les pistes préparées et semi-préparées ont été parcourues. Dans tous les cas, on a considéré que les cas de décollage sans aérodynamique couvrait l'ensemble des cas possibles y compris les conditions de freinage (avec aérodynamique).

Les résultats obtenus sur les bosses des pistes préparées pour les vitesses supérieures à 50kts sont comparables sur le train avant à ceux obtenus sur la piste de San-Francisco (fig13). Pour le train principal, San Francisco couvre également (fig14).

FIGURE 14

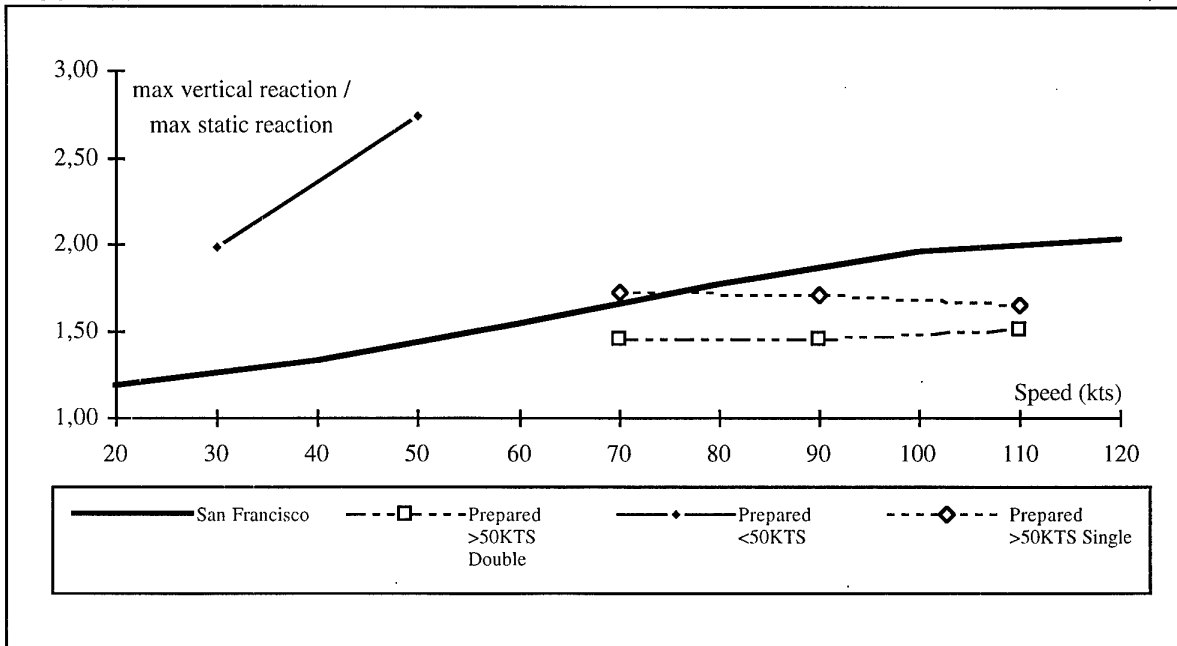
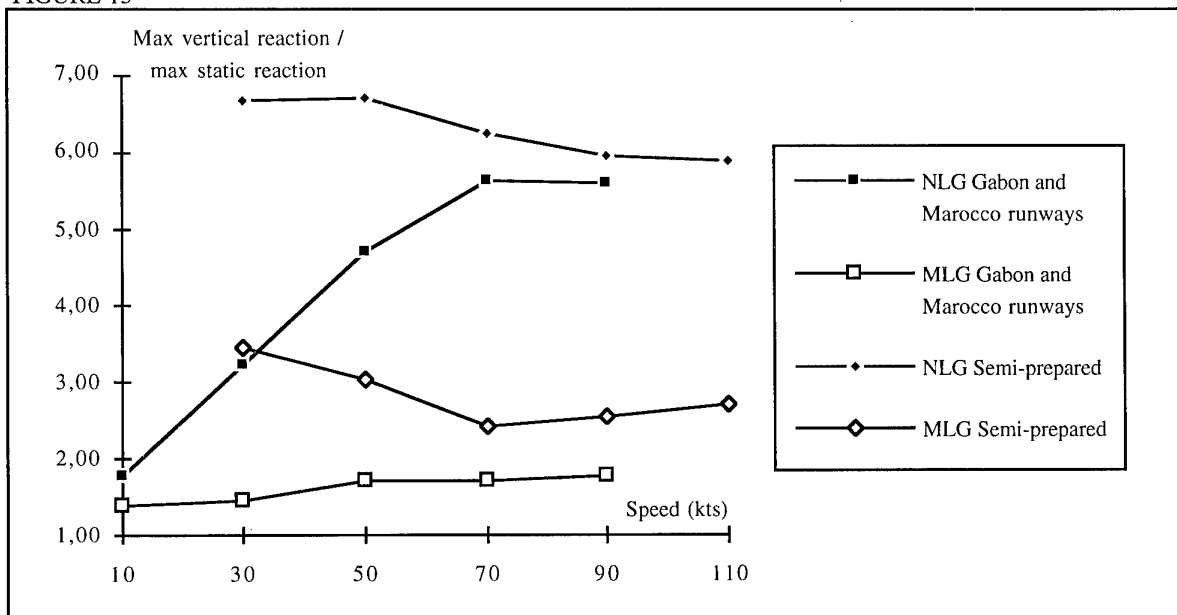


FIGURE 15



En ce qui concerne les pistes semi-préparées sans aérodynamique, les résultats des bosses des normes MIL donnent des résultats bien supérieurs à ceux des pistes réelles et conduiraient pour l'atterrisseur principal à une nouvelle définition (fig15). Le train avant, quant à lui, subirait un nouveau renforcement de moindre importance. Les résultats obtenus pour les vitesses inférieures à 50kts sont une nouvelle fois d'un niveau très élevé mais ne correspondent pas aux contraintes subies sur un taxiway. La piste de San Francisco multipliée par un coefficient à définir pourrait nous donner les mêmes résultats que les pistes réelles ou bien encore les mêmes résultats que les bosses des normes MIL. Cette idée est déjà utilisée dans la norme britannique avec un relevé de piste théorique.

Pour les deux atterrisseurs, les hauteurs de bosses définies pour les vitesses inférieures à 50kts amèneraient à un nouveau dimensionnement. (fig13, fig14 et fig15).

Les résultats obtenus sur les bosses doubles et simples des normes MIL sont identiques (fig9).

#### IV.2 - Coût des calculs

En utilisant la piste de San Francisco dans les deux sens, avec 2 cas de masse (centrage avant et centrage arrière) et 10 vitesses, on obtient environ 40 cas de calculs allant de 15s à 100s de simulation.

En ce qui concerne les normes MIL, un découpage en une vingtaine de longueurs d'ondes, 2 cas de masse, 10 vitesses, les bosses simples et doubles, on obtient 800 simulations de 10s à 20s. Il faut ensuite parcourir tous les types de réparations (15 types ou plus) soit 300 cas de calcul supplémentaires.

Pour couvrir toute la cellule, des répartitions massiques supplémentaires doivent être ajoutées, mais les temps de simulation resteront proportionnels.

Pour un dimensionnement quasi identique sur pistes préparées, il y a donc un rapport très important sur le temps de calcul qui ne semble pas justifié.

#### V - CONCLUSION

La variabilité des réglages atterrisseurs proposée dans la norme MIL (+ ou - 15% de volume d'huile) est extrêmement sévère si on la compare à la variabilité qui est aujourd'hui utilisée dans le domaine civil. Ce point doit donc être clarifié très en amont dans la définition d'un nouvel avion.

Pour un avion n'utilisant que les pistes préparées, les règles civiles couvrent le dimensionnement militaire.

En ce qui concerne les pistes semi-préparées, les réparations définies dans les normes MIL ou britanniques sont couvertes par les bosses de la dernière norme MIL, d'où la disparition de définition des réparations possibles pour un avion autorisé sur des pistes semi-préparées.

Les charges résultantes de la norme MIL sur pistes semi-préparées sont supérieures à celles obtenues sur les pistes réelles de façon théorique ou par mesures,

lors d'essais en vol. Elles amèneraient à un nouveau dimensionnement des deux atterrisseurs de notre avion.

La modélisation des taxiways (bosses utilisées pour  $V < 50$ kts) est extrêmement contraignante, les facteurs de charge de deux (pour le train principal) et de trois (pour le train avant) de la précédente norme MIL-A-8863C sont beaucoup plus proches des situations opérationnelles.

En terme de coût de calcul, sur pistes préparées, suivre les normes MIL entraîne une multiplication des cas de calcul pour un dimensionnement identique des atterrisseurs. Pour les pistes semi-préparées, on doit pouvoir réduire les cas de calcul de la même façon tout en obtenant un bon comportement opérationnel de l'avion.

#### RÉFÉRENCE

- Réf. 1 Agard R-731  
Aircraft Operations on repaired runways
- Réf. 2 Agard CP-484  
Landing gear design loads
- Réf. 3 NATO - R416 - 1963  
Implication of recent investigations on runway roughness criteria
- Réf. 4 NASA TN D5740  
Response of several turbojet airplanes to runway roughness
- Réf. 5 NACA 3305  
Some measurements and power spectra of runway roughness
- Réf. 6 AIAA 83-0927 , Structures structural dynamics and materials conference 24th  
Transient response of taxiing aircraft.

## <sup>1</sup>EVOLUTION OF F-16 LOADS AND REQUIREMENTS

David H. Gibson  
 Weapons System Design Center  
 Analysis Branch  
 Lockheed Martin Tactical Aircraft Systems  
 P.O. Box 748  
 Fort Worth, Texas 76101

### SUMMARY

This article presents a review of the historical background of the growth of external loads and design requirements for the F-16 fighter aircraft. Several scenarios are recounted where analysis assumptions were determined to be inadequate and flight test or operational data presented situations not fully covered by design criteria. Changes in design requirements are discussed and suggestions for future aircraft design analyses are offered.

### INTRODUCTION

The F-16 has been in service for over 20 years and has proven to be the most agile aircraft ever to participate in air-to-air and air-to-ground missions. It has shown that it is possible to design and build an aircraft with a lightweight and strong structure combined with a powerful engine and a fly-by-wire control system, the combination providing a maneuvering advantage over all other aircraft operating in the world today. Its 9g maneuvering capability and fly-by-wire control system are, in large part, responsible for its success. The 9g airframe, the robust design of the control system, and the design of the crew station to enhance pilot g tolerance allow the system to perform beyond anything ever put into service to date.

But, how did the F-16 come to be the aircraft it is? What were its requirements? How have the aircraft loads changed through the years with the various changes to the basic aircraft, new store configurations, and many customers with varying requirements? This paper attempts to bring a small part of that history to light, particularly the part dealing with structural requirements relating to airframe loads. As is evident, the external loads

imparted to an airframe are the defining element for the airframe design, both for strength and for service life.

### SYSTEM DESCRIPTION

The F-16 is a small lightweight fighter aircraft which incorporates a number of innovations to increase its performance and maneuverability. Some of those that affect the structural design include:

- an instrumented, fixed control stick which senses pilot applied control forces rather than pilot induced stick position and then transmits these forces to the flight control system
- a computer controlled flight control system which receives pilot command inputs and translates these commands to control surface deflections
- a seat inclined at 30° to increase pilot g-tolerance
- an aerodynamic design which is statically unstable in subsonic flight
- flight control laws which automatically integrate pilot commands with aircraft motion to maximize stability and enhance handling qualities

These characteristics work together in unique ways to impact structural loads - the inclined seat permits higher g-loading on the aircraft; the fixed stick reduces the "feel" that the pilot has regarding command input; the negative static margin increases maneuver response; the flight control laws blend control surface motion and integrates data from sources not available to the pilot.

These characteristics posed some peculiar situations during the design and development of the F-16. Some were addressed during the design requirements phase, some were encountered during

<sup>1</sup> Copyright © 1996 Lockheed Martin Corporation. All rights reserved. Published by the Advisory Group for Aerospace Research and Development with permission.

development, and some have been discovered as a result of aircraft operations.

### 7.33g to 9g

The original F-16 Air Vehicle Specification (Ref. 1) called for an airframe with the strength capability of withstanding maximum external loads for 7.33g at the Basic Flight Design Gross Weight (BFDGW). Asymmetric maneuvers were to be limited to 80% of the symmetric load factor limit, or 5.86g. In addition, the aircraft must be capable of achieving 9g at off-design symmetric maneuver flight conditions. This requirement first necessitated defining the maximum external loads for the 7.33g condition and then searching the flight envelope for areas where higher load factors could be achieved without exceeding the critical design load.

An alpha-g limiting algorithm was incorporated into the flight control laws to effectively prevent the aircraft from exceeding 9g during symmetric flight. The limiter did not differentiate between symmetric and asymmetric maneuvers. To provide limiting for asymmetric maneuvers, it was originally planned that the aircraft wing be equipped with a strain or load monitoring device to limit wing loads. The device would provide real time feedback to the flight control and would also be useful in limiting wing loads during symmetric maneuvers up to 9g for off-design conditions.

It was discovered that, due to the multiple load path nature of the F-16 wing root design, it was very difficult to install instrumentation to reliably isolate and sense critical wing bending loads. Investigation into the installation of additional structure was conducted in an attempt to design a type of "load cell" which would isolate the loads and provide adequate feedback to the flight control system. This also proved to be very difficult and resulted in the addition of weight to the aircraft.

Due to the difficulty of developing this load limiting system, another study was performed to determine the amount of structural weight that would be required to allow the aircraft to achieve 9g symmetrically at all flight conditions. It was discovered that only about 20 pounds of additional weight were required. Retaining the 5.86g roll limit and designing the aircraft structure to 9g symmetric maneuvers would also provide margin

for overshoots in load factor during asymmetric maneuvers. (The fixed stick reduces the pilot's feel and his ability to prevent pitch-ups during rolls.) (Ref. 2)

These decisions were made very early in the F-16 program, prior to development of the documented Structural Design Criteria (Ref. 3 which reflects the 9g requirement.

### WEIGHT GROWTH

The F-16A/B model originally was designed for a Basic Flight Design Gross Weight (BFDGW) of 22,500 pounds. Various models of the A/B were produced, primarily differing in systems rather than structure. Few structural modifications were made until the Block 40 and then most of the modifications were for service life enhancements rather than for increasing strength. The gross weight of the aircraft has grown through these various models from the original BFDGW of 22,500 pounds to the current Block 50 BFDGW of 28,750 pounds. See Figure 1. For the period from 1980 to 1991 the average weight growth was approximately 1 pound per day. Structural weight growth accounts for approximately 35% of the total weight growth.

There have been no changes in the basic static strength requirements, however, with each model retaining the requirement for 9g at the basic flight design gross weight. Since the weight has increased, this is equivalent to increasing the load requirement from an NzW of 202,500 pounds to 258,750 pounds, an increase of over 25%. There has been a corresponding increase in maximum wing root bending moment. See Figure 2. The Block 25/30 wing load does not follow the linear trend due to its leading edge flap schedule which provides more flap deflection as angle of attack increases than do the pre-Block 25 and the Blocks 40 and 50. This has the effect of producing more leading edge up pitching moment on the wing that must be counteracted by up loads on the horizontal tail which, in turn, relieve the wing load. Different center of gravity positions among the various models also affect the net wing load.

The increase in wing loads for the later F-16 Block 40 and 50 models has required significant structural changes. Over the twenty or so years since the

original design analysis was performed, structural analysis techniques have improved so as to enable increasingly refined stress analyses which have shown the F-16 structure to have adequate strength for these increased loads. However, the Block 30 static test article experienced an upper wing skin buckling failure at 134% of the Block 30 design limit load, requiring fleet wide retrofit of a doubler type enhancement. The Block 40/50 wing was redesigned to provide significantly higher wing bending load capacity.

### **DESIGN CRITERIA AND FLIGHT CONTROL SYSTEM**

The Structural Design Criteria document (Ref. 3), which translates aircraft requirements and USAF Military Specifications into a set of requirements for which the structure must be shown adequate, explicitly defines the aircraft flight envelope, the load factor versus gross weight envelope, and the maneuvers which the aircraft structure must be capable of performing. Not only must the basic aircraft structure be sufficiently strong, but control surfaces must be adequate for providing the necessary control power for performing the required maneuvers. Therefore, the maneuver used for design must wring out maximum loads over all aircraft components.

Design maneuvers described in the USAF Military Specifications (Ref. 4) are intended to generate maximum loads on all lifting and controlling surfaces by performing the maneuvers in such a way as to maximize the effective angle of attack on the surfaces and by maximizing inertial forces. Of course this usually cannot be achieved for all surfaces at one flight condition or for one maneuver. For this reason there are a number of different maneuver types recommended in the Military specifications ranging from balanced symmetric maneuvers to abrupt rolling or sideslip maneuvers with control surface reversals.

These maneuvers were developed prior to the early 1960s when control systems were conventional, mechanical control systems where movement of the control device (stick or rudder pedals) directly resulted in corresponding movement of control surfaces. Accordingly, the design maneuvers

contained in the Military specifications are described in terms of movement the control stick.

The F-16 control system, however, does not link the pilot's control devices directly to the control surfaces. Pilot applied forces, rather than movement or position, are first translated by the flight control computer into commanded aircraft response. The flight control computer then sends electronic instructions to the surface actuators to move the surfaces in such a way as to attain the commanded aircraft response. In general, control surface deflections are proportional to the difference between the pilot commanded response and the aircraft's actual instantaneous condition, or

surface command  $\sim$  (commanded response - current condition).

Longitudinal stick forces in the F-16 produce load factor commands, lateral stick forces produce roll rate commands, and rudder pedal forces produce rudder deflection.

This characteristic is illustrated in Figure 3 for a simulated symmetric pull-up. Note that the elevator deflection does not follow the applied longitudinal stick force but rather it closely resembles the difference between the stick force and the instantaneous load factor,  $N_z$ . Note also the elevator position for the overcheck maneuver (Figure 3b) versus the check to neutral maneuver (Figure 3a). The control system will drive the surfaces to a more extreme position depending on the difference between the command and the instantaneous condition. If the overcheck were held longer, the elevator position would have driven further thus possibly increasing the elevator load. But then  $N_z$  might have been driven negative thus violating the maneuver requirements.

Because the F-16 flight control system does not link control stick deflection with surface position, some military specification maneuvers were not used intact in the design loads analysis. Due to stability augmentation, rate limits, and handling qualities the flight control laws incorporate other parameters into the translation between the pilot input forces and the control surface deflections. While the flight control laws are very predictable when considering known inputs, the actual inputs encountered during flight tests and during fleet operations sometimes offered surprises in terms of external loads acting on the aircraft.

## Roll Maneuvers

Consider rolling maneuvers. For conventional control systems the Military specification requires that the stick be laterally deflected until the target roll rate is achieved and then checked in the same manner as the entry into the maneuver. This implies that once the target roll rate has been achieved, the control stick (and the roll control surfaces for conventional systems) are thrust in the opposite direction, held, and returned to neutral just as the roll rate returns to zero. This control motion will cause the roll control surfaces to move "into the wind" to create high loads on those and associated surfaces.

The F-16 control system, sensing the lateral force applied to the control stick, will first issue commands to the ailerons and horizontal tails to achieve and maintain the desired roll rate and then to stop the roll as quickly as possible when the pilot applied lateral force is removed from the stick (a zero stick force equates to a commanded zero roll rate). If necessary, the control system will drive the control surfaces into a position opposing the roll rate just as the pilot would do with a conventional control system.

This characteristic of the F-16 flight control system led to a change in the criteria roll maneuver description for the F-16. For maneuver simulation and flight test purposes roll maneuvers were initiated normally as described above and then checked or terminated by simply removing the lateral force from the control stick.

However, it became apparent during the F-16A/B flight test program that test pilots were extremely conditioned to checking roll maneuvers by reversing the control stick input. The problem is exacerbated by the lack of positional feedback or feel provided the pilot by the fixed stick. It is especially apparent during elevated g rolls where a constant back pressure must be maintained during the roll. Overchecking during roll termination increases the roll command/roll rate difference, and thus the commanded surface deflection, to higher values than expected in relation to original criteria. See Figure 4 for simulated roll maneuvers both checked to neutral and overchecked. The effect is influenced by control surface rate limits which may preclude maximum deflection, depending on how quickly the aircraft roll rate subsides. Since this control input was inconsistent with the criteria maneuvers, the flight test data was edited and interpreted to remove the control reversal effect.

However, it was realized that the phenomenon could result in higher loads than expected.

The overcheck phenomenon continued to be observed during several flight test programs subsequent to the original F-16A/B flight test program. It was also observed in data retrieved from flight loads recorders installed on operational aircraft. Consequently, criteria for the next airframe loads program, the Block 40 F-16C/D, was modified to include overcheck roll maneuvers.

The revised criteria did not allow for reversals in roll rate, it simply allowed for the pilot to apply reversed stick in order to terminate the roll. When the overcheck roll is performed correctly; i.e., overcheck command but no roll rate reversal, the horizontal tail loads are over 35% higher than for a check to neutral roll. During the Block 40 flight test program, it was observed that pilots had difficulty stopping the roll at exactly zero roll rate and would usually achieve a rate in the opposite direction before stabilizing at zero roll rate. In these cases, the horizontal tail loads spiked shortly after zero roll rate was achieved and the roll rate was reversed. The observed loads were higher than had been predicted during pre-test analyses since the maneuvers were not as described by the criteria. This was due, in part, to the lack of roll stick feedback afforded the pilot.

## Rudder Reversals

For the F-16, the flight control system provides a rudder deflection command proportional to the force applied to the rudder pedals. This command is adjusted by flight control laws which recognize other parameters and reduce or increase rudder deflection in order to maintain aircraft stability and roll coordination. For example, the flight control system will direct rudder deflection as a function of aileron deflection through a parameter referred to as the "aileron/rudder interconnect" or ARI. The purpose of this parameter is to reduce adverse yaw during roll maneuvers just as a pilot would normally do with a conventional system. The flight control system also limits (or fades out) pilot commanded rudder deflection above certain angles of attack. A simplified algorithm for commanded rudder deflection is:

$$\text{Rud Cmd} \sim ((\text{Pilot cmd})(\text{Fadeout}) + \text{ARI} + f(\text{yaw} \text{ \& roll rate, } N_y)).$$



Rudder or sideslip maneuvers were investigated during F-16 design and flight test. The criteria used for these maneuvers was commensurate with criteria maneuvers contained in Military specifications. It was observed during the Block 40 flight test program that rudder reversals can create high loads on the vertical tail. (Rudder reversals are intended to bring the rudder surface into high incidence angles with the airstream and thus to maximize vertical tail and rudder loads.) Flight limits were imposed on rudder maneuvers to preclude encountering high vertical tail loads in operations.

Rudder use during rolling maneuvers was not investigated because the flight control laws are designed to provide automatic rudder control so as to maintain aircraft stability and provide coordinated turns. Therefore, all rolling maneuvers performed during flight test programs were performed with "feet on the floor"; i.e., no rudder commands were provided by the pilot. Although a statement in the flight handbook informs the operational pilot that "...pilot rudder inputs do not improve roll performance...", no specific restrictions were imposed on their using the rudder during roll maneuvers.

During analysis of operational F-16 flight loads recorder data a number of maneuvers were noted as generating very high vertical tail loads. It was originally thought that these maneuvers were rudder reversal maneuvers but subsequent study revealed that they were occurring during roll maneuvers. Extensive investigation determined that F-16 pilots were, indeed using the rudder during roll maneuvers, not always in the conventional manner.

The phenomenon is associated with the normal flight control system rudder command as it is generated during rolling maneuvers. Under certain conditions, relatively high angles of sideslip can be generated. These commands depend on the flight conditions, the load factors, and the pilot's roll commands. The flight control system will command rudder deflection in a manner consistent with the flight control laws in order to maintain coordinated turns. Under normal circumstances rudder and vertical tail loads do not reach levels of concern. The pilot, however, can influence this normal rudder response by providing inputs through the rudder pedals. If he does so at a critical moment during the rolling maneuver, then the rudder deflection in combination with the aircraft

sideslip can result in higher than normal vertical tail loads.

The characteristics of the roll maneuver and the flight condition are very critical to the amount of load generated as is the timing of the pilot rudder command. One maneuver observed in flight loads recorder data which produced high vertical tail loads was investigated thoroughly. The maneuver produced a vertical tail root bending load approximately 20% higher than maximum expected for that aircraft version. A simulation was developed to understand its subtleties and to investigate variations in the pilot rudder input. It was shown in this instance that a delay of 0.2 seconds in the timing of the pilot input caused a reduction in vertical tail load of almost 25%. The simulated maneuver is depicted in Figure 5 where a number of pertinent parameters are plotted versus time. Two maneuvers are actually depicted: the original which simulated the maneuver observed in operational data and one variation where the pilot reversed his rudder command 0.2 seconds later than in the original. Note the reduction in vertical tail bending for the modified maneuver.

### Wing Load

The F-16 was designed at a specified air-to-air loading with full internal fuel. Those requirements were maintained throughout the F-16A/B Block 1, 5, 10, and 15 versions even though the operational gross weights were higher for the later block versions. The increased NzW (load factor times gross weight) limits were cleared by analysis for all F-16A/B aircraft.

A new structural evaluation was deemed necessary for the F-16C/D versions since the gross weight was substantially increasing. The BFDGW for the C/D was defined to be approximately 20% higher than for the A/B and the 9g maneuver requirement was retained. Thus the external loads would be higher.

F-16C/D load predictions were accomplished and were based on analysis techniques which had been correlated to loads flight test results obtained during the F-16A/B flight test program. These predictions were validated through a new flight test program wherein ballast was added to an F-16A aircraft to simulate the C/D mass distribution. It was also fitted with the C/D leading edge flap schedule which was intended to minimize the effect of increased weight on wing loads. The test aircraft

was limited in Nz due to local loading effects of the added ballast and so was not fully able to validate load predictions for the maximum NzW condition. However, test points at NzW up to about 75% maximum NzW were used to validate the prediction methods.

These predictions and the flight test data indicated that the relationship between wing bending moment and NzW would become nonlinear at the higher NzW values. Extrapolation was used to predict the maximum expected wing load at the F-16C/D maximum NzW. Due to the nonlinearity, the load predicted at maximum NzW was lower than would have been predicted had the relationship been assumed linear.

Later flight test programs using F-16C/D loads instrumented aircraft were executed and test results were used to further correlate the load prediction methods. These tests were flown almost to the maximum design NzW values. Test results revealed that the trend of wing load versus NzW did not, in fact, decline in slope at the higher NzW values, that it continued more-or-less linearly up to the maximum design NzW. This was in contrast to test results gathered from earlier test programs using A/B aircraft and to pre-test predictions which were developed from methods correlated to earlier flight test data. The load trend is illustrated in Figure 6.

Studies to explain this phenomenon were accomplished. There was some indication that pilot technique in terminating the maximum g wind-up turn maneuvers contributed to a false relaxation of wing load near peak load factor. However, no satisfactory firm explanation was developed and documented. The linear relationship of wing load versus NzW has continued to be used in load predictions up through the current Block 40 and 50 F-16 models.

## OPERATIONAL EXPERIENCE

### **Vortex Impingement**

Vortex impingement is a phenomenon which is very difficult to capture in actual testing but almost certainly occurs regularly in actual operational activities for air-to-air fighter aircraft. F-16 flight testing was accomplished to investigate loads resulting from flight through jet wake and was initiated as a result of the loss of a tip missile on an

operational F-16. Testing ensued where the aircraft purposely flew through a leading aircraft's wake and measurements were taken of accelerations at various lifting surface tips. It was determined that very high loads could be generated by jet wake but it was concluded that, while under extreme conditions a wing tip missile might be lost, the F-16 wing structure would not be damaged. During this testing a high acceleration approaching 80g was observed on the vertical tail tip. No damage was observed.

Two operational incidents have occurred which caused a re-look into jet wake encounter. In both these incidents, the vertical tail tip was separated from the aircraft. In neither incident did the pilot immediately know that he had sustained damage and both landed safely. No data was available for the first incident; however, flight loads recorder data as well as ground range data was available from the second. This data revealed that the aircraft was performing simulated air-to-air combat and was following a dissimilar target aircraft. The flight recorder data exhibited what appeared to be a transient event during an air-to-air engagement. The pursuit aircraft was maneuvering and had experienced 8g a few seconds before the suspected incident. At the time of the incident, the pursuit aircraft was at approximately 6g. It was assumed that the target aircraft had also been at 6g and had generated wing tip vortices consistent with a 6g maneuver at the target aircraft gross weight and flight conditions.

Subsequent analysis of the target's wing tip vortex characteristics for this condition, based on the model of Ref. 5, revealed that a wing tip vortex would persist for a substantial distance behind the generating aircraft and that the intensity was sufficient to cause damage to the F-16 vertical tail. In particular, the analysis indicated that at a distance of approximately 1900 feet, the vortex core had a diameter of about 8 inches and a circulation velocity of 260 feet per second. Analysis indicated that the circulation would degrade to approximately 122 feet per second at a radius of 7.5 feet from the center of the vortex. Several positions of the vortex center relative to the vertical tail tip were investigated as were several reasonable crossing angles. (The crossing angle determined the duration in the vortex field and thus the time available for aerodynamic load buildup. It was found that a crossing angle of 20° would allow about 90% of the maximum possible load.)

Loads on the vertical tail tip were computed from the presumed vortex flow field and it was determined that the F-16 vertical tail could sustain damage similar to that observed in the two incidents. Nevertheless, it was concluded that this phenomenon should not cause significant concern. In both incidents the aircraft landed safely, there were no adverse handling characteristics, and neither pilot immediately realized his aircraft had sustained damage. There have been two known occurrences of this type damage in over six million flight hours of F-16 operation and so its probability of occurrence is very low. There is little that the pilot can do to avoid a vortex encounter - the vortex is invisible and the pilot has other priorities. With these conclusions there were no safety bulletins or warnings issued.

### Service Loads

Military specifications were used in development of the durability criteria for the F-16A/B (Ref. 6). These specifications contain reference data which can be used to develop a spectrum of maneuvers which are applicable to service life design. Data from these specifications are based in large part on actual experience of pre-1960 aircraft where counting accelerometers or Vgh (velocity, load factor, and altitude) recorders measured operational maneuver activity in terms of exceedance counts of vertical load factor,  $N_z$ , per unit time. Data is available in the specifications for various mission types and for various mission segments. Analysis of the design aircraft's planned mission usage, in this case the F-16, allows a build-up of its expected total service life maneuver experience. These specifications contained the most comprehensive data available at the time of the F-16A/B design.

The F-16, however, was designed to provide a level of agility not available in older aircraft and it was felt that the data contained in the Military specifications was not entirely adequate to represent its expected maneuver activity. Data from F-4 aircraft was available to supplement the specification data and represented a more current operational environment. Therefore, F-4 data was used as a guide to modify the requirements for air-to-air mission segments to what was believed would better represent the F-16 maneuver usage. Spectra were developed to this modified maneuver usage and the aircraft was successfully tested for its durability design life.

The F-16 is equipped with a flight loads recorder which records flight condition and maneuver parameters. This data allows evaluation of the operational environment and calculation of in-flight loads. Analysis of the data preserved by these recorders revealed that the maneuver environment of F-16 operational aircraft was significantly more severe than that predicted through use of military specification and F-4 data.

$N_z$  exceedance distributions are equivalent to a cumulative frequency distribution of load factor peak occurrences and serve to indicate the cumulative number of times a given  $N_z$  level is exceeded. Data in this form is presented in Figure 7 for a maneuver usage based entirely on military specifications, on the modified specification data used for F-16 durability design, and for a sample of data recorded on operational F-16A/B aircraft. Note the mid-range  $N_z$  levels where the operational data is significantly more severe than the design. It is this mid-range that is most significant for crack growth.

The F-16 fleet management program has provided a wealth of data pertaining to F-16 operations. All service life evaluations other than the original design analysis have utilized actual operational data from the flight loads recorder as the data source. Most structural modifications have been made for service life reasons and were based on actual service experience. For the Block 40 redesign, flight loads recorder data was used exclusively with no reliance placed on military specifications or on other aircraft experience.

### CONCLUSIONS

The preceding discussions have presented several instances where F-16 design and analysis assumptions were eventually shown to have been inadequate to cover all loads scenarios that may arise in service. Luckily, a robust structural design for the aircraft has provided room for growth in loads realized through weight growth and test and operational experience. Not all these scenarios should be used in the design process; however, the lessons learned from the F-16 program will prove invaluable for future high performance aircraft. Specific areas which should be considered are:

1. Provide a level of conservatism in initial design loads development to allow for unknown operational activities and for unpredicted

weight growth. Although the conservatism of the F-16 design structural analysis was not deliberate, it has provided room for growth with only one major structural redesign in almost 20 years of production with continued growth in operational capability.

2. Evaluate the characteristics of the flight control system very thoroughly with regard to the pilot's ability to sense his control inputs and with regard to actual operational maneuvers. Criteria maneuvers based on historical experience may not always be adequate, especially for "first of a kind" aircraft. Criteria maneuvers which anticipate operational scenarios should be used for developing design loads
3. Understand the characteristics of the flight control system, especially the control laws for fly-by-wire systems, to evaluate whether it is possible for pilot inputs to combine with normal control system commands in a manner that increases loads beyond those expected from "normal" maneuvers.
4. For durability design do not underestimate the effects that agility can have on operational cyclic loads. This is very difficult to predict rationally for first of a kind aircraft since no historical data is available. At this point it is thought that the F-16 operational experience represents an upper bound on maneuver exceedance levels but new g-tolerance provisions and newer flight controls may allow even more agility.

Luckily, two practices work to the advantage of the loads analyst. One is the design factor of safety, usually 1.5 for ultimate strength for most major aircraft structure. With most current materials, this affords a comfortable yield margin which allows a built-in conservatism for strength design.

The second practice is the standard loads survey which attempts to find the maximum load that may possibly be experienced during a range of maneuver types over a range of flight conditions. Several parameters including gross weight, center of gravity, airspeed, altitude, and maneuver type must come together to result in maximum design loads. In operations, it is rare that the critical combination of these parameters are encountered. Therefore, a margin is available for pilots to

overshoot one or two of the design parameters as long as the other parameters are off-design.

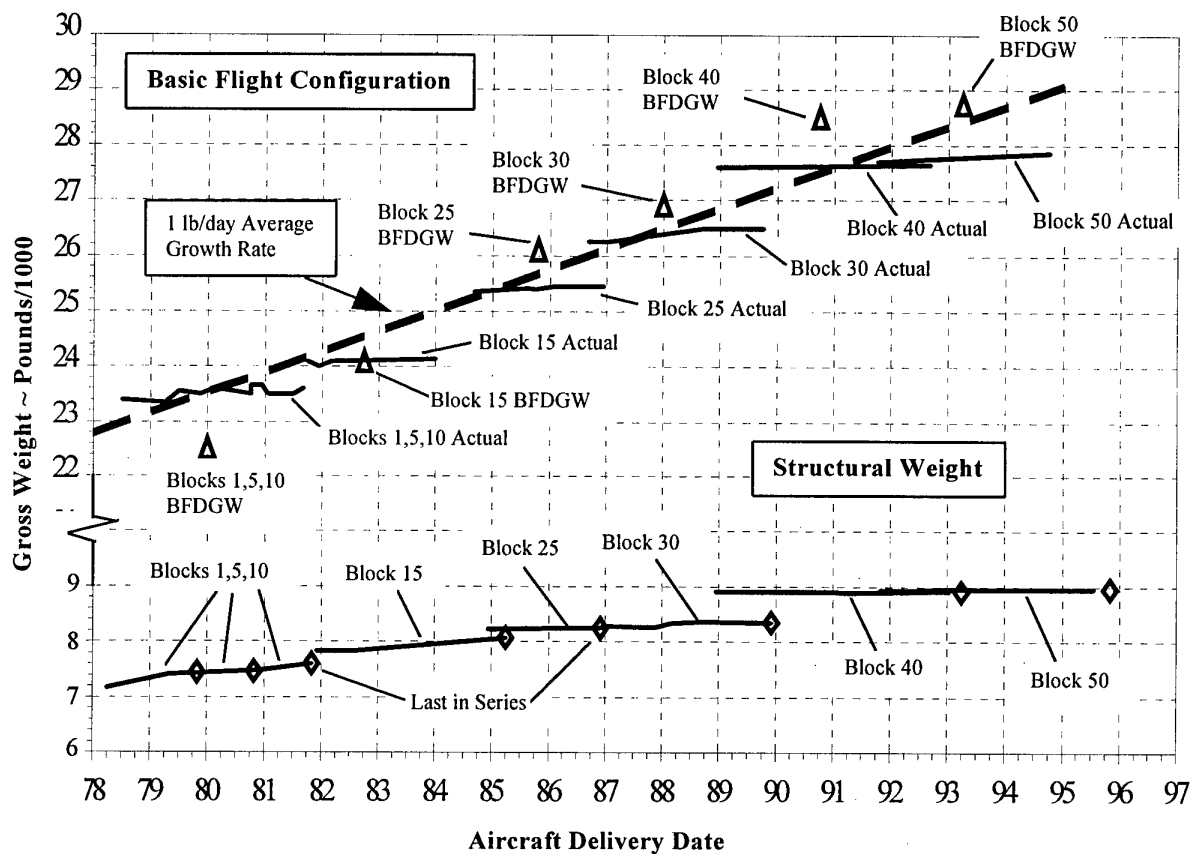
The F-16 has demonstrated that the structural design process can produce a highly efficient, economical, and robust structure. It is anticipated that it will continue to provide exemplary service long into the 21st century and can provide invaluable experience for design of next generation aircraft.

#### ACKNOWLEDGMENTS

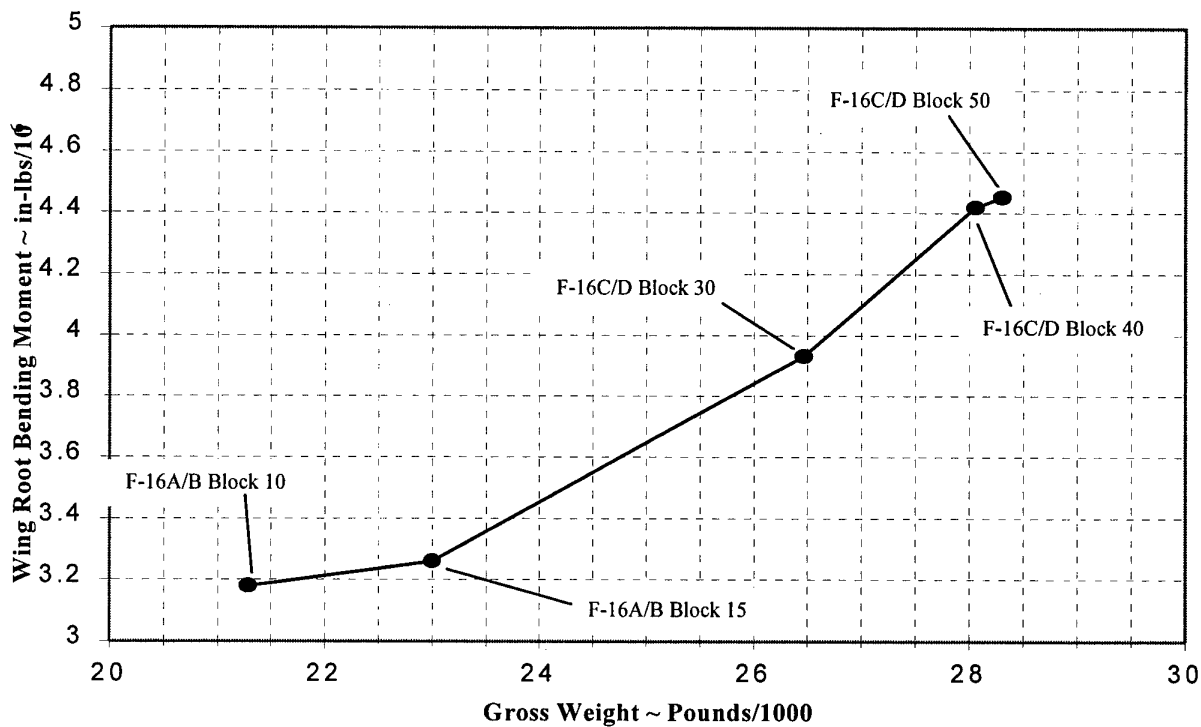
The author wishes to thank Mr. T. K. Miller and Mr. A. L. Stratton who have been involved in the F-16 program throughout its history and who have provided invaluable information in support of this article. Special thanks also are extended to Messrs. S. M. Guest and J. W. Minor who provided details of some of the more recent studies.

#### REFERENCES

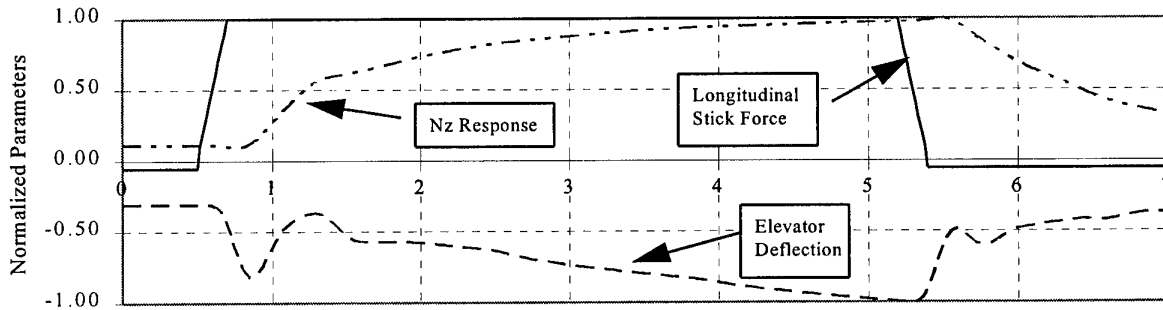
1. General Dynamics Report 16PS002, "Prime Item Development Specification for F-16A Air Vehicle", dated 16 December 1974
2. "Aircraft Structural Integrity Program Master Plan for F-16", prepared by Flight Systems Division, Directorate of Engineering, Deputy for F-16, Wright-Patterson AFB, dated May 1981
3. General Dynamics Report 16PS007B, "F-16 Structural Design Criteria", dated 15 March 1976
4. Military Specification MIL-A-008861A(USAF), "Airplane Strength and Rigidity, Flight Loads", dated 31 March 1971
5. Roberts, Leonard, "On the Structure of the Turbulent Vortex", Stanford Univ., California, AGARD-CP-342, Paper # 3, 1983
6. Military Specification MIL-A-008866B(USAF), "Airplane Strength and Rigidity Reliability Requirements, Repeated Loads and Fatigue", dated 22 August 1975



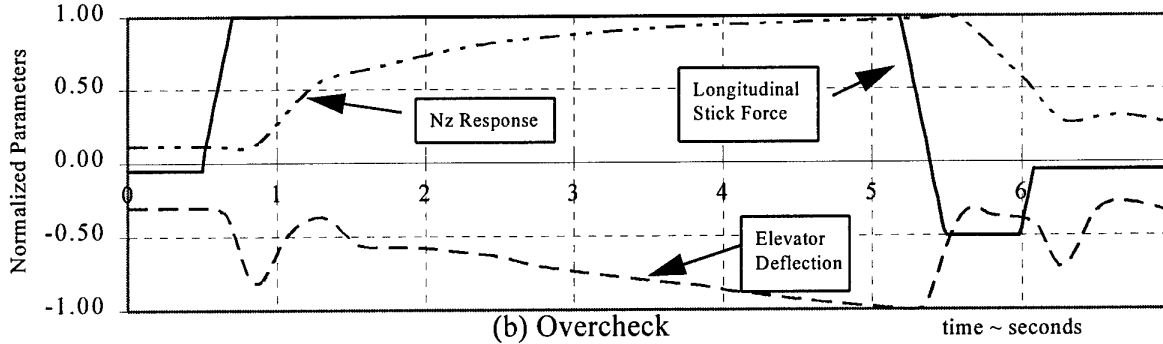
**Figure 1 - F-16 Weight Growth**



**Figure 2 - Growth in Wing Load**



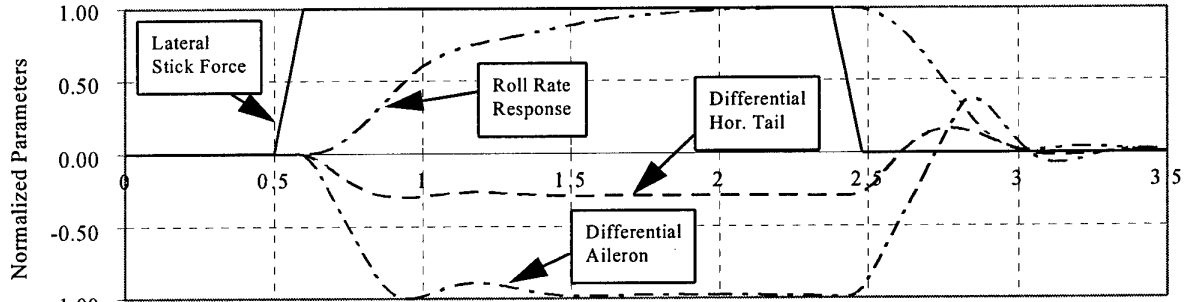
(a) Check to Neutral



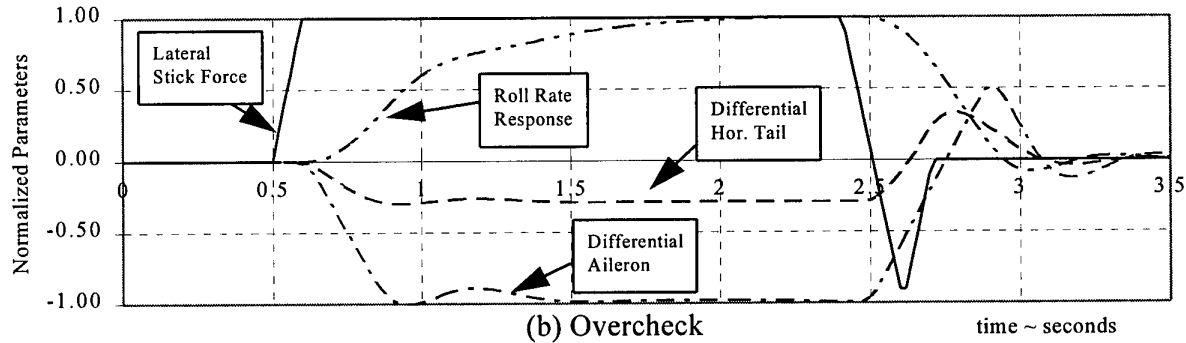
(b) Overcheck

time ~ seconds

**Figure 3 - Simulated Pitch Maneuvers**



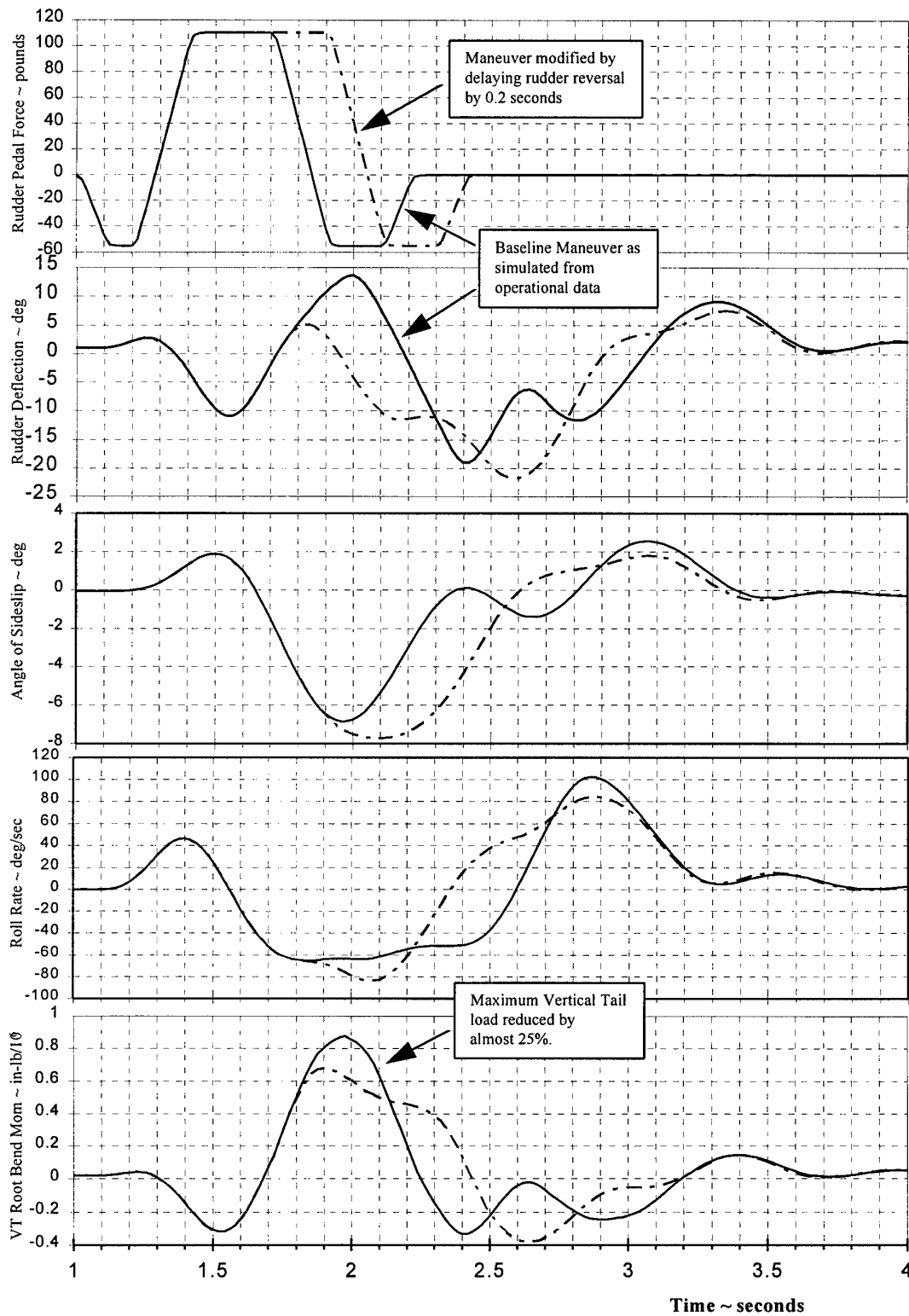
(a) Check to Neutral



(b) Overcheck

time ~ seconds

**Figure 4 - Simulated Roll Maneuvers**



**Figure 5 - Simulated Operational Rudder Reversal**

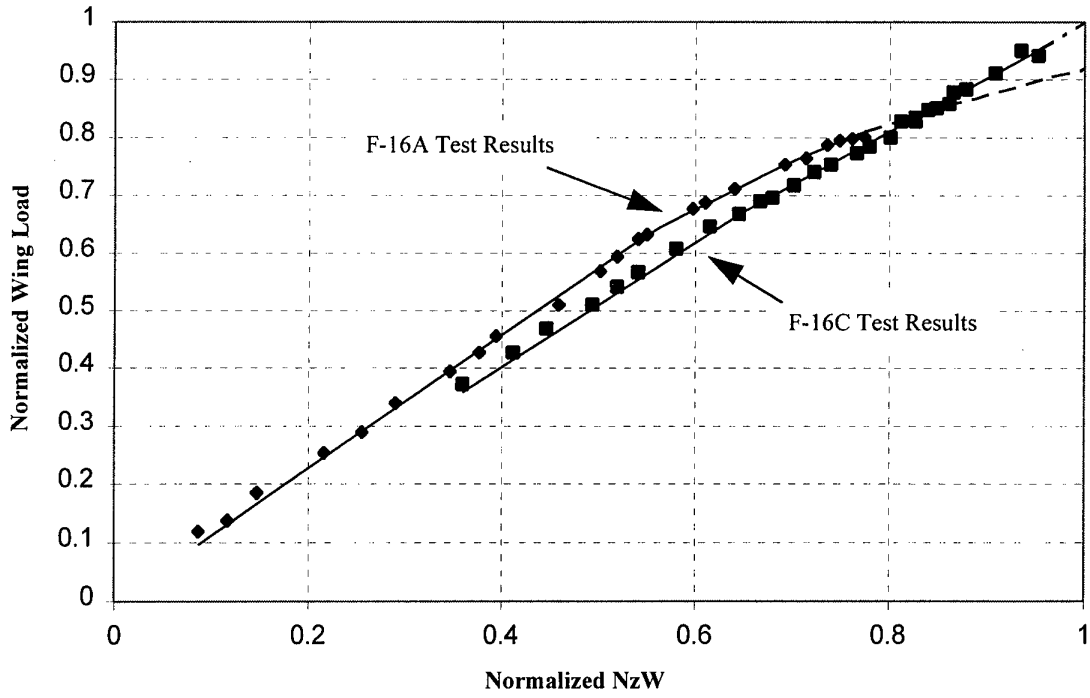


Figure 6 - Flight Measured F-16 Wing Load Trends

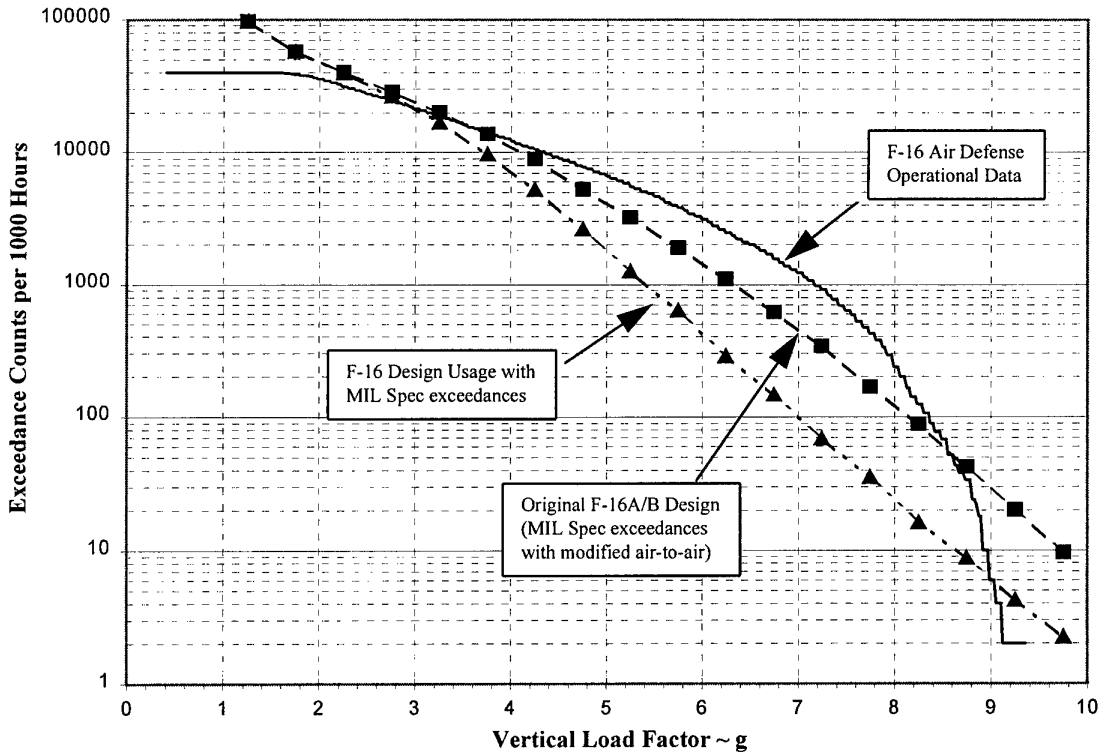


Figure 7 - Vertical Load Factor Exceedances for the F-16



## Impact of Electronic Flight Control System (EFCS) Failure Cases on Structural Design Loads

H.-M. Besch<sup>1</sup>, H.-G. Giessler<sup>2</sup>, J. Schuller<sup>3</sup>  
Daimler-Benz Aerospace Airbus GmbH Hamburg  
Structural Dynamics, Loads Department  
Kreetslag 10  
D-21129 Hamburg  
Germany

### Abstract:

For structural design loads, the most relevant benefits of the advent of fly-by-wire and digital flight control system are drawn from more sophisticated control of the aircraft and from the flight envelope protection functions. In parallel, rarely recognized even by the engineering community, the number of failure cases to be considered in A/C design is significantly increasing due to the growing complexity of the systems, eroding the aforementioned benefits. The monitoring system, designed to detect and to trigger removal of failure cases, can ease but not nullify the impact of failure cases on loads.

Experience gained in the structural design of an A/C with fly-by-wire and digital flight control system is summarized, highlighting the necessity to cover system failures in calculating structural design loads.

The current requirements for structural design of EFCS A/C are explained. By giving several examples of system failures of the new EFCS technology, it will be demonstrated how the requirements are met, whereby the influence on structural loads is especially emphasized.

Generic system-failure cases (software/hardware) having an influence on structural loads, are runaway, jamming and oscillation of control surface(s), the latter we call Oscillatory Failure Cases (OFC). OFC cause significant component loads and can cause resonance phenomena which may generate excessive loads for poorly damped rigid body and flexible modes. This motivated the research programme Oscillatory Failure Case Identification System (OFIS) which, as a future component of the common Monitoring Systems, aims at detection of OFC in time. We describe the current status of OFIS that exploits the specific properties of OFC for detection enhancement.

Furthermore, by investigating the inverse effect, namely, that structure loads have an influence on

system layout (or modification), this presentation will underline the necessity, mentioned above, of co-operation between all disciplines in modern aircraft design.

### List of Symbols

A/C	Aircraft
AFC	Automatic Flight Control
ALE	Adaptive Line Enhancer
AP	Autopilot
ASP	Adaptive Signal Processing
CoF	Continuation of Flight
Conf	Confirmation, issues true when input is true for a confirmation time
DO/OFIS	OFIS based on Deflections-Only measurement
DRP/OFIS	OFIS based on Detection of Resonance Phenomena
EFCS	Electronic Flight Control System, esp. control laws and protection functions
FBW	Fly-By-Wire
FC	Flight Control
FCC	Flight Control Computer
Fh	Flight hour
FIR	Finite Impulse Response
FSF/OFIS	OFIS based on Fault Sensitive Filter approach
FUL	Failure Ultimate Loads
HQ	Handling Quality
IPB	Innovation Process Based
FAR	Federal Aviation Requirements
FDI	Fault Detection and Isolation
JAR	Joint Aviation Requirements
KF	Kalman Filter
LAF	Load Alleviation Function
MLA	Manoeuvre Load Alleviation
MMEL	Master Minimum Equipment List
MS	Monitoring System
NFUL	Non-Failure Ultimate Loads
NOP	Normal Operation

1. H.-M. Besch, Dipl.-Ing., Head of Loads Department, Member of AIAA

2. H.-G. Giessler, Dipl.-Phys., OFIS Project Leader

3. J. Schuller, Dipl.-Ing., Project Engineer System Failures in Loads

OFC	Oscillatory Failure Case
OFIS	Oscillatory Failure Identification System
$P_{Fh}$	Probability of failure per flight hour
PIO	Pilot Induced Oscillations
$q$	Probability of being in failure state
RF	Reserve Factor
$SF$	Safety Factor
SSA	System Safety Assessment
$t_{fail}$	Mean time spent in failure state
TFM/OFIS	OFIS based on Transfer Function Monitoring
TLU	(Rudder) Travel Limitation Unit
TFM/OFIS	OFIS based on Transfer Function Monitoring
ToO	Time of Occurrence

## 1. Introduction

Introduction of EFCS has a profound effect on all disciplines involved in civil A/C design. From Loads point of view, three main interactions with system failure cases exist:

Firstly, the structural design is substantially affected by special functions implemented in the EFCS (via software) to reduce structural design loads (e.g. manoeuvre Load Alleviation Function).

Secondly, EFCS control laws and active flight envelope protection modify the response of the A/C due to any disturbance, and thus have an effect on design inputs as well [1].

And consequently, thirdly, faults or loss of functions enter design conditions, and influence loads level and (if no provision is taken) the level of safety. This is the issue of this paper.

In order to show and to prove that the required safety standard is maintained even in failure condition [2], it is necessary to investigate system failure cases for their influence on structural loads, which requires more effort as for conventional A/C.

Failure case investigations show, that structural design conditions do not cover all system failure conditions. If no provisions were taken, these system failures would become design conditions which is a situation to be avoided. In the course of this presentation we will investigate whether this desideratum can still be met in the new generation of A/C and arrive at what will be, we trust, a convincing conclusion.

In addition, we will demonstrate the influence of EFCS failures on structural design, emphasizing the necessity of co-operation among the different disciplines involved in civil A/C design (here HQ/Systems/Loads/Stress). Further, the new requirement situation arising from this context is discussed and interpreted with special

considerations of how the safety level can be maintained for such an A/C.

We treat in some detail the problematic class of oscillatory failure cases and shortly describe our monitoring solution OFIS.

## 2. Certification Requirements

Loads certification of A/C is reached when it can be shown that the structure complies with all relevant requirements which are JAR-25 [3] and FAR-25 [4].

These requirements specify manoeuvre, gust and ground loads condition, which, via simulation (using an adequate modelling of A/C and systems) and subsequent envelope forming, result in limit loads.

Definition: Limit Load

The maximum load to be expected in service. The structure must be able to support limit loads without detrimental permanent deformation.●

For standard design tasks, a safety factor of normally 1.5 is applied to the limit loads resulting in ultimate loads.

Definition: Ultimate Load:

This is limit load multiplied by a prescribed factor of safety, for static design conditions this factor is 1.5. The structure must be able to support ultimate loads without failure for at least 3 seconds.●

This accounts for uncertainties in the design process and for scatter in material properties and manufacturing.

In addition to the non-failure static design, the influence of flight control system failures on structural design has to be investigated showing compliance with the Notices of Proposed Amendment to JAR-25 (NPA 25C-199 – Interaction of Systems and Structure), which resulted from harmonization of JAR and FAR. The regulations have been established in co-operation between industry and authorities during A320 and A330/A340 design phases.

Definition: Flight Control System Failures

Flight Control System Failures are specified either in terms of control surface movement as a direct consequence of the failure case (runaway or oscillating) or by describing the failure case itself (loss of limiter). For each failure case a probability of failure per flight hour  $p_{Fh}$  and a duration of the failure case  $t_{fail}$  is specified.●

The following two definitions affect the way the failure case is to be investigated.

Definition: Time of Occurrence (ToO)

ToO is the time a transient or a permanent failure with influence on loads occurs by faulty movement of one or more controls including pilot corrective action.●

Definition: Continuation of Flight (CoF)

CoF refers to the time after occurrence of the

failure, lasting until the end of the flight or until the failure condition is removed.●

These definitions replace the former active and passive part of a failure case.

We give examples for ToO and CoF problems:  
 ToO: For failure cases which are likely to become critical at ToO, the conditions as given in the failure case definition are to be simulated resulting in "manoeuvres" not included in the standard design conditions, for instance asymmetrical elevator runaway or oscillatory surface movements (OFC).  
 CoF: For failure cases which remain undetected by the MS or cannot be removed otherwise (pilot action, inspection ...) simulation of design condition with AC in failed state must be done.

The failure limit loads envelope is to be multiplied by a failure case dependent safety factor in order to result in failure ultimate loads. Two different formulas for deriving the safety factor for ToO and CoF respectively have to be applied:

#### At Time of Occurrence

Given the probability of failure per flight hour  $p_{Fh}$  for a specific failure case, the safety factor to be applied to the ToO loads simulation outcomes is given by

$$SF_{ToO} = SF_{ToO}(p_{Fh}) \quad (1)$$

using Fig. 1 :

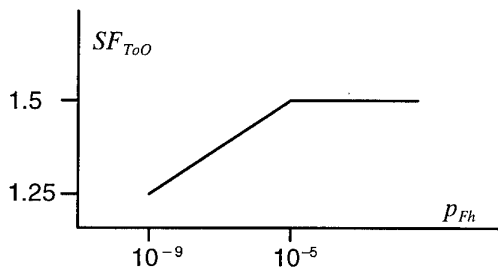


Fig. 1 Safety factor for ToO versus probability of failure per flight hour  $p_{Fh}$

#### For Continuation of the Flight

Given the probability of failure per flight hour  $p_{Fh}$  for a specific failure case and  $t_{fail}$ , the average time the A/C is operating in failure condition, the safety factor to be applied to the CoF loads simulation outcomes is given by

$$SF_{CoF} = \begin{cases} 1.5 & p_{Fh} \geq 10^{-3} \\ SF^*_{CoF}(p_{Fh} t_{fail}) & else \end{cases} \quad (2)$$

using Fig. 2 :

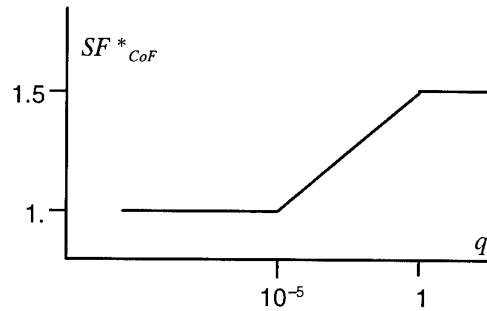


Fig. 2 Contribution to Safety factor for CoF versus probability of being in failure state  $q = p_{Fh} t_{fail}$ , the product of  $p_{Fh}$  and time spent in failure state  $t_{fail}$

Summarizing we have to show for ToO, that the structure can withstand the loads due to system failure cases. For CoF we have to show, that in addition to loads due to the persisting system failure case, the structure can withstand loads resulting from design criteria on top.

For system failures that can be shown to be extremely improbable, i.e.  $p_{Fh} < 10^{-9}$ , no investigation is required.

### 3. EFCS failures

The basic rule for System Failure Cases in A/C design is to show, that the standard level of safety is maintained during the incident itself and for the completion of the flight.

A catastrophic consequence has to be shown to be extremely improbable and is thereafter not considered for the structure. This evokes the following requirements:

- the flight handling of the A/C with systems in failure state must not overload the crew's ability to counteract the possible A/C reaction and to complete the flight, and
- the A/C structure must not be overstressed by the incident itself or during the completion of the flight.

To meet these requirements, a justification is carried out as done for all large transport A/C and is documented in the so called System Safety Assessment (SSA) established by the System Departments. A lot of defined failure cases consist of single cases which are comprised to a worst case scenario. Each of these defined system failures has to be analyzed for its impact on the structural loads.

All possible failure cases are investigated in detail by establishing fault trees and performing an analysis on the probability of each failure. The total work is summarized in the SSA mentioned above.

Two main lists of system failures have been drawn up:

- automatic flight control (AFC) failures (autopilot (AP))
- flight control (FC) failures.

AFC-failures are not considered here as they are well known for conventional A/C. Their influence on the structure is of minor importance except those involving oscillatory failure cases which are treated in connection with the FC-failures.

FC-failures (above all, those of structural relevance) are all failures affecting any control surface, its control unit (jacks, servo valves etc.) or the associated computers. These failures may be indicated in the following as failures of the EFCS.

All further discussions are restricted to failures having their origin in a computer error.

Before giving types of EFCS-failures, something shall be said about the "Monitoring System" (MS), which keeps the EFCS under surveillance. This MS checks the computer output (and all control surface deflections/rates) for their compatibility with the A/C flight condition (configuration, pilot command etc.) and controls the computer operation itself.

For example during normal operation Flight Control Computer 1 (FCC1) is on line where Flight Control Computer 2 (FCC2) is in stand-by mode. When FCC 1 fails, FCC 2 takes over the job after being initiated by the MS.

If the MS has recognized an error within the air data computers, the loss of the normal control laws is the consequence, and the alternate ones come on line, again initiated by the MS.

EFCS-failures having an influence on structural loads are mainly as follows:

- unintended runaway of any control surface by computer error or mechanical damage
- loss of control over any control surface by disconnection or during change from one computer to another
- unintended retraction of any control surface
- loss of limitations (e.g. rudder travel limiter)
- oscillation of control surfaces
- degradation of rate of deflection (e.g. because of low hydraulic pressure)
- loss of special functions (load alleviation).

In the next chapter, several system failures are described and their consequences on the structure are demonstrated as basic examples for the complete failure case analysis process. The complete work of system failure case analysis requires an extended (and iterative) effort, and is far beyond the scope of this presentation.

Before concluding this chapter, an economic aspect should be mentioned. Up until now, all system failures described have been Normal Dispatch Cases. But there is also the approach of dispatching the A/C under known system failures.

Airlines are interested in being able to fly the A/C to the next maintenance center without repairing the A/C at a remote airport lacking facilities.

Furthermore, it might be allowed to operate the A/C under some restrictions up to the next planned maintenance check.

The minimum system (hardware or software) required for dispatching the A/C, that is which have to be in normal operating mode, are laid down in the so called Master Minimum Equipment List (MMEL). Two kinds of MMEL-dispatch cases are distinguishable:

- Failures, which allow dispatch of the A/C under MMEL and
- subsequent failures after the A/C has been dispatched under MMEL-conditions.

The second item is of especial importance for the level of safety because the A/C no longer retains its original redundancy of the EFCS. Thus it is more likely that any further subsequent failure will have consequences. This is expressed by the higher probability of the MMEL failures. The MMEL approach is used particularly for failures affecting the LAF/MLA, because this function reduces the loads in severe turbulence but has – for some failure states – no effect on A/C handling. An example is given in the next but one chapter.

4. Procedure to handle Failure Cases in Loads

As mentioned above, possible system failures are summarized in the SSA. Each item of the SSA is to be processed according to Fig. 3 which we are going to describe now.

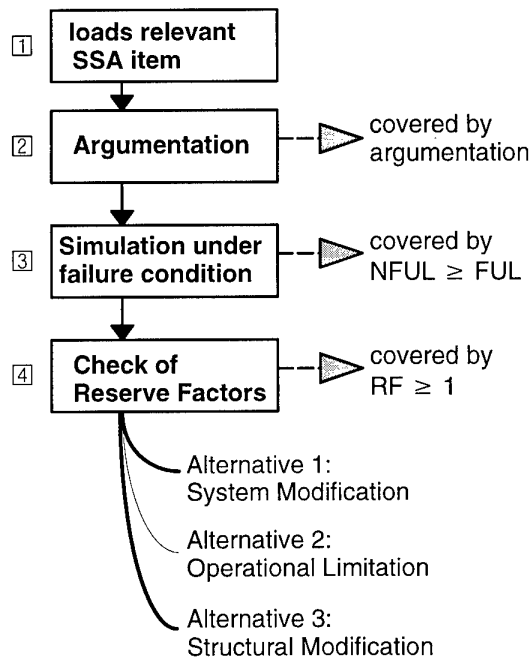


Fig. 3 Investigation of SSA items

The first step 1 of the investigation of system failures having an influence on the structure is to

select the loads–relevant failure cases from all failures of the SSA. The co–operation between System and Loads Department starts at this point. Both Systems and Loads derive a scenario for each selected case which generally includes the worst conditions in order to have a pessimistic approach for the impact on structural loads.

For many cases it may be sufficient to cover the failure loads by argumentation [2] and therefore satisfy the requirements.

If it is not possible to solve a case by arguing (i.e. failure loads expected to be close to or greater than the design envelope loads) a loads calculation has to be carried out [3]. For each affected component the ultimate loads under failure conditions (FUL–Failure Ultimate Loads) are calculated according to the requirements and then compared with the non–failure ultimate loads envelope (NFUL–Non Failure Ultimate Loads). It should be noted, that the non–failure ultimate loads are obtained by multiplying the limit loads by a SF depending for time of occurrence on the probability of occurrence of the failure and for continuation of flight on the probability of being in failure state.

If the failure loads are below the non failure ultimate loads  $NFUL \geq FUL$ , the investigation for this case is finished.

If, however, the FUL exceed the NFUL, there is a problem. Fortunately, there are also several ways to solve it. Especially at this stage of the failure case investigation, good–working co–operation between the different involved disciplines becomes of particular importance.

One possibility is to use structural margins [4]. The structure can stand the design ultimate loads at the least. This means that it can often stand higher loads. The proportion between the ultimate loads level and the real capability of the structure is figured in the Reserve Factor (RF).

If the RF for loads under failure condition is greater than 1. the investigation is finished; however this special failure case has now become a design case which must be considered in all later stress calculations. This is an undesirable situation.

To avoid this or in case of a RF being less than 1., the following alternatives remain:

- Alt.1: System Modification  
This can lead directly to a decrease of failure loads or can result in a reduction of the probability of occurrence (the system is now more reliable), so that a lower required safety factor can be applied.  
Another way is to apply system modifications that change the parameters defining the failure case in a way favorable for loads.
- Alt. 2: Introduction of appropriate flight limitation to reduce loads.
- Alt. 3: Reinforcement of structure.

The selection of the alternatives will be done in the light of timing, cost and feasibility.

## 5. Consequences on Design

In the following, some basic examples of system failures are given to demonstrate how they influence the structure and/or how they may affect system design.

The first example is an antisymmetrical runaway of elevators caused by a computer error, Fig. 4 .

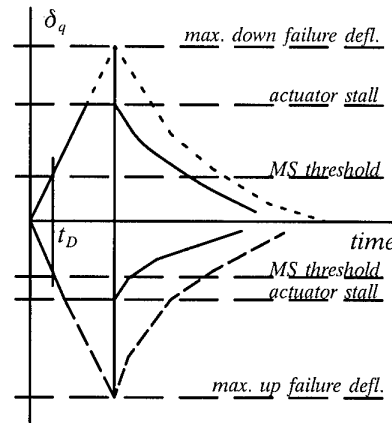


Fig. 4 Supervision of antisymmetrical elevator runaway ( $\delta_q$ ) detected by MS at  $t_D$

The elevators are signalled to deflect up to the stops if not limited by the aerodynamic hinge moment. The MS recognizes the sudden full command as a fault and holds up the surface at a certain position. Then a stand–by computer device takes over control of the surfaces, moving them back to the originally commanded position using the manual normal pitch law of AP pitch law. The probability of occurrence of, say,  $p_{Ph}^{ToC} = 10^{-5}$  requires using a SF of 1.5 to obtain the ultimate failure loads for this failure that is critical at ToO. The component affected mainly by this failure is horizontal tailplane (HTP) and the associated structure (attachments, rear fuselage).

Resulting FUL caused by this runaway exceed the total NFUL envelope applying the normal design condition. Due to the fact that the system can not be modified at this late stage, a stress check is required with the aim of using structural margins. The responsible stress offices have to show that the HTP–structure as dimensioned can sustain the high failure loads. But, at this point we should emphasize, that a failure case has now become one of the design cases for the HTP and reserve factors are not fully usable for further A/C versions.

Another type of failures is the group of control law reconfiguration failures. Table 1 shows the different combinations of pitch and lateral control law degradations with their appropriate probabilities.

Pitch	Normal	Alternate with Static Stability	Alternate without Static Stability	Direct	Mechanical Back-up
Lateral	Normal	Extremely Improb.	Extremely Improb.	Extremely Improb.	Extremely Improb.
Roll Direct with Alternate Yaw Damper	Extremely Improb.	10 <sup>-5</sup>	10 <sup>-8</sup>	Extremely Improb.	Extremely Improb.
Roll Direct without Alternate Yaw Damper	Extremely Improb.	10 <sup>-7</sup>	10 <sup>-7</sup>	10 <sup>-8</sup>	Extremely Improb.
Yaw Mechanical Back-up	Extremely Improb.	Extremely Improb.	Extremely Improb.	Extremely Improb.	Extremely Improb.

Table 1 Typical probabilities of Control Law Reconfigurations

Pitch and yaw mechanical back-up laws normally are extremely improbable ( $p_{Fh} < 10^{-9}$ ), therefore it is not required to investigate consequences on A/C structure.

The remaining five cases (roll direct laws and pitch alternate laws) have to be investigated only for continuation of flight (CoF) because the effect on loads during reversion to another law (ToO) is neglectable which has to be demonstrated. Here all relevant design conditions have to be calculated using the different control laws. Due to the low safety factor which has to be applied for these probabilities for CoF these failure cases have always been covered by the non-failure design loads envelope.

A third failure demonstrates the behavior of the transition from a computer which has failed to a standby one.

Again we have a runaway of control surfaces, this time of the ailerons, Fig. 5, limited by the aerodynamic loads or the stops. The rate of deflection is the maximum allowed by the electrical rate limiter of the control law. After a certain time while the electrically actuated valve is signalled with the maximum input, the MS detects (threshold) the failure automatically and gives a stop command to the valve. Having done this, the function of the faulty FCC1 is transferred to a standby FCC2. During this transition time, Fig. 5, no control of ailerons is present: they automatically go to zero hinge moment and simultaneously – as always when not powered – return to damping mode.

After the standby computer has been initiated by the MS with aid of the air data computer etc., A/C control is resumed and the control surfaces are commanded to the original flight conditions: that is the aileron is not frozen.

This system scenario has to be investigated for loads at all A/C stations in detail. The result must show that all failure loads are covered by the non-failure ultimate loads envelope.

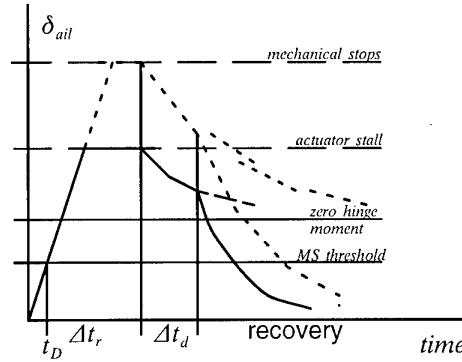


Fig. 5 Supervision of aileron runaway ( $\delta_{ail}$ ) detected by MS at  $t_D$ ,  $\Delta t_r$  is runaway time,  $\Delta t_d$  is time spent in damping mode

The next example describes, how the solution of a failure case problem was achieved by modifying the system.

It is a failure concerning the rudder with its so-called rudder travel limitation unit (TLU). The TLU limits the maximum allowed rudder deflection for structural purposes as a function of the speed VCAS (Fig. 6).

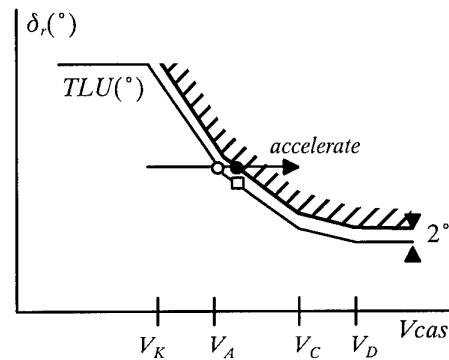


Fig. 6 Limitation of rudder deflection ( $\delta_r$ ) by TLU, solid line is 2° jamming detection threshold.

- occurrence of TLU jamming,
- detection of TLU jamming
- commanded TLU value

In case of TLU failure the TLU immobilizes at the last commanded rudder position. If the failure occurs at low speed with a higher commanded rudder deflection than the TLU allows at high speeds, it might be dangerous for the structure if the A/C operates at increased speed.

In the beginning of this failure case investigation, it was found that this failure was not detected by any system (e.g. MS) and therefore not reported to the crew. Thus, we were confronted with the unpleasant fact that rudder deflections at high speed, producing loads at fin and rear fuselage which could not be sustained by the structure, were possible. After many solutions had been

discussed and a lot of additional calculations had been done, the only economic way of covering this failure and maintaining the required level of safety was to perform a system modification.

It was decided to implement an additional function in the MS which would detect the failure as soon as the commanded position of the TLU decreased to  $2^\circ$  below the jammed position providing a warning on the crew's warning display "AUTO FLT RUD TRV LIM SYS" with the additional remark to use the rudder with care, Fig. 6 .

The fifth interesting example of a severe system failure case with consequences for both system and structure design is the oscillatory failure case (OFC), leading to oscillation of one or more control surfaces as a consequence of a system failure. Potential locations of OFC sources are shown in Fig. 7 .

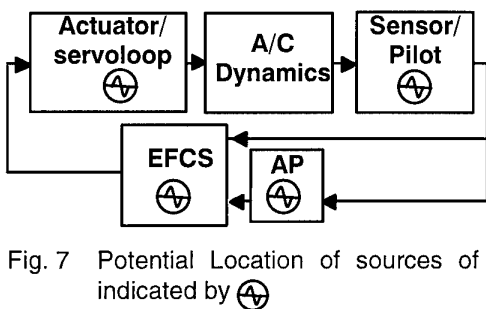


Fig. 7 Potential Location of sources of OFC indicated by  $\textcircled{A}$

The OFC may manifest itself as liquid or solid at the control surface. In liquid OFC, the OFC signal adds to the normal operation (NOP) signal issued by the EFCS and the control surface(s) deflects according to the superimposition. In solid OFC the control surface executes a pure periodic motion.

Solid OFC of control surface occurs, when OFC of actuator/servoloop is solid or when we have an upstream OFC in the EFCS, AP or in the sensor system with no pilot input or feedbacks from the control system. Upstream OFC (i.e. OFC that occur in the EFCS or AP or even in the sensor system) in general manifest itself as liquid at the control surface, because feedbacks from different paths can add. Solid OFC is most severe, because the oscillating control surface cannot execute any damping action that can ease the impact of the OFC on the structure.

OFC frequencies are uniformly distributed over the frequency range where the structure responds to excitation. Amplitudes are determined by A/C and control law dynamics. They are limited by the capability of the associated hydraulic jacks or by the detection levels of the MS.

The requirement demands investigation of the full frequency range, i.e. from the lowest body mode (rigid or elastic) up to the highest elastic mode. However frequencies below 0.2 Hz need not be regarded [5].

The determination of loads is carried out as follows:

The complete, full flexible A/C model from design load calculations in dynamic response analysis is the basis for OFC simulation. A harmonic disturbance is used to analyze the structural A/C response whereby the frequency is varied over the entire range, and the amplitude is kept at unit (1 degree). Thus the transfer functions for unit control surface deflections for different critical stations at all relevant A/C components over frequency are determined. The transfer functions show several peaks for different frequencies, characterizing the eigenvalues (eigenfrequencies) of the A/C structure.

It must be demonstrated, that loads due to OFC with amplitudes as high as the detection level of the MS can be sustained by the structure. This is tested using Fig. 8 : the dashed line is the MS detection level (or, if lower, the actuator performance curve); the solid line represent allowed angles. They are constructed by dividing the non-failure design loads by the unit load per degree, i.e. allowed angles would generate design loads when used in OFC simulation.

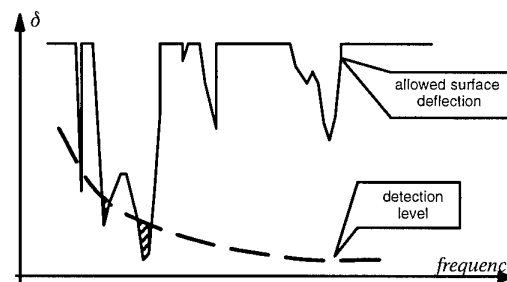


Fig. 8 Allowed Control Surface Deflection

As can be seen from Fig. 8 , some peak values of allowed angle fall below the detection level. Thus, loads due to oscillating for this frequency are not covered by the design loads at this station.

Since it may not be possible to reinforce the structure at that time, and since it is not economical to do this for a small frequency range, another solution has to be chosen. There are several options:

- a structural filter to avoid critical frequency
- system modification (e.g. rate limiter in the respective frequency region)
- more restrictive motoring; a special OFC detection device (see Oscillatory Failure Case Identification System (OFIS) below).

A final solution to the problem of OFC is obtained only, when OFIS can be put into practice: occurrence of OFC must be detected by the MS before the loads on the A/C can damage the structure.

When the OFC is such that design loads will ultimately be exceeded, detection must be very fast in order to neutralize the OFC before design loads are reached. This defines the ToO problem.

If OFC remains undetected or cannot be cut-off before completion of flight, then simultaneous occurrence of OFC and standard design conditions must not exceed ultimate loads level. This defines the CoF problem. Even if this can be achieved, an undetected OFC can cause severe fatigue problems even (when small amplitudes) which is due to the relatively large frequency of loads cycles and to the long inspection intervals. This is the fatigue problem associated with OFC.

## 6. OFIS, Approaches to OFC detection

Process monitoring is an indispensable prerequisite for the design of reliable, fault tolerant systems. The realm of Fault Detection and Isolation (FDI) ranges from simple voting systems to the concept of model based FDI or analytical redundancy which is recommended in situations where replication of hardware becomes prohibitively expensive. Model based FDI with deep roots in Decision Theory and Estimation Theory is currently the subject of extensive research. As mentioned above current A/C are equipped with a MS, but we believe that it can be improved with respect to OFC detection performance – the add-on system we call OFIS, Oscillatory Failure Identification System. In the literature on FDI, the problem of OFC seems to be rather unknown and the procedures there were not readily applicable. For OFIS, we utilize some classical approaches for FDI, but also introduced new ones (Adaptive Signal Processing (ASP) and resonance condition monitoring).

The different types and sources of OFC lead to a family concept for OFIS, which up to now has four members, Fig. 9. The underlying algorithms are based partly on Kalman Filtering and on Adaptive Signal Processing and adaption procedures developed there, but also on the observation of basic properties of response characteristics of an harmonic oscillator. We explain now the working principle for the different members, more details are given in [14].

**FSF/OFIS:** In [7] the Fault Sensitive Filter (FSF) was proposed as a fast responding detector for the ToC problem of liquid actuator/servoloop OFC. Roughly speaking, the FSF/OFIS is based on a comparison of actuator/servoloop input with output, approximately taking into account the actuator/ servoloop dynamics. More precisely, a Kalman Filter is used to estimate the states of a simple model of the actuator/servoloop plus additional failure states that respond in case of OFC. A subsequent detection state examines the failure state and derives a quantity to be subject to threshold test. It is clear, that this procedure can only detect OFC that occurs inside the actuator/ servoloop (or, more generally between input/output (I/O) measurement points). First results were given in [8] while [9] addresses the false alarm issue of FSF. Improvements of the

present day MS (smaller detection levels in the most critical frequency regions) shifted our interest to CoF and Fatigue problem area which was the genesis of [10], where Adaptive Signal Processing (ASP) for detection of sinusoids in noise was involved, working either on the states of the FSF or on the Innovation Process (i.e. prediction error) of a KF (without failure model).

**DRP/OFIS:** In order to cover upstream OFC we gave a procedure for "Detection of OFC causing Resonance Phenomena", which was offered as an extension to OFIS [12][13]. DRP/OFIS is confined to frequency ranges, where a couple can be found showing resonance. To fix ideas, think of the dutch roll frequency range and the couple rudder deflection and sideslip response. From an ongoing forced oscillation we conclude, that OFC has occurred. We found an easy way to monitor the forcing condition by investigating the sense of rotation in a phase plane plot of sideslip versus rudder. As we detect forcing conditions in general, we note, that there might be a chance of applying this procedure to the phenomena of Pilot Induced Oscillation (PIO) too, although it was not designed for it.

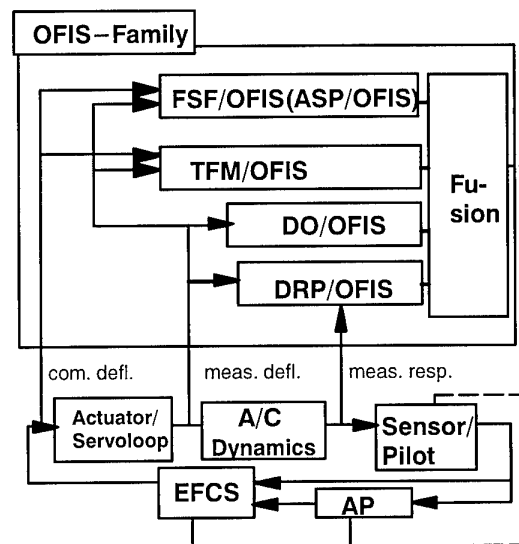


Fig. 9 OFIS-Family

**DO/OFIS:** The variation of OFC types: actuator/servoloop-OFC, upstream OFC, liquid OFC, solid OFC and the experience we gained within our part in the Loads Certification Loop leads us to pursue an alternate approach, the "Deflections Only-" component of OFIS [12]. This is an Innovation Process Based method using Kalman Filtering and Adaptive Filtering, processing only deflection measurements of the control surface to be supervised. It is directed towards detection of solid OFC in specific frequency ranges (no resonance of structure needed) that turned out to be critical during our certification work. The main assumption is, that



there exist frequency regions in which a sustained periodic signal is neither commanded nor desired and thus is indicative of OFC. From Adaptive Signal Processing, we borrow the Adaptive Line Enhancer (ALE) concept, which adapts a FIR (all zero) filter to become a prediction filter for the deflection measurement. In case of Solid OFC, the Innovation Process of the ALE becomes a minimum, because of the splendid predictability of periodic processes. The low power in the innovation process and a 'system active criteria' is used to decide on occurrence or absence of OFC.

TFM/OFIS: The realm of application of Transfer Function Monitoring OFIS is the same as that for FSF/OFIS. But it utilizes ASP algorithms, which, this time, are cast into a system identification algorithm, used on-line in order to monitor the occurrence of oscillations between points where input/output measurements are taken. Presence of OFC will result in extra large gains at the respective frequency of the OFC and can be detected by comparing the continuously updated system transfer function with an envelope of the transfer function of the healthy system. As the TFM/OFIS adapts a FIR filter to match the transfer function of the system to be supervised (in Fig. 9 this is the actuator/servoloop) using various ASP algorithm, the model of the healthy system (transfer function envelope) can be identified and must not be provided a priori. Clearly, this approach also can be applied to any part of the controlled A/C where I/O measurements are available.

We note, that the individual members of the OFIS-Family are designed to do their own job and not all of them are needed in order to remove the impact of the most severe OFC on A/C design. However, a subsequent fusion step, as indicated in Fig. 9, can enhance the overall performance and even add new features to the scheme which are not displayed by the single OFIS member itself.

## 7. Conclusion

The development of A320 and A330/A340 has shown that system failure cases for EFCS controlled A/C have an increasing influence on structural loads investigation.

In the past for non-EFCS A/C, apart from some failures of lesser importance, it always could be demonstrated for conventional A/C that no system failure case would become a design condition for any part of the structure.

From system failure case analysis for EFCS A/C, we have learned that this must no longer be true; now several system failures do affect the design of A/C structure and, vice versa, structural loads do influence the system layout. This has shown how

important close co-operation among all disciplines involved in A/C design has become.

The increasing complexity of flight control systems leads to a rising number of failure cases with the tendency of becoming a structural design condition.

This calls for a continuous improvement of the monitoring system.

Especially for oscillatory failures the current monitoring systems have turned out to border on. Therefore an additional oscillatory failure identification system – OFIS has been created.

A family concept for OFIS has been developed tailored for detection and identification of OFC in modern FBW/EFCS AC, the current status of which was sketched. The basic working principles of the various OFIS-Family members are presented. The methods are based on Kalman Filtering, Adaptive Signal Processing (ASP) and "Detection of Resonance Phenomena". While ASP is widely used in other areas, to our knowledge the application in the framework of fault detection is new, and so is the specific approach to resonance detection. Our conjecture is, that the ladder method also presents a solution to the PIO problem, which will be investigated in parallel. OFIS is offered as a potential part of EFCS and MS providing the basis for system reconfiguration after occurrence of OFC, which are OFC detection and estimation of OFC amplitude and OFC frequency range.

## 8. Literature

- [1] Influence of EFCS-Control Laws on Structural Design of Modern Transport Aircraft  
M. Besch, C.L. Tanck  
Messerschmitt-Bölkow-Blohm GmbH  
ICAS-86-2.1.2
- [2] Is it Safe?  
The Safety Assessment of Aircraft Systems  
W. Tye, T. Lloyd  
Aircraft Engineering, Jan. – May 1981
- [3] Joint Airworthiness Requirements JAR-25
- [4] Federal Airworthiness Requirements FAR-25
- [5] Joint Airworthiness Requirements JAA ACJ 25.1329. § 5.4.1 and IM S-17
- [6] Besch, H.-M., Schuller J. 1988: Influence of EFCS-Failure on Structural Design of Modern Transport Aircraft, 16th ICAS Congress Jerusalem/Israel ICAS-88-1.72
- [7] Besch, H.-M., Giessler H.-G. 1991: OFIS, Oscillatory Failure Identification System, Proposal for application of Failure Detection Methods in Dynamical Systems to the Problem of Control Surface Oscillation, Deutsche Airbus EF 32 -18/91

- [8] Besch, H.-M., Giessler H.-G. 1991: OFIS Progress Report A.1: First Results from OFIS simulation: Performance of Fault Sensitive Filter operating on artificial I/O, Deutsche Airbus EF 32 – 35/91
- [9] Besch, H.-M., Giessler H.-G. 1992: Progress Report A.3: Towards a Robust OFIS: Reduction of False Alarm Rate Due to Low Frequency Mismatch of System Model, Deutsche Aerospace Airbus EF 322 – 41/92
- [10] Besch, H.-M., Giessler H.-G. 1992: Progress Report B.1: Adaptive Signal Processing (ASP) for detection of sinusoids and frequencies, directed to solve the OFIS very low amplitude detection problem P2/3 Deutsche Aerospace, Airbus EF 322 – 35/92
- [11] Besch, H.-M., Giessler H.-G. 1992: OFIS Oscillatory Failure Identification System, Proposal for Detection of Forced Oscillations Causing Resonance Phenomena, Deutsche Aerospace Airbus EF 322 – 36/92
- [12] Besch, H.-M., Giessler H.-G. 1992: Progress Report B.2: Daimler-Benz Aerospace Airbus EF 322 – 35/94
- [13] Besch, H.-M., Giessler H.-G. 1992: Progress Report X.2: Daimler-Benz Aerospace Airbus EF 322 – 35/94
- [14] Besch, H.-M., Giessler H.-G. 1995: The Oscillatory Failure Identification System OFIS, 36th AIAAS/ASME/ASCE/AHS/ASC Structures, Structural Dynamics and Materials Conference and AIAA/ASME Adaptive Structures Forum New Orleans, LA April 10–13 1995

## **Influence of Thrust Vectoring System (TVS) on Structural Design Loads**

Konrad Füllhas, Dr. Martin Neubauer  
Daimler-Benz Aerospace AG  
Militärflugzeuge  
Postfach 80 11 60  
81663 München (Germany)

### **Summary**

The manoeuvrability and performance of modern fighter aircraft can be enhanced by a Thrust Vectoring System (TVS).

This paper will show the benefits for the aircraft (e.g. Poststall) and identify the change in the structural design loads when a TVS will be adapted to an existing fighter aircraft. The requirement is:

to minimise structural changes under consideration of the benefits from the TVS for aircraft manoeuvrability and performance.

The capabilities and properties of new fighter aircraft to be designed initially including TVS will be touched.

## **Introduction**

The German-American experimental aircraft X-31 developed by Daimler Benz Aerospace (Dasa) and Rockwell International (RI) has demonstrated successfully that it is possible to fly safely in the high angle-of-attack area (PST). The aerodynamic efficiencies of the aircraft control surfaces are supplemented respectively replaced by a Thrust Vectoring System (TVS) because the Flight Control System (FCS) was especially designed to handle the aircraft at low speeds and high angle of attacks ( $\alpha \leq 70^\circ$ ).

The manoeuvrability was extremely increased as shown by the close-in combat effectiveness of the X-31 and the F 18 (Fig. 2).

In addition Thrust Vectoring has a big potential to increase the performance for ground handling (take-off and landing) and for the conventional flight regime (e.g. supercruise capability).

Another significant advantage of thrust vectoring is the reduction of the aircraft loss rate.

Based on the X-31 experience an upgrade of modern fighter aircraft (e.g. EF2000) seems to be possible using all the benefits of thrust vectoring for poststall (PST) and the conventional flight regime.

To take advantage of all the benefits from thrust vectoring a well matched TVS has to be developed :

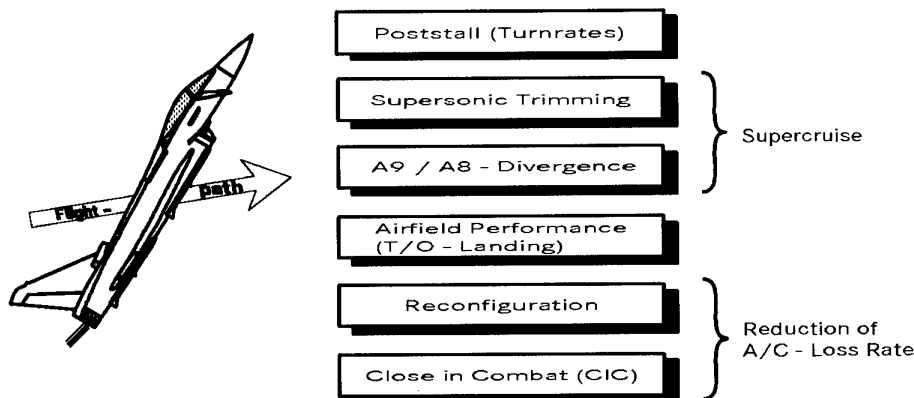
e.g. Thrust Vectoring Nozzle, Advanced Air Data System (AADS), FCS (redesign).

The subject of this paper however is the change of the Structural Design Criteria and with it the change of the aircraft design loads and of the aircraft structure for an upgraded modern fighter aircraft with TVS.

The influence on design loads for new fighter aircraft initially designed including TVS can be touched only.

### **1.0 Benefits of Thrust Vectoring for Fighter Aircraft**

A fighter aircraft with thrust vectoring capability has new important characteristics compared to a conventional aircraft (s. Fig. 1). The PST capability increases the manoeuvrability and with it the close-in combat effectiveness extremely. The aircraft loss rate can be reduced remarkably and an increase of the aircraft performance (supercruise, airfield performance) is possible.



**Fig. 1 Thrust Vectoring System (TVS) Benefits**

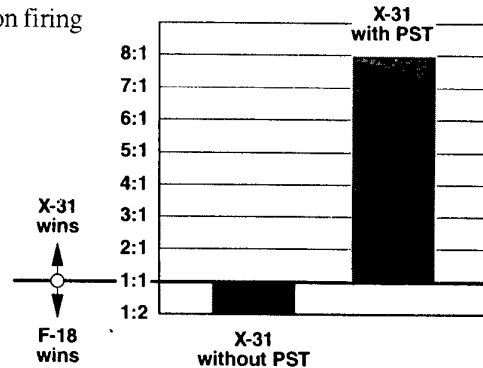
■ A fighter aircraft with thrust vectoring capability will increase extremely the manoeuvrability and with it the close-in combat effectiveness. The important basic manoeuvres are:

- ⇒ safe flight and manoeuvring at  $70^\circ$  angle of attack (AOA)
- ⇒  $360^\circ$  rolls about the velocity vector at  $70^\circ$  AOA
- ⇒ PST manoeuvres at high load factors
- ⇒  $180^\circ$  J-turn (or Herbst turn) with extremely small turn radii and high turn rates

PST manoeuvres are accomplished by roll around the aircraft velocity vector while the sideslip angle  $\beta$  should be kept to a minimum ( $\sim \pm 2^\circ$ ) by the flight control system. The advantages of PST manoeuvres are:

- ⇒ rapid aircraft deceleration capability because of high drag
- ⇒ high turn rates and tight turn radii
- ⇒ improved pointing capability for weapon firing

The superiority of a fighter aircraft with thrust vectoring compared to a conventional aircraft is shown on Fig. 2 (win and loss rate of the X-31 and the US-Navy F 18).

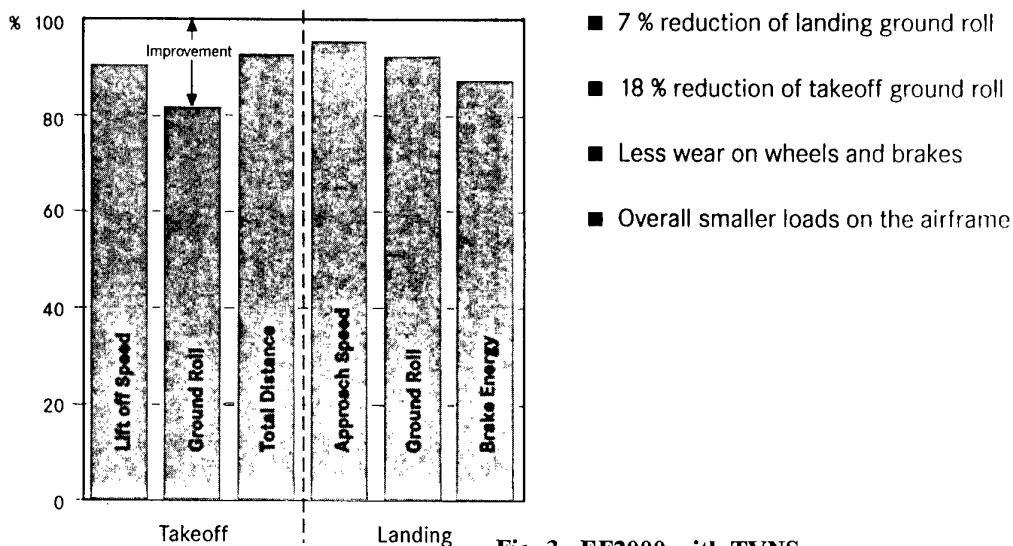


**Fig. 2 Tactical Utility of PST for Close-in Combat  
X-31 Flight Test Results**

■ During peace as well as in war time the aircraft loss rate can be reduced remarkably by using a TVS. A prerequisite is that a failure of the TVS shall not effect the aircraft safety. The main points for a safer aircraft are:

- ⇒ Failure of canard, rudder or trailing edge flaps can be compensated by TVS and FCS reconfiguration
- ⇒ carefree handling can be enlarged throughout the PST envelope at improved agility level
- ⇒ improved battle damage survivability of the aircraft
- ⇒ significantly reduced loss rate in close-in combat

■ The airfield performance can be improved by using a TVS (s. Fig. 3). For take-off and landing the lift off speed respective the approach speed will be reduced and with it the ground roll for both. The aircraft needs less brake energy and the wear of wheels and brakes is lower. The overall loads on the airframe are smaller and the fatigue conditions are reduced.



**Fig. 3 EF2000 with TVNS  
- Airfield Performance Improvements**

- An additional advantage for fighter aircraft with a Thrust Vectoring Nozzle System (TVNS) is the supercruise capability.

The optimisation of the A9/A8 thrust vector nozzle area schedule allows the improvement of installed net thrust.

The supersonic performance can be improved with thrust vector trimming thereby reducing drag.

The combat/emergency power setting can be increased at max. dry.

The sum of these improvements leads to the „supercruise“ capability.

This short description shows that the possible advantages for an aircraft with thrust vectoring capability can be impressive and it was demonstrated above all from the X-31 that the increase of manoeuvrability (PST) will remarkably increase the close-in combat effectiveness and the aircraft loss rate.

## **2.0 X-31 Experience**

The successful German - American X-31 experimental aircraft program was performed to demonstrate that it is possible to fly safely at low speed and high angle of attack (PST). The program was then extended for take off and landing performance tests and for quasi tailless flying demonstration. In the following the loads point of view is considered in more detail.

### **2.1 Design Loads**

The difficulty for the design of the aircraft was the small experience with PST and a FCS in order to simulate loads critical PST manoeuvres was not available in the beginning.

But the theoretical analysis of new unconventional manoeuvres led to the assumption that PST conditions are less critical for the aircraft structure than the conventional conditions:

The Mach number was limited to  $\leq 0.7$  (including PST-entry) at which the load factor  $n_z$  was lower than for the normal flight regime. The corresponding angular velocities/accelerations were very low compared to the conventional manoeuvres.

The result was to design the aircraft to conventional flight conditions with the exception of the rear fuselage where the influence of thrust vectoring from the 3 thrust vector vanes had to be considered.

Very important was the decision to design the aircraft structure (fin, rear fuselage) to fin buffet conditions (F-18 experience !!).

In a second load phase (interim loads) the design loads where checked and updated with nonlinear aerodynamics (high angle-of-attack).

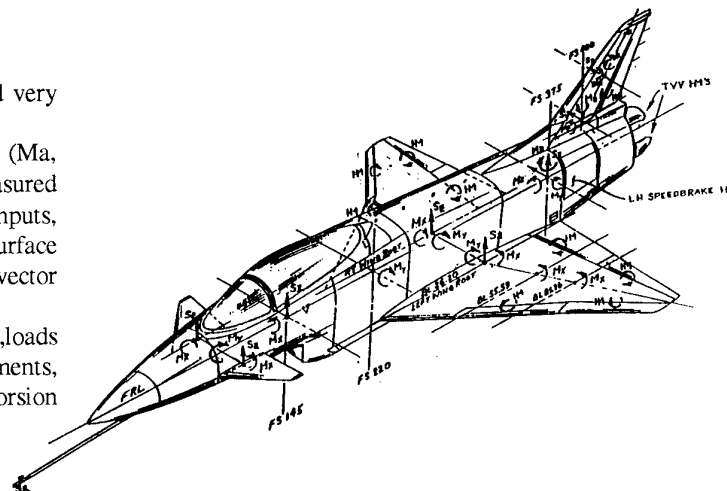
For both X-31 aircraft a 80% structural loads clearance was given while no ultimate static airframe test was done.

### **2.2 X-31 Flight Test Results**

The X-31 flight test was performed very carefully.

The total list of flight parameters ( $Ma$ , alt.,  $\alpha$ ,  $\beta$ ,  $n_z$ , etc.) where measured together with control stick inputs, actuator positions and control surface deflections (including the thrust vector vanes).

Aircraft number one was the „loads aircraft“. The loads like hinge moments, shear forces, bending moments, torsion moments where measured at several fuselage, wing, fin, and foreplane stations (s. Fig. 4) with calibrated strain gauges. The first flight test steps were



**Fig. 4 X-31 - Structural Flight Test Load Measurement Items Shears, Bending Moments, Torques and Hinge M.**

performed without thrust vectoring in the conventional flight envelope ( $\alpha < 30^\circ$ ). The loads analysis from this flight test results gave the confirmation that the design loads were correct. The defined loads critical design parameter ( $n_z$ ,  $n_y$ ,  $\beta \cdot q$ ,  $p$ , etc.) were attained during flight test and the corresponding measured loads compared well to the calculated design cases.

Before starting the PST manoeuvre flight test the X-31 configuration was changed.

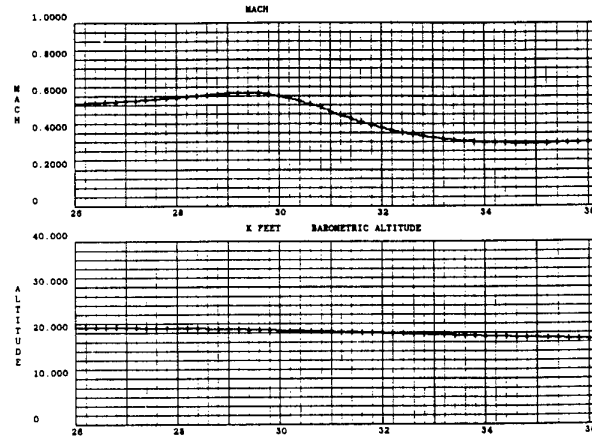


Fig. 5 X-31 - 6g abrupt WUT (Split -S) to 70° Alpha Mach/Altitude versus time

Nose- and aft fuselage strakes were necessary for aerodynamic reasons for the high angle of attack area.

The analysis of the PST flight test results confirmed the design assumption that the PST manoeuvres are less loads critical than the conventional conditions (s. para. 2.1 Design Loads).

Fig. 5 to 9 shows the loads critical flight parameters Mach, altitude,  $\alpha$ ,  $\beta$ ,  $n_z$ ,  $n_y$ ,  $n_x$ ,  $p$ ,  $q$ ,  $r$ ,  $\dot{p}$ ,  $\dot{q}$  and  $\dot{r}$  versus time for one representative X-31 typical PST flight manoeuvre.

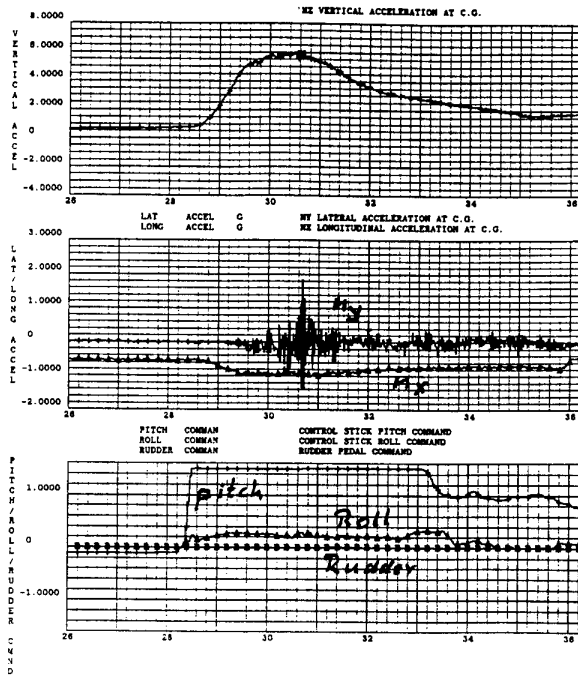
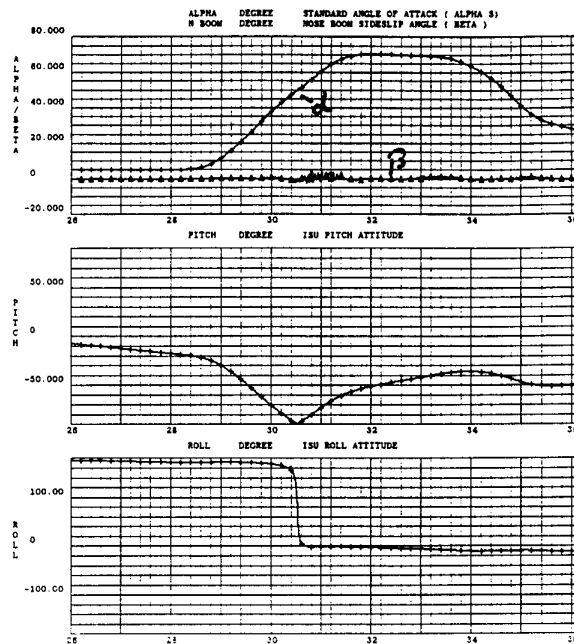


Fig. 6 X-31 - 6g abrupt WUT (Split -S) to 70° Alpha  $n_x$ ,  $n_y$ ,  $n_z$  and Stick/Pedal Command v. time

For better understanding of the flight manoeuvre the corresponding control stick commands (pitch, roll)/pedal command and the pitch- and roll attitude are shown too.

It can be seen that the aircraft deceleration ( $n_x$ ) is remarkable during the  $\alpha$  increase up to 70°. The mach number decreases from 0.6 to ~0.3 at nearly the same altitude (decrease of dynamic pressure).

Fig. 7 X-31 - 6g abrupt WUT (Split -S) to 70° Alpha Alpha/Beta and Pitch/Roll Attitude v. time



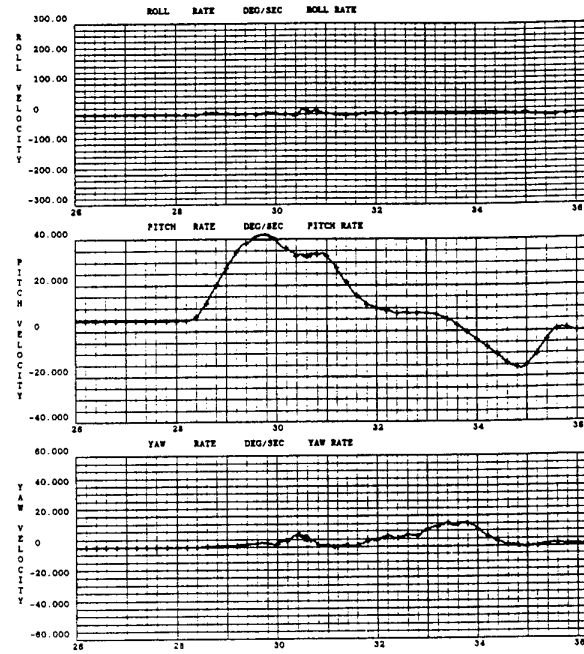
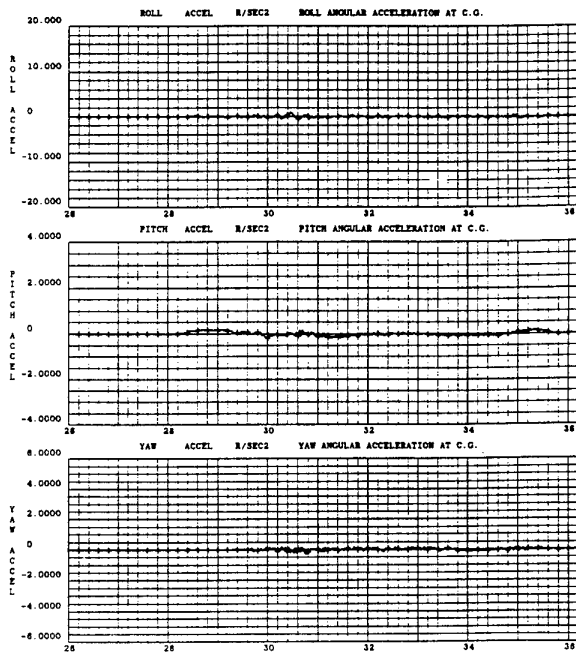


Fig. 8 X-31 - 6g abrupt WUT (Split-S) to 70° Alpha Roll/Pitch/Yaw Acceleration at c.g. v. time

Fig. 9 X-31 - 6g abrupt WUT (Split-S) to 70° Alpha Roll/Pitch/Yaw Rate (p, q, r) versus time

The sideslip angle  $\beta$  and the aircraft fixed angular velocities (p, q, r) and accelerations (p $\dot{}$ , q $\dot{}$ , r $\dot{}$ ) are low while the FCS handles the aircraft very well and with it the influence on loads from these parameters was very low. Beside some nonlinear aerodynamic effects it can be said that the static loads are driven mainly from symmetric load conditions ( $n_z$ ,  $\alpha$ , control surface deflections) and the thrust vectoring. All static loads measured during PST flight test were inside the 80% flight load envelopes.

X-31 flight test has shown that for the high angle of attack area dynamic loads - in this case fin buffet - are more critical than static loads. Fin buffet peak loads occurred regularly in each PST test flight in the  $\alpha$ -range of 45° to 55° (s. Fig. 10 and 11) but all measured fin buffet loads during flight test were inside the 80% fin design load envelopes. The dynamic response of fin buffet can be seen also in Fig. 6 were the linear acceleration  $n_y$  in the aircraft c.g. is measured.

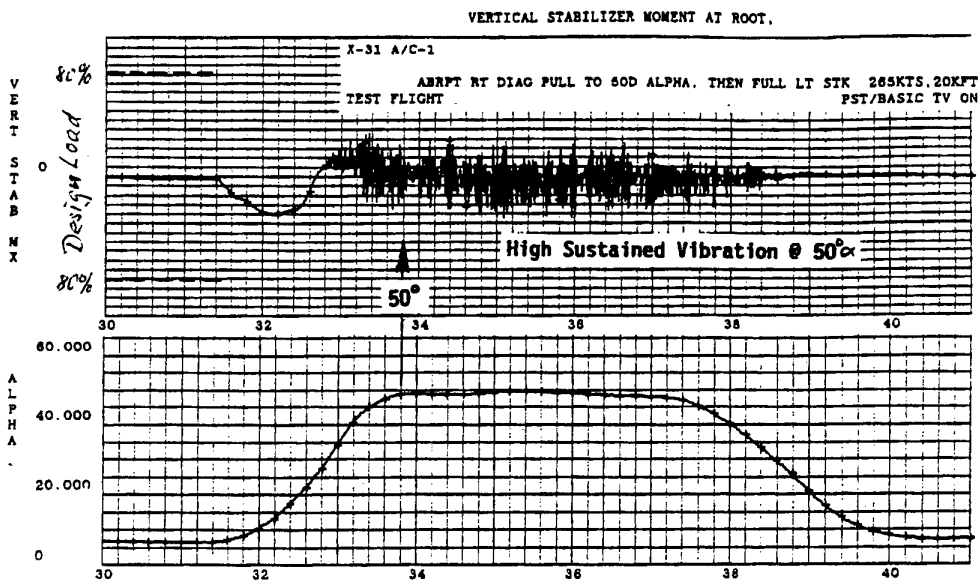


Fig. 10 X-31 - Diagonal Pull to 50° Alpha Fin Buffet - High Sustained Vibration



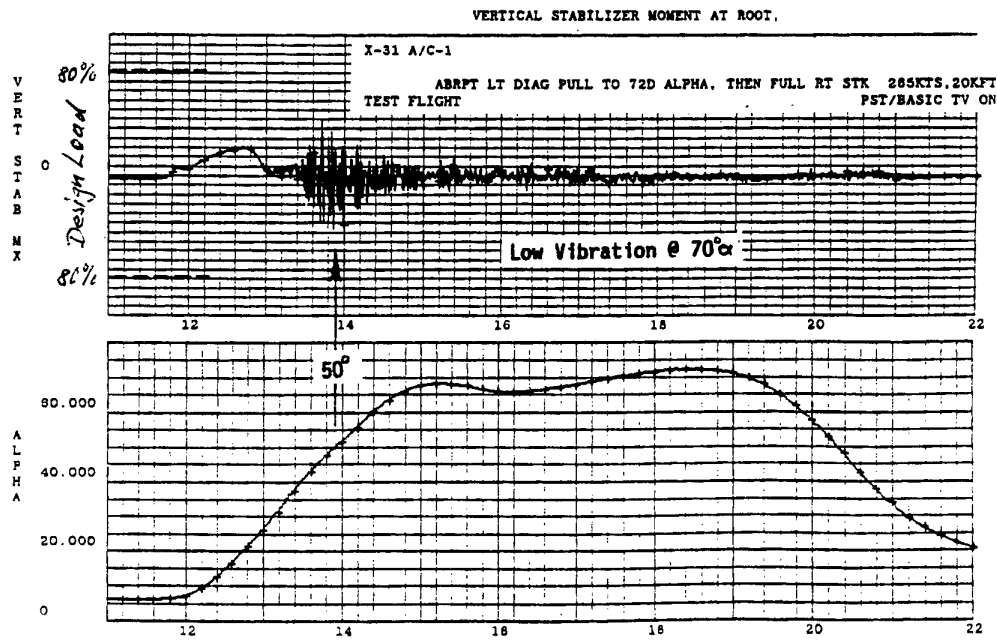


Fig. 11 X-31 - Diagonal Pull to 70° Alpha  
Fin Buffet - Low Vibration at 70°

**3.0 EF2000 with Thrust Vectoring Nozzle System (TVNS)**

The good test results with the X-31 led to first investigations for an upgrade of the EF2000 with TVNS. For the improvement of the close-in combat capability for EF2000 and the usage of the other benefits (airfield performance, supercruise, aircraft loss rate) three main columns for the development of TVNS for EF2000 (s. Fig. 12) were identified:

- The development of an Advanced Air Data System (AADS)
- The redesign of the Flight Control System (FCS) and control laws
- The integration of the thrust vectoring nozzle into the aircraft structure

The development of the thrust vectoring nozzle itself is the task of an engine manufacturer.

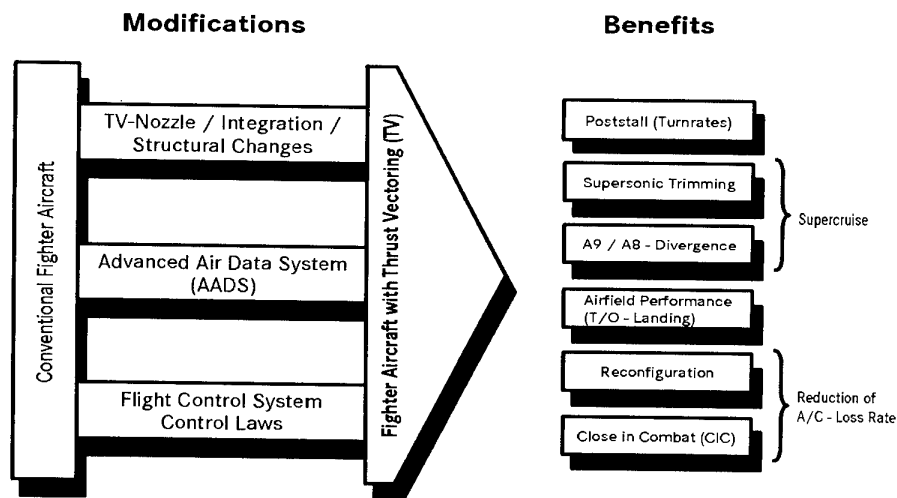


Fig. 12 EF2000 with TVNS - Modifications and Benefits

### 3.1 Advanced Air Data System (AADS)

The expansion of the flight envelope into the poststall regime (s. Fig. 15) requires an AADS which has to cover

- high angles of attack
- low dynamic pressure

The noseboom (e.g. X-31) has to be removed for a production aircraft whereas new sensor technics can provide the required accuracy (tolerances) of measurements.

### 3.2 Flight Control System

The FCS and with it the control laws have to be redesigned to include the vector nozzle control and to achieve a carefree manoeuvring performance for the conventional flight regime (supercruise, airfield performance) and for PST. A single engine recovery from PST manoeuvring should be possible.

The remarkable increase of the turn rate for EF2000 with TVNS (s. Fig. 13) in the conventional flight regime and especially in the high alpha range (PST) which is possible with thrust vectoring controlled by a redesigned FCS is also important for the check of the design loads.

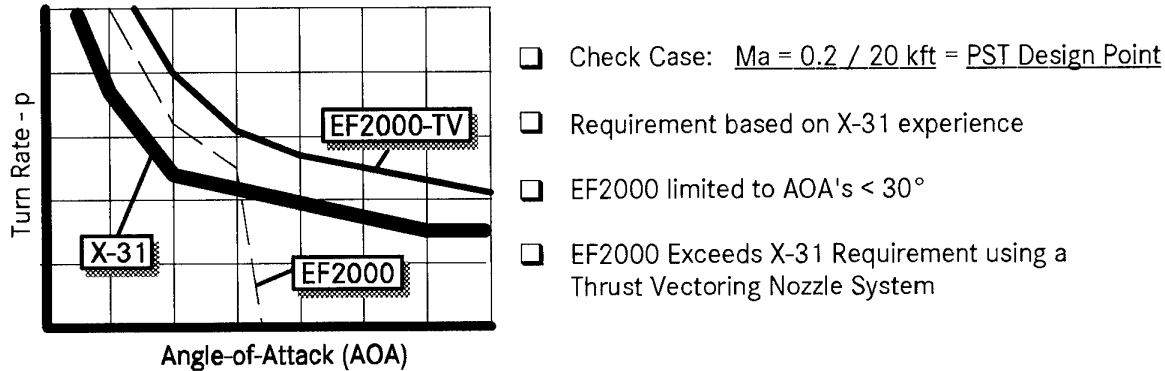


Fig. 13 EF2000 with TVNS - PST Performance

### 3.3 TV-Nozzle Integration and Structural Changes

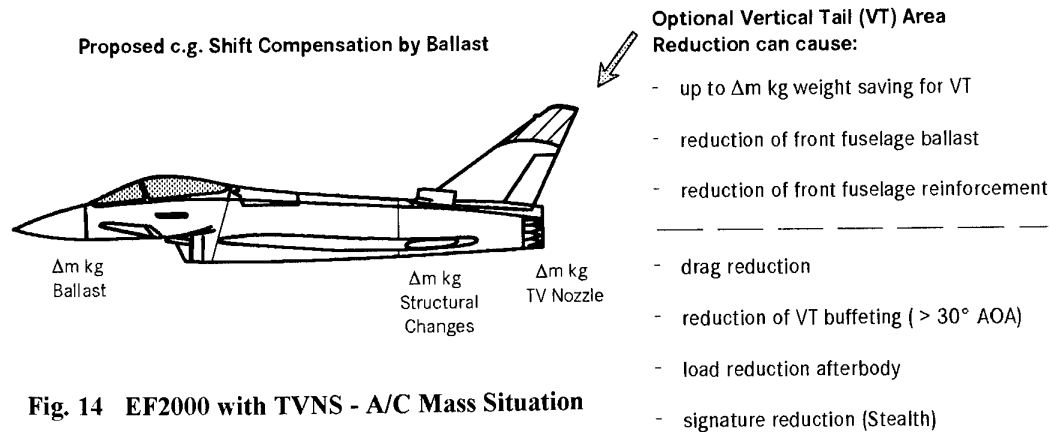
The experience of the X-31 is very helpful for the definition of the Structural Design Criteria for the upgraded aircraft with TVNS while the knowledge of PST manoeuvres and the influence on static and dynamic loads is now improved. The proof that the FCS can handle the aircraft in high angle of attack and low speed and the information about the loads critical flight parameter in PST ( $Ma$ ,  $n_z$ ,  $n_y$ ,  $p$ ,  $q$ ,  $r$ ,  $\dot{p}$ ,  $\dot{q}$ ,  $\dot{r}$ ) is important to define the design conditions for critical loads for the aircraft components. The measured loads in flight test for the main aircraft components - front fuselage, rear fuselage, fin, wing - and for the control surfaces gave an impression about the differences of loads in the conventional flight envelope compared to PST. It could be identified - for example - that nonlinear aerodynamic effects in high angle-of-attack (PST) are not very important for the critical design loads of the aircraft.

#### 3.3.1 Aircraft Mass Situation

The integration of a TVNS will change the mass situation of the aircraft (s. Fig. 14). The two vector nozzles are increasing the mass at the rear end of the rear fuselage and shift the aircraft c.g. rearward out of the tolerated c.g.-range for the FCS. For compensation of this aircraft c.g.-shift front fuselage ballast is therefore needed. An additional mass increase should be taken into account from local loads changes and load increase - especially in the rear fuselage area.

These mass changes are locally important but will not change the overall mass situation of the aircraft remarkably. The definition of the aircraft design mass has not to be changed while the total mass increase can be covered by a small reduction of internal fuel (3 ÷ 4 %) in the centre fuselage and the wings.

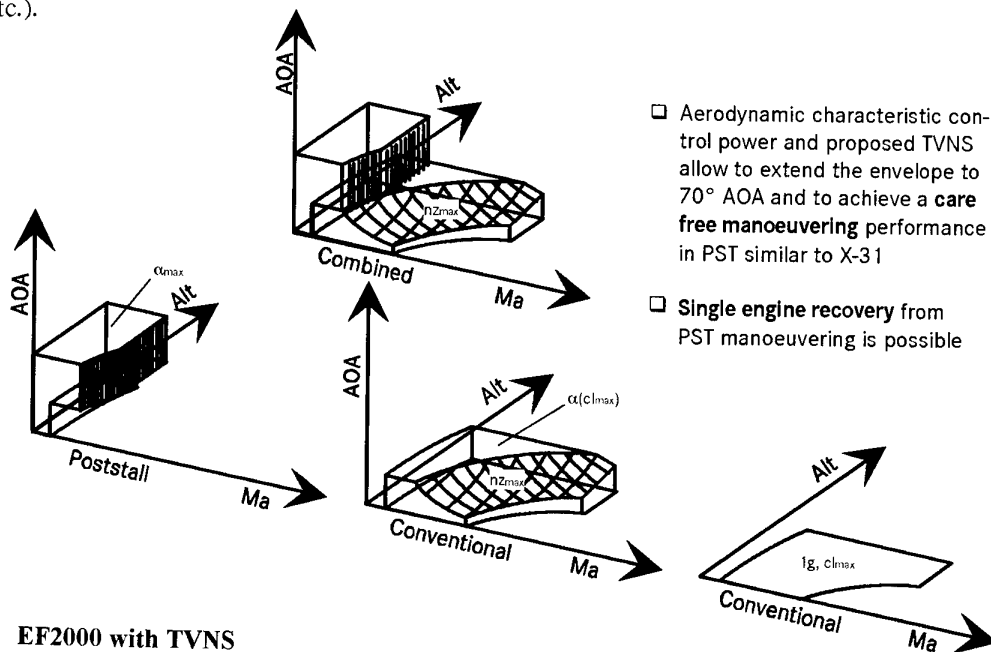
An additional option for the aircraft with TVNS is to reduce the vertical tail (VT) area. In this case the rear fuselage mass increase will be less resulting in a lower front fuselage ballast.



**Fig. 14 EF2000 with TVNS - A/C Mass Situation**

### **3.3.2 Definition of Loads Critical Flight Manoeuvres**

Fig. 15 shows the expansion of the flight envelope for an aircraft with thrust vectoring capability (e.g. EF2000). PST manoeuvres (including PST-entry) will be flown only in the subsonic region. A prerequisite for the extended envelope is that in the conventional part of the envelope no additional flight limitations should occur ( $Ma$ ,  $n_z$ , etc.).



**Fig. 15 EF2000 with TVNS**  
- Expansion of Flight Envelope into the PST Regime

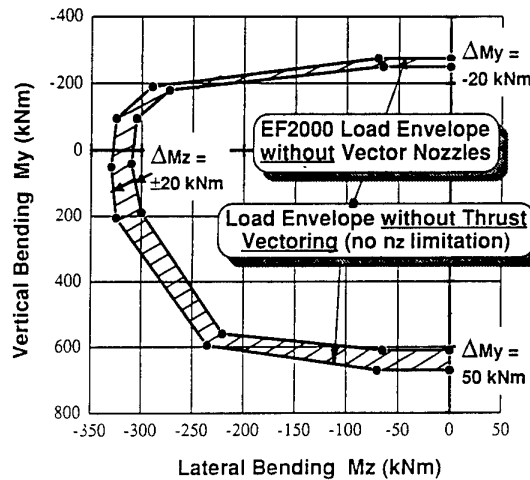
The analysis of the increased manoeuvre capability of the upgraded aircraft with TVNS showed that the loads critical manoeuvres can be grouped into three different segments:

1. PST manoeuvres
2. Manoeuvres without thrust vectoring throughout the conventional flight envelope
3. Manoeuvres with thrust vectoring throughout the conventional flight envelope

The loads criticality of the three different manoeuvre types in combination with the changed mass situation of the aircraft can be defined now.

⇒ The lessons learned from X-31 were that PST manoeuvres are less critical for the overall aircraft static loads situation than the conventional manoeuvres. The reasons are explained in para. 2.2 X-31 Flight Test Results. The maximum load factor  $n_z$  for PST will be ~ 80 % of the design load factor. However local load changes in the rear fuselage area resulting from thrust vectoring condition during PST have to be checked. As the X-31 has shown, Fin Buffet will be a critical design condition. The actual fin buffet loads from PST have to be checked against the design buffet conditions statically and for fatigue.

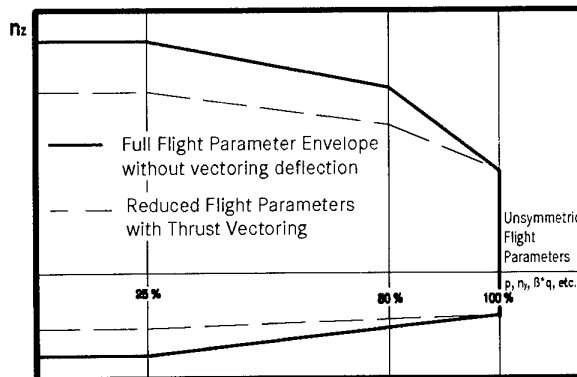
⇒ The 2nd manoeuvre type where the aircraft with TVNS is flying throughout the conventional flight envelope without using the TVNS and without any additional flight limitations resulting from TVNS will be critical for the update of the aircraft structure. The local mass increase for the rear fuselage (thrust vector nozzles) and the front fuselage (additional ballast) will increase the mass dominated overall fuselage loads and defines the new design loads envelopes for front- and rear fuselage. Fig. 16 shows the increase of rear fuselage design loads for the aircraft with TVNS compared to the design loads for the aircraft without a TVNS.



**Fig. 16 EF2000 with TVNS  
- Increase of Rear Fuselage Design Loads**

The influence to the aerodynamic dominated wing loads is very small because the aircraft design mass and aircraft c.g. position has not changed (s. para. 3.3.1 Aircraft Mass Situation) respective the wing mass is nearly the same (minor reduction of wing fuel). The fin loads are not affected if the fin geometry has not changed.

⇒ For the 3rd manoeuvre type where the aircraft is using the thrust vectoring capability throughout the conventional flight envelope the load factor  $n_z$  can be limited in a sense that only local design conditions for the rear fuselage (engine attachments, etc.) may become critical. The potential benefits from the use of thrust vectoring are not affected by the necessary flight limitations. The overall aircraft loads are inside the new defined fuselage loads envelopes (s. 2nd manoeuvre type). The possible limitation for the 3rd manoeuvre type is shown in Fig. 17



**Fig. 17 EF2000 with TVNS  
- Flight Parameter Envelope for Structural Design**



## Eurofighter 2000 Structural Design Criteria and Design Loading Assumptions

G.J. Watson  
Aerodynamics Department  
British Aerospace - Military Aircraft Division  
Warton Aerodrome, Preston, Lancs. PR4 1AX  
United Kingdom

### SUMMARY

This paper provides an overview of the assumptions employed in the preparation of Design Loads for the Eurofighter 2000 aircraft. For loading purposes, a set of Design Criteria have been defined, which summarise the principal manoeuvre requirements for the aircraft. Additional assumptions on aircraft Control usage have been necessary to allow Design Loads to be defined without a detailed knowledge of the final standard of Flight Control System. The assumptions employed have been aimed at providing a robust structural design for the airframe, an aim which is now being validated through the Flight Clearance and Test activities on which the first Prototype aircraft are currently engaged.

### 1. INTRODUCTION

The Eurofighter 2000 (EF2000) aircraft is a 4-Nation project between Italy (Alenia), Spain (CASA), Germany (DASA) and the UK (BAe). Each Partner Company is responsible for the design and build of portions of the airframe, and the definition of Structural Design Loads has also been shared between Companies. To ensure a consistent approach, it has therefore been essential to closely define the assumptions to be employed in the definition of Design Loads.

The aircraft features a highly augmented Flight Control System (FCS), offering artificial longitudinal stability in subsonic flight, and extensive control augmentation throughout the flight envelope. The FCS is also planned to provide a full Carefree Manoeuvre capability, with automatic load protection achieved through careful control of manoeuvre response parameters.

Given the very high levels of control augmentation and the multiple control surfaces, the loads developed on the airframe during manoeuvring flight are dependent to a significant degree on the detailed design of the FCS Control Laws as well as the fundamental Aerodynamics of the airframe. This presents a problem for the definition of Design Loads, as such loads must be defined early in the project life, when only a very limited understanding of the FCS Control Laws is available.

To provide both a consistent framework of assumptions for

the derivation of Design Loads and to pre-empt the detailed manoeuvre characteristics of the FCS Control Laws, manoeuvre requirements have been summarised into a set of flight parameter envelopes and collated into a Structural Design Criteria document. The existence of a single set of Design Criteria permits each Partner Company to work semi-independently on the production of Design Loads for each major aircraft component, and provides clear visibility to the FCS designers of the manoeuvre capability being designed into the airframe structure. This allows the Structure and FCS Control Laws to be developed concurrently, and ensures that when they are brought together during Flight Clearance assessments, the Structural capability will be well matched to the requirements placed on it by the FCS Control Laws, and the final aim of an agile and Carefree load limiting FCS can be realised.

### 2. EUROFIGHTER 2000 GEOMETRY

Figure 1 shows the general lay-out of the EF2000 aircraft, which features a delta-canard configuration, with a single vertical fin and twin engines fed by a chin mounted intake. Control is provided by all moving Foreplanes for pitch control, four Trailing Edge Flaperons for pitch and roll control, and a Rudder for Yaw control. Secondary Leading Edge devices are also used for wing drag optimisation, and provide some secondary pitch benefits. Further secondary devices under the FCS control include a Spine Mounted Airbrake and an Intake Varicowl for controlling mass flow to the engines.

To produce a minimum mass solution, Design Loads are required to be defined in some detail. A number of Monitor Station locations were therefore identified at which Design Loads were required to be produced. These monitor stations included the obvious major component build joints such as the Wing, Foreplane and Fin root, and Front and Rear Fuselage Build Joints. However many additional locations were also identified, to include all the primary control surfaces, and additional 'semi-arbitrary' cuts across the wing surface as shown in Figure 2. By defining a large number of critical loading locations, the structural design can be optimised to ensure that appropriate strength (with the attendant mass implications) is tailored precisely to the loading distribution across the airframe.

Figure 1. EF2000 General Lay-out

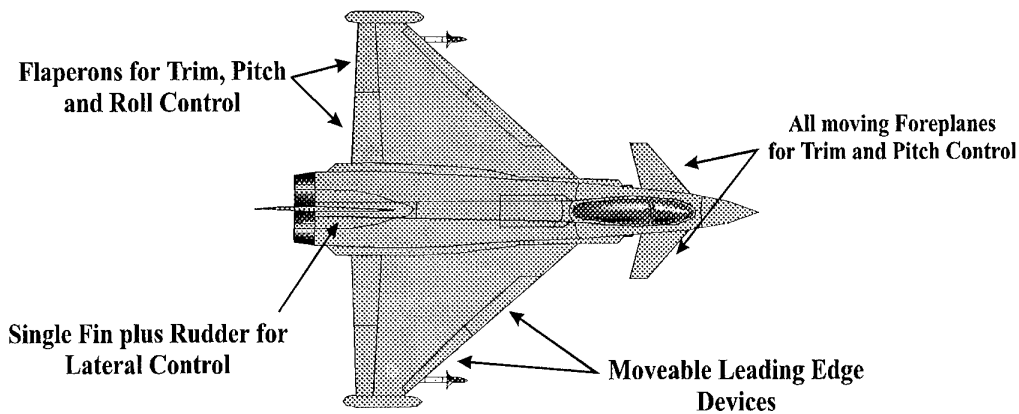
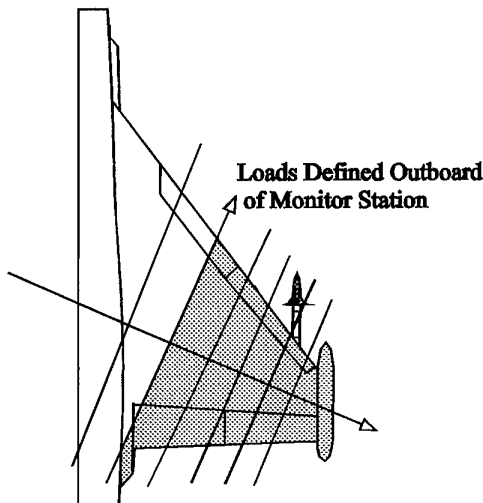


Figure 2. Wing Monitor Stations



The production of the Design Loads therefore involved identifying the particular manoeuvre conditions that maximised the loading at each Monitor Station, whilst falling within the Design Criteria manoeuvre envelopes. Furthermore the Design Cases were also required to contain sensible assumptions regarding the use of the various control surfaces.

**3. STRUCTURAL DESIGN PHILOSOPHY AND LOADING PHASES**

Prior to discussing the Structural Design Criteria, it is worthwhile to note certain points regarding the overall philosophy adopted for the design of the Eurofighter structure, and the various phases of loading work conducted on the project. All the following design assumptions were aimed at providing the minimum mass solution to meet the overall performance requirements of the project

**3.1 Ultimate Factor Reduction**

Previous aircraft designed by the each of the four Partner Companies have generally adopted an Ultimate/Load Limit factor of 1.5, in line with requirements such as the US Mil-Spec and the UK Def-Stan. In part this derives from the

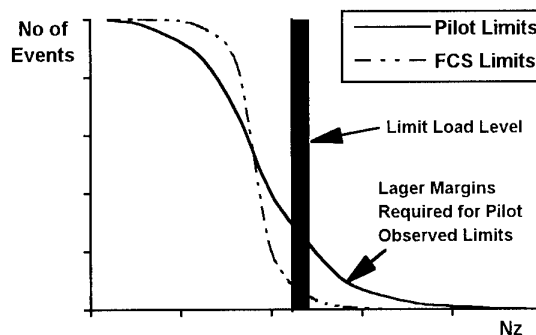
structural performance of conventional materials, where it is conceded that although plastic deformation may occur beyond Limit Load, no failure should occur up to Ultimate Load Levels. Over the years, this factor has gained credibility simply because aircraft designed to it have exhibited satisfactory structural performance, under both static and fatigue loading conditions.

To save mass on Eurofighter, it was decided that for those areas of the structure where the Loads were controlled in some manner by an Aircraft System, the Ultimate Factor could be relaxed to 1.4. In particular, this was to be applied to general manoeuvre loads, as the Flight Control System will provide Carefree Manoeuvring, with automatic Load protection during extreme manoeuvres.

This decision is supported structurally by the extensive use of composite materials in the airframe construction. As such materials generally exhibit linear characteristics almost up to failure, it becomes safe to reduce the margin between Limit and Ultimate levels without undue concern over premature deformation of the airframe.

The use of the FCS to provide automatic Load Limiting ensures that when extreme manoeuvres are flown, Limit Load levels may be achieved more frequently, but will be exceeded only rarely. Figure 3 illustrates the expected situation.

Figure 3. Effect of FCS On Load Criticalities



### 3.2 Design to 90% Loads

Design Loads produced early in a project life are subject to many assumptions to ensure they adequately cover the eventual manoeuvre demands of the aircraft. Arbitrary increasing of Design Loads to cover uncertainties is not generally performed, however it is inevitable that when early Design Loads are produced, they contain a significant degree of conservatism. Once the structure has been designed to these loads, it becomes very difficult to subsequently remove any mass added due to this conservatism.

To achieve the minimum possible mass, it was therefore decided to design the airframe to just 90% of the Design Loads. The philosophy then applied was that during subsequent Check Stress work, when the Loads could be more accurately defined, the Structure would be re-checked and it was anticipated that in many cases sufficient strength would be demonstrated, despite only designing to 90% of the original loads. For those areas where a short-fall in strength remained, repairs would be required, but as these would target only the essential areas, an overall lower mass was expected than would be achieved with a conventional design philosophy.

### 3.3 Reduced Parameter Envelopes

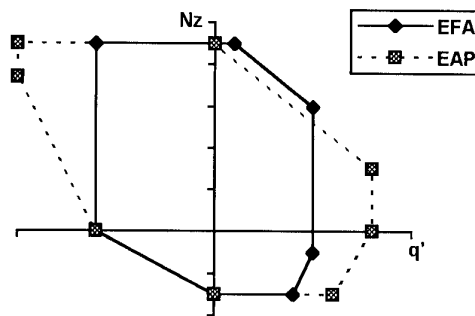
The Eurofighter aircraft is an agile air superiority design, therefore it must demonstrate significant agility under a wide range of manoeuvre conditions. Early in the project however, some investigations were conducted into exactly how the various manoeuvre parameters may be required to be combined to meet these agility requirements.

The starting point for this assessment was the UK Experimental Aircraft Programme (EAP). The EAP Demonstrator was intended to bring together and demonstrate the maturity of a number of new technologies that would be required by the next generation of agile combat aircraft. In particular, the aircraft featured a similar delta-canard configuration to Eurofighter, and possessed a reasonably mature Flight Control System. It was therefore possible to assess through flight simulation the manoeuvre combinations achievable with a mature FCS, and compare these against the parameters used for the original design. This demonstrated that significant reductions in the design parameter envelopes could be achieved whilst still achieving the required agility. As the EAP demonstrator represented the first attempt within the four Eurofighter partners to produce a highly agile delta-canard configuration, this was not unexpected. The experience gained with the EAP structural and FCS designs therefore permitted the Design parameters for Eurofighter to be better optimised, thus avoiding excessive Design Loads, and hence undesirable mass penalties. Figure 4 shows for example a comparison of the required normal and pitch accelerations for design of the EAP and Eurofighter airframes, illustrating the magnitude of the reductions. Despite these reductions, the EAP study demonstrated that the required aircraft manoeuvrability would still be achieved, and with the saving in mass, the agility of the aircraft could actually be enhanced.

### 3.4 Project Loading Phases

The cycle of loads activities on the EF2000 project have been divided into a series of phases, categorised by the source of loading information used at each stage.

Figure 4. Comparison of EAP and EFA Design Parameters



At the very earliest stages of the project, preliminary loads are issued for sizing and lay-out purposes. These are based on empirical calculations or previous experience on other projects, and are not generally sourced from a single loading model.

Once the basic aircraft lay-out and control sizes are defined, it is possible to construct a Loads Model to describe the loading contributions of aircraft attitude and control deflections. On Eurofighter, two standards of semi-empirical Loads Model were constructed. The Phase 0 Model was used for the issue of Design Loads for the detailed design of the airframe structure. Subsequently, a refined Phase 1 Model was constructed and used for the issue of Check Stress Loads. The Check Stress Loads were required to assess the capability of the Structure against a more accurate set of loads, and thereby to identify any necessary repairs prior to flight of the Prototype Aircraft, in line with the philosophy of a design to 90% loads. In addition, the Check Stress loads were used to define the Ground Test load cases, and to provide Allowable Loads describing the airframe strength for use by Loads engineers in subsequent Flight Clearance assessments. Both the Design and Check Stress loads were developed without specific reference to the FCS Control Laws and therefore required similar assumptions regarding control usage.

The Phase 0 and Phase 1 Loads Models were linear in nature, being based on theoretical Computational Fluid Dynamic calculations. This was considered adequate as Design Loads generally arise at high-speed conditions where the aerodynamics remain within the linear regime. Adjustment of the theoretical CFD data was however performed to account for known Wind Tunnel results, with the most precise matching being performed for the Phase 1 Loads Model in a two stage process:-

- 1) Extensive pressure and loading distribution data was available from EAP Pressure Plot testing. CFD calculations were performed for the EAP configuration and compared with this Wind Tunnel database. Where necessary, adjustments to the shape of the theoretical pressure distributions were defined to provide a better match to the Wind Tunnel data. These adjustments were then applied to the theoretical results for the Eurofighter configuration.
- 2) At the time of the Phase 1 Loads Model, a significant amount of 6-component Wind Tunnel data was available for



the Eurofighter configuration. This data was used to scale the magnitude of the theoretical pressures after they had been adjusted to the appropriate distribution using the EAP data. This two-stage matching therefore aimed to ensure that both the shape and magnitude of the pressure and load distributions were representative of all relevant Wind Tunnel sourced data.

After the Check Stress loads were issued, a further Phase 2 Loads Model was constructed by performing Pressure Plot testing of a definitive Eurofighter Wind Tunnel model. Due to the cost and complexity of the model, it could not be designed and tested until after the final lines freeze for the airframe, and as a result was aimed at feeding into the Flight Clearance stage of the project. The Phase 2 Loads Model provides a full non-linear description of the aircraft loading, which is highly desirable as it permits flight clearances to take advantage of any non-linear relief present at high Angle of Attack conditions, thereby increasing the clearances in less critical regions of the flight envelope. At the clearance stage, the Phase 2 Loads Model is used to calculate component loading based on definitive aircraft manoeuvres generated using an FCS and Aerodynamic model of the aircraft.

The overall Loads philosophy for Eurofighter can therefore be summarised as a continuous refinement process, using increasingly complex loading models and progressing from assumed parameter envelopes during design to actual aircraft responses for flight clearance work. The following sections first discuss the parameter envelopes of the Structural Design Criteria and their method of application, and then goes on to review areas of over or under prediction based on the current understanding of the Flight Control Laws.

#### 4. STRUCTURAL DESIGN CRITERIA AND DESIGN LOADS

The Structural Design Criteria for EF2000 aims to capture in a single document all the assumptions required for the definition of Design Loads. A major portion of the document concerns itself with the requirements for manoeuvring flight. However, for a comprehensive design, additional assumptions relevant to local areas of the airframe are also considered. Therefore requirements for such loading actions as Ground Loads, Engine Surge Pressures and Gun-firing effects etc. are also defined, along with Aeroelastic stiffness and Flutter requirements.

The following sections concentrate on the Static manoeuvre loading aspects of the criteria, as these have the main bearing on the interface with the FCS design. Various aspects of the Design Criteria and their application are discussed, along with the manner in which they influence the airframe loads.

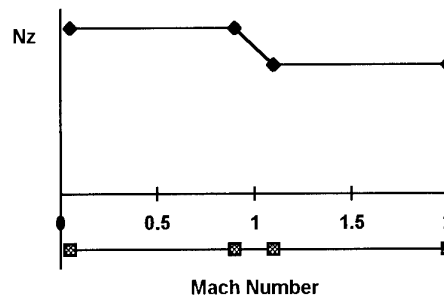
##### 4.1 Normal Acceleration Requirements and Wing Loads

Wing Shear and Bending Loads are primarily a function of normal acceleration and aircraft mass, whilst Wing Torque effects are maximised by roll conditions due to the use of trailing edge flaperons for roll control.

Figure 5 shows the normal acceleration requirements of the Design Criteria as a function of Mach Number. The sharp reduction in required normal acceleration at transonic Mach Numbers makes identification of critical wing Shear and

Bending cases relatively easy. The wing spanwise centre of lift generally moves outboard transonically, therefore Bending is maximised at the highest transonic Mach Number at which maximum normal acceleration is still maintained.

**Figure 5. Normal Acceleration Requirements**



The normal-g requirements are defined as a function of aircraft mass, with the maximum normal-g requirement applying up to a specified mass (denoted as the Basic Flight Design Mass or BFDM), and with constant NzW scaling applied to masses above this level. This scaling applies for all Air-to-Air Store configurations, regardless of the specific configuration details. Thus the external Aerodynamic wing loads are maintained at a constant level for the heavy aircraft masses that can arise, particularly when external fuel tanks are carried. Maximum Wing Bending cases therefore occur for transonic flight conditions, for masses at or above the BFDM.

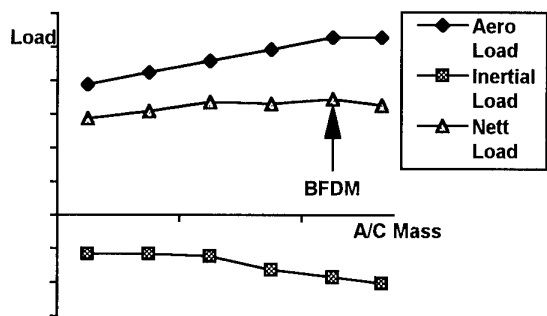
The detail of the critical store configuration depends on the wing inertial relief. The BFDM can be achieved by a variety of external store configurations simply by adjusting the internal fuel load to restore the required total mass. As the wings on EF2000 are used as fuel tanks, this fuel adjustment affects the wing mass, and hence the wing inertial loads. The critical nett wing loading cases therefore arise for BFDM cases with the lightest possible wing mass - i.e. the configuration with the maximum Under-fuselage store load with no under-wing stores. If additional fuel is added to increase the mass above the BFDM, the Aerodynamic lift remains constant, but the wing inertial relief increases, thus reducing nett wing loads. If on the other hand, fuel is removed from the BFDM, the Aerodynamic lift reduces more rapidly than the reduction in inertial relief, therefore the nett wing loads again reduce.

The trade-off between Aerodynamic and Inertial loading is illustrated in Figure 6, where it can be seen that although the nett wing loads are maximised at the BFDM case, they are held almost constant across a wide range of aircraft masses. The fuel sequence has been carefully tailored to offset the increase in Aerodynamic lift as mass increases to ensure that the aircraft is not overly optimised against a single critical design point.

##### 4.2 Roll Rate and Acceleration Requirements

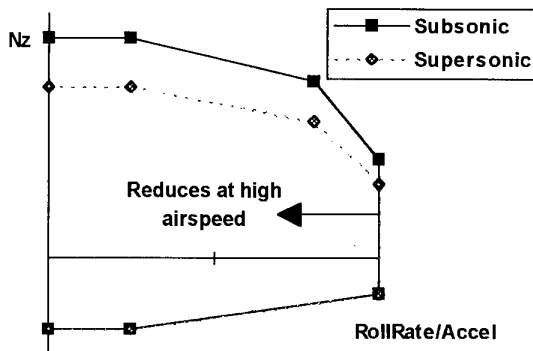
Wing torque loading is primarily produced by rapid roll manoeuvres, due to the use of wing trailing edge flaperons

Figure 6. Variation of Wing Load



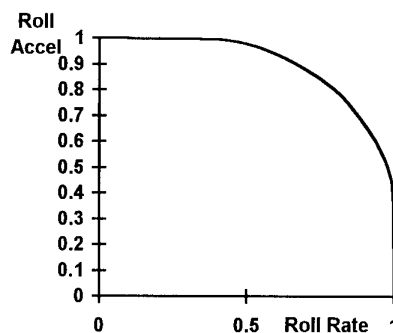
for roll control. Figure 7 shows the shape of the Design Criteria Nz/roll rate envelope. Maximum roll rates are only achieved within a limited Nz range, and are reduced significantly as maximum Nz is approached, though the aircraft is required to maintain 80% of its roll capability at up to 80% of its maximum normal acceleration. Note that some small degree of Roll capability (25%) is always maintained under all normal acceleration conditions and therefore roll manoeuvres at extreme positive and negative normal acceleration levels will slightly increase the wing Shear and Bending loads above those of steady trim conditions discussed above. Roll acceleration requirements follow exactly the same shape of relationship as the roll rate term. This is sensible as the FCS controls the application of differential flap for rolling such that it initially applies the correct amount of flap to achieve the desired roll rate under steady rolling conditions. The resulting roll acceleration produced by this differential flap is therefore directly proportional to the demanded roll rate.

Figure 7. Roll Rate/Acceleration vs Normal-g



To avoid simultaneous application of maximum Rate and Acceleration terms, the Design Criteria defines a weighting function for combining these terms, as shown in Figure 8. This illustrates that for design purposes, maximum roll rate is to be combined simultaneously with up to 40% of maximum roll acceleration. This implies a severe requirement as no further acceleration should be possible once the maximum rate is achieved, however this apparently severe combination is necessary to adequately cover the dynamic interchange between rates and

Figure 8. Roll Rate/Acceleration Combinations



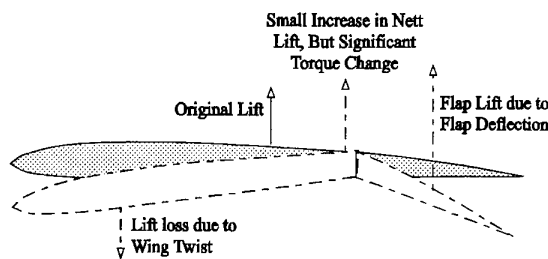
accelerations that may arise during agile roll reversal manoeuvres.

4.3 Trim Assumptions for Rolling Manoeuvres

The Design Criteria envelopes fully specify the manoeuvre requirements for rolling, however as the flaperons are used for both roll and pitch control, certain assumptions must be made about how these differing control requirements may be combined within the FCS Control Laws.

Flap strength and actuator requirements are fairly readily deduced purely from the roll requirements. Loads acting on the flaps are maximised at supersonic flight conditions, as only in supersonic flow can large differential pressures be maintained at the rear of the wing. At high speed conditions, wing aeroelastic effects become important, and deflection of the flaps results largely in inducing wing twist, with little overall lift change. Roll requirements are therefore significantly relaxed at such high speed flight conditions, but even though the required rates are low, very large flap deflections are required to overcome the wing twist losses, and hence induce sufficient differential lift to achieve even the fairly low roll requirements. Although the nett wing lift is little changed, large loads are carried locally by the flaps, giving rise to the Flap design cases, as shown in Figure 9.

Figure 9. Lift Distribution During High Speed Rolling



Flap actuator sizing requirements are based around achieving the required high speed supersonic roll performance within 70% of the Dual Hydraulic System capability. This retains a proportion of the actuator capability for trim and other pitch control functions.

The above roll conditions give rise to large wing torque

loads, as indicated in Figure 9, but may not maximise the wing torque, as even more severe conditions can arise subsonically. At subsonic conditions, the additional wing loading due to roll is not carried directly by the flaps, but flap deflection still generates significant wing torque by changing the pressure distribution across the wing chord. Since the roll rate and normal-g requirements are maintained at a higher level subsonically, overall wing torques tend to be maximised at subsonic flow conditions, even though the flaps themselves may be fairly lightly loaded.

At subsonic flight conditions, the aircraft is longitudinally unstable. It is therefore essential to ensure that all manoeuvre conditions can be achieved within the capability of a Single Hydraulic System. If this were not the case, failure of one Hydraulic System could lead to an unstable condition leading to catastrophic loss of the aircraft. In practice, all manoeuvres are maintained within 70% of Single System to provide a further margin of safety.

Having sized the flap actuators for the supersonic roll conditions, the Single System requirement dictates the maximum flap load that may be carried subsonically. This may be used in the definition of assumptions about splitting flap responsibilities between trim and roll control to define wing design cases. The flaps on one wing can be fixed to give the maximum permitted subsonic Hinge Moment (respecting the 70% of Single System rule). This immediately provides the maximum wing torque case, but further checks of the other controls must be performed to investigate the legitimacy of the case. The flaps on the opposite wing can be deflected in the opposite sense to achieve the maximum allowable roll rate or acceleration condition. This combination of flaps will imply a certain level of pitch response on the aircraft, which must be adjusted by using the Foreplane to maintain the pitch response within the permissible combinations of the Design Criteria. In establishing an acceptable pitch manoeuvre, it is assumed that the pitch authority will be shared between the flaps and Foreplane, and that no more than 70% of the authority will be assigned to each individual surface. Furthermore, maximum permissible foreplane loads must also be respected, as discussed in Section 4.5 below. This limits the scope for simply applying more foreplane angle to balance the pitch induced by the flap deflections.

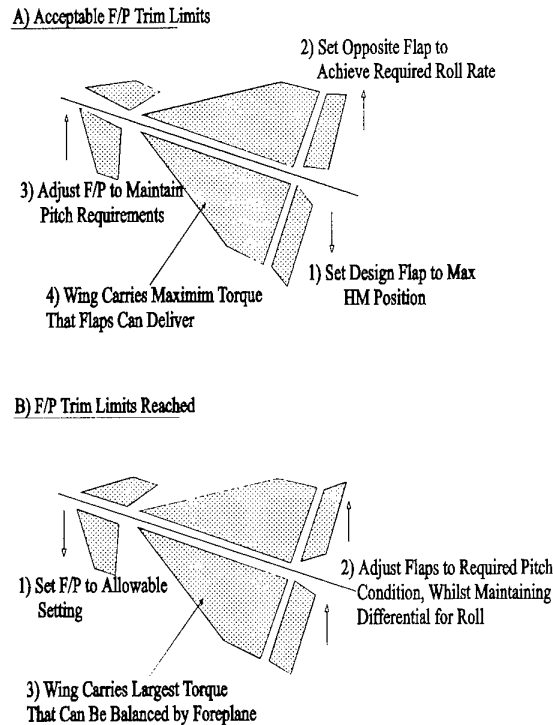
In the above process, if the limits on foreplane pitch control are reached, the mean flap deflections on both wings must be adjusted to return to a legitimate pitch response. This will reduce the flap setting on the original design wing, thus leading to lower torque levels than originally sought. This is acceptable, as the case still represents the maximum wing torque condition that the Flight Control System is likely to be capable of sustaining. This process allows maximum wing torque cases to be defined without detailed attention being paid to exact trim schedules, and arrives at an implied split between roll and pitch responsibilities for the flaps by considering the balancing capability of all of the control surfaces. This process is illustrated in Figure 10.

**4.4 Fin Design Loads**

The Design Criteria specifies the allowable sideslip during manoeuvres in terms of a constant  $q\beta$  (sideslip times Dynamic Pressure) product. This is basically derived from the magnitude of sideslip resulting from the design lateral

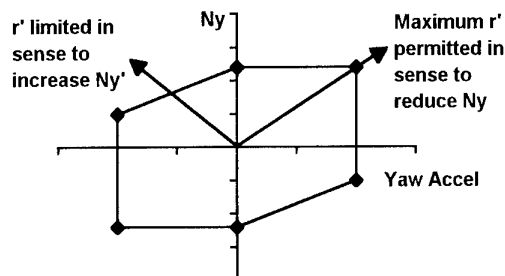
gust case, on the assumption that designing to this level to cater for the gust effect gives adequate capability for all expected manoeuvres. During roll manoeuvres for example, the FCS will aim to limit sideslip by introducing a rudder input to co-ordinate the yawing moment produced by differential flaps. However, although the design criterion may be scaled from the gust requirement, fin design loads are maximised by careful balancing of Aerodynamic and Inertial loads.

**Figure 10. Flap Settings for Wing Torque Design Cases**



Given that the maximum  $q\beta$  is fixed by the requirements, additional fin side-load can only be generated if rudder inputs are permitted to be superimposed. During a Steady-Heading Sideslip manoeuvre, the rudder is used to balance the sideslip load, and relatively low nett fin loads result. However if a rapid reversal of the rudder is then made, both the sideslip and rudder terms become additive. The Design Criteria envelope of interest is the combination of Lateral acceleration and yaw acceleration, shown in Figure 11. This demonstrates that superposition of maximum positive yaw acceleration is permitted in combination with the full level of lateral acceleration permitted within the  $q\beta$  requirement.

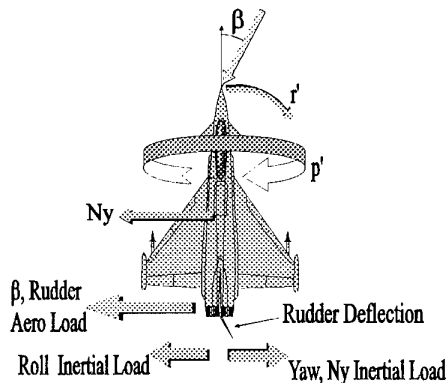
**Figure 11. Combination of Lateral and Yaw Accelerations**



The introduction of a rudder induced yaw acceleration still does not produce the fin design case, as the inertial loads created by the yaw and lateral accelerations both oppose the aerodynamic loads. The inertial loads can be reduced to almost zero if an appropriate roll acceleration is also introduced, as this may be set to counteract the inertial loads arising from the yaw and lateral acceleration. This combination of roll and yaw accelerations may at first appear unlikely, however during rolling manoeuvres at high-g, the aircraft must perform a coning motion about the Stability axes to control sideslip. To initiate such a roll requires simultaneous input of roll and yaw accelerations, as identified for the Fin Design case.

Figure 12 shows the combination of terms involved in the Fin design case, illustrating the complexity of the manoeuvre required to maximise the fin loads.

**Figure 12. Loading Assumptions for Fin Design Case**



#### 4.5 Foreplane Design Loads

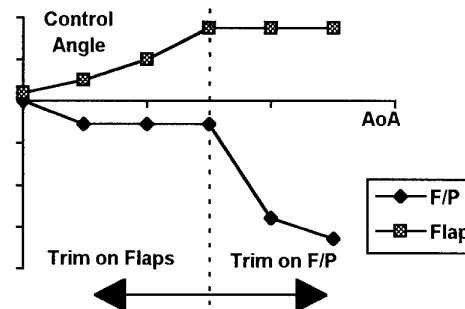
Similar to the fin situation, the Front Fuselage design cases are produced only by careful balancing of several counteracting effects. Due to the presence of the foreplane, the Front Fuselage achieves a close balance between Aerodynamic lift and Inertial down-load under many flight conditions. Significant loads at the Centre Fuselage interface only arise very transiently during manoeuvre initiation or termination, when the natural balance of the Front Fuselage loading is upset by control surface demands.

As the primary loading action on the Front Fuselage is the Foreplane, down-bending load cases are therefore produced by applying the maximum possible foreplane down-load, then adjusting the other loading effects to add to this action, or at least to minimise their relief. To define the Front Fuselage loads, it is therefore necessary first to define the Foreplane load carrying capability.

The Foreplane loading is intimately bound up with assumptions regarding trim scheduling. As the aircraft is longitudinally unstable subsonically, additional nose-down pitch is required to be generated to trim the aircraft as Angle of Attack increases. This nose-down moment could be generated by the flaps, foreplane, or a combination of both, therefore to provide a unique solution, the foreplane is driven by an Angle of Attack related trim schedule, whilst the flaps adopt whatever setting is required to trim out any residual moment. Once the flaps achieve their limit of

allowed travel, then they are fixed, and the foreplane is free to perform the trim function. Examples of the resulting control settings are shown in Figure 13.

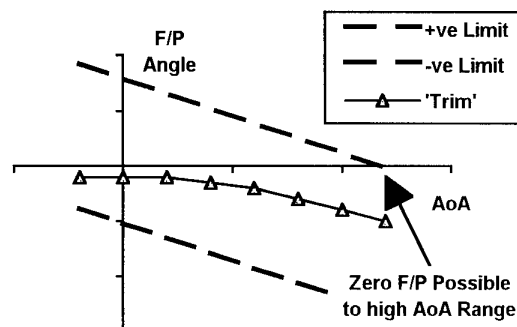
**Figure 13. Flap and Foreplane Subsonic Trim Settings**



The choice of schedule for the foreplane over the initial Angle of Attack range is dictated by balancing Performance and Stability and Control considerations. To minimise Lift Induced Drag, it is necessary to increase the wing camber by introducing positive down flap settings as Angle of Attack increases. As seen from Figure 13, this is automatically achieved by limiting the amount of trim control assigned to the Foreplane and allowing the unstable nature of the configuration to demand down flap to trim. The drag benefits could be further enhanced by scheduling up-foreplane, as then the flap demand would apply much more quickly. However in this case, the available flap deflections for trim would quickly become saturated, reducing the available flap control for rolling.

Since the detailed drag/control trade-off is unlikely to be exactly defined when Design Loads are required, the Foreplane load capability should be set such that it does not place further undue constraints on the selection of the schedule. At high-g conditions, positive foreplane settings are unlikely to be practical due to the flap saturation concerns noted above. However negative foreplane settings will reduce the required flap setting, hence increasing induced drag. Prior to a detailed trade-off study, it is sensible to assume that the final schedules may require zero foreplane setting to be maintained up to high-g, at least at high speed conditions, therefore the foreplane design load

**Figure 14. Foreplane Load Boundaries**



should be defined to permit this possibility. Once the critical design point and required load capability is defined, a permissible corridor of Foreplane settings can be defined across the Angle of Attack range, as shown in Figure 14. The final optimised Foreplane trim schedule can be placed anywhere within this corridor, ideally close to the centre to maximise the foreplane deflection available for pitch control. This may however become slightly compromised to achieve the optimum drag solution.

**4.6 Front Fuselage Design Cases**

Having sized the Foreplane Spigot loads to cope with a variety of possible trim schedules, the Front Fuselage loads can now be deduced. The main Down-Bending load conditions on the Front Fuselage are provided by applying the maximum permissible F/P Down-Load, then adjusting the other Aerodynamic and Inertial parameters. The primary parameter envelope is the permissible combinations of normal and pitch accelerations, which is defined in the Design Criteria as shown in Figure 15.

**Figure 15. Normal and Pitch Acceleration Combinations**

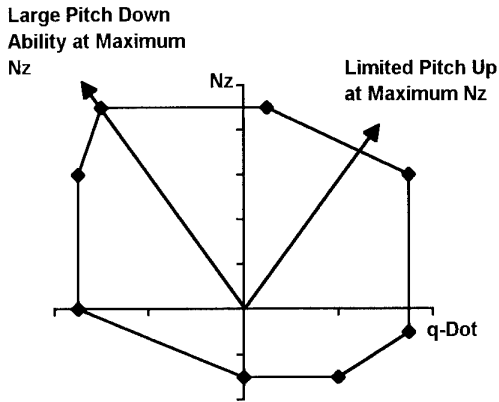


Figure 15 shows that simultaneous combination of maximum pitch and normal accelerations is disallowed by the Design Criteria. Clearly it is sensible that no pitch up can be permitted if the aircraft is already at its maximum normal acceleration level, however a small cut-off is also present in conditions involving pitch down from maximum acceleration. This provides a small level of protection against accidental increase in normal acceleration when the flaps are used to initiate the pitch down manoeuvre, but in reality the consequences of this cut-off are minor.

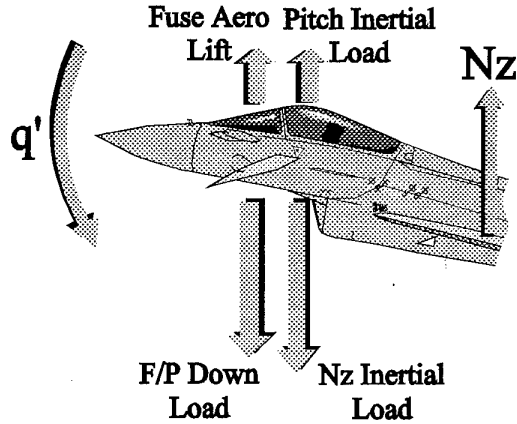
The Front Fuselage Down Bending case can now simply be set up by combining maximum Foreplane down-load with the maximum permissible Normal-acceleration to maximise both the Aerodynamic and Inertial down-forces. The presence of a large Foreplane down-load inevitably leads to a significant pitch acceleration, which acts to reduce the Inertial down-load, but this is a small penalty compared with the Aerodynamic foreplane load. Aerodynamic lift on the fuselage also acts to slightly reduce the nett Down-Bending loads. The balance of forces is shown in Figure 16.

**5. RESULTS FROM FLIGHT CLEARANCES**

The preceding sections outline some important assumptions involved in the definition of design loads for the

Eurofighter aircraft, and show how the parameter envelopes

**Figure 16. Balance of Forces for Front Fuselage**



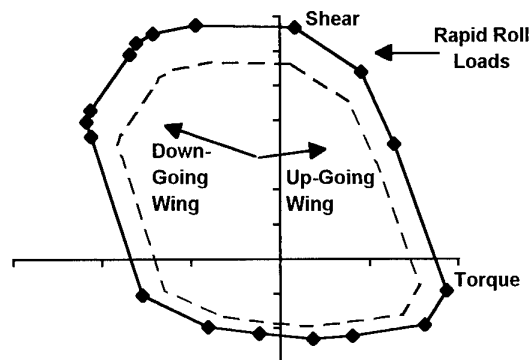
of the Structural Design Criteria were used to arrive at critical load cases for some of the primary component loads. Following Check Stress of these load cases, the proven strength of the airframe has been reported back to the Loads Engineers in the form of Allowable Load Envelopes (ALE's) for the various airframe Monitor Stations.

As the Flight Clearance phase is now in full progress, it is possible to review some of these Allowable Loads envelopes resulting from the Design assumptions outlined above. This will demonstrate whether the overall design process has resulted in envelopes that are too large, too small or about right once manoeuvres produced by a definitive FCS standard are considered. The latest standard of FCS (designated Phase2A) has been designed to respect 84% manoeuvre envelopes, therefore loads during critical manoeuvres would be expected to lie close to this percentage of the Allowable Loads.

**5.1 Wing Root Loads during Roll Manoeuvres**

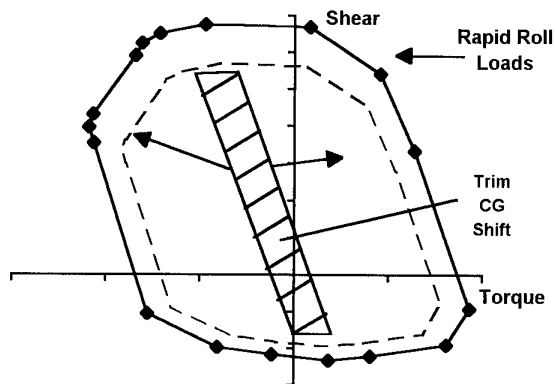
Figure 17 illustrates the typical Wing Root loading produced by roll manoeuvres at moderate-g, generating maximum conditions of roll rates and accelerations. It can be seen that the Allowable Load envelope, even when scaled to 84%, is easily sufficient to cover the full Torque range experienced on both wings. At first sight this implies that the assumptions regarding flap usage during rolling

**Figure 17. Wing Root Loads During Rolling**



may have been pessimistic, resulting in an over-definition of the Design Loads. However, for the current FCS standard, the cg of the prototype aircraft has been ballasted some 2% forward of the Design requirement. For the Production aircraft cg, the wing torque at trim will therefore shift further aft, resulting in torque requirements much closer to the ALE boundary during rolling, as shown in Figure 18.

**Figure 18. Effect of CG Range on Rolling Loads**



From Figure 18, a significant margin clearly remains at the positive torque boundary, however this is essential to cater for some of the forward cg store configurations that the aircraft will be required to fly with. The design philosophy has therefore resulted in a wing torque capability which appears adequate, but is in no way excessive when the various configuration requirements and resulting cg ranges are considered.

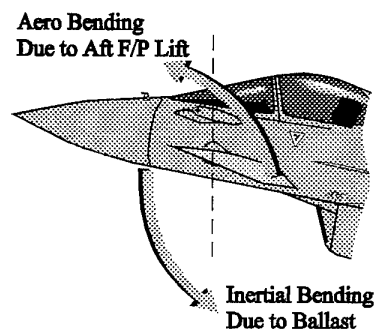
### 5.3 Front Fuselage Manoeuvre Loads

During clearance manoeuvres assessed to date, Front Fuselage loads have shown only small loading criticalities at the major build joint. As explained above, Front Fuselage loads are a fine balance between Aerodynamic loads acting on the Foreplanes, and inertial loads due to the fuselage mass. The Design cases were generated by applying the full Foreplane down-load during a pitch down from high-g. The current FCS Control Laws utilise both flaps and foreplane to initiate such pitch manoeuvres, with the foreplane providing only 40% of the control input.

As a result, significant foreplane loads have not been seen to date, and consequently the Front Fuselage loads have also remained small. This implies that the design assumptions on foreplane usage may have been pessimistic compared with realistic FCS designs.

Despite the above, significant fuselage loading conditions have been seen locally at the Foreplane Attachment Frame. As explained above, the Prototype aircraft have been ballasted to a forward cg location. This ballast mass has been added to the front fuselage forward of the foreplane and generates significant local inertial loads. At supersonic flight conditions the foreplane lift moves behind the spigot attachment, resulting in a Down-Bending action which combines with the Ballast loads to generate a Bending couple about the Foreplane Attachment frame, as shown in Figure 19. This illustrates that localised configuration changes can give rise to loading conditions not fully covered

**Figure 19. Combination of Ballast and Foreplane Loads**

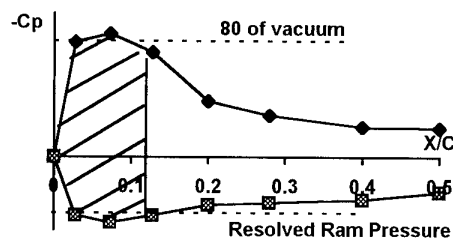


by the Design assumptions, and it is therefore dangerous to be too specific in the configurations and assumptions permitted at the design stage.

### 5.5 Leading Edge Loads

On a highly agile aircraft, the Wing Leading Edges will experience pressure conditions close to the physical maximum. Design Loads for such components can often be defined by considering 80% of vacuum acting over the upper surface, and a ram pressure resolved for the Leading Edge sweep angle acting on the lower surface, as shown in Figure 20.

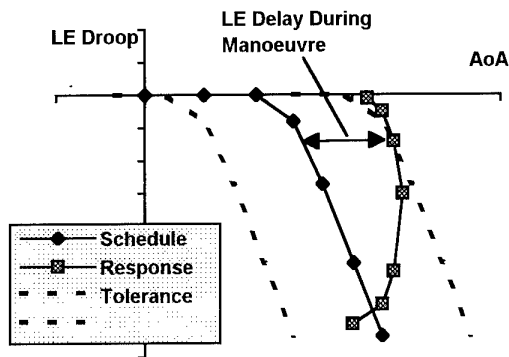
**Figure 20. Pressure Distribution for Leading Edge Design Loads**



On Eurofighter, the Leading Edge is scheduled to droop with Angle of Attack to optimise the wing drag characteristics, an action which tends to off-load the Leading Edge devices at high-g conditions. The assumptions regarding physical maxima therefore led to excessive loads, which gave problems for design of the actuation system. The alternative approach adopted was to produce Design Loads based on the drag optimisation schedule, with a tolerance to cater for the lags in the deflection of the Leading Edge during rapid pitch manoeuvres. As this approach depended on the precise relationship between loading due to Angle of Attack and Leading Edge deflection, it was sensitive to the loading terms contained within the Loads Models.

Recent clearance work with the Phase 2 Loads Model has shown higher than expected Leading Edge loads at high transonic Mach numbers. These are maximised during

**Figure 21. LE Deflections During Pitch Manoeuvres**



rapid pitch manoeuvres, when the Leading Edge can lag some way behind the optimised schedule as shown in Figure 21, however this effect was catered for during the Leading Edge design stage. The principal reason for the high loading arises due to differences between the Phase 1 Design Loads Model, and the wind tunnel based Phase 2 Loads Model used for clearances. Despite the careful adjustments to correlate the Phase 1 Loads Model to overall 6-component wind tunnel data, the Leading Edge loads remained very much lower than seen in the definitive Eurofighter pressure plot wind tunnel tests.

For future clearances, a re-appraisal of the allowable strength of the Leading Edges is under way to resolve this concern. This particular case however highlights that when the Design Loads are tailored too closely to expected manoeuvre conditions, some problems may result due to change later in the project. In this instance, the tolerances considered within the Design Loads were just adequate to cater for the delays in the motion of the Leading Edge device, but proved insufficient to cover the additional Loads Model changes.

## 6. CONCLUSIONS

This paper has discussed some of the loading issues related to Eurofighter 2000 Design Loads, and explained how manoeuvre parameter envelopes contained in the Design Criteria have been employed. In particular it is noted that various assumptions have had to be made to cater for uncertainty in the precise manner in which the final Flight Control System will utilise the controls to achieve the required manoeuvres.

A brief comparison with some results from Flight Clearance work has shown the design assumptions have generally not led to excessive loads when compared with realistic Control System demands for most of the major component loads. However in some localised instances, subsequent changes to the Loading data or aircraft configuration have led to cases where the loads have been higher than anticipated, resulting in further work being required to provide adequate flight clearances. This highlights the attention to detail that is required to ensure that the design assumptions adequately cover all regions of the airframe and to provide a robust design capable of accommodating change.

The project is now well into the Flight Test phase, with three aircraft currently flying, and the remaining four prototypes expected to join the Test Programme within the next few months. After the initial envelope expansion work has been completed, it is intended to perform an extensive flight pressure survey to validate the Phase 2 Loads Model used for flight clearances. Following validation, this Model will be used to provide clearance for the final FCS Control Laws standard for Prototype Testing, and subsequently to provide Service Release clearances for the Production aircraft. Full confirmation of the adequacy of the design parameters contained in the Structural Design Criteria can therefore only finally be given when the production manoeuvres which the Eurofighter aircraft will be required to perform.

## 7. ACKNOWLEDGEMENTS

The Eurofighter Loads programme is a four-partner company responsibility, therefore the author wishes to acknowledge the contributions made by ALN, CASA and DASA to aspects of the loads philosophy reported within this paper.

Work performed by BAe on the Eurofighter loading programme has been carried out with the support of the Procurement Executive, Ministry of Defence.

## REPORT DOCUMENTATION PAGE

<b>1. Recipient's Reference</b>	<b>2. Originator's Reference</b>  AGARD-R-815	<b>3. Further Reference</b>  ISBN 92-836-0037-1	<b>4. Security Classification of Document</b>  UNCLASSIFIED/ UNLIMITED
<b>5. Originator</b> Advisory Group for Aerospace Research and Development North Atlantic Treaty Organization 7 rue Ancelle, 92200 Neuilly-sur-Seine, France			
<b>6. Title</b>  Loads and Requirements for Military Aircraft			
<b>7. Presented at/sponsored by</b>  The 83rd Meeting of the AGARD Structures and Materials Panel, held in Florence, Italy, 4-5 September 1996			
<b>8. Author(s)/Editor(s)</b>  Multiple			<b>9. Date</b>  February 1997
<b>10. Author's/Editor's Address</b>  Multiple			<b>11. Pages</b>  176
<b>12. Distribution Statement</b> There are no restrictions on the distribution of this document. Information about the availability of this and other AGARD unclassified publications is given on the back cover.			
<b>13. Keywords/Descriptors</b>			
Military aircraft Loads (forces) Flight loads Aviation safety Design Structural analysis Buffeting		Stochastic processes Gust loads Fatigue life Flight control Thrust vector control Tolerances (mechanics)	
<b>14. Abstract</b>			
<p>Since the beginning of aircraft design and certification, the loads and the loads-related requirements have continued to evolve, while initial conservative assumptions related to safety factors have remained essentially the same over the years.</p> <p>With the increased use of technologies such as Electronic Flight Control Systems (EFCS) and thrust vectoring systems, and the improved quantification of factors influencing the loads, the initial concept of safety factors needed to be re-visited.</p> <p>It was concluded in the Workshop that new criteria and methods should be investigated in order to propose standards for future aircraft design.</p>			



Aucun stock de publications n'a existé à AGARD. A partir de 1993, AGARD détiendra un stock limité des publications associées aux cycles de conférences et cours spéciaux ainsi que les AGARDographies et les rapports des groupes de travail, organisés et publiés à partir de 1993 inclus. Les demandes de renseignements doivent être adressées à AGARD par lettre ou par fax à l'adresse indiquée ci-dessus. *Veillez ne pas téléphoner.* La diffusion initiale de toutes les publications de l'AGARD est effectuée auprès des pays membres de l'OTAN par l'intermédiaire des centres de distribution nationaux indiqués ci-dessous. Des exemplaires supplémentaires peuvent parfois être obtenus auprès de ces centres (à l'exception des Etats-Unis). Si vous souhaitez recevoir toutes les publications de l'AGARD, ou simplement celles qui concernent certains Panels, vous pouvez demander à être inclu sur la liste d'envoi de l'un de ces centres. Les publications de l'AGARD sont en vente auprès des agences indiquées ci-dessous, sous forme de photocopie ou de microfiche.

CENTRES DE DIFFUSION NATIONAUX

## ALLEMAGNE

Fachinformationszentrum Karlsruhe  
D-76344 Eggenstein-Leopoldshafen 2

## BELGIQUE

Coordonnateur AGARD-VSL  
Etat-major de la Force aérienne  
Quartier Reine Elisabeth  
Rue d'Evere, 1140 Bruxelles

## CANADA

Directeur - Gestion de l'information  
(Recherche et développement) - DRDGI 3  
Ministère de la Défense nationale  
Ottawa, Ontario K1A 0K2

## DANEMARK

Danish Defence Research Establishment  
Ryvangs Allé 1  
P.O. Box 2715  
DK-2100 Copenhagen Ø

## ESPAGNE

INTA (AGARD Publications)  
Carretera de Torrejón a Ajalvir, Pk.4  
28850 Torrejón de Ardoz - Madrid

## ETATS-UNIS

NASA Goddard Space Flight Center  
Code 230  
Greenbelt, Maryland 20771

## FRANCE

O.N.E.R.A. (Direction)  
29, Avenue de la Division Leclerc  
92322 Châtillon Cedex

## GRECE

Hellenic Air Force  
Air War College  
Scientific and Technical Library  
Dekelia Air Force Base  
Dekelia, Athens TGA 1010

## ISLANDE

Director of Aviation  
c/o Flugrad  
Reykjavik

## ITALIE

Aeronautica Militare  
Ufficio del Delegato Nazionale all'AGARD  
Aeroporto Pratica di Mare  
00040 Pomezia (Roma)

## LUXEMBOURG

Voir Belgique

## NORVEGE

Norwegian Defence Research Establishment  
Attn: Biblioteket  
P.O. Box 25  
N-2007 Kjeller

## PAYS-BAS

Netherlands Delegation to AGARD  
National Aerospace Laboratory NLR  
P.O. Box 90502  
1006 BM Amsterdam

## PORTUGAL

Estado Maior da Força Aérea  
SDFa - Centro de Documentação  
Alfragide  
2700 Amadora

## ROYAUME-UNI

Defence Research Information Centre  
Kentigern House  
65 Brown Street  
Glasgow G2 8EX

## TURQUIE

Millî Savunma Başkanlığı (MSB)  
ARGE Dairesi Başkanlığı (MSB)  
06650 Bakanlıklar-Ankara

**Le centre de distribution national des Etats-Unis ne détient PAS de stocks des publications de l'AGARD.**

D'éventuelles demandes de photocopies doivent être formulées directement auprès du NASA Center for Aerospace Information (CASI) à l'adresse ci-dessous. Toute notification de changement d'adresse doit être fait également auprès de CASI.

AGENCES DE VENTE

NASA Center for Aerospace Information  
(CASI)  
800 Elkridge Landing Road  
Linthicum Heights, MD 21090-2934  
Etats-Unis

The British Library  
Document Supply Division  
Boston Spa, Wetherby  
West Yorkshire LS23 7BQ  
Royaume-Uni

Les demandes de microfiches ou de photocopies de documents AGARD (y compris les demandes faites auprès du CASI) doivent comporter la dénomination AGARD, ainsi que le numéro de série d'AGARD (par exemple AGARD-AG-315). Des informations analogues, telles que le titre et la date de publication sont souhaitables. Veuillez noter qu'il y a lieu de spécifier AGARD-R-nnn et AGARD-AR-nnn lors de la commande des rapports AGARD et des rapports consultatifs AGARD respectivement. Des références bibliographiques complètes ainsi que des résumés des publications AGARD figurent dans les journaux suivants:

Scientific and Technical Aerospace Reports (STAR)  
publié par la NASA Scientific and Technical  
Information Division  
NASA Langley Research Center  
Hampton, Virginia 23681-0001  
Etats-Unis

Government Reports Announcements and Index (GRA&I)  
publié par le National Technical Information Service  
Springfield  
Virginia 22161  
Etats-Unis  
(accessible également en mode interactif dans la base de  
données bibliographiques en ligne du NTIS, et sur CD-ROM)



AGARD holds limited quantities of the publications that accompanied Lecture Series and Special Courses held in 1993 or later, and of AGARDographs and Working Group reports published from 1993 onward. For details, write or send a telefax to the address given above. *Please do not telephone.*

AGARD does not hold stocks of publications that accompanied earlier Lecture Series or Courses or of any other publications. Initial distribution of all AGARD publications is made to NATO nations through the National Distribution Centres listed below. Further copies are sometimes available from these centres (except in the United States). If you have a need to receive all AGARD publications, or just those relating to one or more specific AGARD Panels, they may be willing to include you (or your organisation) on their distribution list. AGARD publications may be purchased from the Sales Agencies listed below, in photocopy or microfiche form.

NATIONAL DISTRIBUTION CENTRES

## BELGIUM

Coordonnateur AGARD — VSL  
Etat-major de la Force aérienne  
Quartier Reine Elisabeth  
Rue d'Evere, 1140 Bruxelles

## CANADA

Director Research & Development  
Information Management - DRDIM 3  
Dept of National Defence  
Ottawa, Ontario K1A 0K2

## DENMARK

Danish Defence Research Establishment  
Ryvangs Allé 1  
P.O. Box 2715  
DK-2100 Copenhagen Ø

## FRANCE

O.N.E.R.A. (Direction)  
29 Avenue de la Division Leclerc  
92322 Châtillon Cedex

## GERMANY

Fachinformationszentrum Karlsruhe  
D-76344 Eggenstein-Leopoldshafen 2

## GREECE

Hellenic Air Force  
Air War College  
Scientific and Technical Library  
Dekelia Air Force Base  
Dekelia, Athens TGA 1010

## ICELAND

Director of Aviation  
c/o Flugrad  
Reykjavik

## ITALY

Aeronautica Militare  
Ufficio del Delegato Nazionale all'AGARD  
Aeroporto Pratica di Mare  
00040 Pomezia (Roma)

## LUXEMBOURG

*See Belgium*

## NETHERLANDS

Netherlands Delegation to AGARD  
National Aerospace Laboratory, NLR  
P.O. Box 90502  
1006 BM Amsterdam

## NORWAY

Norwegian Defence Research Establishment  
Attn: Biblioteket  
P.O. Box 25  
N-2007 Kjeller

## PORTUGAL

Estado Maior da Força Aérea  
SDFA - Centro de Documentação  
Alfragide  
2700 Amadora

## SPAIN

INTA (AGARD Publications)  
Carretera de Torrejón a Ajalvir, Pk.4  
28850 Torrejón de Ardoz - Madrid

## TURKEY

Millî Savunma Başkanlığı (MSB)  
ARGE Dairesi Başkanlığı (MSB)  
06650 Bakanlıklar-Ankara

## UNITED KINGDOM

Defence Research Information Centre  
Kentigern House  
65 Brown Street  
Glasgow G2 8EX

## UNITED STATES

NASA Goddard Space Flight Center  
Code 230  
Greenbelt, Maryland 20771

**The United States National Distribution Centre does NOT hold stocks of AGARD publications.**

Applications for copies should be made direct to the NASA Center for AeroSpace Information (CASI) at the address below. Change of address requests should also go to CASI.

SALES AGENCIES

NASA Center for AeroSpace Information  
(CASI)  
800 Elkridge Landing Road  
Linthicum Heights, MD 21090-2934  
United States

The British Library  
Document Supply Centre  
Boston Spa, Wetherby  
West Yorkshire LS23 7BQ  
United Kingdom

Requests for microfiches or photocopies of AGARD documents (including requests to CASI) should include the word 'AGARD' and the AGARD serial number (for example AGARD-AG-315). Collateral information such as title and publication date is desirable. Note that AGARD Reports and Advisory Reports should be specified as AGARD-R-nnn and AGARD-AR-nnn, respectively. Full bibliographical references and abstracts of AGARD publications are given in the following journals:

Scientific and Technical Aerospace Reports (STAR)  
published by NASA Scientific and Technical  
Information Division  
NASA Langley Research Center  
Hampton, Virginia 23681-0001  
United States

Government Reports Announcements and Index (GRA&I)  
published by the National Technical Information Service  
Springfield  
Virginia 22161  
United States  
(also available online in the NTIS Bibliographic  
Database or on CD-ROM)

